Characterization of Chromosomally Encoded Toxin-Antitoxin Systems in *Streptococcus pyogenes*

D I S S E R T A T I O N

zur Erlangung des akademischen Grades

Doctor of Philosophy
(Ph.D.)

eingereicht an der
Lebenswissenschaftlichen Fakultät der Humboldt-Universität zu Berlin

von
Lina Johana Zarate Bonilla
Master of Science in Molecular Biology

Präsidentin
der Humboldt-Universität zu Berlin

Prof. Dr.-Ing. Dr. Sabine Kunst

Dekan der Lebenswissenschaftlichen Fakultät
der Humboldt-Universität zu Berlin

Prof. Dr. Bernhard Grimm

Gutachter/innen

1. Prof. Dr. Kenn Gerdes
2. Prof. Dr. Emmanuelle Charpentier
3. Prof. Dr. Marc Erhardt

Datum der Einreichung: Januar 29, 2019
Tag der mündlichen Prüfung: April 24, 2019

ZUSAMMENFASSUNG

Streptococcus pyogenes ist ein bedeutender Krankheitserreger des Menschen, welcher den Oropharynx und verschiedene Epithelien inklusive der Haut besiedeln kann und dadurch ein Spektrum an verschiedenen Krankheiten verursacht. Die Eigenschaft des Bakteriums verschiedene Gewebe zu infizieren beruht auf dessen Fähigkeit verschiedene, vom Wirt induzierte Stresskonditionen zu ertragen. Die Mechanismen, die zu dieser enormen Anpassungsfähigkeit beitragen sind jedoch noch nicht vollständig verstanden. Eine Strategie, die in diesem Zusammenhang eine Rolle zu spielen scheint, sind Toxin-Antitoxin (TA) Systeme. Typ II TA Systeme sind genetische Module, die für zwei Proteine kodieren, ein Toxin und ein Antitoxin. Beide Proteine bilden einen stabilen TA Komplex, der das bakterielle Wachstum nicht beeinträchtigt. Verschlechtern sich jedoch die Wachstumsbedingungen durch äußere Einflüsse, kann das Antitoxin proteolytisch abgebaut werden, wodurch das freigesetzte Toxin essentielle zelluläre Prozesse des Bakteriums beeinflussen oder inhibieren kann. TA Systeme haben Einfluss auf Vorgänge wie *post-segregational killing (PSK)*, *abortive infection (Abi)* und bakterielle Persistenz, welche das pathogene Potenzial eines Erregers steigern können. In dieser Studie charakterisierte ich zwei chromosomal kodierte TA Systeme der ParDE Proteinfamilie des humanpathogenen Bakteriums *S. pyogenes*. Beide Systeme sind hochkonserviert in verschiedenen Serotypen. Die Hauptziele meiner Untersuchungen bestanden in: 1) der funktionellen Validierung der Eigenschaften des putativen Toxins und Antitoxins, 2) der Charakterisierung des molekularen Targets des Toxins, 3) Untersuchungen zur Rolle beider TA Systeme in unserem Modellorganismus und 4) der Erforschung von Regulationsmechanismen der TA Systeme.

Beide Systeme (*parDEF1* und *parDE2*) zeigten *bona fide* Charakteristika von TA Systemen, aber auch spezifische Eigenschaften, die in der ParDE TA Familie noch nicht beschrieben wurden. Ähnlich zu anderen Systemen werden das Toxin und das Antitoxin co-transkribiert und werden durch Stresseinwirkung wie Ethanolbehandlung und Aminosäuremangel induziert. Wenn *S. pyogenes* einem Aminosäuremangel ausgesetzt war, konnte ich zudem die Prozessierung der *parDE2* mRNA beobachten, was auf eine putative posttranskriptionelle Regulation unter Stressbedingungen hindeutet. Zusätzlich konnte in beiden Systemen der Abbau des Antitoxins durch die Protease ClpXP *in vivo* nachgewiesen werden. Dies ist ein bedeutender Faktor zur Kontrolle von TA Systemen.

Die extrachromosomale Expression der Toxine ParE1 und ParE2 führten in *S. pyogenes* und *Escherichia coli* zum Zelltod, wobei die Co-expression der entsprechenden Antitoxine ParD1 und ParD2 die Toxizität deutlich minderte. Zusätzlich zu der Fähigkeit die

Toxizität von ParE1 und ParE2 zu vermindern zeigte auch eine Überexpression der Antitoxine allein einen negativen Effekt auf das Zellwachstum. ParD1 hemmte die Zellteilung in *E. coli*, wobei der N-Terminus des Proteins entscheidend für diesen Effekt zu sein schien. Diese Ergebnisse deuten auf einen neuen TA Mechanismus hin, bei dem beide Proteine, das Toxin und das Antitoxin, präsent sein müssen, um das Zellwachstum nicht zu blockieren.

Neben der verminderten Überlebensrate bei Expression der Toxine, konnte ich zeigen, dass ParE1 und ParE2 die normale DNA Topologie der Zelle schädigen und dadurch zu einem deutlichen Phänotyp führten. Wir haben die molekularen Targets beider Toxine identifiziert und konnten dadurch die erstaunliche Plastizität der Toxine verdeutlichen, da sowohl die Funktion des Enzyms Gyrase, als auch Topoisomerase IV durch die Toxine beeinträchtigt wurden. Beide Enzyme gehören zur Gruppe der essentiellen Topoisomerasen, welche die korrekte DNA Topologie in der Zelle aufrechterhalten und zudem bei Behandlung von Infektionen als Ziele für Antibiotika dienen können. Die Fähigkeit von ParE beide Topoisomerasen zu inhibieren, impliziert eine höhere Effizienz bei der Modulierung des bakteriellen Wachstums im Vergleich zu bekannten Toxinen wie CcdB, welche nur die Gyrase hemmen.

Zusammengefasst erweitern die Ergebnisse dieser Arbeit unser Verständnis von ParE Toxinen, derer molekularen Targets und verdeutlichen außerdem die diversen Mechanismen, welcher sich TA Systeme bedienen, um die bakterielle Physiologie zu beeinflussen. Zusätzlich gibt diese Arbeit einen Einblick in mögliche Mechanismen, die *S. pyogenes* implementiert, um Stresskonditionen im Wirt zu überdauern und dadurch effizienter Krankheiten bedingt.

ABSTRACT

Streptococcus pyogenes is an important human pathogen that colonizes the oropharynx and epithelium including the skin and causes a wide spectrum of diseases worldwide. Its remarkable ability to colonize different tissues relies on the capacity to endure diverse host-induced stress conditions through mechanisms that have yet to be fully understood. One strategy employed by bacteria to cope with changing and potentially stressful environments are toxin-antitoxin (TA) systems. Type II TA systems are genetic modules encoding two proteins that permit growth when forming a tight antitoxin-toxin complex. Under non-ideal conditions, the antitoxin is subject to proteolysis and thus the freed toxin can target crucial pathways in the cell modulating bacterial growth. TAs have been connected to some important cellular functions such as post-segregational killing (PSK), abortive infection (Abi) and bacterial persistence, all of which can support the pathogenic potential of bacteria. In this study, I characterized two chromosomally encoded ParDE-like TA systems from the human pathogen *S. pyogenes*, both of which are well conserved in different serotypes. In this context, I aim to, 1) validate the function of the putative toxin and antitoxin molecules, 2) characterize the toxins' molecular targets, 3) elucidate the role of the respective TA systems in our model organism and, 4) investigate the putative TA regulation.

I found that both *parDEF1* and *parDE2* presented commonly described bona fide TA characteristics, but also some particular features that have not been described for this TA family. Like other TA systems, the antitoxin-toxin genes are co-transcribed and triggered by ethanol treatment and amino acid starvation conditions. I detected *parDE2* mRNA processing which may suggest a putative post-transcriptional regulation under amino acid starvation, implying an additional layer of TA regulation upon stress exposure. Additionally, both systems are controlled by ClpXP antitoxin-protein degradation *in vivo*, an important factor for TA triggering.

Moreover, plasmid-based expression of the toxins ParE1 and ParE2 resulted in cell death in our model organism *S. pyogenes* and in the heterologous system *Escherichia coli*. Most importantly, the antitoxin molecules ParD1 and ParD2 were able to prevent ParE1 and ParE2 toxicity, respectively. In addition to their capacity to prevent the ParE1 and ParE2 toxic effect, unlike canonical antitoxins, both ParD1 and ParD2 molecules displayed a deleterious effect when over-expressed in *S. pyogenes*. Furthermore, ParD1 arrested *E. coli* cell division, and its activity seemed to be exclusive and related with its N-terminus domain potentially involved

in DNA-interaction. These findings might suggest a new TA mechanism where the two molecules – antitoxin and toxin – need to co-exist to permit bacterial growth.

Besides decreasing cell viability upon expression, ParE1 and ParE2 toxins induced DNA topology damage and an altered phenotype. We identified the toxin molecular targets and interestingly the ParE toxins presented remarkable plasticity, able to harm not only gyrase but also topoisomerase IV. Both topoisomerases belong to the group of essential enzymes, which are involved in the maintenance of DNA topology and constitute interesting targets to treat bacterial infections. The ParE ability to target both proteins implies more efficacy to modulate bacterial growth in comparison with for instance the well-known CcdB toxin that only targets gyrase.

Overall, the results of this thesis expand the view on the molecular targets of ParE toxins and highlight the diverse mechanisms TAs employ to modulate bacterial physiology. In particular, this thesis provides more insights into possible mechanisms that *S. pyogenes* employs to endure stress in the host and efficiently cause disease.

SCHLAGWÖRTER

Streptococcus pyogenes, Toxin-Antitoxin (TA) Systeme, Gyrase, Topoisomerase IV

KEYWORDS

Streptococcus pyogenes, toxin-antitoxin (TA) systems, Gyrase, Topoisomerase IV

TABLE OF CONTENTS

DEDICATION

"Two roads diverged in a yellow wood, and sorry I could not travel both and be one traveler…

Two roads diverged in a yellow wood, and I took the one less traveled by, and that has made all the difference"

By Robert Frost

To my family and to Eric JC Galvez B, my best traveling partner

LIST OF FIGURES

LIST OF TABLES

LIST OF ABBREVIATIONS

GAS	Group A *Streptococcus*
TA	Toxin-antitoxin
AT	Antitoxin
T	Toxin
PSK	Post-segregational killing
ORF	Open reading frame
SD	Shine-Dalgarno (ribosome binding side)
TSS	translational start side
nt	Nucleotide
ds	double-stranded
ss	single-stranded
PNPase	polyribonucleotide phosphorylase
RSS	ribosome standby site
RBS	ribosome binding site
CRISPR	clustered regularly interspaced short palindromic repeats
Abi	Abortive infection
ssDNA	Single stranded DNA
dsDNA	Double stranded DNA
CPX	Ciprofloxacin
NOV	Novobiocin
STSS	Streptococcal toxic shock syndrome
cDNA	complementary DNA
ORF	open reading frame
rRNA	ribosomal RNA
tRNA	transfer RNA
sRNA	small RNA

1 INTRODUCTION

Regulation of cell growth and death is essential for all living organisms, especially in eukaryotic cells processes such as senescence, apoptosis, necrosis, or autophagy are important for maintaining normal homeostasis (Galluzzi et al., 2018). All these processes are triggered under specific conditions. For example, in eukaryotic cells, the pathway of apoptosis is initiated by a variety of external signals related to stressful conditions such as nutrient deprivation or infection (Galluzzi et al., 2018). Similarly, in bacteria, analogous processes of regulated cell growth and death exist to provide an advantage in response to environmental stimuli (Tanouchi et al., 2013). Toxin-antitoxin (TAs) systems are ubiquitous molecular switches genetically encoded, that control bacterial growth and in some cases their cellular effect may cause cell death in an apoptotic-like fashion. It has been hypothesized that the TA capacity to kill its bacterial host might have come from a maladaptive trait resulting from a process that would provide fitness; e.g. some TAs control gene expression under non-ideal conditions rather than killing (Tanouchi et al., 2013). Another possibility is that cell death induced by TAs might represent an altruistic trait since the sacrifice of some cells in a population can benefit survivors by the provisioning of some nutrients which active cells can benefit (Tanouchi et al., 2013). The study of cell growth and/or death modulation by TA systems in bacteria involves a more complex network of not only one genetic TA copy, but normally several TA copies encoded within the same genome. In addition, numerous features make TA modules versatile systems: they come in six different types, they have different modes of genetic regulation, diverse cellular targets to modulate bacterial growth and/or cell death and a variety of roles that will be summarized in the following section.

1.1 TOXIN-ANTITOXIN SYSTEMS IN BACTERIA

TA systems are abundant genetic elements composed of two molecules: a normally stable protein toxin that modulates bacterial growth by interfering with vital functions and a comparatively unstable non-coding RNA or protein antitoxin that counteracts the toxin's effect. The toxin molecules modulate bacterial growth by targeting important elements that are essential to fulfill successful DNA replication, transcription or translation. They can also affect for example the function of the inner cell membrane homeostasis, peptidoglycan synthesis or cytoskeleton conformation (reviewed by Unterholzner et al., 2013).

TAs are classified into six major types (I- VI) based on the nature and mechanism by which the antitoxin molecule counteracts the toxic effect (Unterholzner et al., 2013). In TA type I and III the antitoxin is an RNA molecule while in type II, IV, V and VI the antitoxin is a protein. The main features of the different TA types are summarized in **Figure I**, and the specific toxin targets of each type will be described in detail later in this section. Moreover, the most studied TA type II system will be described in greater detail in section 1.2.

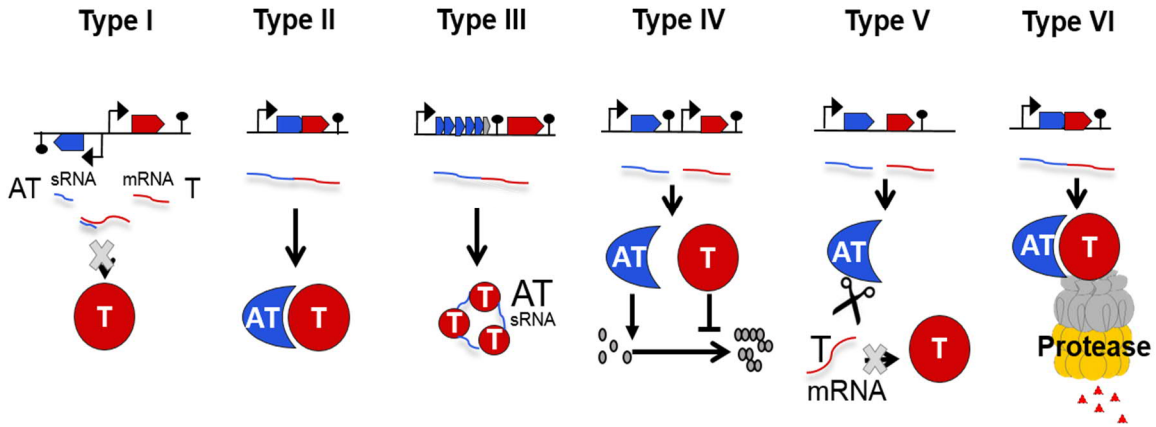

Figure I. TAs are divided in VI types

The figure summarizes the modes by which the antitoxin (blue) control the toxin (red) in the different TA types. Promoters are shown with black arrows and terminators with a black bubble. Curly lines represent RNAs and a protease is shown in grey and yellow for the type VI. The antitoxin is a sRNA in type I and II and a protein in type II, IV,V and VI. **Type I:** the antisense sRNA antitoxin counteracts the toxin activity by binding to the mRNA encoding toxin molecule avoiding its translation. **Type II:** the less stable antitoxin protein counteracts toxicity by forming a complex with the more stable toxin molecule. **Type III:** The sRNA antitoxin directly interacts with the active side of the toxin protein molecule. **Type IV:** AT-T do not interact, the antitoxin protein has the capacity to stabilize the toxin target that will disassemble in the presence of the toxin molecule. **Type V:** The antitoxin is a RNase that degrades the mRNA encoding the toxin. **Type VI**: The antitoxin protein is an adaptor that interacts with both the toxin and the ClpX ATPase stimulating the toxin proteolytic degradation by the ClpXP protease.

TAs were first discovered as addiction molecules that play a role in plasmid maintenance by post-segregational killing (PSK) of plasmid-free daughter cells (Ogura and Hiraga, 1983). Intriguingly, beside such plasmid-located TA systems, several bacterial chromosomes contain multiple TA copies that belong to the same or distinct types or families displaying different roles (reviewed by Harms et al., 2018). *E. coli* K-12 for instance encodes 19 type I TA systems and 13 type IV TA loci as well as many other putative (reviewed by Harms et al., 2018). The human pathogen *Mycobacterium tuberculosis* has been also highlighted due to the abundant and redundant TA modules encoded in the chromosome (79 in total), which may contribute to its pathogenesis and persistence (Ramage et al., 2009; Sala et al., 2014). Similarly,

Salmonella enteritica serovar Typhimurium encodes 6 type I TAs and 21 type II TAs in its genome, highlighting redundancy that might lead to different biological outcomes under diverse conditions (Lobato-Márquez et al., 2015).

1.1.1 BIOLOGICAL FUNCTIONS OF TA MODULES

Different functions have been attributed to TA modules, some of which are still controversial and some others are well supported by experimental data (Magnuson, 2007; Van Melderen, 2010). The stabilization of mobile genetic elements through PSK constitutes one of the best-described TA functions, not only important for plasmidic TA copies but also for chromosomally encoded TA modules, e.g. within pro-phage encoded regions. The abrogation of bacteriophage infections - abortive infection (Abi) - through altruistic suicide of phage-infected cells constitutes another important trait of some chromosomally encoded TAs (Fineran et al., 2009). Finally, the formation of dormant cells – antibiotic tolerant cells – known as persisters, represents the most controversial proposed function of TA systems (Helaine et al., 2014). The three concepts are depicted in **Figure II** and will be discussed in the following sections.

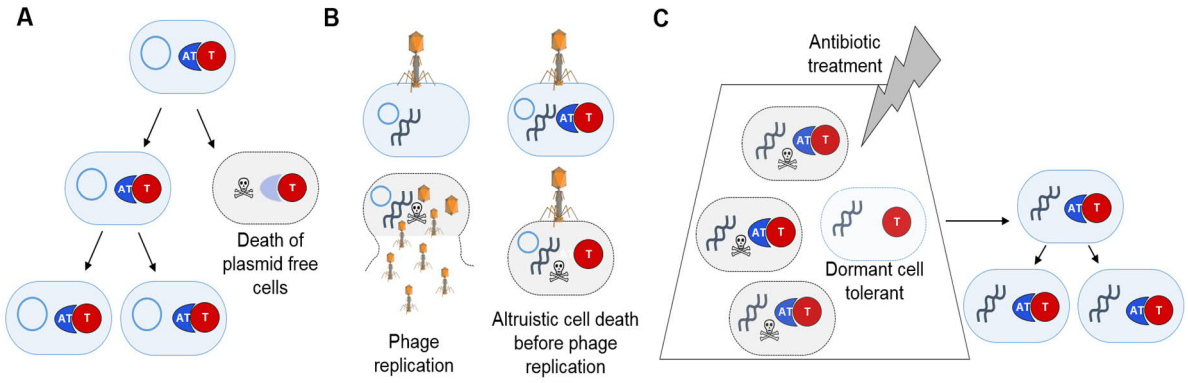

Figure II. Biological functions of TA modules

The main TA biological functions are depicted; plasmids and chromosomes are represented by a small circle and by a black spiral, respectably. Light blue cells are alive while light grey cells are dead. **A**. Post-segregational killing (PSK) by TA system encoded in a plasmid (or in the chromosome). Plasmid-free cells (light grey cell) loss the TA genes and therefore cannot supply antitoxin molecules to counteract the toxin. The already present antitoxin is rapidly degraded and thus the toxin is released. **B**. Abortive infection (Abi) by TA system encoded in a plasmid (or in the chromosome) gets triggered upon phage infection, the free toxin kills the cells before the phage can replicate. **C.** Persistent cell formation, less than 1% of the whole population stochastically enters into a dormant stage where they are tolerant to environmental insults (e.g. antibiotic treatment). The dormant cells can resume growth in ideal conditions.

1.1.1.1 Post-segregational Killing

Type I and type II TAs were the first ones implicated in PSK, but this function is also attributed to some type IV TAs (reviewed by Harms et al., 2018). These “addiction modules” prevent the loss of plasmid but can also use this mechanism to maintain the genomic mobile regions in which they are encoded, throughout bacterial generations (Szekeres et al., 2007; Wozniak and Waldor, 2009). PSK relies on the different stability of the two TA molecules wherein the antitoxin is less stable than the toxin. Upon cell division, the locus encoding the TA module needs to be inherited to the offspring so that the antitoxin molecule continues being produced to keep the toxin in check. Conversely, if upon cell division the offspring loses the TA module, the antitoxin remaining molecule will be rapidly degraded, while the toxin molecule will target specific cellular functions leading to cell death. As a consequence, this mechanism ensures that the TA-free cells die (Gerdes et al., 1986; Jensen and Gerdes, 1995; Ogura and Hiraga, 1983).

The first characterized TA system was the *ccdAB* operon (couple cell division) involved in the maintenance of the F plasmid (Ogura and Hiraga, 1983). This TA system operates by coupling host cell division to plasmid proliferation, since cell host division is inhibited when the copy number of a plasmid carrying the *ccdAB* segment decreases (Ogura and Hiraga, 1983).

Notably, Partition Systems (PS) also promote stability of plasmids during cell division, but the mechanism of PS is not related to TA systems. PS direct segregation of plasmids into the daughter cells with a nucleoside triphosphatase (NTPase) and a centromere binding protein (CBP) which binds the DNA *par* sites forming a partition complex (Pilla and Tang, 2018). Based on this function, another crucial element for the RK2 plasmid maintenance, was first named *parDE,* from “partition system” due to induction of a similar phenotype compared with PSs (Roberts and Helinski, 1992). Now it is known that *parDE* constitutes a type II TA system and is not associated with the partition mechanism of a cognate PS (Roberts et al., 1994a).

1.1.1.2 Abortive Infection

Although bacteria are the most abundant organisms on earth, then times more phages (predator) exist per bacterial cell (prey) (Chibani-Chennoufi et al., 2004; Lima-Mendez et al., 2007). This predator-prey relationship has caused bacteria to evolve multiple strategies of protection such as: 1) surface alterations to avoid phage absorption, 2) prevention of phage

DNA injection, 3) restriction of incoming DNA, via both innate (restriction enzymes) and adaptive mechanisms by clustered regularly interspaced short palindromic repeats system (CRISPR) (Sorek et al., 2008), and 4) abortive infection (Abi) (Petty et al., 2007). Abi systems encoded in plasmids and chromosomes provide population protection by promoting "altruistic suicide" of infected cells (Forde and Fitzgerald, 1999). One of the main characteristics of Abi systems is that they harbor a highly effective toxin that when activated, targets a crucial cellular function to inhibit phage DNA replication, transcription and translation (Chopin et al., 2005).

TA modules that constitute Abi systems encoded for a toxin that interfere with processes such as DNA replication and translation or with the inner membrane homeostasis. The TA type II *rnlAB* which is a chromosomally encoded in *E. coli,* has been shown to abort bacteriophage T4 infection, wherein the toxin RnlA degrades mRNA (Koga et al., 2011). The MazEF (type II) and hok/sok (type I) were also shown to abort T4 infection, by degrading mRNA in the case of the MazF toxin or by damaging the bacterial inner membrane in the case of the Hok toxin (Alawneh et al., 2016; Pecota and Wood, 1996). The type III TA modules, e.g. *toxIN* and *tenpIN,* wherein the toxins interfere with the bacterial membrane, were also described to protect a wide range of bacteria from bacteriophage infection (Goeders et al., 2016)

Regarding the bacteriophage's resistance to Abi systems, several interference mechanism have been studied. Interestingly, one of these mechanisms constitutes an antitoxin-like molecule (Dmd "the master key") encoded in the T4 phage that can counter the effect of several toxins from the LsoA and RnlA family by direct interaction (Otsuka and Yonesaki, 2012). Moreover, the protein Alt from the T4 bacteriophage, ADP-ribosyltates the MazF toxin in a specific position rendering the toxin inactive. Some bacteriophages (e.g. T7) also encoded protease inhibitors, since proteases are important for the depletion of the antitoxin protein molecules (TA type II and IV) to release the toxins. However, cellular proteases are also responsible for many important function in the cell (e.g. protein quality control), thus phage protease inhibitors not only impair abortive infection by TAs but can also interfere with essential bacteria cellular processes (Sberro et al., 2013).

1.1.1.3 Bacterial Persistence

Persistent bacterial infections (or recurrent infections) are commonly due to difficult to eradicate pathogens that have not evolved classical resistance (genetically-encoded) but

antibiotic tolerance (Lewis, 2010; Mulcahy et al., 2010). This antibiotic tolerance is stochastically induced in less than 1% of a clonal bacterial population that enters in a "dormant stage" called persistence where molecular antibiotic targets are inactive and therefore unaffected (Balaban, 2004).

Studies in *E. coli* allowed the identification of the first bona fide persister gene *hipA* (high persistence) from the type II TA system HipAB (Moyed and Bertrand, 1983). HipA is a protein-serine kinase toxin that phosphorylates glutamyl-tranfer RNA synthase in the absence of its cognate antitoxin HipB (Germain et al., 2013; Korch and Hill, 2006). Thus, HipA inhibits protein synthesis, which induces cell dormancy. Another example highlights the importance of the toxin TisB (TA Type I) induced upon DNA damage. TisB affects the bacterial cell membrane by forming channels that disrupt the proton motive force resulting in a drop in ATP levels (Dörr et al., 2010). Importantly, the activity of many antibiotics is typically ATP-dependent; therefore a decrease in cellular energy leads to increased drug-tolerance (Conlon et al., 2016; Shan et al., 2017). A recent finding from the group of Kim Lewis suggested that low ATP levels lead to persister formation and that this might be an important aspect of this bacterial trait (Shan et al., 2017). However, a drop in cellular ATP can be also due to other factors not related to TA systems (Shan et al., 2017).

The stress-induced expression of mRNAase toxins from 10 type II TA loci was claimed to have major contribution to persister formation in *E. coli* (retracted Maisonneuve et al., 2013). This process involved the alarmone ppGpp, the PPK phosphatase and the Lon proteases. Careful reexamination of *E. coli* mutants lacking either 10 TAs (Δ10 TAs), Lon (*Δlon ΔsulA*) or the polyphosphate operon (*Δppx Δppk*), did not reproduce the persister phenotype, disproving the model (Chowdhury et al., 2016; Harms et al., 2017; Shan et al., 2017). The misleading findings arose as a result of a cryptic prophage contaminant (Harms et al., 2017). Moreover, a controversial more recent publication confirmed that the 10 TA copies from *E. coli* are not essential for persister cell formation (Goormaghtigh et al., 2018a).

David Holden (Imperial College-London) has recently published his opinion and highlighted three important points with regard to TA modules and persister formation (Holden and Errington, 2018): 1) The relevance of TA systems on persister cell formation should be addressed under different physiological conditions – e.g. biofilm formation (Harrison et al., 2009) - and not only in optimal growth conditions where the TA systems might not be active. 2) The involvement of TAs in persistence should be considered during infection. There have been evidences in pathogenic bacteria that support the involvement of TAs in persister cell

formation; in favor to this idea, one report suggested that the YefM-YoeB, YbaJ-Hha and PasTI TAs are important for niche-specific colonization of uropathogenic *E. coli* using a murine infection model (Norton and Mulvey, 2012). Another study highlighted the involvement of TAs in *Burkholderia cenocepacia* persistence during biofilm formation, wherein expression of these TAs relied on the mode of growth and antibiotic used (Van Acker et al., 2014). In addition, recent publications have demonstrated that the persister cell formation of *Salmonella* in macrophages depends on TAs, specifically three tRNAs acetyltransferase toxins (Cheverton et al., 2016; Helaine et al., 2014; Rycroft et al., 2018). 3) The role of single TA copies in persistence should be highlighted. The naturally acquired *hipA7* mutant (toxin from TA type II *hipAB*), was the first hint of TAs implicated in this process (Moyed and Bertrand, 1983), afterwards RelE (Keren et al., 2004) and MazF (Tripathi et al., 2014) toxin expression was shown to significantly increase persister cells in a population. However, experiments relying on artificial overexpression of a toxin or gain-of-function alleles of TA systems do not present enough evidence for TA being causative agents of a phenotype, and the information of those experiment should be carefully analyzed (Goormaghtigh et al., 2018b).

Overall, these information present enough evidence to conclude that TAs are somehow involved in the persistence stage (Holden and Errington, 2018). However, persistence is a phenomenon that involves several factors among which TA systems might be only one.

1.1.1.4 Other Functions

Besides Abi, PSK and persister cell formation, TAs have been implicated in biofilm formation, a trait that is still under debate. One report showed in *E. coli,* five TAs modulating biofilm formation due to the induction of the gene *yjgK*, potentially involved in adherence (Kim et al., 2009). Moreover, a clearer phenotype was observed also in *E. coli* where five TAs were compared for the capacity to mediate cell death in both planktonic and sessile cells; it was observed that *mazEF* was activated under both conditions, whereas *dinJ-yafQ* was shown to play a role only during biofilm formation (Kolodkin-Gal et al., 2009). As mentioned before some papers have also suggested the involvement of TAs in persister cell formation only under biofilm formation conditions (Sun et al., 2017; Van Acker et al., 2014).

Interestingly, a recent publication concluded that the toxin ParE (from the type II TA *parDE*) protects *Pseudomonas aeruginosa* under antibiotic treatment with fluoroquinolones

that target the same molecule targeted by ParE, the DNA gyrase. In this model the toxin will compete with the antibiotic to bind gyrase thereby protecting it. In addition, this mechanism depends on the ParE/ParD ratio that in excess of the toxin with respect the antitoxin will lead to cell death (Muthuramalingam et al., 2018).

Many reports have shown that some TA systems are up-regulated under stress conditions (Christensen et al., 2001a, 2003; Christensen-Dalsgaard et al., 2010; Wang et al., 2011). In some cases TA systems modulate growth under non-ideal conditions by reducing the rate of cell division in a reversible manner, while in some other cases TA elements might lead to cell death as an altruistic mechanism by which a subpopulation die to provide nutrients to the remaining cells (Erental et al., 2012; Tanouchi et al., 2013).

Finally, TAs might also play a regulatory role in the cell, e.g. some of them specifically degrade mRNA thereby modulating translation. MazF for instance is an endoribonuclease (of the MazEF type II TA), that cleaves multiples sites in most mRNAs while blocking ribosome biogenesis by targeting ribosomal-protein transcripts and ribosomal RNA (rRNA) precursors. In addition, MazF generally cleaves mRNAs in a sequence specific manner, which might inhibit growth, but also modulate the translation of its targets (Culviner and Laub, 2018).

1.1.2 TYPE I TA SYSTEMS

The type I TA systems is constituted by an unstable antisense sRNA antitoxin (AT) molecule that base-pairs with the mRNA toxin (T) molecule thereby down-regulating its expression (Brantl, 2012). The genes are normally arranged in the same genetic locus where the AT can be a cis-encoded antisense RNA or a trans-encoded sRNA with respect to the toxin ORF. The sRNA AT-mRNA T complex blocks the T mRNA ribosome binding side sequence Shine-Dalgarno (SD) sequence, by binding the T mRNA translational start side (TSS) or binding to the open reading frame (ORF), thereby arresting translation of the T molecule (Fozo et al., 2008a). However, formation of this sRNA AT-mRNA T complex can also promote mRNA T degradation. Thus, the regulation of type I TAs often involves RNases providing an additional layer of control (Reviewed by Brantl, 2012). Some examples are described in **Table 1**.

Table 1: Representative type I TA modules

Antitoxin	Toxin	Organism	Regulation	Reference
symR	*symE*	*E. coli*	*symE* expression by LexA (SOS induced) SymE degradation by Lon	(Fernández de Henestrosa et al., 2002; Kawano et al., 2007)
istR-1	*tisB*	*E. coli*	Transcription of the T controlled by LexA (SOS induced). Inhibitory 5' UTR structure masks the RSS preventing translation of TisB, relive by a processing event. Binding of the AT *istR-1* to *tisB* triggers cleavage by RNase III	(Berghoff et al., 2017; Wagner and Unoson, 2012)
ibs	*sib*	*E. coli*	Transcription of the T controlled by LexA (SOS induced)	(Fozo, 2012)
sok	*hok*	Plasmid R1 *E. coli*. Genomes of several entorebacteria. Five copies in the *E. coli* K12 genome.	Processing by RNase II to allow translation and biding of *sok*. *mRNA mok* overlaps with mRNA *hok*. *sok* preventing transcription therefore no *hok* is translated. *hok* mRNA/*sok*-RNA is degraded by RNaseIII	(Franch et al., 1997; Gerdes et al., 1992; Pedersen and Gerdes, 1999; Thisted and Gerdes, 1992)
txpA	*ratA*	*B. subtillis*	AT RNA binds SD of T mRNA. The complex is degraded by RNase III	(Durand et al., 2012a)
sr4	*bsrG*			(Jahn et al., 2012)
as-yonT	*yonT*			(Durand et al., 2012a)
tisA	*tisB*	*E. coli*	AT RNA binds SD of T mRNA.	(Gurnev et al., 2012)
agrB	*dinQ*	*E. coli*	Transcription of the T controlled by LexA (SOS induced). Translation of DinQ depends on mRNA processing. AT *agrB* binds to *dinQ* mRNA sequestering the SD sequence.	(Berghoff et al., 2017; Weel-Sneve et al., 2013)
orzO	*zorO*	*E. coli* O157:H7	Antisense encoded antitoxin *orzO* binds the mRNA *zorO*.	(Wen et al., 2014, 2017)

			zorO mRNA processing in response to nutrient shift.	
ohsC	*shoB*	*E. coli*	*shoB* mRNA processing. *ohsC* binds the mRNA *shoB*	(Fozo et al., 2008b; Kawano, 2005)

Hok/Sok is one of the most studied and complex members of the type I TA family (Reviewed by Berghoff et al., 2017). Its regulatory mechanism has been studied in detail and is summarized in **Figure III**. Translation of the *hok* (host killing) T depends on a third component *mok* (modulation of killing) that together with *hok* forms a single translationally inert transcript (*mok-hok*). RNase II and the polyribonucleotide nucleotidyltransferase (PNPase) process and remove 39nt (nucleotides) respectively from the 3' end of the *mok-hok* transcript thereby inducing structural rearrangements of the mRNA that lead to translation of *hok.* Moreover, the *sok* (suppressor of killing) AT is able to bind to the hok transcript thereby blocking its translation (Berghoff and Wagner, 2017). Interestingly a second regulatory event involves the RNase III, which cleaves the *sok-hok* RNA heteroduplex to decay the transcript (reviewed by Gerdes and Wagner, 2007)

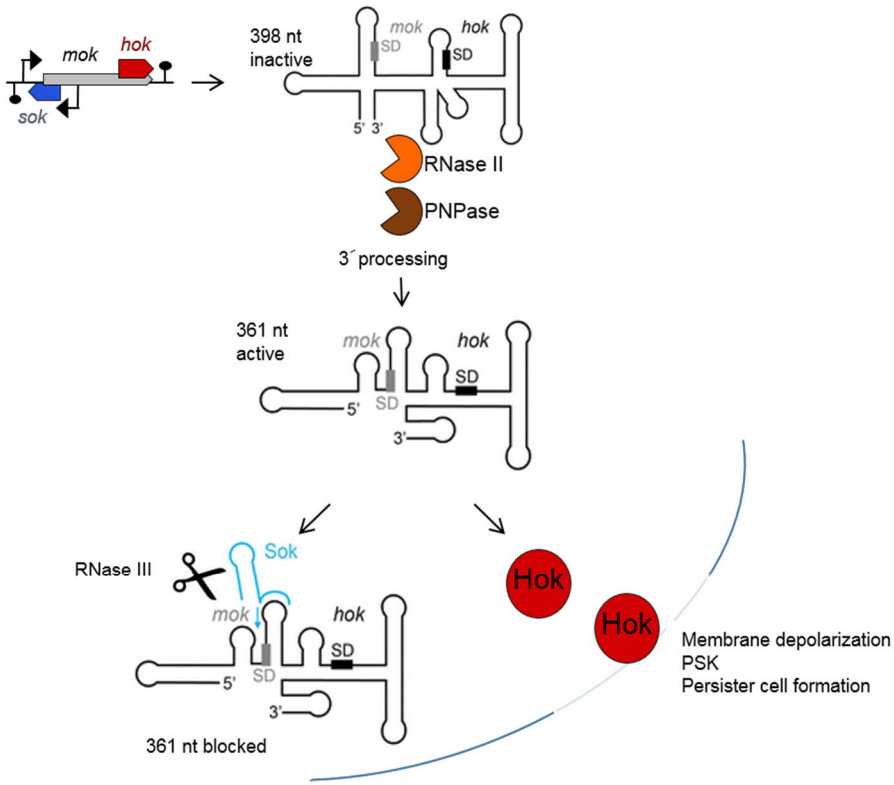

Figure III. Translation of the Hok toxin is controlled by several regulatory RNA elements

The *sok-hok* locus is depicted in colors where the toxin *hok* (red) gene overlaps the sequence of the regulatory element *mok* (grey). The antitoxin *sok* (blue) RNA is transcribed in cis. The *mok-hok* RNA is processed by RNase II (orange) and PNPase (brown) allowing the antitoxin sRNA *sok* to bind the mRNA of *hok.* RNase III (scissors) processes the double stranded *sok-hok* sRNA-mRNA complex to deplete the toxin transcript. In the absence of sRNA *sok,* the Hok protein is translated (modified from Berghoff and Wagner, 2017).

Except for SymE, all type I toxins are hydrophobic proteins with a putative transmembrane domain, similar to phages holins and are therefore able to introduce pores into cell membranes (Reviewed by Brantl, 2012). Thereby, membrane depolarization can occur and ATP synthesis can become impaired resulting in the inhibition of vital functions such as, replication, transcription and translation leading to cell death.

Type I TA systems are known to interfere with phage propagation by affecting the bacterial cell membranes or preventing the maturation of phage particles (Kawano, 2012). The toxins SymE and TisB (regulated by the LexA repressor) have been shown to recycle damaged mRNAs which are produced under SOS stress conditions or to prevent infection by RNA phages (Kawano, 2012). Other type I toxins affect the maintenance of prophages within bacterial chromosome, e.g. TxpA, BsrG, YonT (Durand et al., 2012b), in a manner which resembles the PSK plasmidic-TA function. Some of the TAs type I have been reported to be bacteriostatic and are induced under oxygen or glucose limitation conditions (Durand et al., 2012b). Moreover, type I TAs have been also related with persister cell formation since deletion of *tisAB* abrogates persistence and over-expression of the toxin TisB increased the level of persister cells (Dörr et al., 2010). This is due to the cellular effect of TisB which destabilizes membrane integrity leading to a decrease in ATP levels shutting down antibiotic targets resulting in multidrug tolerance (Reviewed by Brantl, 2012).

1.1.3 TYPE III TA SYSTEMS

Similar to type I TA systems, in type III TA systems the antitoxin is a small RNA, but instead of interacting with the toxin mRNA, the antitoxin sRNA forms pseudoknots that bind directly to the active side of the toxin protein molecule. Recently, a classification of TA type III have been proposed according to the amino acid sequence similarities consisting of: ToxIN, CptIN and TenpIN (reviewed by Goeders et al., 2016). The most studied member of TAs type III is the ToxIN module discovered on a cryptic plasmid from *Pectobacterium atrosepticum* (*Erwinia carotovora subsp. atroseptica*), also present in *Bacillus thuringiensis* (plasmid pAW63), *Histophilus somni* 129PT and within the chromosome of many Firmicutes and proteobacteria (Blower et al., 2012; Fineran et al., 2009). The toxNI distribution implies

horizontal gene transfer as the plasmid pAW63 from *B. thuringiensis is* conjugal (Short et al., 2015). The *toxNI* operon is co-transcribed from a single promoter wherein the toxin *toxN* gene is preceded by the *toxI,* a short palindromic repeat and a tandem array of nucleotide repeats. The ToxN toxin is an RNase that cleaves the *toxIN* transcript to activate the sRNA *toxI* antitoxin transcripts that fold into an RNA pseudoknot, and three ToxI monomers bind three ToxN proteins in a trimeric ToxI/ToxN complex to inhibit toxicity of ToxN. Interestingly, most of the TA transcripts end right after the antitoxin *toxI*, leaving on average only 10% of read-through into the *toxN* sequence, thus the presence of the *toxI* terminator ensures an appropriate ToxI:ToxN stoichiometry (Fineran et al., 2009).

The ToxN toxin has endoRNase activity and cleaves other mRNAs to inhibit growth in a bacteriostatic and reversible manner, highlighting its important regulatory function in the cell (Brantl and Jahn, 2015). ToxIN provides viral resistance against multiple phages (Fineran et al., 2009). In a similar fashion, the second TA type III described *abiQ/AntiQ* is required for promoting cell death and limit phage replication where the AbiQ (abortive phage infection) toxin also acts as an RNase (Samson et al., 2013). It has been reported that plasmidic TA types III also play a role in PSK (Short et al., 2015). Finally, the *cptIN* TA module is the only chromosomally encoded TA type III that has been reported to date, and a physiological function has not been described.

1.1.4 TYPE IV TA SYSTEMS

The antitoxin and toxin elements of the type IV TA systems never interact. In this group the toxin molecule prevents growth by binding and inhibiting the polymerization of the bacterial cytoskeletal proteins MreB and FtsZ (Brown and Shaw, 2003; Masuda et al., 2012). MreB is the actin-homolog in bacteria, it is important for maintaining cell shape and polarity and is also involved in chromosome segregation. FtsZ is the tubulin-like protein that serves as scaffold during assembly of the divisome (Shih and Rothfield, 2006). Maintaining the homeostasis of these molecules constitute an important step during cell division. The antitoxin prevents the toxic effect by stabilizing the same molecules and therefore promoting the bundling of the MreB and FtsZ filaments. The YeeU-YeeV (CbtA for cytoskeletal bundling-toxic) encoded in the chromosome of *E. coli* is the main representative of this type where both molecules bind to the MreB and FtsZ proteins (Masuda et al., 2012). The CbtA toxin was found to have a profound effect in cell morphology and division (Tan et al., 2011), while the YeeU antitoxin not

only neutralized the CbtA toxicity but also the effect of other MreB and FtsZ inhibitors, such as A22 [S-(3, 4-dichlorobenzyl) isothiourea], SulA or DicB (Masuda et al., 2012).

In order to respond to environmental insults, bacteria need to rapidly modulate the bundling of filaments; the direct manipulation of these dynamics by type IV TA systems may allow bacteria to quickly change their physiology under unfavorable conditions. Moreover, the *yeeU-cbtA* operon is part of a prophage sequence (CP4-44) that might give to the host a potential selective advantage to easily manipulate cell division (Masuda et al., 2012).

1.1.5 TYPE V TA SYSTEMS

In the only known type V TA system in *E. coli* and *Shigella spp*, the antitoxin GhoS (YjdK) is an RNase that cleaves the toxin *ghoT* (*yjdO*) mRNA. Under stress condition the antitoxin *ghoS* mRNA is degraded by the type II toxin MqsR (from the *mqsRA* "motility quorum sensing regulator" TA type II) resulting in translation of GhoT (Wang et al., 2011, 2012) **(Figure IV)**. Moreover, the antitoxin GhoS is stable during stress (not proteolytically degraded) and does not bind the promoter-DNA to regulate its own transcription, like a typical type II antitoxin. Interestingly, its structure resembles the CRISPR-associated-2 (CAS2) sequence-specific endo-RNase, indicating a putative evolutionary of post-translational regulation for serving several purposes in the cell, from controlling cell growth to preventing phage attack (Wang et al., 2012).

The toxin GhoT (toxin producing ghost cells) is an inner membrane lytic peptide, known to function similar to the type I toxins, which targets the integrity of the cell membrane leading to membrane depolarization and cellular ATP depletion **(Figure III)** (Wang et al., 2012).

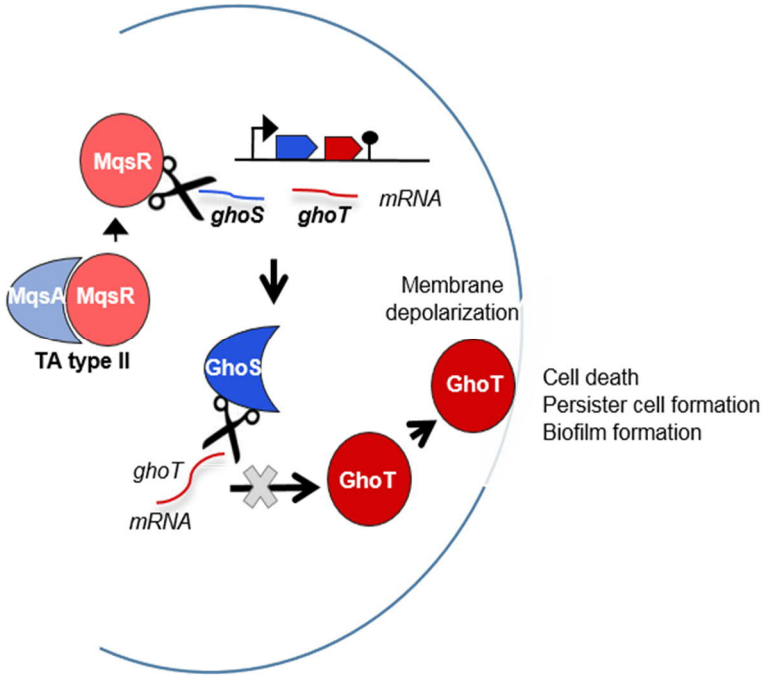

Figure IV. The antitoxin GhoS is an RNase that degrades the GhoT toxin mRNA

The *ghoST* locus is depicted in colors; the toxin *ghoT* (red) mRNA is degraded by the antitoxin protein GhoS (blue). Under stress conditions the toxin MqsR (light red) (form the MqsAR TA type II, light blue and red) enriches the GhoT toxin by degrading the *ghoS* antitoxin mRNA leading to the toxin accumulation that targets the inner membrane (modified from Wang et al., 2013).

It has been suggested that GhoS-GhoT plays a role in persister cell formation since GhoT not only kills the cells but can also to a certain extent reduce cell growth. Remarkably, the toxin GhoT has been shown to also prevent cell elongation upon the addition of low levels of ampicillin (Wang et al., 2013). Furthermore, GhoT increases early biofilm formation and swimming motility (Wang et al., 2013).

1.1.6 TYPE VI TA SYSTEMS

SocAB is the only TA type VI systems representative known up to date, encoded in a bisistronic operon within the *Caulobacter crescentus* chromosome (Aakre et al., 2013). Unlike canonical TA systems the atypical toxin SocB is unstable and degraded by the ClpXP proteolytic complex via the adaptor SocA antitoxin molecule. The SocA antitoxin is therefore able to bind both the toxin SocB and the N-terminal domain of ClpX. In the absence of SocA, the toxin SocB blocks the replication elongation through direct interaction with the essential sliding clamp (DnaN) important for DNA replication, leading to replication fork collapse **(Figure V)**. This effect leads to induction of the SOS response and eventually cell death. The SocB toxin might accumulate and compete for binding to the clamp with polymerase III (Pol III) and

other important replication factors such as DNA repair proteins, Pol IV and Pol V (translesion synthesis), MutS and MutL (DNA mismatch repair) and Had (regulation of initiation) that are also able to bind DnaN (Aakre et al., 2013).

The *socAB* operon is induced by the DNA-damaging agent mitomycin C (MMC), suggesting that it may play a regulatory role during the DNA-damage response. Aakre and coworkers suggested that DNA damage or other stress conditions might lead to accumulation of SocB to regulate the rate at which DNA replication occurs (Aakre et al., 2013).

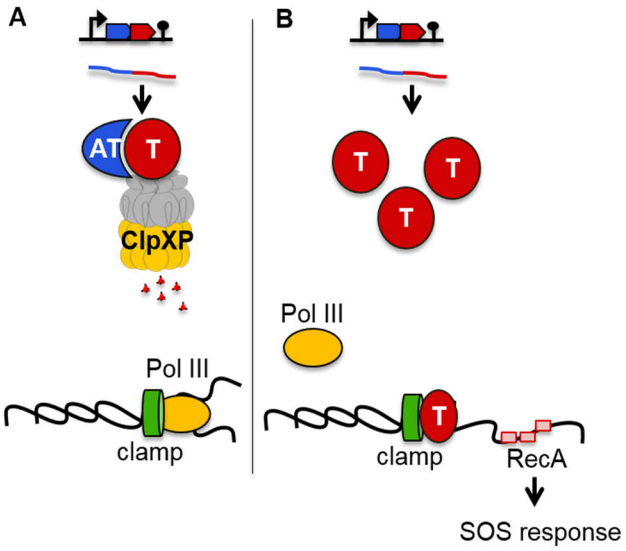

Figure V. SocAB mode of regulation

A. Under normal growth conditions, the antitoxin SocA binds and delivers the SocB toxin protein for degradation by the ClpXP proteolytic complex, leading to normal DNA replication. **B.** In the absence of ClpXP or SocA, the toxin SocB accumulates and reaches the DNA β clamp thereby collapsing the replication forks. SocB abolish the interaction of important protein such as the Pol III to the clamp inducing the RecA-mediated SOS response (modified from Aakre et al., 2013a).

1.2 TYPE II TA SYSTEMS

Type II TA systems is the best-studied class. They are composed of two proteins, an unstable antitoxin and a stable toxin. In this type, the antitoxin forms a tight complex with the toxin resulting in its neutralization (Wang et al., 2011). The TA type II genes are typically encoded in a small operon where the upstream gene encodes the antitoxin that overlaps with the beginning of the toxin-encoding gene. However, there are some exceptions to the typical AT-T operon configuration, e.g. the operon *higBA* harbors the opposite operon organization where the toxin *higB* is the first gene followed by the antitoxin *higA* gene (Tian et al., 2001), however the implication of this genetic organization have not been characterized. The

regulation of TAs type II occurs at two different levels, i) transcriptional repression by the antitoxin molecule alone or in complex with the toxin and ii) posttranslational degradation of the unstable antitoxin protein. Both mechanisms are important for triggering the system - summarized in the **Figure VI** - and will be discussed in the next sections.

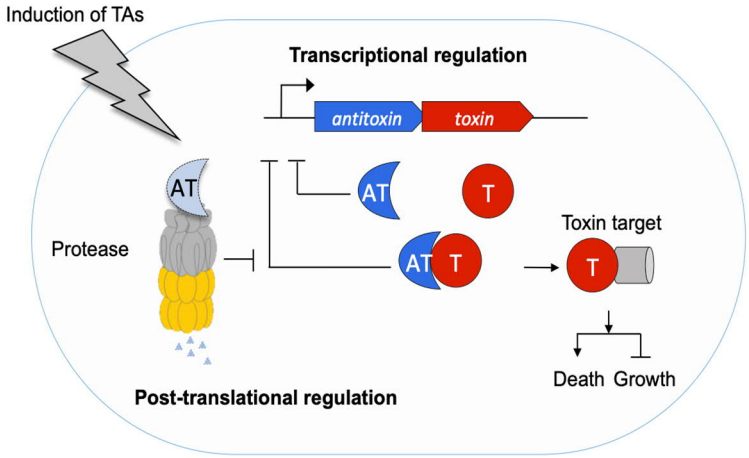

Figure VI. TA type II mode or regulation

The AT-T operon is composed of two genes, one encoding the antitoxin unstable protein (blue), and the second gene encoding the stable toxin molecule (red). The antitoxin or antitoxin-toxin complex can bind to the TA promoter to block its own transcription. The unstable antitoxin molecule can be degraded by cellular proteases, which leads to TA transcription and toxin release. The freed toxin molecule accumulates and therefore modulates bacteria growth by targeting vital functions. In the absence of the antitoxin the toxin will kill the cells.

1.2.1 Transcriptional Regulation

In type II TA systems the antitoxins molecules normally have three important features: one domain that binds DNA, a second region that binds the cognate toxin and a segment that is recognized by a proteolytic machinery. The domain that directly interacts with DNA is normally located at the N-terminal end of the protein and specifically recognizes its own promoter DNA sequence. Thus, at the transcriptional level, the expression of type II TA systems is tightly regulated by presence of the antitoxin, which has the ability to repress expression of its own operon, either alone or in complex with the cognate toxin. The formation of the AT-T complex will then result in a more potent transcriptional repression that might be due to the toxin capacity to stabilize the antitoxin by binding to the same region recognized for its proteolysis, located at the C-terminus of the protein. Thus, a more stable antitoxin will efficiently reach and bind its promoter (reviewed by Page and Peti, 2016).

Interestingly, an excess of the toxin molecule will also drive transcription but in the opposite direction; one of the first reports about TA transcriptional autoregulation was characterized in the Doc/Phd TA system, where the excess of toxin activated rather than repressed transcription (Magnuson and Yarmolinsky, 1998). Therefore, the level of transcriptional auto-regulation depends on the formation of TA complexes with different stoichiometries and distinct affinities for their own operator (Afif et al., 2001; Garcia-Pino et al., 2016a; Tsuchimoto and Ohtsubo, 1993). The toxin enhances cooperative auto-repression at low T:A ratios in steady state conditions, whereas it acts as activator at high T:A ratios, thereby stimulating TA transcription (reviewed by Harms et al., 2018). This phenomenon has been named conditional cooperativity (Garcia-Pino et al., 2010) and has been reported for other type II systems such as *ccdBA* (Afif et al., 2001), *parDE* (Johnson et al., 1996), *relBE* (Overgaard et al., 2008), *kid/kis* (Monti et al., 2007) and *vapBC* (Dienemann et al., 2011). Nevertheless, some TA type II copies do not regulate transcription by conditional cooperativity, e.g. MqsRA, where the MqsR toxin does not enhance MqsA antitoxin binding to the promoter but instead destabilize it (Brown et al., 2013).

Some other TAs type II operons are composed of three molecules where the third gene might also play a role in the TA transcriptional regulation. As an example, the TA module *ω-ε-ζ*, encoded within the pSM19035 plasmid from *Streptococcus pyogenes* constitutes of a three-component system. In this model the *ε* antitoxin dimer counteract the *ζ* toxin effect by forming a heterotetramer complex while *ω* plays a regulatory role by binding to the TA promoter (Camacho et al., 2002; Meinhart et al., 2003; Zielenkiewicz et al., 2009). The TA locus *parR-paaA-parE* in *E. coli* 0157:H7 is also composed by the AT-T elements and a regulatory protein, ParR which is necessary for the TA transcriptional control (Hallez et al., 2010). In addition, both the PaaA antitoxin and the PaaA-ParE AT-T complex can bind to its own promoter and regulate transcription of the TA operon (Hallez et al., 2010). Moreover, other examples of tripartite TA subtypes exist where the third molecule does not play a role in transcription, e.g *pasA-pasB-pasC* encoded in the plasmid pTF-FC2 from *Thiobacillus ferrooxidans*, where the third component PasC enhances AT-T complex formation, helping to control the toxin (Smith and Rawlings, 1997).

Another mechanism of post-transcriptional regulation has been recently suggested in which the TA mRNA transcripts can be processed by RNases (Altuvia et al., 2018; Lybecker et al., 2014). These studies, reported cleavages in the transcripts of the antitoxins *hipB* (*hipA/hipB*), and *dinJ* (*yafQ/dinJ*) from type II TAs and *ghoS* (*ghoS/ghoT*) from the type V TA systems, but interestingly also in the transcripts encoding the toxins *cptA* (*cptA/sdhE*) and

yafO (*yafO/yafN*) (Altuvia et al., 2018; Lybecker et al., 2014). These results imply a putative additional layer of regulation at the TA mRNA level, which needs to be explored.

1.2.2 Post-translational Regulation

Bacterial proteases are important for general protein quality control and also play a role in the regulation of various cellular processes such as cell cycle, cellular development and adaptation by controlling the stability of a regulatory protein (Lehnherr and Yarmolinsky, 1995; Melderen et al., 1994; Tsuchimoto et al., 1992). They are responsible for the proteolytic degradation of misfolded or aggregated proteins and are normally composed of two parts the ATPase or unfoldase and the peptidase. Hsp100/Clp proteins from the AAA+ ATPase (ATPase associated with diverse cellular activities) unfold and translocate the substrates into the proteolytic chamber of a peptidase such as ClpP (caseinolytic protease) which is in charge of the substrate hydrolysis (reviewed by Kirstein et al., 2009). In both Gram-positive and Gram-negative bacteria, the ATPase ClpX is an example of an hexamer that interacts with the ClpP 14-mer to form the proteolytic complex; ClpXP **(Figure VII)**. Alternatively, in Gram-negative and to a lesser extent in Gram-positive bacteria, the protease Lon harbors both the ATPase or unfoldase and the peptidase functions on the single polypeptide (reviewed by Kirstein et al., 2009).

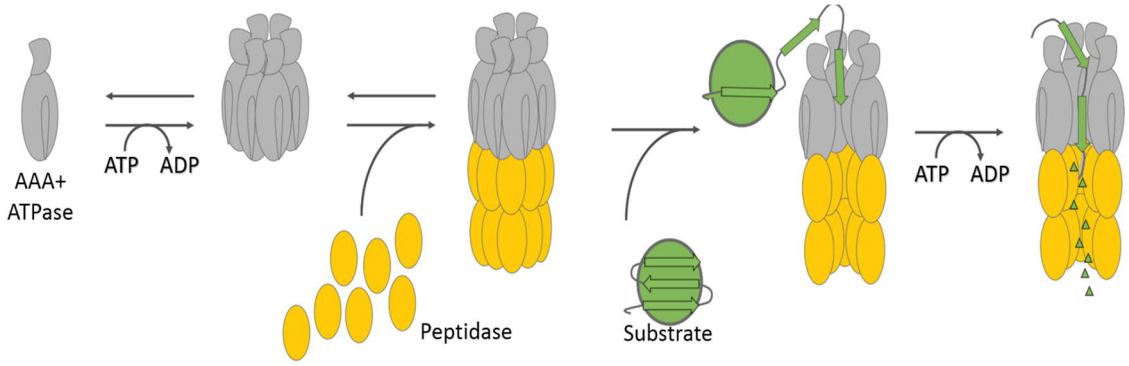

Figure VII. Bacterial AAA+ proteases mechanism of assembly with the peptidase.

The formation of the protease complex is depicted, where single monomers of the ATPase (grey) form a hexamer upon ATP hydrolysis. The ATPase hexamer then assembles with the 14-mer peptidase complex (yellow). The substrate (green) is recognized by the ATPase and subsequently unfold and driven through the peptidase channel for its hydrolysis in a process that is ATP dependent (adapted from Kirstein et al., 2009).

Antitoxin degradation has been reported to be mediated by ATP-dependent proteases such as, Lon, ClpCP, ClpXP and ClpAP (reviewed by Muthuramalingam et al., 2016). In some cases degradation of the antitoxin is the key process that leads to the release and thus

activation of the toxin (Wang et al., 2011). As mentioned before, the mechanism by which the system is activated relies on the different stability of the two molecules. Upon stress exposure, binding of the AT-T complex is disrupted. This causes the loosely structured C-terminal domains of the AT, which are most commonly associated with binding the T molecule, to become sterically available to cellular proteases. Thus, the AT molecules may be rapidly degraded, whereas the unpaired T molecules are generally more resistant to protease-degradation, leading to an accumulation of catalytically active toxins (Ruangprasert et al., 2017)

CcdA constitutes an example of an antitoxin with an intrinsically unstructured C-terminal domain, which explains its high susceptibility to proteolysis by the Lon protease in *E. coli* **(Figure VIII)** (Madl et al., 2006). CcdA can form a tight complex with its cognate toxin molecule, similar to the PhD antitoxin (Phd/Doc) (Garcia-Pino et al., 2016b) and this complex formation protect it from degradation. On the other hand, the ParD antitoxin (*parDE*) from the RK2 plasmid in *E. coli*, is a protein with an unstructured C-terminal domain, in the absence of its cognate binding partner ParE **(Figure VIII)** (Oberer et al., 2007), similar to HipB (Hansen et al., 2012). Conversely, the DinJ (from the dinJ/yafQ TA system) **(Figure VIII)** is an antitoxin degraded by both, the ClpXP and Lon protease in *E. coli,* which contains a structured C-terminus in the absence of the toxin molecule, similar to YefM (Kumar et al., 2008) and MqsA (Brown et al., 2009), leading to a higher stability. This antitoxin structural diversity suggests its stability alone might not be the only factor that determines antitoxin recognition for degradation.

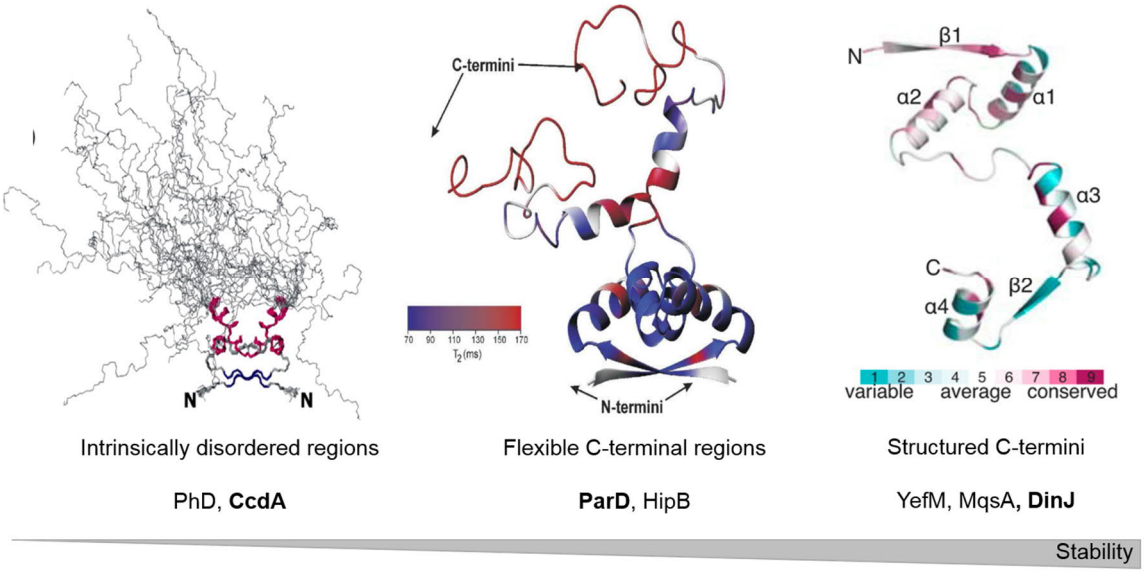

Figure VIII. Antitoxin lability alone may not fully explain susceptibility to proteolysis.
Three different antitoxins type II structures are shown: CcdA (Madl et al., 2006) harbors an intrinsically disorder C-terminal region similar to the PhD antitoxin. ParD (Oberer et al., 2007) have a flexible but not completely deserter C-terminus similar to HipB. DinJ (Ruangprasert et al., 2017) contains a structured C-terminal region that renders the protein more stable, similar to the YefM and MqsA antitoxins.

Bacterial proteases are not only able to recognize unstructured or aggregated protein but also specific domain or proteolytic tags. The ClpXP protease recognizes flexible domains but also structured peptide tags within protein substrates (reviewed by Baker and Sauer, 2012) **(Figure IX)**. The protease direct recognition of a substrate involves binding to short unstructured peptide sequences called degradation tags or degrons at the end of the N-terminus or C-terminus of a substrate (Baker and Sauer, 2012; Jana et al., 2016). Nevertheless, to date there are no reports that suggest a specific antitoxin domain or sequence that will lead to proteolysis. The ClpXP protease can also recognize substrates after endo-proteolytic event (Flynn, 2004; Neher, 2003) a process that has not been described for antitoxins. Adaptor molecules can also mediate proteolysis since they recognize and enhance the substrate recognition by the unfoldase (Levchenko et al., 2000). Interestingly, protein adaptors such as TrfA, but also chaperones such as SecB, have been reported to enhance or assist antitoxin degradation (Bordes et al., 2016; Donegan et al., 2014). Finally, free substrates with solvent expose domain as described for the antitoxin DinJ can be also recognized for proteolysis by the ClpXP protease (Ruangprasert et al., 2017).

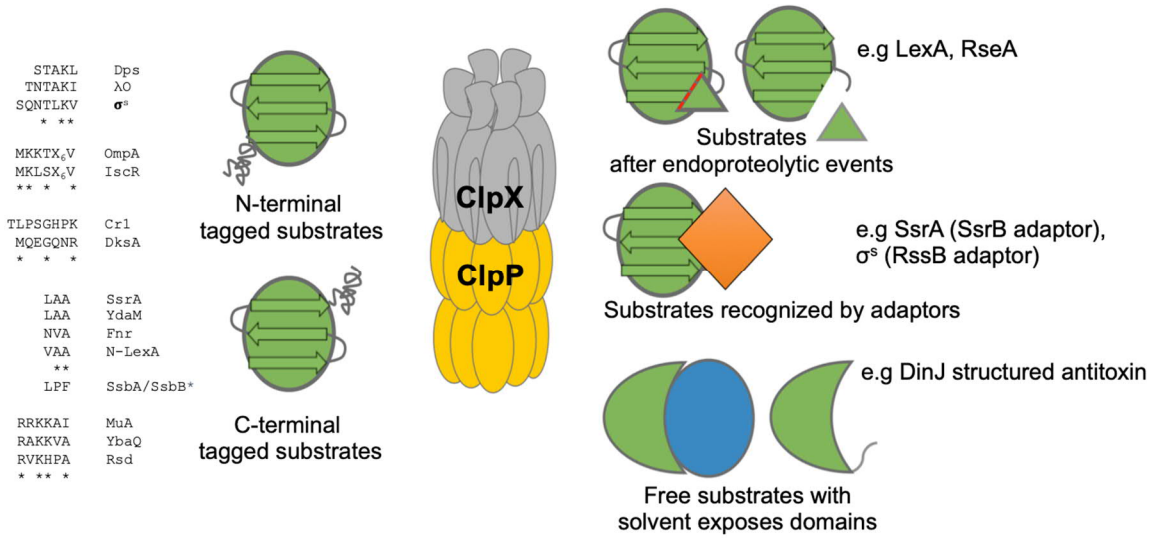

Figure IX. Mechanism of ClpX substrate recognition

In the left part of the figure, C-terminal or N-terminal sequence degrons in the substrates (green) can be recognized by ClpXP (ClpX ATPase in grey and ClpP peptidase in yellow) for degradation, the amino acid sequence and representative proteins containing this tags are shown (Baker and Sauer,

2012; Jana et al., 2016). Right part of the figure: ClpXP can also recognize substrates after proteolytic events e.g. LexA and RseA (Flynn, 2004; Neher, 2003), the substrate recognition can be enhance by adaptor molecules (orange) (Levchenko et al., 2000), and free substrates with solvent exposes domains such as DinJ can be also targeted for degradation (Ruangprasert et al., 2017).

Finally, a recent report has suggested that a DNA molecule can stimulate antitoxin degradation (Dubiel et al., 2018). In *Pseudomonas aeruginosa*, the ClpAP protease is in charge of ParD recognition, which is enhanced in the presence of DNA as ClpA interaction with DNA enhances its ATPase activity and thus substrate proteolysis (Dubiel et al., 2018).

1.2.3 Molecular Toxin Type II Targets

Toxins from the type II TA systems have a broad variety of targets; the majority that have been studied are mRNA endonucleases or kinases that phosphorylate proteins implicated in ribosome function and therefore reversibly interfere with protein translation (i.e., RelE, HipA) (Christensen and Gerdes, 2003a; Germain et al., 2013). Another group of type II toxins interfere with DNA replication by interacting with and thereby inactivating essential molecules, such the DNA gyrase (Yuan et al., 2010) **(Figure X)**.

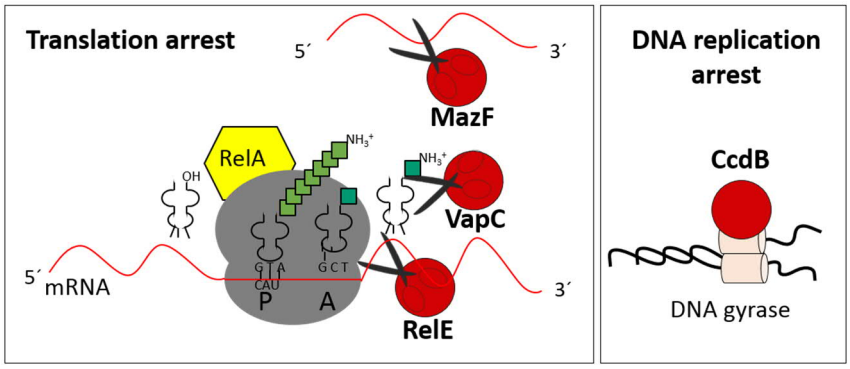

Figure X. Toxins type II affect either DNA replication or translation

Two main functions are targeted by toxins type II: the protein translation by degradation of free mRNA, mRNA within the ribosome or tRNAs or the DNA replication by for instance inhibiting the DNA gyrase.

Toxins that arrest translation comprise ribosome-dependent mRNA endonucleases such as RelE (Christensen and Gerdes, 2003b), ribosome-independent mRNA endonucleases of the MazF family (Culviner and Laub, 2018) or toxins that cleave tRNAs or rRNAs like the VapC toxin (Winther and Gerdes, 2011) **(Figure X)**. Other toxins modify their targets post-transcriptionally by introducing a modification. Remarkably, TacT is a toxin that also targets tRNAs, but instead of cleaving tRNA, TacT is an acetyltransferase that blocks the

primary amine group of amino acids on the already charged tRNA molecules. This effect also inhibits translation and is known to promote persister cell formation in *Samonella* (Cheverton et al., 2016).

Toxic kinases are examples of toxins that modify their targets post-translationally, such as the Doc toxin that phosphorylates the translation elongation factor EF-tu. This phosphorylation renders EF-Tu unable to bind aminoacylated tRNAs, thereby arresting translation (Castro-Roa et al., 2013). HipA is another kinase toxin, which phosphorylates the glutamyl-tRNA synthetase GltX that inhibits aminoacylation. This leads to the generation of so-called “hungry codons” at the ribosomal A site that trigger the synthesis of the second messenger (p)ppGpp, leading to a persistent phenotype (Germain et al., 2013). Interestingly, the ζ zeta toxins (from the epsilon/zeta ε-ζ family) is also a kinase, which does not target cellular factors involved in translation. Instead, the ζ toxin phosphorylates the peptidoglycan precursor uridine diphosphate-N-acetylglucosamine (UNAG) impairing cell wall synthesis, thus displaying a bacteriotoxic effect in Gram-positive bacteria (Mutschler et al., 2011). Recently, another report has suggested that the ζ toxin displays a broader substrate specificity. This kinase can phosphorylates multiple UDP-activated sugars that are not only precursors of peptidoglycan but also required for lipopolysaccharide synthesis in the Gram-negative bacteria *Neisseria gonorrhoeae* (Rocker et al., 2018).

Other type II toxin arrest DNA replication, e.g. a recent report has shown that the toxin DarT (*darTG*) from *M. tuberculosis,* ADP-ribosylates thymidines on ssDNA in a reversible and sequence-specific manner. The DarT activity leads to induction of the SOS response, a cellular stress response triggered upon DNA damage, thus having important implications at the level of DNA maintenance (Jankevicius et al., 2016).

Importantly, they are many reports about toxin proteins targeting the DNA gyrase as poisons that lead to stronger cellular effects in comparison with RNase or kinases **(Figure XI)**. The DNA gyrase, a type II topoisomerases together with topoisomerase IV (topo IV) are important for cellular survival as they relieve DNA-topological stress. Gyrase is essential during initiation, elongation, and termination of DNA replication, while topo IV mainly influences chromosomal stabilization during cell division. Both enzymes act via double strand breakage and re-joining process in an energy-dependent manner (reviewed by Sissi and Palumbo, 2010). Type II toxin inhibitors such as the acetyltransferase FicT (*ficAT*) abrogates the function of both gyrase and topo IV in a reversible manner (Harms et al., 2015) **(Figure XI)**. In contrast, toxins such as CcdB (from the CcdAB system) and most of the ParE-like toxins

(from the ParDE-family) have been reported to target the gyrase resealing capacity of the transient double strand DNA breaks resulting in a bactericidal effect (Bernard and Couturier, 1992; Jiang et al., 2002) **(Figure XI)**. Conversely, the MtbParE toxin from *M. tuberculosis* leads to a bacteriostatic effect (Gupta et al., 2016) by interacting with a different gyrase domain **(Figure XI)**. Moreover, some short-ParE synthetic peptides, designed based on the *E. coli* ParE plasmidic toxin, displayed the capacity to inhibit both gyrase and topo IV *in vitro* (Barbosa et al., 2012). However, the broader spectrum of targets has not been studied for native ParE-like toxins. Since gyrase, and to a lesser extent topo IV, are present in prokaryotes – and some eukaryotes – but absent in humans, they represent interesting cellular drug targets (Forterre et al., 2007). Due to the importance of topoisomerase IIA as toxins type II targets, they will be discuss in the next section.

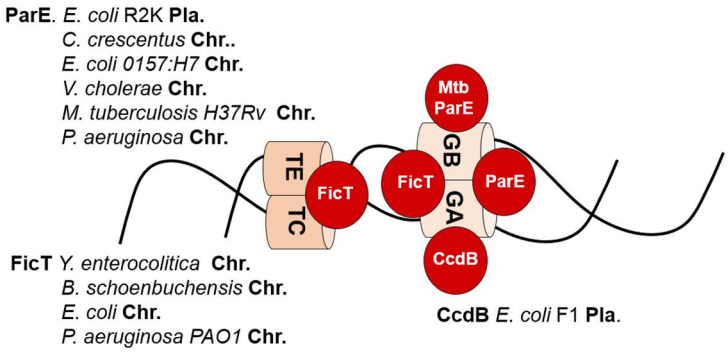

Figure XI. Toxins type II that affect DNA replication

Four toxins ParE, MtbParE, FicT, and CcdB (depicted in red), encoded in chromosomes (Chr) or in plasmid (Pla) of different bacteria, have been predicted to arrest DNA replication by interacting with topoisomerase IIA: topoisomerase IV (TE-TC) or gyrase (GB-GA).

1.3 Bacterial DNA Topoisomerases

The normal biological function of DNA and processes related to this molecule - RNA transcription and DNA replication - will not occur, happen very slowly, or will be aberrant if the DNA lacks the proper super-helical tension. A geometric property of the DNA is that the number of times one strand wraps around the other cannot be altered without first cleaving at least one of its polynucleotides. Topoisomerases (classified in type I and II) have a remarkable role of changing the topological state of circular DNA by introducing DNA breaks and re-sealing them without changing its covalent structure, thus keeping the molecule accessible but in correct shape (Sissi and Palumbo, 2010).

Type I topoisomerases play an important role in creating transient single strand breaks in DNA and are further classified in type IA and type IB topoisomerases based on their amino acid sequences and catalytic mechanism. They are in charge of catalyzing the relaxation of supercoils in DNA by single turns until the supercoil is entirely relaxed. Type IA topoisomerases are present in all living cells and relax only negatively supercoiled DNA, reversibly catenate two single-stranded circles or unwinds duplex DNA by one turn. Conversely, type IB topoisomerases are present in many prokaryotes but not in *E. coli*, and eukaryotes. They can relax both negatively and positively coiled DNA. As of this writing, there have been no previous reports of toxins from TA modules affecting type I topoisomerases in bacteria.

In contrast, they are several reports about toxins type II that target type II topoisomerases (**Figure XI)** (Barbosa et al., 2012; Bernard and Couturier, 1992; Fiebig et al., 2010; Gupta et al., 2016; Hallez et al., 2010; Harms et al., 2015; Jiang et al., 2002). Type II topoisomerases, are complex enzymes that act by transiently cutting both strands of a duplex, passing the duplex through the break and resealing it. The main representatives are the gyrase and topoisomerase IV. They help to remove the torsion in the DNA and remove positive supercoils ahead of the DNA polymerase.

While eukaryotic type II topoisomerases are single subunit enzymes that are active as homodimers, prokaryotic topoisomerases type II are composed by two subunits. DNA gyrase is a hetero-tetramer of approximately 375 kD A_2B_2, where the subunit GyrA wraps the DNA and GyrB is in charge of ATP hydrolysis. Importantly, gyrase catalyzes the stepwise negative supercoiling of DNA with the concomitant hydrolysis of an ATP molecule to ADP + P. Gyrase prepares the negatively supercoiled template for DnaA to initiate replication. Another function of gyrase is to remove the positive supercoils that form ahead of the growing fork during elongation of the growing strands. It can also catenate and decatenate double-stranded circles as well as tie knots in them, while the topoisomerase I antagonizes the action of the DNA gyrase. In addition, the gyrase can complement the function of the topoisomerase IV but the topo IV cannot complement the activity of Gyrase. The gyrase is therefore vital, important during initiation elongation and termination of the DNA replication, chromosome segregation, DNA decatenation prior to cellular division (Sissi and Palumbo, 2010).

Topoisomerase IV (Topo IV) is also a hetero-tetramer composed of two molecules topo C (ParC) that share a 46% sequence homology to GyrA and contains the active site tyrosine residue and topo E (ParE), that is 40% similar to gyrB and contains the ATPase

domain. Despite the strong sequence similarity between gyrase and topo IV, the C-termini of the A subunits are not well conserved. This domain of the protein is involved in topology recognition and allows gyrase, but not topo IV, to generate supercoils in DNA. Topo IV activity is important in chromosome partitioning, decatenation and relaxation of DNA, it decatenates during replication more than the gyrase and therefore plays an important role in passive separation of the chromosomes during cell elongation. Topo IV might be associated with the replication complex (DnaE) and is a membrane-associated enzyme (Sissi and Palumbo, 2010).

Topoisomerases type II can be inhibited by a variety of substances such as novocin (NOV) and quinolones such as ciprofloxacin (CPX). NOV associates with GyrB thereby inhibiting the enzyme, whereas CPX associates with GyrA and poisons the enzyme (Aldred et al., 2014). Thus, bacterial NOV treatment results in the arrest of DNA replication and RNA transcription, while CPX treatment enhances the rate at which gyrase cleaves double stranded DNA and reduces the rate at which it reseals these breaks. Upon gyrase poisoning, there are higher level of transient protein-bridges breaks in the DNA that are easily ruptured by the passage of the replication machinery, thereby rendering the breaks permanent. Although all cells possess, extensive enzymatic machinery to repair damaged DNA, a high level of DNA damage can result in cell death (Aldred et al., 2014). Interestingly, one of the quinolones target-mediated resistance is cause by specific mutations that weaken the interactions between quinolones and these enzymes, highlighting the importance of finding new drugs.

1.4 Streptococcus pyogenes

Group A *Streptococcu*s (GAS; *Streptococcus pyogenes*) is a non-motile bacterium that grows in chains and belongs to the Firmicutes phylum, the Bacilli class and the Lactobacillales order. *S. pyogenes* colonizes the oropharynx, epithelium, skin of humans and causes a wide spectrum of diseases worldwide (Cunningham, 2000). Although GAS is a frequent agent of mild infections like pharyngitis and uncomplicated impetigo infections, penetration of GAS into deeper tissues can lead to devastating invasive infections, such as necrotising fascilitis, myonecrosis or “flesh-eating” syndrome or lead to severe systemic complications such as, sepsis or streptococcal toxic shock syndrome (STSS), as well as sequelae of rheumatic fever and acute poststreptococcal glomerunophritis (Stevens et al., 2014; Tsatsaronis et al., 2014; Walker et al., 2014).

The complex surface of *S. pyogenes* includes conventional globular proteins, polysaccharides and the M protein, which has specifically evolved to enable survival in different host tissues (Cunningham, 2000). The M protein, in particular, has developed to allow this bacterium to persist while avoiding the human immune response, specifically phagocytosis. Thus, the M protein is considered the archetypical surface molecule. At the moment of this writing there are more than 200 different serotypes based on the M protein, one of the most studied streptococcal proteins (Lancefield, 1962). *S. pyogenes* also harbors a pili structure that plays important roles during pathogenesis by mediating bacterial adhesion to host tissues and biofilm formation (Bessen and Kalia, 2002; Mora et al., 2005). The capsule is produced by most of the group A streptococci, and also plays an important role for pathogenicity. It is associated with the cell surface during exponential growth and shed during stationary phase and is mainly composed of hyaluronic acid (linear polymer of N-acetylgrucosamine and glucuronic acid)(Wilson, 1959).

Among the virulence related transcriptional regulators, *S. pyogenes* harbors 13 two-component regulatory systems and at least 30 transcriptional regulators known. The most important master regulators are CovR/S (Gryllos et al., 2003) and RofA-like proteins (RALPs) that control the activity of multiple virulence regulators (Granok et al., 2000). Some other regulators are relevant for sensing environmental conditions and response to stress e.g. CcpA, Mga that response to carbohydrates (Deutscher et al., 2006) or Rsh, CodY that response to different nitrogen sources (Steiner and Malke, 2001). Regulators such as VicR/S, MtsR, CiaH/R influences the expression of metabolism-related genes. Moreover, PerR is also an important regulator that response to oxidative stress, Rgg2/3 is involved in quorum sensing, and SalK/R response to environmental signals from the host (Le Breton et al., 2015).

S. pyogenes has also a wide variety of extracellular virulence factors which include: streptokinase, proteinases, esterases, DNAase, CAMP factor, hyaluronidases, complement inhibitor, superoxide dismutase, immunoglobulin degrading enzymes, and the hemolysins SLO and SLS (reviewed by Ferretti et al, 2016). All these secreted factors provide to *S. pyogenes* different abilities to cope with the host response and can vary between different serotype. Interestingly, some of the most studied are SLO and NADase that can destroy cell tissues, red blood and immune cells, SLS lyses a variety of host cell types and SpeB that degrades tissues and immune response molecules. Importantly, Ska converts host plasminogen into plasmid and SodA converts oxygen radical into hydrogen peroxide. All of these virulent factors among many others, make GAS an efficient pathogen (reviewed by Hynes and Sloan, 2016).

While the mechanism by which GAS evades elements of the innate immune response have been the focus of extensive research, less attention has been paid to the molecular mechanisms that facilitate its remarkable ability to persist. Certain conditions might lead to asymptomatic carriage of GAS causing common recurrent episodes of pharyngitis (Osterlund and Engstrand, 1997). There are a few reports about *S. pyogenes* antibiotic tolerant cells, an in vitro study has reproduce a persistent behavior (Wood et al., 2005), but the basis of this phenotype is not yet elucidated.

Finally, the TA type II module ω- ε -ζ encoded in the streptococcal plasmid pSM19035 is the only reported TA system in our model organism (Zielenkiewicz et al., 2009), and its implications in virulence have not been described. Nevertheless, bioinformatic predictions have revealed the presence of four hypothetical type II TA copies within the chromosome of *S. pyogenes*, which are still uncharacterized **(Figure XII).**

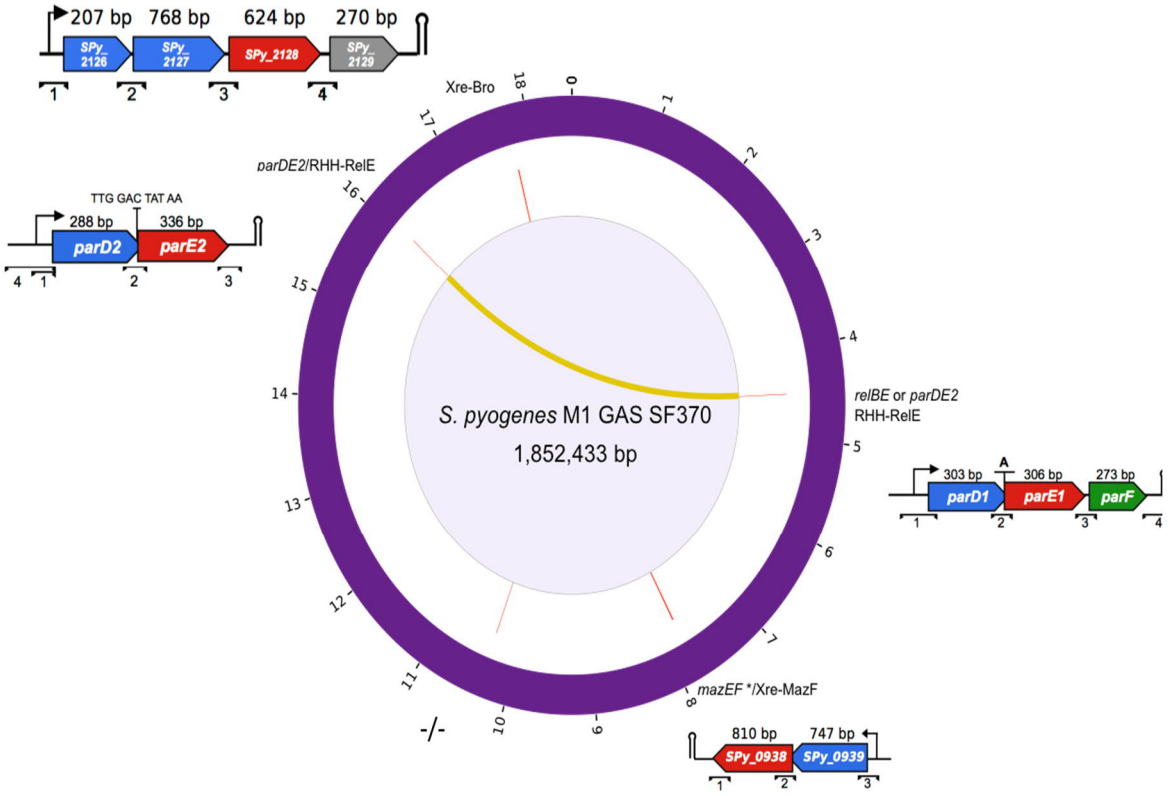

Figure XII: Type II TA copies predicted within the chromosome of *S. pyogenes* M1 GAS

TA type II systems predicted by TADB (Y. Xie et al., 2018). The purple circle represents the bacterial chromosome. In blue the predicted antitoxins and in red the predicted toxins. Grey and green genes represent hypothetical ORFs non-predicted as TA elements. 4 genes compose the hypothetical Xre-Bro TA system: SPy_2126, SPy_2127, SPy_2128 and SPy_2129. Two genes typically compose the putative MazEF TA system: SPy_0938, SPy_0939. Two hypothetical RelBE/ParDE-like TA systems are predicted, the first one composed by three genes SPy_0550, SPy_0552 and SPy_0553 and the second one compose by two genes: SPy_1926 and SPy_2127.

1.5 AIMS OF THE STUDY

Four type II TA systems are predicted to occur in the chromosome of the human pathogen *S. pyogenes* and two of these loci are putative ParDE-like TA modules (Xie et al., 2018). The ParDE-like TA family was first described as an addiction molecule within the RK2 plasmid, playing a role in PSK. Chromosomal ParDE-like TA systems have been predicted in several bacterial genomes (Sevin and Barloy-Hubler, 2007; Xie et al., 2018), but are poorly studied or not completely characterized. In *Caulobacter crescentus,* a set of four functional *parDE* modules were reported, which are differentially expressed under certain stress conditions (Fiebig et al., 2010). *E. coli* 0157:H7 encodes for a typical ParDE TA system as well as two tripartite homologs for which the physiological role is currently unknown (Hallez et al., 2010), and three ParDE homologs in the *Vibrio cholerae* superintegron were reported to be required for the inheritance of chromosome II (Yuan et al., 2011). Moreover, in *Mycobacterium tuberculosis* H37Rv two bacteriostatic ParDE-like copies were reported to be expressed upon oxidative stress (Gupta et al., 2016; Ramage et al., 2009). All ParE-like toxins described in Gram-negative bacteria and *M. tuberculosis* are known to influence DNA replication, stability and maintenance by targeting the gyrase. Interestingly, ParDE-like TA systems located on the chromosome of Firmicutes have not been characterized.

Characterization of hypothetical genes helps us to understand the mechanism that pathogens use to endure diverse conditions within the host and cause diseases. In this work, I used the Firmicute *S. pyogenes* as a model organism to shed light on the features that render two chromosomally encoded ParDE-like TA systems functional and relevant for this human pathogen. In this context, I specifically aimed to:

1) Functionally validate the putative ParDE-like TA systems.
2) Characterize the ParE-like toxin molecular target.
3) Elucidate the role of these ParDE-like modules in *S. pyogenes*.
4) Investigate their regulatory mechanism.

2 MATERIALS AND METHODS

2.1 Bioinformatic and statistical analysis

The genome of *S. pyogenes* M1 GAS NC_002737.2 (Ferretti et al., 2001) was used as a reference of our study (*SPy_0550: parD1, SPy_0552: parE1, SPy_0553: parF1, SPy_1926: parD1, SPy_1927: parE1)*. To determine the subfamily of the predicted ParE-like toxins or ParD-like antitoxins, non-redundant ParE/RelE or PhD, RelB, PaaA and ParD proteins were retrieved from the TADB database (Xie et al., 2018) and global alignments were computed using Mafft V.7 with default parameters (Katoh et al., 2002). Principal component analysis based on protein sequence similarity was performed in Jalview V2.8 (Waterhouse et al., 2009) using the substitution matrix BLOSUM62. Phylogenetic analysis was inferred by the GGDC web server (Meier-Kolthoff et al., 2013) available at http://ggdc.dsmz.de/. A multiple sequence alignment was created with MUSCLE (Edgar, 2004). Maximum likelihood (ML) and maximum parsimony (MP) trees were inferred from the alignment with RAxML (Stamatakis, 2014) with a 1000 bootstrapping replicates.

The TA conservation and synteny among the distinct *S. pyogenes* M serotypes was performed with SyntTax web tool (Oberto, 2013) using the ParE-like nucleotide sequence as a reference to map the locus of interest and further analyzing a 15 Kb genomic window. The genomic percentage of guanine/cytosine content (GC%) was calculated in R package *Biostrings*. The identification of the *parDEF1* transcription start site (TSS) and confirmation of operon architecture was assessed using previously published RNAseq data from our model organism (Le Rhun et al., 2017), the operon image was captured from Integrative Genomics Viewer (Robinson et al., 2011; Thorvaldsdottir et al., 2013) and the Rho-independent terminator (TransTermHP v2.07) prediction was downloaded from http://transterm.cbcb.umd.edu/tt/Streptococcus_pyogenes_M1_GAS.tt.

Protein sequences were analyzed in Pfam (Finn et al., 2016) and secondary structure predictions were performed using SWISS-MODEL (Waterhouse et al., 2018) and Phyres2 (Kelley et al., 2015) websites tools. Protein alignments and oligonucleotide design were performed in Geneious 10.2.6 software (https://www.geneious.com). Statistical analyses were performed using R v3.5.1 (2018-07-02). For all experiments at least 3 biological replicates were done each with 3 technical replicates. For T tests, p values < 0.05 were considered as significant.

2.2 Bacterial strains and growth conditions

Bacterial strains and - restriction or Gibson mediated cloned - vectors and their usages are listed in **Table 2** in the appendix. *E. coli* MG1655 was used for growth rescue and killing assays and *E. coli* TOP 10 was used for cloning. *E. coli* strains were grown under standard conditions (37°C, 180 rpm) in LB media (Becton Dickinson) supplemented with antibiotics if required at the following concentrations: 50 µg ml^{-1} kanamycin (Sigma-Aldrich), 30 µg ml^{-1} chloramphenicol (Sigma-Aldrich) or 100 µg ml^{-1} carbenicillin (Roth). Heat-shock competent cells (0.1 M $CaCl_2$ method) were used for transforming vectors following standard procedures (Sambrook and Russell, 2001).

S. pyogenes SF370 (M1 GAS) and isogenic derivatives **(Table 2)** were cultivated at 37°C, 5 % CO_2, without shaking in THY medium (Todd Hewitt Broth THB, Bacto, Becton Dickinson) supplemented with 0.2% yeast extract (Servabacter) and TSA (tryticase soy agar, BD Difco) supplemented with 3% sheep blood (defibrinated; Oxoid). Antibiotics were added when required at the following concentrations: 300 µg ml^{-1} kanamycin (Sigma-Aldrich), 3 µg ml^{-1} erythromycin (Sigma-Aldrich) or 100 µg ml^{-1} spectinomycin (Sigma-Aldrich). Pre-cultures were always diluted 1:100 in fresh THY medium and grown at 37°C, 5% CO2 until mid-exponential phase at OD_{620nm} 0.25 (plate reader; BioTek™ Cytation 3) or OD_{620nm} 0.6 (cuvette reader Eppendorf BioSpectrometer® basic) for the antitoxin stability assays, or until early logarithmic phase at OD_{620nm} 0.1 (plate reader; BioTek™ Cytation 3) or OD_{620nm} 0.4 (cuvette reader Eppendorf BioSpectrometer® basic) for the stress response experiments.

S. pyogenes electrocompetent cells were prepared following the ice-cold method (Caparon and Scott, 1991). Briefly, the cells were grown in THY medium until mid-exponential phase of growth (OD_{620nm} 0.25; plate reader BioTekTM Cytation 3). The cells were washed twice with ice-cold water and suspended in 20% glycerol and kept at –80 °C or immediately used. Transformation of *S. pyogenes* was performed as previously described (Caparon and Scott, 1991) by electroporation (1.8 kV, 25 µF and 400 Ω; Gene Pulse Xcell Biorad), followed by a recovery step in 3 ml of THY pre-warm media incubating for 3 hours at 37°C, 5% CO_2 before spreading on the appropriate selection TSA blood plates.

2.3 DNA and RNA manipulation

S. pyogenes SF370 (M1 GAS) (NC_002737.1; Ferretti et al., 2001) was used as a reference for oligo design. Vectors and oligonucleotide primers (Sigma-Aldrich and Biomers)

used in this study are listed in the **Table 2** and **Table 3** respectively. Plasmid extraction (QIAprep Spin MiniPrep Kit), polymerase chain reaction (PCR) (Phusion High-Fidelity DNA Polymerase, and Q5® High-Fidelity DNA Polymerase, New England Biolabs), DNA digestion (fast digest restriction enzymes, Fermentas), DNA ligation (T4 DNA ligase, Fermentas), DNA purification (QIAquick PCR and gel Purification Kit, Qiagen) were done according to the standard techniques (Sambrook and Russell, 2001). For cloning PCR fragments into vectors two strategies were used: restriction (Fastdigest restriction enzymes; Thermo Scientific) and ligation (T4 DNA ligase, Thermo Scientific) mediated cloning for pBAD33P_{ara}, pZE12$P_{lac,}$ pUC19 and pEC85P_{tet} plasmids, and Gibson mediated cloning for pAH160P_{rha} and pEC85P_{tet} (refer to appendix **Table 3**).

RNA extractions were performed following protocols pre-set by our lab (Fonfara et al., 2014); a minimum of 20 ml of growing bacterial were mixed with an equal volume of ice-cold acetone/ethanol (1:1) solution and harvested (1500 x g, 4°C, 10 minutes) for RNA extraction using TRIzol (Life Technologies)/chloroform (Sigma-Aldrich) and precipitated with isopropanol (Sigma-Aldrich). RNA concentrations were measured (NanoDrop, Thermo Scientific) and RNA integrity was determined by electrophoresis in agarose gel (1.8% agarose in 1X TBE (Tris-borate-EDTA pH 8) and ethidium bromide (Merck) staining. *S. pyogenes* DNA extractions were performed from exponentially growing cells (OD_{620nm} 0.25; plate reader BioTekTM Cytation 3) following the instructions from the kit (NucleoSpin® Microbial DNA; Macherey-Nagel).

The DNA from *Escherichia coli* Serotype O157:H7 (Migula 1895); was obtained from the DSMZ (Deutsche Sammlung von Mikroorganismen und Zellkulturen GmbH, DSM No: 17076). The DNA from *Mycobacterium tuberculosis* was share by Prof. Kaufman laboratory at the Max Planck Institute for Infection Biology. Vectors harboring the *Vibrio cholearae* and *Vibrio fischeri* TA systems were share by the Prof. Waldor laboratory at the Brigham and Women's Hospital- Boston MA (Yuan et al., 2010).

2.4 *S. pyogenes* methods

2.4.1 Construction of *S. pyogenes* mutants

Chromosomal deletion of the complete *parDE1* and *parDE2* TA operons, the *clpP* peptidase, *clpX, clpE* and *clpC* ATPase were generated using the Cre-Lox system (Lambert

et al., 2007). Oligonucleotides were designed to delete the complete genes except for *clpX* (Δ60-1161bp) where 60 bp were maintained at the beginning of the ORF to avoid polar effects, and ensure translation of the second gene *yihA* in frame.

Around 1 Kb of the upstream and downstream regions of each gene of interest were PCR amplified from the wild type genomic DNA using primers described in **Table 2.** The fragments were then PCR ligated (LongAmp Taq DNA-polymerase; NEB) with the lox71-ermAM/B-lox66 PCR fragment (amplified from the plasmid pEC454). The resulting 3 Kb fragments were gel purified (QIAGEN Gel Extraction Kit) and cloned either by restriction-ligation into pUC19 (suicide vector for *S. pyogenes*) or by poly A mediated ligation into TOPO XL PCR cloning vector (Thermo Fisher), following the manufacturers instructions. Plasmid preparations were performed according to manufacturer's protocols (Plasmid Miniprep Kit QUIAGEN), and vectors were linearized using NcoI (Thermo Fisher) restriction enzyme that cleaves the kanamycin resistance cassette in the vector. The gel purified linear plasmids (up to 1 µg) were transformed into freshly prepared *S. pyogenes* electro-competent cells and after the recovering time (3ml THY, 37°C, 5% CO_2) the cells were spread on TSA blood plates supplemented with 3 µg ml^{-1} erythromycin.

Erythromycin-resistant growing clones were collected and genomic DNA was extracted following the instructions from the kit (NucleoSpin® Microbial DNA; Macherey-Nagel) to perform PCRs and DNA sequencing (Microsynth, Switzerland) of the region of interest in order to confirm the insertion of the fragments in the correct position (SEQ mutant or Upstream/Downstream oligonucleotides **Table 3** Mutants construction). Positives clones were transformed with pEC455 encoding the Cre recombinase (Laboratory collection) to remove the DNA between the lox sites (replaced with a lox72 site). Moreover, blue colonies were selected in TSA blood supplemented with 80 µg ml^{-1} XGal (5-Brom-4-chlor-3-indoxyl-β-D-galactopyranosid; Sigma-Aldrich) and 300 µg ml^{-1} kanamycin. Kanamycin-resistant and erythromycin-sensitive mutants should have excised the DNA between the two lox sites and have replaced the cassette with the lox72 site. Finally, mutants were grown in TSA medium without antibiotics until they lost the pEC455 plasmid. The integrity of the generated mutant strains was confirmed by PCR and DNA sequencing (Microsynth, Switzerland) (SEQ mutant or Upstream/Downstream oligonucleotides **Table 3** Mutants construction).

2.4.2 Growth curves and biofilm formation

Overnight cultures of *S. pyogenes* wild type, *ΔparDE1* and *ΔparDE2* mutant backgrounds were used (1/100) to inoculate 50ml of fresh THY media to follow growth. Samples were taken 60, 120, 180,140, 300 and 360 minutes after inoculation, serial diluted ((10^{-1} to 10^{-6}), spotted on TSA blood plates and incubated overnight (37°C, 5% CO_2). 4 biological replicates each with 3 technical replicates were considered to plot the $\log_{10}$ CFU ml^{-1} versus the time course.

To perform the biofilm formation assays, overnight cultures were normalized to OD_{620nm} 0.2 (plate reader BioTekTM Cytation 3), and 1.5 ml of each sample was inoculated in triplicates in a 24 well plate for cell culture (Tissue culture 24-well plate (Flat bottom) for adherent cells; Hain life science). After 24 hours of incubation at 25°C or 37°C (5% CO_2), the media was gently removed by flipping the plate upside down on a disposal container followed by three washing steps with distilled water (gently addition and removal with a plastic 25 ml pipette). The plates were kept under the hood for 30 minutes to dry and then 200 µl of 0.2% Crystal violet (C.I. 42555; Roth) was added per well and the plates were incubated for 10 minutes at room temperature. The Crystal violet was gently removed in a disposal container and plates were washed three times as described before and air-dried out for 10 minutes. To elute the biofilm Crystal violet- stained 1 ml of 1% SDS (sodium dodecyl sulfate; Applichem) solution was used and transferred into a plastic cuvette to measure the absorbance at OD_{540nm} (cuvette reader Eppendorf BioSpectrometer® basic).

2.4.3 *S. pyogenes* stress induction, survival measurement

S. pyogenes growing cultures in THY (500 ml) were divided in early-logarithmic phase (OD_{620nm} 0.1, plate reader BioTek™ Cytation 3 measured) into 5 different flasks, 100 ml of the culture was used as a control and 100 ml was treated independently with each of the stress inductors: 4 mM H_2O_2, 1.25 M NaCl, 3 µg ml^{-1} mitomycin or 8% ethanol (10% ethanol when stated). Cell growth was monitored at OD_{620nm} and samples were serial diluted and spotted in TSA blood plates to register the CFU ml^{-1}. Samples were taken (20 ml) at time zero, 5, 15, 30, 45 and 60 minutes upon ethanol treatment, and at zero, 10, 20 and 30 minutes upon SHX treatment (DL-Serine hydroxamate; Sigma-Aldrich) to induce amino acid starvation, mixed with an equal volume of ice-cold acetone/ethanol (1:1) solution and harvested (1500 x g, 4°C, 10 minutes) for RNA extraction (as described in the section 2.3 DNA and RNA manipulation).

2.4.4 Killing assay in *S. pyogenes*

S. pyogenes was transformed with the low copy empty vector pEC85 (control) or pEC85P$_{tet}$ harboring the either *parE1*, *parD1, parD1-parF1, parE2*, *parD2* or *parD2-parE2* genes under the control of the anhydrotetracycline (AHT) promoter (P$_{tet}$ from Bugrysheva and Scott, 2010). Single colonies were used to start overnight cultures in 3 ml of THY medium supplemented with 300 µg ml^{-1} kanamycin. The day after the optical density at OD$_{620nm}$ was normalized to 0.2 (plate reader BioTekTM Cytation 3 measured) and serial dilutions were prepared (10^{-1} to 10^{-6}) and spotted on TSA media plates supplemented with 3% sheep blood, 300 µg ml^{-1} kanamycin without inductor (control conditions) or with 50 µg ml^{-1} of AHT to induced the toxin expression (experimental conditions). After 16 hours of incubation, the grown plates were scanned (CanoScan LiDE 700F).

To evaluate the toxicity of ParE2* L48A (start codon ATG versus TTG variants) OD-standardized overnight pre-inoculums (1/100) were used to inoculate 3 ml of THY fresh media with two different concentrations of the inductor (either 25 µg ml^{-1} or 50 µg ml^{-1} AHT) to evaluate growth after 16h of incubation under the same conditions. Finally, to prepare samples for phenotypic analysis by microscopy (refer to methods below), 50 ml of cultures were inoculated as described above with 25 µg ml^{-1} AHT and samples were collected at mid exponential growth phase (OD$_{620nm}$ 0.25; plate reader BioTekTM Cytation 3).

2.4.5 Antitoxin stability and western blot experiments

S. pyogenes wild type, Δ*clpP*, Δ*clpX*, Δ*clpC* and Δ*clpE* mutant strains were transformed with the pEC85P$_{tet}$ empty vector or harboring either the N-terminal FLAG-tagged *parD1* (pEC1487: pEC85P$_{tet}$ΩN-FLAGtaqSPy_ParD1) or the N-terminal FLAG-tagged *parD2* (pEC1488: pEC85P$_{tet}$ΩN-FLAGtaqSPy_ParD2) gene under the control of the P$_{tet}$ promoter. Overnight cultures (1/100 dilution) were sub-cultured in fresh THY medium supplemented with 300 µg ml^{-1} kanamycin and 25 µg ml^{-1} of the inductor AHT. At exponential growth phase (OD$_{620nm}$ 0.6, cuvette reader Eppendorf BioSpectrometer® basic, t = 0) translation was inhibited by adding 100 µg ml^{-1} spectinomycin and 15 ml of each sample was collected every 20 minutes for 2 hours. After centrifugation (4000 rpm, 4°C, 10 minutes) pellets were washed twice with 1X PBS pH 7.4 and lysed by bead beating with 0.1 mm glass beads (BioSpec) in a FastPrep instruments (MP Biomedicals™ FastPrep-24™ 5G) using 500 µl of disruption buffer (50 mM Tris-HCl pH 7.5, 10 mM EDTA, 150 mM NaCl, 0.1% Triton X-100) to extract cytoplasmic proteins. The suspension was then centrifuged (21000 x g, 4°C, 10 minutes), the

supernatant was collected and total protein concentration was determined using the Bradford method. Normalized protein samples at 10 µg were separated on a 15% SDS-PAGE gel (sodium dodecyl sulphate – polyacrylamide gel electrophoresis; 180 V for 1 hour) blotted via wet transfer (at 60 V for 1 hour in transfer buffer, 39 mM glycine, 48 mM Tris, 0.037% SDS and 20% methanol) on a Nitrocellulose membrane (Protran BA83, pore size 0,2µm, 30x300cm; GE Healthcare) for western blot (WB) analysis. Membrane blocking was performed by incubating overnight at 4°C in 5% Skim Milk (Sigma) in 1X TBST (TBST 10X: 100 mM Tris, 1.5 M NaCl, 0.5% Tween 20), pH 8). After the incubation time the membrane was incubated for at least 1 hour at 4°C with mouse monoclonal ANTI-FLAG® M2 antibody (1/5000 dilution) in 1X TBST 5% Skim Milk (Sigma-Aldrich Chemie GmbH), then washed 3 times for 5 minutes in the same buffer and incubated with the anti-mouse (ECL Mouse IgG, HRP-Linked Whole Ab from sheep; GE Healthcare, 1/10000) in 1X TBST for 1 hour at 4°C. The HtrA-protein (Rabbit Polyclonal, 1/1000 dilution; secondary antibody Amersham ECL Rabbit IgG, HRP-linked whole Ab from donkey; GE Healthcare, 1/10000) was used as loading control measured on the same membrane (antibody provided by Prof. Jeffrey Weiser; New York University School of Medicine). The WB was developed (Clarity Western ECL Substrate; Bio-Rad) and signals were registered in the Molecular Imager Gel-Doc system (Bio-rad) and analyzed in ImageJ (Schneider et al., 2012).

2.4.6 Antitoxin pull-down experiments

Exponentially growing *S. pyogenes* cells harboring either the N-terminal FLAG-tagged *parD1* (pEC1487: pEC85P_{tet}ΩN-FLAGtaqSPy_ParD1) or the N-terminal FLAG-tagged *parD2* (pEC1488: pEC85P_{tet}ΩN-FLAGtaqSPy_ParD2) gene under the control of the P_{tet} promoter were grown and induced as described for the antitoxin stability experiments. A total of 50 ml of culture was collected on ice, centrifuge (4000 rpm, 4°C for 10 minutes) and lysed using 800 µl of disruption buffer (50 mM Tris-HCl pH 7.5, 10 mM EDTA, 150 mM NaCl, 0.1% Triton X-100) and prepared as described above (section 2.4.5 antitoxin stability experiments). The antitoxin pull-down was performed while incubating the samples at 4°C with gently rotation the total protein extract with the ANTI-FLAG M1 agarose affinity gel following the manufactures instructions (Sigma Aldrich) overnight. After 3 washing steps with 0.5 ml of TBS (Tris-buffered saline: 150 mM NaCl, 50 mM Tris-HCl, pH 7.6; 8200 x g for 30 seconds each), the elution was performed by mixing the samples with SDS-page loading dye without β–mercaptoethanol and boiled at 95°C for 15 minutes. Samples were then centrifuged (8200 x g, 30 seconds, 4°C) and the supernatant was resolved on a 15% SDS-PAGE gel (sodium

dodecyl sulfate – polyacrylamide gel electrophoresis) and visualized with Coomassie Brilliant Blue (Sigma-Aldrich) staining and imaged using CanoScan LiDE 700F. Different fractions were gel-extracted and sent for mass spectrometry analysis (see below).

2.5 RNA assays

2.5.1 RT-PCR analysis

For quantitative RT-PCR (qRT-PCR), a total of 100 ng μl^{-1} of each RNA sample was treated twice with DNase I at 37°C for 1 hour following the manufacturer protocols (1 unit/µl, RNase-free, Thermo Fisher). DNA-free RNA samples were measured (NanoDrop, Thermo Scientific) and normalized to 50 ng μl^{-1} to perform retro-transcription following the manufacturer instructions (High-Capacity cDNA Reverse Transcription Kit; Applied Biosystems). To test the operon architecture, PCRs were performed using DNA copy (cDNA) as a template and the oligonucleotides listed in **Table 3**. PCR samples were separated in a 1.5% agarose gel (1X TBE) and bands were visualized by staining with ethidium bromide, imaged with a Molecular Imager Gel-Doc system (Bio-Rad) and analyzed in Image Lab (Bio-Rad).

qRT-PCRs to assess the level of mRNA transcripts were performed by monitoring the cDNA amplification rate by real time PCR (SensiFAST™ SYBR® No-ROX Kit, Bioline), targeting the genes of interest using the oligos listed in **Table 3**, in a Lightcycler 480 instruments (Roche)**.** The crossing point values (CP) were analyzed relative to the CPs obtained with the housekeeping gene *tufA,* using the Pfaffl formula (Pfaffl, 2001) and the $\log_{10}$ relative fold change was plotted versus the time. At least three biological replicates were considered in the analysis.

2.5.2 Polyacrylamide Northern blots analysis

The qRT-PCR results were confirmed by polyacrylamide Northern blot analysis following standard protocols as described in (Fonfara et al., 2014). Briefly, a total of 15 µg of RNA per sample was separated on a 5% polyacrylamide gels (Tris-base buffer containing 8M urea) at 100 V for 90 minutes and transferred onto a nylon membranes (Hybrond™ N+, GE healthcare; Trans-Blot SD semi-dry transfer apparatus, Biorad; 1X TBE, 90 minutes, 20 V), followed by crosslinking using EDC ((1-Ethyl-3-3-dimethylaminopropyl) carbodiimide

hydrochloride; Sigma-Aldrich) (Pall and Hamilton, 2008) at 60 °C for 1 hour, and pre-hybridization using Rapid-hyb buffer (GE healthcare), 1 h at 42°C, in glass tubes. Probes (40 pmol) listed in **Table 3** targeting the *parE1* or *parE2* mRNA transcript and the 16S rRNA as loading control **(Table 3)** were radioactively labeled with gamma-^{32}P ATP (0.75 MBq; Hartmann Analytics) using T4 Polynucleotide Kinase (T4-PNK, Fermentas) and purified over G-25 columns following the manufactures protocols (GE Healthcare) as previously described in (Le Rhun et al., 2016). The hybridization in Rapid-hyb buffer with the purified ^{32}P labeled probes was performed over night at 42°C. After the incubation time, membranes were washed with 5x SSC, 0.1 % SDS and 1x SSC, 0.1 % SDS (20 X SSC; NaCl 350.6 g, sodium citrate 177.4 g, ddH_2O water for 2 L, pH 7) for 15 minutes each and the exposure was performed for 1 week (phosphorimager screen). Visualization of the radioactive signal was possible using FLA-9000 (Fujifilm) and pictures were analyzed using ImageJ software.

2.6 In vitro topoisomerase assays

In vitro translation was performed to produce and purify the ParE-like proteins of interest following the manufacturer instructions (PURExpress® In Vitro Protein Synthesis Kit, NEB), using PCR products as templates (100ng µl^{-1}each) that included the T7 promoter and T7 terminator **(Table 3)**. *In vitro* topoisomerase assays were performed with recombinant DNA gyrase and topo IV from *E. coli* (TopoGEN) or *S. pneumoniae* (Inspiralis) following the manufacturer instructions. In brief, relaxed plasmid DNA (provided in the kits) was used as a substrate to assess the gyrase supercoiling activity, while supercoiled DNA and kDNA (TopoGEN or Inspiralis) were used as substrates to test the topo IV relaxation and decatenation activities. The antibiotics Ciprofloxacin (5 µg ml^{-1}) and Novobiocin (5 µg ml^{-1}) were used as positive controls. Upon 1 hour of incubation at 37°C the reactions were quenched by adding 2% of SDS and 1 mg ml^{-1} of proteinase K followed by 30 minutes of incubation at 37°C. Chloroform: isoamyl alcohol (24:1) organic extractions were done for the relaxation and supercoiling assays. Topoisomers were analyzed by electrophoresis (50 V for 3 hours) in 1% agarose gels and visualized by ethidium bromide staining. Images were acquired with a Molecular Imager Gel-Doc system (Bio-Rad) and analyzed in the Image Lab software (Bio-Rad).

2.7 Experiments involving *E. coli* as host

2.7.1 Killing assay

The effect of the different ParE proteins on bacterial viability was investigated in *E. coli* MG1655 using the low copy plasmid pBAD33P$_{ara}$ harboring each of the ParE-like toxins under the control of the arabinose promoter (P$_{ara}$). An additionally strategy was applied for depleting the toxin expression to allow successful cloning by decreasing the distance between the Shine-Dalgarno sequence and the start codon to 6nt (Ringquist et al., 1992a), maintaining the same ribosome binding side sequence for all toxins tested (**Table 2)**. Cells harboring the toxins were grown taking 1/100 dilution of an overnight culture in LB media supplemented with 30 µg ml^{-1} chloramphenicol. Exponentially growing cultures (OD$_{600nm}$ 0.5, cuvette reader Eppendorf BioSpectrometer® basic, t = 0) were divided in two; one half was treated with glucose 0.2% (control conditions), while the toxin was induced in the second half by adding 0.2% of arabinose (experimental conditions). Samples were taken every 30 minutes for two hours to perform serial dilutions (10^{-1} to 10^{-6}) and which were spotted on LB agar plates supplemented with 30 µg ml^{-1} chloramphenicol and 1% glucose for CFU ml^{-1} counting.

The effect of ParD1 or ParD1-ParF1 on bacterial viability was investigated by cloning either the *parD1* gene alone or together with *parF1* in the high copy plasmid pAH160P$_{rha}$, under the control of the rhamnose promoter (P$_{rha}$), provided by Prof. Dr. Christoph Dehio (Harms et al., 2015). The experiments were performed by growing the cells in LB media supplemented with 50 µg ml^{-1} kanamycin. Exponentially growing cultures (OD$_{600nm}$ 0.5, cuvette reader Eppendorf BioSpectrometer® basic, t = 0) were divided in two; one half was treated with glucose 0.2% (control conditions), while the toxin was induced in the second half by adding 0.2% of rhamnose (experimental conditions). Samples were collected, prepared and spotted on LB agar plates supplemented with 50 µg ml^{-1} kanamycin and 1% glucose for CFU ml^{-1} counting. The *parD1* titration of expression was performed by growing the cells in a bigger amount of LB media and dividing the exponentially growing culture into 6 different flasks. One flask served as a control and the others were treated independently with different concentrations of rhamnose (0.001, 0.005, 0.01, 0.05 and 0.2%). To assess the viability, samples were taken, diluted and spotted following the same protocol described above.

2.7.2 SOS response

The *E. coli* MG1655 AT15 strain (*λatt::P$_{sulA}$-gfp*) was used to evaluate the SOS-response where the promoter of the gene *sulA* has been fused to the GFP-encoding gene (McCool et al., 2004). Cells were transformed with the empty pBAD33P$_{ara}$ vector or harboring

each of the ParE-like toxins or the pAH160P$_{rha}$ empty vector or harboring the *parD1* or *parD1-parF1* and experiments were performed as described for the killing assays. After 2 hours of expression 1 ml of each culture was washed twice and suspended in 1X PBS; then 200 µl were placed in a 96 well plate (microplates, 96 well, clear, flat bottom with lid; Sarstedt) and the GFP signal was measured (Cytation3, BioTek Instriments Inc; Excitation: 475, Emission: 509, Optics: Bottom, Gain: 70). The data was normalized to the OD_{600nm} measurements.

2.7.3 Death prevention experiments

The capacity of the antitoxin to prevent the toxic effect was performed in *E. coli* MG1655 using a two plasmids system. For the characterization of the *parDEF1* locus the toxin was cloned in the pBAD33P$_{ara}$ as previously stated for the killing assays and the antitoxin *parD1* or the hypothetical gene *parF1* in the low copy vector pZE12P$_{lac}$ under the control of the isopropyl β-D-1-thiogalactopyranoside (IPTG)-inducible promoter. An overnight culture (1/100 dilution) was use to inoculate 100ml of LB media supplemented with 30 µg ml^{-1} chloramphenicol and 100 µg ml$_{-1}$ carbenicillin. Exponentially growing cultures (OD_{600nm} 0.5, cuvette reader Eppendorf BioSpectrometer® basic, t = 0) were divided in two: half of the culture was supplemented with 0.2 % arabinose to induce the toxin, while the second half was supplemented with both 0,5 mM IPTG and 0.2% arabinose to induce both the antitoxin and toxin. Samples were taken every 30 minutes for 2 hours to perform serial dilutions (10^{-1} to 10^{-6}) that were spotted on LB agar supplemented with 30 µg ml^{-1} chloramphenicol, 100 µg ml $^{-1}$ carbenicillin and 1% D-glucose for CFU ml^{-1} counting.

To assess the putative ParE targets each toxin in the pBAD33P$_{ara}$ vector was co-induced with each of the putative targets: *gyrA, gyrB*, *gyrase*, *topo IV E*, *topo IV C* or *topo IV,* cloned in the high copy vector pAH160P$_{rha}$, (Harms et al., 2015) **(Table 2)**. Cells were grown taking 1/100 dilution of an overnight culture in 100ml of LB media supplemented with 50 µg ml^{-1}, kanamycin, 30 µg ml^{-1} chloramphenicol and 0.2 % rhamnose to pre-induce the expression of the target. At mid-exponential growth phase (OD_{600nm} 0.5, cuvette reader Eppendorf BioSpectrometer® basic, t = 0) the grown culture was split in two flasks (control and experimental conditions). The toxin was induced by adding 0.2% of arabinose in one of the flasks. Samples were taken every 30 minutes for 2 hours after expression of the toxin and serial dilutions (10^{-1} to 10^{-6}) from each time-point were plated on LB media supplemented with 1 % D-glucose, 50 µg ml^{-1} kanamycin and 30 µg ml^{-1} chloramphenicol to quantify the CFU ml^{-1}. For the characterization of the *parDE2* operon, to further study the dual ParD1-ParE1 TA

system and to assess the TA cross talk, the same set of vectors was used (pBAD33P$_{ara}$ toxins, pAH160P$_{rha}$ antitoxins) **(Table 2),** following the protocol described above, unless otherwise stated.

2.7.4 Growth rescue experiments

To assess the ParD1 capacity to rescue the ParE1 effect and vice versa, *E. coli* MG1655 cells were transformed with two plasmids: the pBAD33P$_{ara}$ harboring the *parE1* (start codon TTG-SD6) gene (pEC1484) and pAH160P$_{rha}$ harboring the *parD1* gene (pEC2189). Bacteria cells were grown in LB media (50 ml) supplemented with 30 µg ml^{-1} chloramphenicol, 50 µg ml^{-1} kanamycin and 0.2% D-glucose to repress both P$_{ara}$ and P$_{rha}$ until mid-exponential phase of growth (OD$_{600nm}$ 0.5, cuvette reader Eppendorf BioSpectrometer® basic, t = 0). At this point, the culture was divided in two and washed twice with fresh LB media (25°C, 1500 xg, 10 minutes), and re-suspended in LB supplemented with the same antibiotics and either 0.2% arabinose to firstly induce *parE1* expression (experiment 1) or 0.2% rhamnose to induce *parD1* expression (experiment *2)*. After one hour, cells were washed again twice as previously described and re-suspended in fresh LB media supplemented with the same antibiotics and the opposite sugar to induce the second molecule (*parD1* for experiment 1 and *parE1* for experiment 2). Samples were taken from time zero every 30 minutes for 3 hours and serial dilutions were spotted on LB agar plates supplemented with 30 µg ml^{-1} chloramphenicol, 50 µgml^{-1} kanamycin and 1% D-glucose for CFU ml^{-1} counts. Subcultures were only one of the molecules was induced were used as controls.

2.8 Microscopy

Sample preparation for fluorescence microscopy was performed by collecting 1 ml of grown cultures from the killing (section 2.7.1) or SOS response (section 2.7.2) assays in *E. coli* or 1ml from the killing assays (section 2.4.4) in *S. pyogenes*. After 2 washes with the same volume of 1X PBS (centrifugations at 21000 x g, 4°C, 10 minutes) the pellets were re-suspended in 1 ml of a membrane dye (2.5 mg/ml FM4-64 in 1X PBS, Molecular Probes) and incubated at room temperature in the dark for 30 minutes. Afterward, cells were centrifuged and pellets were fixed with 1ml of 4% paraformaldehyde (Sigma) for at least 1 hour at 4°C. Subsequently a second step of washes as described before was performed and cells were re-suspended in a DNA stain solution (5 mg/ml Hoechst in 1X PBS, Sigma-Aldrich), incubated at room temperature in the dark for 30 minutes and 4 µl were transferred onto microscopy slides

coated with 1X PBS 1.5 % agarose pads. Images were acquired with an Inverted Microscope (Leica DMi8, DFC9000 GT VSC-D6212 camera), and a 100X phase contracts objective (HC LP APO 100X/1.40 oil). Filter sets were as follows: excitation, 390/18; emission 435/48 for Hoechst; and excitation, 542/27; emission, 594/45 for FM4-64. The images were further analyzed in ImageJ (Schneider et al., 2012).

S. pyogenes samples for electron microscopy were prepared by re-suspending the pellet of 20 ml (centrifugation step at 1500 x g, 25°C and 10 min) of grown cultures in 0.1 M of HEPES buffer pH 6.9 (HEPES (4-(2-hydroxyethyl)-1-piperazineethanesulfonic acid), 0.09 M sucrose, 10 mM $CaCl_2$, 10 mM $MgCl_2$) containing 5% formaldehyde and 2% glutaraldehyde (refer to section 2.8.2).

2.8.1 Image processing

To calculate the overall *E. coli* DNA content per cell, ImageJ to filter (Gaussian Blur) was used (threshold (Otsu) the original images of both fluorescent dyes). Small non-specific outliers were removed and a mask with the information of both channels was created. The overall DNA content was calculated: area (mask DAPI) / area ((mask DAPI) * (mask FM4-64)). The cell size /length was determined manually. At least 80 cells from the controls and 51 cells from the toxin-induced conditions were taken into account for performing the analysis.

2.8.2 Field emission scanning electron microscopy

Bacteria were fixed overnight with 5% formaldehyde and 2% glutaraldehyde at 4° C. After washing with HEPES buffer, an aliquot of 50 µl of the bacterial solution was placed on poly-l-lysine coated coverslips and allowed to settle for 10 min. After fixation with 1% glutaraldehyde in TE buffer (20 mM Tris-HCl, 1 mM EDTA, pH 6.9) for 10 min at room temperature, the coverslips were washed with TE buffer before dehydrating in a graded series of acetone (10, 30, 50, 70, 90, and 100%) on ice, each step for 10 minutes. Samples in 100% acetone were allowed to reach room temperature (exchange with fresh, room temperature 100% acetone after 10 min) before critical point drying with liquid CO_2 (CPD 30, Balzers, Liechtenstein). Dried samples were covered with a palladium–gold film by sputter coating (SCD 500, Bal-Tec, Liechtenstein). The samples were examined with a field emission scanning electron microscope (Merlin, Zeiss, Germany) using the HESE2 Everhart Thornley SE detector and the in-lens SE detector in a 25:75 ratio at an acceleration voltage of 5 kV. The SEM analysis was performed in collaboration with the Central Facility for Microscopy, at The Helmholtz Centre for Infection Research, Braunschweig, Germany.

2.8.3 Transmission electron microscopy

The fixed samples (refer to section 2.8.2) were further exposed to osmium tetroxide (1% in HEPES buffer) for 1 h at room temperature. After washing with HEPES buffer, samples were dehydrated in a graded series of ethanol on ice interrupted by an overnight incubation with 2 % uranyl acetate (UAc) at 4 °C (10, 30, 50, 70 +UAc, 70, 90, 100%). Samples were allowed to reach room temperature and subsequently infiltrated with the aromatic acrylic resin LRWhite (1:1, 2:1, 100%). After polymerization for 2 days at 50 °C, ultrathin sections were cut with a diamond knife (approx. 50-70 nm), collected onto butvar-coated 300 mesh grids, and counterstained with 4% aqueous uranyl acetate for 3 min and lead citrate for 30 seconds. The samples were examined with the transmission electron microscopes TEM 910 and Libra 120 Plus (Zeiss, Germany) with an acceleration voltage of 80 kV, respectively 120 kV and at calibrated magnifications. Contrast and brightness was adjusted using the WinTEM software. The TEM analysis was performed in collaboration with the Central Facility for Microscopy, at The Helmholtz Centre for Infection Research, Braunschweig, Germany.

2.9 Mass spectrometry analysis

The SDS-PAGE gel fragments of interest were excised and transferred into 0,5 ml Eppendorf tubes. For de-staining the gel bands were incubated with 500 µL of 200mM ammonium bicarbonate (ABC) and 50% acetonitrile (ACN) for 30 min at 37°C, followed by incubation with 500 µl of 50mM ABC, 5% ACN for 30 min at 37 °C. Gel pieces were then dried at 37°C for 30 min. Protein digestion was performed overnight at 37°C with 0,1-0,2 µg modified trypsin (Promega V5111) per 25 µl 50mM ABC, 5% ACN. The supernatant was transferred into an Eppendorf tubes and peptides were extracted by first applying 25 µL of 60% ACN, 0.5% Trifluoroacetic acid (TFA) for 10 min, followed by 25 µL of 100% ACN for 10 min. All supernatants were combined and dried in an Eppendorf Concentrator at 45°C. For desalting the samples were solubilized with 15 µl 0,1% TFA and bound to ZipTips (Millipore) according to the manufacturer's instructions. The peptides were eluted with 5 mg/ml α-Cyano-4-hydroxycinnamic acid in 60% ACN, 0.5% TFA onto the MALDI template.

Mass spectra were acquired with a 4700 Proteomics Analyzer (AB Sciex) MALDI-TOF/TOF instrument. The MS mass range was set to 800-4000 Da and MS/MS precursor selection for the 5 most intensive peptides was performed automatically; using the 4000 Series Explorer Software. Proteins were identified using Mascot 2.6.2 (Matrix Science) allowing a mass tolerance of 50 ppm for peptides and 0,3 Da for fragment masses. The search parameters for the MSMS ion search were a maximum of one missed cleavage, oxidation of

methionine, N-terminal acetylation of the protein, propionamide at cysteine residues and N-terminal pyroglutamic acid formation. The data were searched against a manually created database containing ParD1, ParE1, ParF1, ParD2 and ParE2 and the UniRef100 (133853533 sequences; 49656227882 residues) database. A protein was accepted as identified when the Mascot protein score was significant ($p < 0,05$) and the sequence coverage was > 30% or at least two peptides were confirmed by MSMS. The mass-spectrometry analysis was performed in collaboration with Monica Schmid at the Max Planck Institute for Infection Biology.

3 RESULTS

3.1 ParDEF1 is a bona-fide Toxin-Antitoxin System from *S. pyogenes*

This chapter describes the characterization of the *parDEF1* operon, an atypical TA system from the human pathogen *Streptococcus pyogenes*. The results demonstrated that *parDEF1* is a bona-fide TA system: 1.) The toxin-antitoxin- genes are co-transcribed 2.) Ectopic expression of the toxin ParE1 resulted in cell death and 3.) Co-expression of the toxin together with its cognate antitoxin prevented but did not reverse ParE1 toxicity. Unlike canonical antitoxins and in addition to its capacity to prevent ParE1 toxicity, ParD1 expression had a reversible effect in growth. This activity appeared to be exclusive for *S. pyogenes* ParD1 compared to previously characterized ParD-like proteins. The experimental results indicated that ParD1 impairs cell division and that the phenotype can be rescued by the presence of ParE1. These findings advocate a new type of TA system where both molecules target important cellular processes and their coexistence permits bacterial growth. Collectively, this chapter expands the knowledge about TAs and the diversity of mechanisms employed by these elements to modulate bacterial behavior.

The *parDEF1* locus is an operon conserved among different *S. pyoge*nes serotypes

Five different type II TA systems encoded in the chromosome of *S. pyogenes* were predicted (Xie et al., 2018). Among them, two loci are hypothesized to encode ParDE-like TA modules. In this chapter, I focused on the *parDEF1* locus which is an operon composed of three genes **(Figure 1.1A).** The operon architecture was validated by RT-PCR **(Figure 1.1B)**. *SPy_0550* is the first gene of the operon encoding the putative ParD1 antitoxin protein. As in other TA modules, one nucleotide of the stop codon from the antitoxin gene overlaps the first nucleotide of the toxin gene-encoding region. *SPy_0552* encodes the putative ParE1 toxin molecule, while the last gene of the operon *SPy_0553* encodes a hypothetical protein named ParF1. With the aim to identify the transcription start site (TSS) and confirm the operon architecture, we used previously reported transcriptome data of our model organism (Le Rhun et al., 2017). The analysis showed that the *parDEF1* operon is expressed at mid-exponential growth phase and that the *parD1* TSS differs from the predicted start site; therefore we have accordingly re-annotated the *parD1* start codon (coordinate 448386) **(Figure 1.1A)**.

The *parDEF1* operon is highly conserved among *S. pyogenes* serotypes **(Figure 1.1C)**. However, in some genomes the *parF1* gene is truncated leading to a potentially non-functional peptide **(Figure 1.1D)**. The genomic context of the *parDEF1* locus is also well conserved among most of the serotypes. Namely, it is located in a region encoding three hypothetical prophage proteins: a phage terminase, a phage portal protein and a transposase-encoding gene. In addition, putative cell division and multidrug resistance elements are encoded close to the *parDEF1* operon **(Figure 1.1C)**. The GC content of these features differs from the rest of the genome, suggesting that this operon may be located in a hypothetical prophage-like area **(Figure 1.1E)**. These findings could highlight the origin and/or role of the *parDEF1* locus in our model organism; if the putative prophage region is prone to excision, this TA module could stabilize the chromosomal DNA region surrounding it under certain conditions.

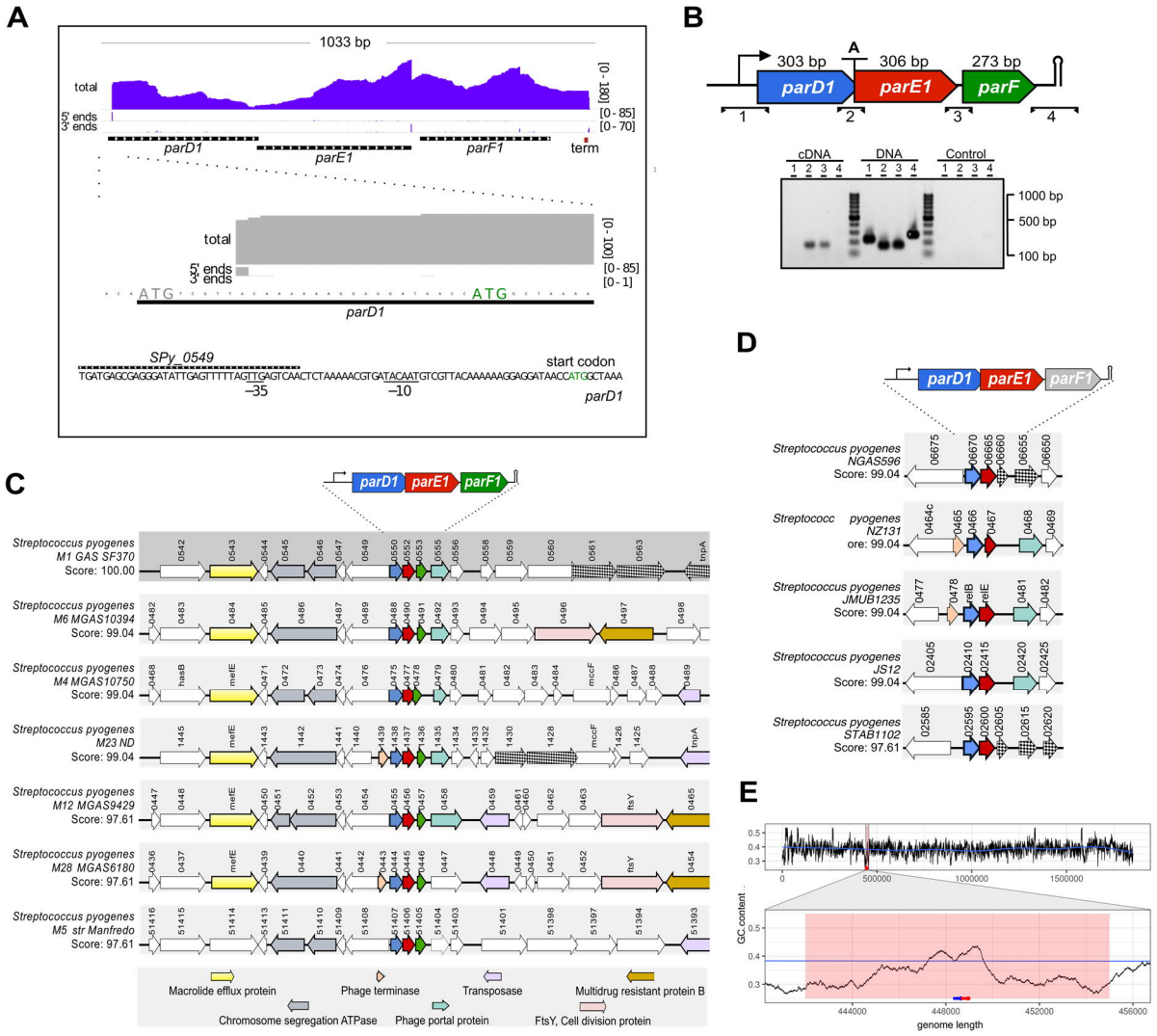

Figure 1.1: *parDEF1* is an operon highly conserved among *S. pyogenes* serotypes.

A. The *parDEF1* locus was shown to be co-transcribed in the *S. pyogenes* M1 GAS RNAseq analysis (expression signal depicted in purple). The coverage of reads and the coverage of the 5' and 3' ends are given into brackets (image captured from Integrative Genomics Viewer) (Robinson et al., 2011; Thorvaldsdottir et al., 2013). The *parD1* start codon was re-annotated based on the genome NC_002737.2 at the coordinate 448386 (green colored ATG sequence). The red box indicates the predicted Rho-independent terminator (TransTermHP v2.07 prediction downloaded from Le Rhun et al., 2017). Analysis performed in collaboration with Dr. Anaïs Le Rhun from the Max Planck Unit for the Science of Pathogens. **B.** The *parDEF1* operon architecture is depicted: *parD1* antitoxin in blue, *parE1* toxin in red and the hypothetical *parF1* gene in green. An adenine, indicated by an "A" overlaps the antitoxin and toxin sequences. Gene sizes are shown above the open reading frames (ORFs) and lines with arrows below the ORFs represent RT-PCRs performed to confirm the operon conformation. *parD1, parE1* and *parF1* formed a three-gene operon (positive PCR line 2 and 3 and negative PCR line 1 and 4 from cDNA). Positive (DNA) and negative (water) controls are shown. **C.** The *parDEF1* operon is conserved among different *S. pyogenes* serotypes and the genomic context includes putative pro-phage and antibiotic resistant genes depicted in colors. A BLAST-base analysis was performed using SyntTax web server (http://archaea.u-psud.fr/synttax). **D.** The *parF1* gene is truncated and/or non-annotated in some serotypes shown. **E.** Guanine/cytosine (GC) content analysis shown that the *parDEF1* operon is located in a genomic region with low GC-content. The zoomed panel indicates a window of 15Kb (pink squared, antitoxin in blue and toxin in red). The genomic GC% content was calculated in R, package *Biostrings* using a genome window of 1000bp.

The *parDEF1* operon encodes a bona-fide TA system

I next aimed to evaluate whether the predicted TA system is functional. For this purpose I first examined whether ParE1 has a toxic effect in the heterologous host *E. coli*. Multiple cloning strategies applied to express the wild-type *parE1* gene from the low copy plasmid pBAD33P$_{ara}$ under the control of the arabinose promoter failed due to the acquisition of random mutations that led to the recovery of non-toxic variants. To reduce the expression level of *parE1* the start codon was changed from ATG to TTG and 6 nucleotides between the ribosome binding site and the methionine-encoding triplet were left, as previously described to reduce the expression level in *E. coli* (Ringquist et al., 1992b). Growth rescue experiments revealed killing of *E. coli* cells upon overexpression of the ParE1 toxin **(Figure 1.2A and 1.2B).** Whereas, expression of the ParE1*L47A variant with a randomly acquired mutation during cloning allowed growth**,** displaying the importance of the L47 residue for toxicity or protein stability **(Figure 1.2A)**. Next, I wanted to evaluate the phenotype of *E. coli* cells overexpressing ParE1. Two hours of ParE1 expression caused strong cell elongation, absence of septum and nucleoid condensation compared to the non-induced conditions **(Figure 1.2C)**. Moreover, by live and dead staining we could determine that ParE1 expression indeed resulted in cell killing, since the elongated cells were dead **(Figure 1.2C).**

To determine whether *parDEF1* is a typical TA module I assessed the antitoxin capacity by cloning *parD1* in the low copy vector pZE12P$_{lac}$. Co-expression of ParD1 efficiently counteracted the toxicity of its cognate toxin ParE1, but also in the absence of the inducer.

This is most likely due to the leakiness of the isopropyl β-D-1-thiogalactopyranoside (IPTG)-inducible promoter that controls antitoxin expression **(Figure 1.2D)**. Repeated attempts to clone the wild type *parD1* gene also lead to various suppressor mutations. Some of these ParD1 variants showed reduced antitoxin capacity. For instance, the ParD1* F49L variant partially counteracted ParE1 toxicity in comparison with the non-induced conditions, highlighting the potential importance of the F49 residue for the interaction of ParD1 with its toxin or for ParD1 stability **(Figure 1.2D)**. The highly toxic phenotype upon ParE1 expression and the growth prevention upon co-expression of the two molecules suggest that *parDE1* is a bona-fide TA system.

Furthermore, I have also investigated the function of the third gene of the operon. ParF1 did not show any antitoxin capacity when co-expressed with the ParE1 toxin, nor toxicity when solely express in *E. coli* **(Figure 1.2E).** Finally, I have assessed the interaction of the TA components in the natural host *S. pyogenes*. For this purpose, I cloned extra-chromosomally the N-terminal FLAG-tagged ParD1 variant which retained its antitoxin function **(Figure 1.2F)** into *S. pyogenes*. *In vivo* pull downs from total cell extracts of cells expressing this ParD1 variant, followed by mass spectrometry analysis, have revealed the presence of ParE1 **(Figure 1.2G)**, suggesting that indeed ParD1 and ParE1 can interact *in vivo*. Conversely, in the same analysis ParF1 was not detected in any of the fractions, possibly due to a weaker or absent interaction with ParD1 under the conditions tested, or an interaction with ParE1 that we have not studied yet.

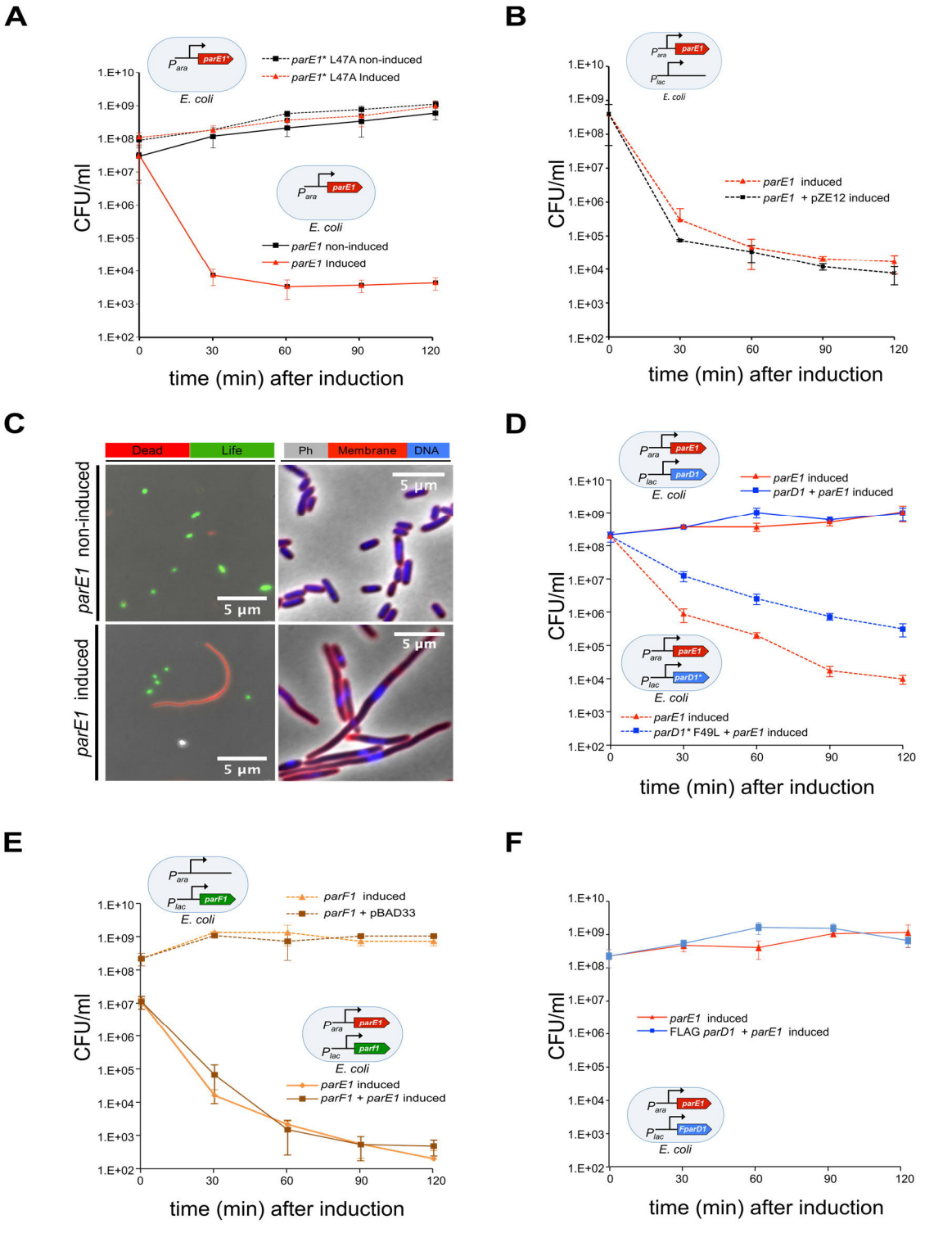

Bands	MS prediction
1, 2, 3	Unspecific bands
4, 8	ParD1 (putative dimer)
5, 9	ParE1 (putative dimer)
6, 10,12	ParD1 (putative monomer)
7, 11, 13	ParD1 (putative degradation product)

Figure 1.2: *parDEF1* is a bona fide TA system encoding the ParE1 toxin that induces cell elongation and nucleoid condensation in *E. coli*.

A. Exponentially growing *E. coli* cells harboring the toxin *parE1* (TTG-SD6) under the control of the arabinose promoter (P_{ara}) were divided in two (time zero); one half was treated with 0.2% D-glucose to repress P_{ara} (black) while 0.2% of arabinose was added to the second half (red) to induce toxin expression. Colony-forming units (CFU ml^{-1}) were counted every 30 min during 2 hours. Expression of the ParE1 toxin resulted *E. coli* cell death while the toxin variant ParE* L47A did not have an effect in growth. Error bars represent the standard deviation of at least three biological replicates. **B.** Exponentially growing *E. coli* cells harboring *parE1* (TTG-SD6) under the P_{ara} control and the pZE12P_{lac} empty vector were divided in two (time zero): i) half of the culture was treated with 0.2% arabinose to induced the toxin (red dotted line), ii) the second half was treated with 0.2% arabinose and IPTG 0.5 mM to induced the $P_{lac.}$ (black dotted line). ParE1 expression led to killing while the empty pZE12P_{lac} vector did not rescue ParE1 toxicity. Error bars denote standard deviation of at least three biological replicates. **C.** *E. coli* cells from A, 120 minutes after ParE1 (TTG-SD6) expression were prepared for dead (cell depicted in red)/live (cell depicted in green) analysis, as well as stained with FM4-64 (membranes; red) and Hoechst (DNA; blue) and observed by fluorescence and phase contrast (Ph) microscopy. The toxin ParE1 led to cell death, induced cell elongation and nucleoid condensation indicating that DNA-topology and cell division is strongly affected. Representative images are shown. **D.** The death prevention experiment in exponentially growing *E. coli* cells harboring *parE1* (TTG-SD6) under the P_{ara} control and *parD1* under the control of the lactose promoter (P_{lac}), was performed as described in B. At mid-exponential phase the culture was divided in half: i) the toxin was induced by adding 0.2% of arabinose (red), ii) both the toxin and the antitoxin were induced by adding IPTG 0.5 mM and 0.2% of arabinose (blue). ParD1 effectively prevent ParE1 toxicity even in absence of the inductor while the ParD1* F49L variant partially prevent death. Error bars represent the standard deviation of at least three biological replicates. **E.** Death prevention experiment in *E. coli* cells harboring *parF1* under the P_{lac} promoter and either the toxin *parE1* (TTG-SD6) under the P_{ara} promoter or the empty pBAD33P_{ara} vector. The experiment was performed as described in D. ParF1 was not toxic (dotted orange and brown lines) and ParF1 did not shown antitoxin activity since expression of only the toxin ParE1 (orange line) as well as both ParF1 and ParE1 (brown line) led to killing. **F.** Death prevention experiment in exponentially growing *E. coli* cells harboring *parE1* (TTG-SD6) under the P_{ara} control and the N-terminal FLAG-tagged *parD1* variant under the control of the lactose promoter (P_{lac}), performed as described in B. The FLAG-tagged parD1 variant efficiently prevent ParE1 toxicity (blue), even in absence of the inductor (red). **G.** Exponentially growing *S. pyogenes* cells expressing extra-chromosomally the N-terminal FLAG-tagged ParD1 protein under the control of the AHT promoter (P_{tet}) were grown until mid-exponential phase to perform antitoxin pull-downs (Anti-FLAG M2 agarose beads) where ParE1 was detected. Samples were run in a 15% polyacrylamide gel and different fractions were analyzed by Mass-spectrometry. ParD1 was detected in three fractions: a putative dimer at 22 kDa, a monomer at 11 kDa and a potential degradation product below 10 kDa. A putative ParE1 dimer was detected at around 19 kDa. The mass-spectrometry analysis was performed in collaboration with Monica Schmid at the Max Planck Institute for Infection Biology.

Both ParD1 and ParE1 cause cell division halt in *S. pyogenes*

To ascertain the ParDEF1 TA function in the natural host *S. pyogenes*, I studied the phenotype of the wild type and *ΔparDE1* mutant strain upon extra-chromosomal expression of each TA component. Multiple attempts to clone independently the wild type toxin gene in the low copy plasmid pEC85P_{tet} under the control of the tetracycline promoter failed. Still, while the mutation ParE1*L47A (start codon TTG) leads to a non-toxic variant in *E. coli* **(Figure 1.2A)**, ParE1* L47A (start codon ATG) reduced growth in the wild type *S. pyogenes* strain

when compared with the empty vector control **(Figure 1.3A)**. The phenotype was stronger in the *ΔparDE1* mutant, which we attributed to the absence of ParD1 **(Figure 1.3B)**, thus implying that ParD1 is the antitoxin that neutralizes ParE1 toxicity.

Next, I assessed the phenotype upon antitoxin expression. As for ParE1, multiple attempts to clone the antitoxin in the same vector were unsuccessful. Therefore, I used the N-terminal FLAG-tagged ParD1 variant that was previously shown to counteract ParE1 toxicity and interact with the cognate toxin (**Figure 1.2F and 1.2G)**. Strikingly, expression of the ParD1 variant caused growth defects in the *S. pyogenes* wild type strain **(Figure 1.3A)**. This phenotype was stronger in the *ΔparDE1* mutant strain where the reduction in CFU ml^{-1} was also evident under non-induced conditions **(Figure 1.3B)**. This result could suggest that ParD1 is unexpectedly toxic and that ParE1 is also acting as the cognate antitoxin. In addition, multiple attempts to delete only *parE1* on the chromosome failed, suggesting a potential ParD1-mediated deleterious outcome that leads to unviable cell. The ParE1 molecule could possibly counter this effect and therefore the two TA components need to co-exist.

I was also interested in confirming the ParD1 antitoxin phenotype upon ParE1 co-expression in *S. pyogenes.* Molecular tools to ectopically co-express different genes under distinct promoters are not available for *S. pyogenes* M1 GAS. In order to validate the TA function in its natural host, we attempted to clone the *parD-parE1* genes or the complete *parDEF1* operon in the same vector. Unfortunately, we were not able to obtain a clone using the pEC85P_{tet} backbone for *S. pyogenes* or by using a different set of vectors for *E. coli*. This inability to evaluate antitoxin: toxin ratios in *S. pyogenes* prohibits us from confidently concluding whether these two molecules act as a dual TA system. Nevertheless, it could suggest that the 1:1 antitoxin: toxin ratio is not enough to lead to viable cells when attempting to clone the two components under the control of the same promoter. Furthermore, since ParF1 showed neither antitoxin nor toxin activity in *E. coli* **(Figure 1.2E),** we assessed the effect of ParF1 when expressed with ParD1. Cloning and co-expression of ParD1 and ParF1 was possible. Nevertheless, the phenotype is similar to the solely ParD1 expression condition in both the wild type and the *ΔparDE1* mutant strain **(Figure 1.3A and 1.3B)**, suggesting that ParF1 does not act as an antitoxin of ParD1.

These experiments also indicated that the ParE1 toxin arrests DNA replication since I observed prominent cell elongation and nucleoid condensation when ParE1 was expressed in the heterologous system *E. coli* **(Figure 1.2C)**. I was interested in describing the phenotype in the natural host where defects at the level of DNA replication via TA systems have not been

characterized. Furthermore, having seen impaired of growth upon ParD1 overexpression, I also wanted to elucidate the basis of this intriguing outcome. For this purpose, I grew in liquid medium wild type *S. pyogenes* cells overexpressing either ParE1 or ParD1 and prepared the samples for DNA-labeled fluorescence microscopy (FL), scanning (SEM) and transmission electron microscopy (TEM). As depicted in **Figure 1.3C** *S. pyogenes* cells harboring the pEC85 empty vector showed a normal DNA staining pattern (FL). In addition, chains were well defined and cell sizes were homogeneously distributed (FL, SEM). Finally, by TEM we could see the septum positioned in the middle of the cells undergoing cell division **(Figure 1.3C)**. When ParE1 was expressed the DNA staining pattern appeared weaker (FL), some cells were swollen in size (SEM) and the septum was displaced and multi-positioned (TEM) **(Figure 1.3D)**. Surprisingly, expression of ParD1 also had a clear impact on the cells (**Figure 1.3E);** namely it caused cell elongation and a single clump of DNA was positioned at the cell poles (FL). In addition, elongated cells seemed to have started cell division (SEM), while the misplaced septum appeared to be incomplete (TEM). Taken together, I hypothesized that the ParD1 antitoxin is also toxic when overexpressed in *S. pyogenes.*

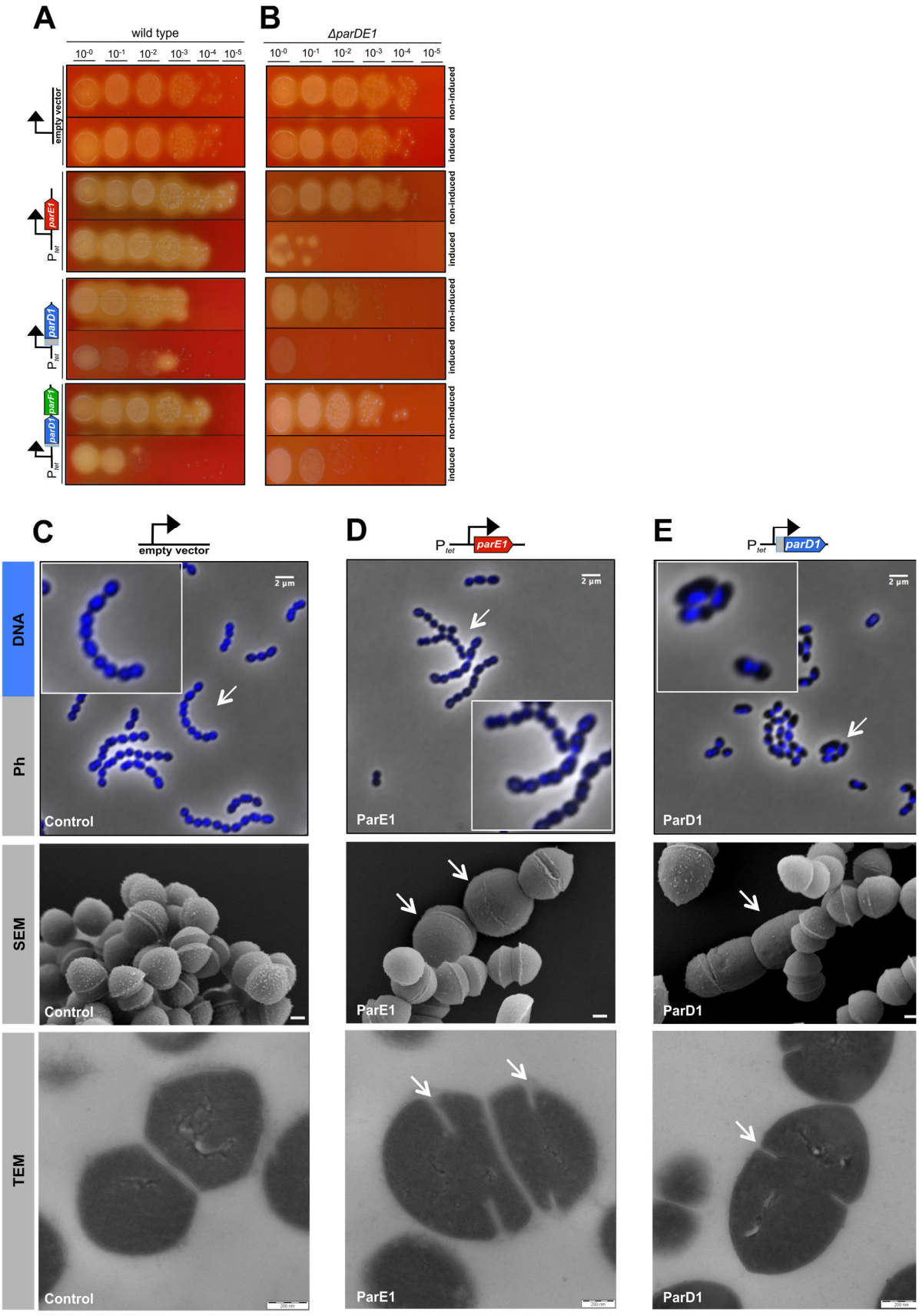

Figure 1.3: Both ParE1 and ParD1 are toxic in *S. pyogenes*

A-B. *S. pyogenes* overnight cultures of cells harboring the pEC85P$_{tet}$ empty vector or harboring either *parE1** (ATG L47A), N-terminal FLAG-tagged *parD1* or N-terminal FLAG-tagged *parD1-parF1* under the control of the tetracycline promoter (P$_{tet}$), were normalized to the same optical density (OD$_{620nm}$ 0.2), and serial dilutions (10^{-1} to 10^{-5}) were spotted in TSA-blood agar plates with and without the inductor (AHT 50 ng ml^{-1}). Expression of all of the three constructs led to a small reduction of viable *S. pyogenes* wild type cells (A) a stronger effect in the *ΔparDE1* mutant background (B). Representative pictures of at least 6 biological replicates are shown. **C-D-E.** Exponentially wild type growing *S. pyogenes* cells with the constructs described in A were induced for 2 hours (AHT 25 ng ml^{-1}) and subjected to fluorescence (DNA stained with Hoechst; blue), phase contrast (Ph), scanning (SEM) and transmission (TEM) electron microscopy. **C**. The DNA molecule was spread in the cells, a typical cocci shape was evident and the septum was right positioned. **D**. The DNA staining pattern looked weaker than when the empty vector was induced and nucleus seemed to be condensed, cells were swollen and the septum was misallocated upon ParE1 expression. **E**. The DNA molecule is highly condensed, cells are swollen, elongated, and the septum is uneven positioned. Representative pictures of at least three biological replicates are shown. SEM and TEM analysis were performed in collaboration with the Central Facility for Microscopy, at The Helmholtz Centre for Infection Research, Braunschweig, Germany.

ParD1 is a novel antitoxin that has a deleterious effect in *E. coli*

The results demonstrated that ParD1 is an antitoxin in *E. coli* **(Figure 1.2D)** and in *S. pyogenes* **(Figure 1.3B).** Furthermore, experiments in *S. pyogenes* support the idea that ParD1 and ParE1 may be toxins that cancel their effect when coexisting in an unknown ratio **(Figure 1.3A and 1.3B)**. To further characterize ParD1 I analyzed the protein features *in silico*. According to this analysis, ParD1 typically harbors two important domains with distinct functions **(Figure 1.4A)**. The N-terminal domain adopts a ribbon-helix-helix (RHH) fold that harbors a DNA-binding domain (DNA-BD) and allows the interaction of ParD-like proteins with the *parDE* promoter sequence, thus regulating the transcription of the whole operon (Oberer et al., 2002). On the other hand, the C-terminal domain of ParD-like proteins encoded in plasmids harbors the toxin-neutralization domain (TND), an intrinsically unstructured region prompt to be recognized for degradation by the bacterial protein quality machinery (Oberer et al., 2007). Interestingly, the ParD1 C-terminus appears to be rather structured with two well-defined α-helical shapes **(Figure 1.4A)**, which could lead to a more stable protein as previously described for other chromosomally encoded ParD antitoxins (Dalton and Crosson, 2010). Besides these features, there are no other obvious characteristics that would allow me to predict the nature of ParD1 toxicity. However, I cannot exclude the possibility that the N-terminal domain could nonspecifically bind nucleotide sequences in the genome that could lead to deleterious effects.

We assessed the toxicity of ParD1 using killing experiments by overexpressing ParD1 in *E. coli* from the pAH160 high copy vector. As expected, ParD1 expression led to a 10^5-fold decrease in CFU ml^{-1} compare to the non-induced conditions, confirming its deleterious effect.

Intriguingly, the N-terminal tag appeared to reduce ParD1 toxicity in *E. coli*, as it showed only 10^1-fold decrease in CFU ml^{-1} in comparison with the non-induced conditions **(Figure 1.4B)**. Since multiple cloning attempts led to different mutations in the ParD1 protein, we also studied the toxicity of some of these variants including a C-terminal FLAG-tagged ParD1 protein; all of these ParD1 variants retained their antitoxin capacity **(Figure 1.4C)**. The C-terminal tag did not have an influence on ParD1 toxicity as this variant has shown a 10^4-fold decrease in CFU ml^{-1} in comparison with the non-induced conditions, similar to the wild type ParD1 protein **(Figure 1.4D)**. Conversely, mutations in the amino acid at position 8 (N8I) and position 3 (K3A) led to non-toxic ParD1 protein variants. Next, we designed mutations in different N-terminal residues to further understand their implications and found that a mutation in the position 5 (G5A) lead to a stronger phenotype in *E. coli* when compared with the wild type ParD1 **(Figure 1.4D)**. These results suggest that the ParD1 N-terminus could potentially carry the features that render the protein toxic.

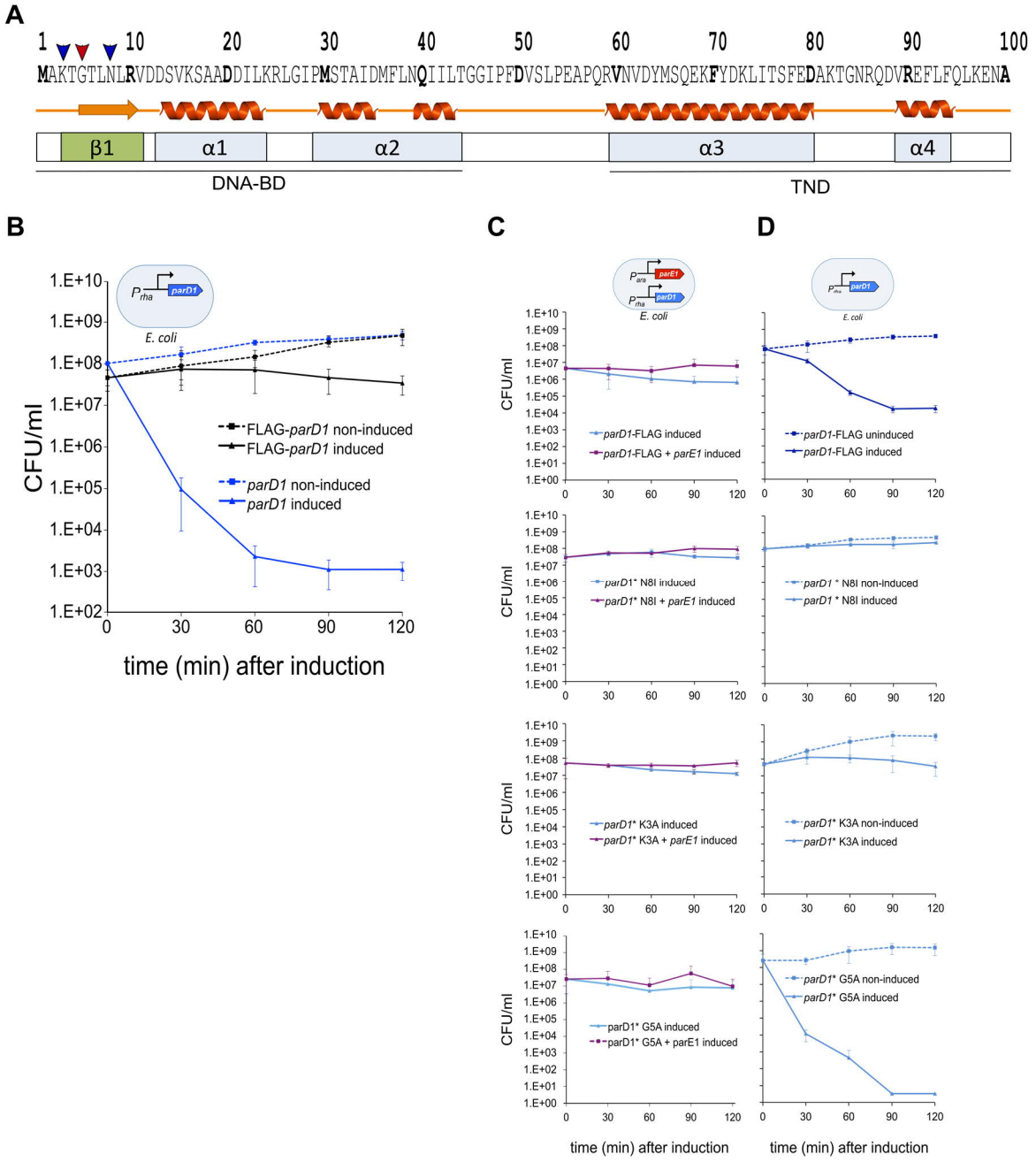

Figure 1.4: ParD1 has a deleterious effect in *E. coli* and its N-terminus might be implicated in toxicity.

A. The ParD1 secondary structure prediction (Waterhouse et al., 2018), showed a β-sheet (β1: orange arrow) and two α-helix (α1, α2: orange spirals) on the hypothetical DNA-binding (DNA-BD) domain located at the N-terminus while two α-helix (α3, α4: orange spirals) on the putative toxin neutralization domain (TND) at the C-terminus of the protein. Three arrows at the N-terminus represent hypothetical key residues for its toxicity (2 blue arrows, K3 and N8 and one red arrow G5). **B.** *E. coli* exponentially growing cultures harboring either *parD1* or N-terminal FLAG-tagged *parD1* under the P_{rha} control, where divided in two (time zero) to perform the killing assays: half of the culture was treated with 0.2% D-glucose to repress the P_{rha} expression (dotted blue and black lines), while the second half was treated with 0.2% rhamnose to induced expression of either *parD1* (blue line) or the FLAG-tagged *parD1* variant (black line) and the CFU ml^{-1} were followed for two hours. ParD1 led to a growth reduction while the FLAG-tagged ParD1 had a mild impact in *E. coli* growth. **C.** *E. coli* cells harboring either *parD1* C-terminus FLAG-tagged, *parD1** N8I, *parD1** K3A or *parD1** G5A

variants under the P_{rha} control with the ParE1 (TTG-SD6) toxin under the P_{ara} control, were grown inducing expression of *parD1* variants (0.2% rhamnose) until mid-exponential phase (time zero), and then divide in two to perform the death prevention experiment: half of the culture served as a control (blue line) while the second half was treated with 0.2% arabinose to co-induce expression of the toxin (purple line). All ParD1 variants prevent ParE1 toxicity. **D.** Killing assays (as described in B) of *E. coli* cells harboring each of the different ParD1 variants tested in C displayed that the ParD1 C-terminal FLAG-tagged variant led to a reduction of CFU ml^{-1} similar to the wild type *parD1* (B), while the mutations N8I and K3A led to less toxicity and G5A to stronger killing compared to the native ParD1 (B).

Deleterious effects of antitoxins have never been reported. In fact, *parD1* might be a new type of antitoxin/toxin gene assigned to the incorrect family of antitoxins. In addition, toxins belonging to a given superfamily can be associated to antitoxins that belong to different superfamilies (Leplae et al., 2011). A typical ParE-like toxin could potentially be associated to at least four different superfamilies: PhD, RelB, PaaA (Hallez et al., 2010) and ParD1-like antitoxins. With the aim to find antitoxins closely related to ParD1 and test their possible toxicity, we retrieved all antitoxins belonging to the ParD, PhD, RelB and PaaA superfamilies from the TADB database (Xie et al., 2018) and performed a sequence-base comparison. Principal component analysis has revealed 4 different clusters grouped by the antitoxin superfamilies included in the test and not by phylum **(Figure 1.5A)**. As expected, ParD1 forms a cluster with typical ParD proteins; nevertheless, phylogenetic analysis of the ParD cluster revealed that ParD1 branches only with a hypothetical antitoxin from another strain of *S. pyogenes* **(Figure 1.5B)**. These analyses support assigning ParD1 to a new, uncharacterized type of antitoxins that share some sequence features with the ParD1 superfamily.

Moreover, we were interested in comparing the effect of ParD1 with other proteins assigned to this superfamily of antitoxins. Thus, we have performed growth arrest experiments upon expression of $ParD_{EDL933}$ from *E. coli* 0175H7 (EcoParD3) (Hallez et al., 2010) and ParD2 from *M. tuberculosis* H37Rv (MtbParE3) (Gupta et al., 2016). Interestingly, only ParD1 from *S. pyogenes* showed a 10^5-fold decrease in CFU ml^{-1} in comparison to the non-induced conditions **(Figure 1.5C)**. These data suggest that ParD1 toxicity in *E. coli* is an intrinsic characteristic of this protein and not a feature more widely extended to its ParD homologs.

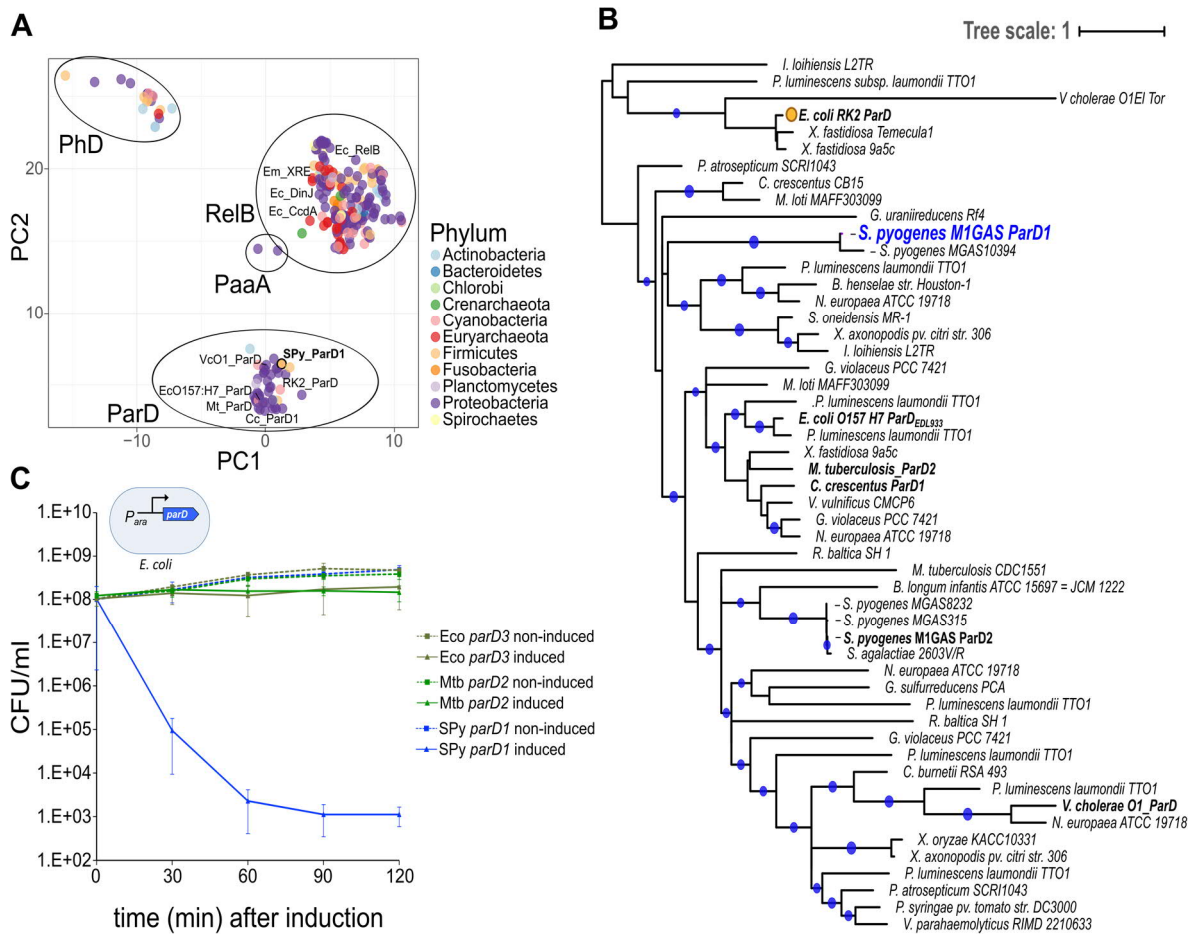

Figure 1.5: The toxic phenotype is exclusive from ParD1.

A. Principal component analysis of the PhD, RelB, PaaA and ParD family members that have been reported to interact with ParE-like toxins, retrieved form the TADB database (Xie et al., 2018) showed that these toxin families are more abundant in proteobacteria and the members are not grouped by phylum. ParD1 (SPyParD1) clustered with typical ParD-like antitoxins such as EcParD3 and MtbParE2. **B.** Phylogenetic analysis of the ParD family cluster from A showed that SPyParE1 (blue) group with an hypothetical protein from other *S. pyogenes* specie as well as the second ParD-like proteins SPyParE2 (black bold) located in other cluster. The plasmidic ParD from *E. coli* is highlighted with a yellow circle. The previously characterized ParD-like copies are also depicted in bold letters. The blue circles represent the bootstrap support bigger than 70% (raxml). **C.** Killing assays as described in **1.4B** showed that EcParD3 (dark green) and MtbParD2 (light green) did not have an effect in growth when express in *E. coli* in comparison with SPyParD1 (blue), implying that its toxicity is exclusive. The principal component and phylogenetic analysis were performed in collaboration with Dr. Eric JC. Galvez from the Max Planck Unit for the Science of Pathogens.

As previously described in **Figure 1.3A and 1.3B** ParD1-ParF1 expression prevented growth in the natural host *S. pyogenes.* To determine if this was the case in *E. coli* we co-expressed *parD1-parF1* and performed killing assay. The results showed the same trend of killing when compared with single ParD1 expression **(Figure 1.6A)**, confirming that ParF1 does not counteract the toxicity of ParD1 in *E. coli*.

Given that ParD1 was toxic when produced from a high copy plasmid in *E. coli*, we speculated that the toxic effect could be due to the amount of protein produced. In order to validate that the phenotype is a direct consequence of ParD1 and is also detectable at low levels of expression, titration experiments were performed with *E. coli* harboring the same high copy vector, in which different concentrations of the inducer rhamnose (from 0% to 0.2%) were used. When a small quantity of inducer (0.001%) was added, the number of CFU ml^{-1} increased or was maintained over time, which meant that cells were growing normally **(Figure 1.6B)**. However, as higher concentrations of the inducer were added, there was a progressive reduction of CFU ml^{-1} after two hours **(Figure 1.6B and 1.6C)**. These results confirmed that the observed phenotype is a direct consequence of ParD1 and its ability to cause an effect even at small quantities.

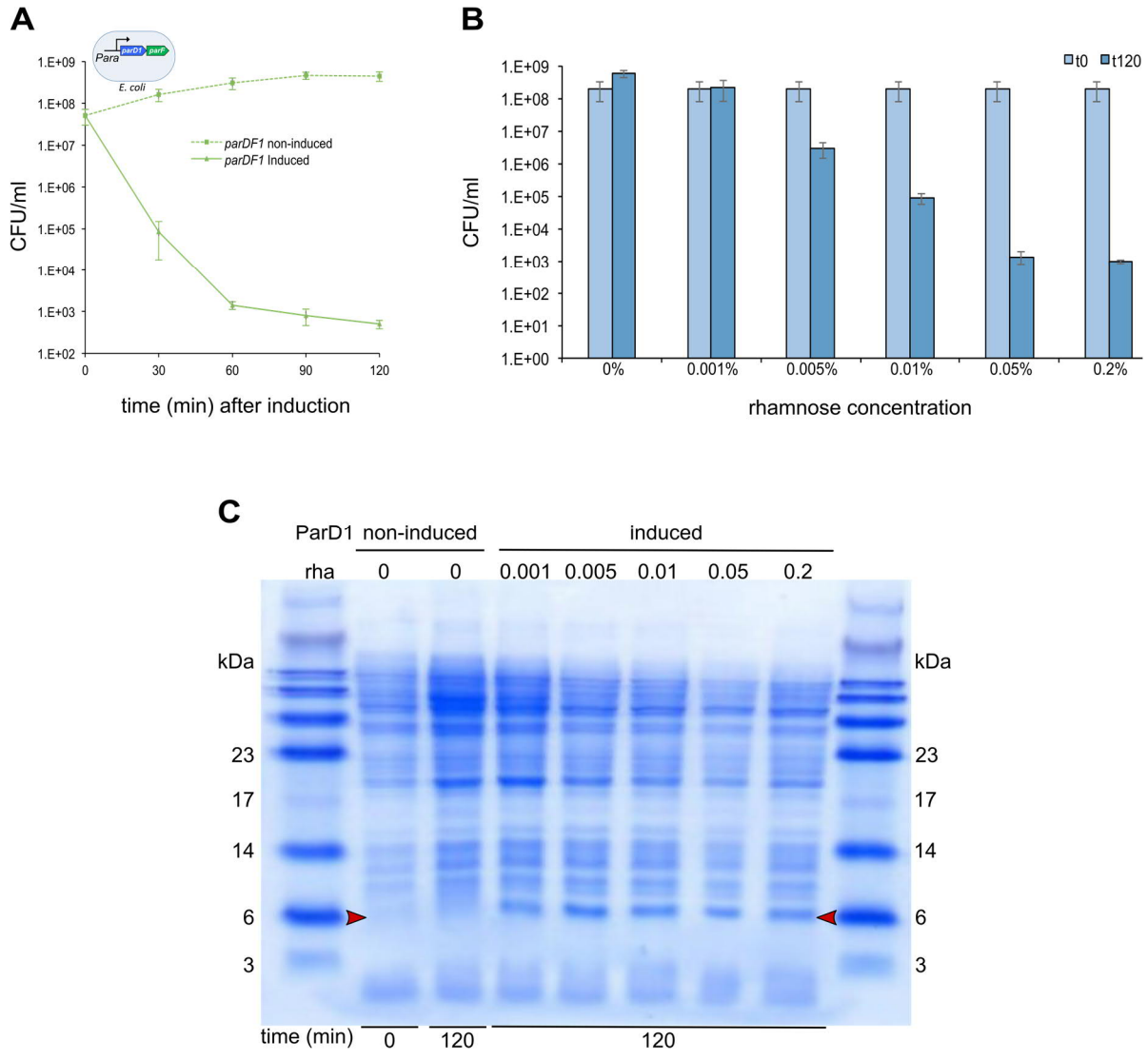

Figure 1.6: The ParD1 effect is not prevented by ParF1 and is dose dependent.

A. Killing assays as described in **1.4B** of *E. coli* cells harboring *parD1-parF1* under P_{rha} control showed a CFU ml^{-1} reduction upon expression implying that ParF1 does not prevent the ParD1 toxic

effect. **B.** Killing assays in *E. coli* where induction of the *parD1* wild type expression was done in subcultures at different concentration of the inductor rhamnose (0, 0.01, 0.005, 0.01, 0.05 and 0.2 %). The reduction of CFU ml^{-1} is ParD1 dose dependent since increasing concentration of the inductor led to stronger killing in comparison with the non-induced conditions. Experiments were performed in triplicates. **C.** SDS-PAGE gel from experiment described in B, total cell lysates, confirmed the expression of the ParD1 protein. B.S Leticia Rodriguez-Montes contributed to the analysis of the ParD1 phenotype in *E. coli*.

ParD1 is a toxin molecule that arrests cell division

Expression of ParD1 in *S. pyogenes* causes nucleoid condensation, cell elongation and incomplete septum formation **(Figure 1.3E)**. A similar phenotype has been reported for Gram-positive bacteria in cells lacking proteins important for septum formation (Fleurie et al., 2014; Stamsås et al., 2018). Since ParD1 expression also impacts *E. coli* growth, we speculated that its target might be highly conserved between these two species. In order to better characterize the ParD1 influence I assessed the phenotype of *E. coli* cells upon 2 hours of ParD1 expression. Interestingly, ParD1 rendered the cells slightly larger, while the nucleus was condensed in an uneven position **(Figure 1.7A and 1.7B)**. I also quantified the DNA content per cell and found that upon expression of ParE1, ParD1 and the more toxic variant ParD1* G5A there were significant differences in DNA content in comparison with the non-induced conditions, while the expression of the non-toxic variant ParD1* K3A did not lead to statistically significant change **(Figure 1.7B)**. Similarly, single DNA condensation and slight cell elongation is evident when cells are treated with ciprofloxacin that arrest DNA replication (will be described in section 3.3)**,** suggesting that ParD1 could also potentially target this process. However, the SOS response was not induced upon ParD1 overexpression implying that the primary effect is not to disturb DNA topology **(Figure 1.7C)**. Moreover, TEM showed that the cells seemed to have replicated DNA and further decatenation appeared to have started **(Figure 1.7D)**; we observed defects on septum formation while the DNA tends to be positioned at the pole of cell division **(Figure 1.7D)**. Intriguingly, when ParD1 and ParF1 were co-induced this phenotype is more obvious since daughter DNA molecules were more evident, but still the septum is misallocated in the cell and some cells presented two condensed DNA marks next to each other **(Figure 1.7E)**. Finally, at lower concentration of the inducer, a single DNA clump was evident and then resolved in two different clumps while inductor concentration increased the septum was no longer visible **(Figure 1.7F).** These observations support the hypothesis that ParD1 might have an effect at the level of cell division via a mechanism that still needs to be understood.

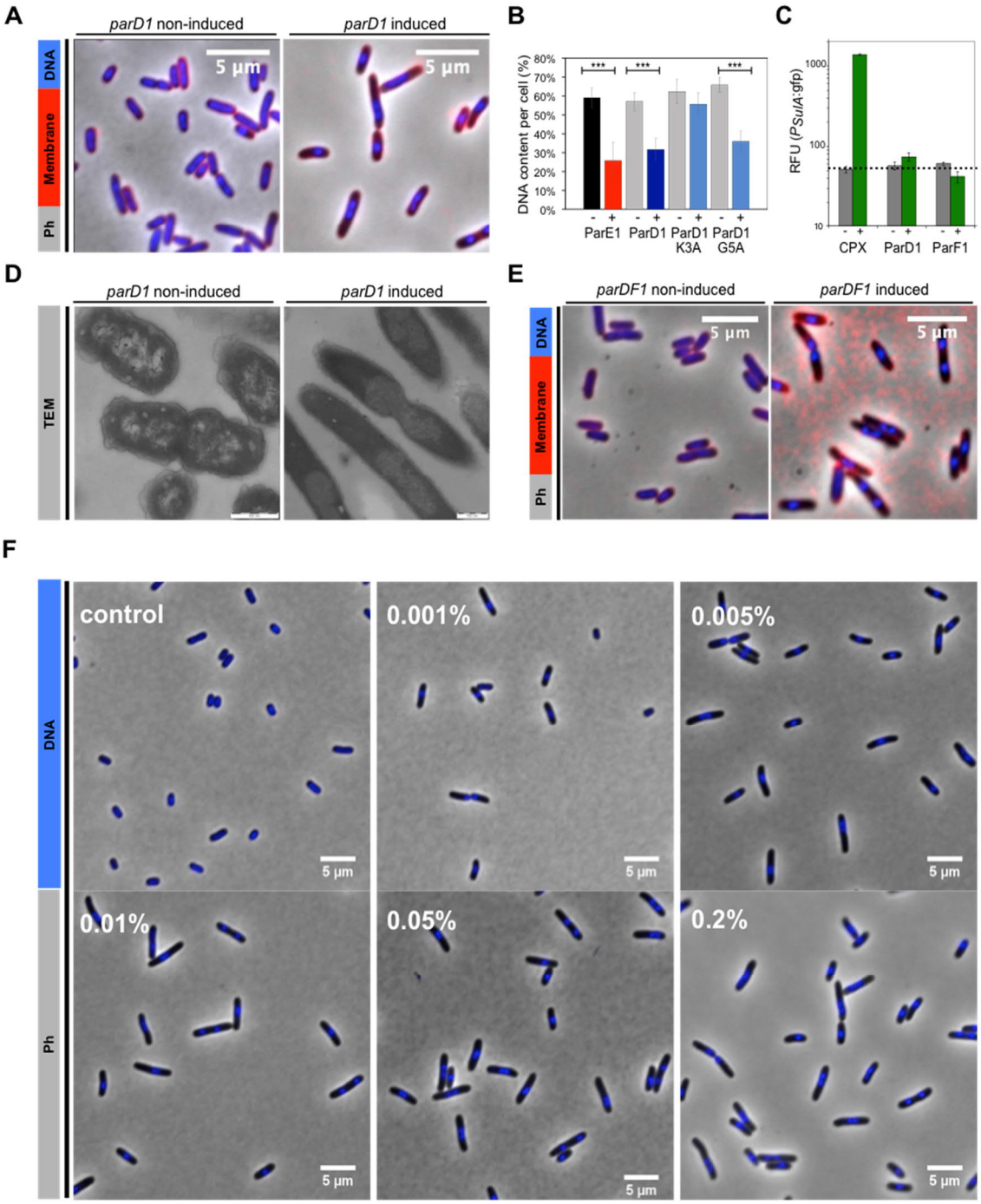

Figure 1.7: The ParD1 has an effect on cell division in *E. coli*.
A. Cells from the experiment described in **1.4B**, 2 hours upon ParD1 expression were stained with FM4-64 (membranes; red) and Hoechst (DNA; blue) and visualized by fluorescence and phase contrast (Ph) microscopy. Expression of ParD1 led to mild cell elongation and DNA condensation. **B.** The DNA content per cell was quantified from experiments described in **1.2A**, **1.4B** and **1.4D**. ParE1 (red bar), ParD1 (dark blue bar), or ParD1 G5A expression (light blue bar) led to a significant reduction ($p \leq 0.05$) of DNA content in comparison with the non-induced conditions (black and grey bars) while the less toxic ParD1* K3A variant presented statistically insignificant differences. **C.** Exponentially growing *E. coli* cells (*λatt::psulA-gfp*) harboring either *parD1* or *parF1* under the P_{rha} control were grown as described in **1.4B** and expression was induced (green bar) or repressed (grey

bar) for 2 hours, to measure the GFP signal. The SOS response was not induced by the proteins tested. Ciprofloxacin (CPX) treated samples were used as controls. The data was normalized to the OD_{600nm} measurements and relative fluorescence units (RFU) were plotted in a log_{10} scale. Error bars represent standard deviation of at least three biological replicates. **D.** *E. coli* cultures from **1.4B** were prepared for transmission electron microscopy (TEM). Expression of ParD1 led to nucleoid condensation in the cell pole and cells are slightly elongated in comparison with the non-induced conditions. TEM analysis was performed in collaboration with the Central Facility for Microscopy, at The Helmholtz Centre for Infection Research, Braunschweig, Germany. **E.** *E. coli* cells from the experiment described in **1.6A** were prepared for fluorescence and Ph microscopy as described in A. Co-expression of ParD1 and ParF1 led to the same phenotype observed in A, however two condense DNA molecules were more prominently observed. **F.** Cells from the experiment described in **1.6B** were also observed by fluorescence microscopy and Ph and the DNA condensation pattern got stronger as the concentration of the ParD1 inductor increased.

ParDE1 migth be a dual toxin-antitoxin system

The previous results indicated that both ParE1 and ParD1 are toxic for the cells **(Figure 1.2A, 1.3 and 1.4B)** and ParD1 efficiently counteracts ParE1 toxicity **(Figure 1.2D)**. The findings also revealed that in the natural host ParD1 toxicity is stronger in the absence of the chromosomal ParE1 copy **(Figure 1.3B)**. Therefore, I speculated that ParE1 could also act as an antitoxin of ParD1. In order to test this hypothesis, I have performed growth rescue experiment in *E. coli* harboring two vectors; *parE1* in the low copy vector pBAD33P_{ara} and *parD1* in the high copy vector pAH160P_{rha}. This time, I grew the cells under repression conditions until mid-exponential growth phase, and then split the culture in two and independently induced either ParE1 or ParD1. A 10^2-fold reduction in CFU ml^{-1} was detected upon 3 hours of only ParE1 expression **(Figure 1.8A left panel, light red line)**. I assumed that the smaller effect when only ParE1 is expressed could be due to the small quantities of ParD1 coming from the leakiness of the promoter being enough to partially counter ParE1 toxicity **(Figure 1.8B)**, or small amounts of glucose inside the cells that still partially repress expression of P_{ara}. Conversely, when ParD1 was co-expressed after 1 hour of ParE1 expression there was a 10^6-fold reduction in CFU ml^{-1} **(Figure 1.8A left panel dark red line)**. These results suggested that the ParE1 effect plus overloaded quantities of ParD1 do not rescue growth but kill *E. coli* faster, therefore a cumulative defect in growth was evident **(Figure 1.8A left panel)**. Interestingly, when only ParD1 was induced, there was a 10^7-fold reduction in CFU ml^{-1} after 3 hours **(Figure 1.8A right panel, dark blue line)**, but when ParE1 is co-expressed after 1 hour of ParD1 expression the cells resumed growth **(Figure 1.8A right panel, light blue line)**. We therefore conclude that ParE1 can counteract ParD1 toxicity. This is further supported by another growth rescue experiment with the same strain wherein the ParD1 molecule was expressed from the beginning of the experiment. Even though ParD1 disturbs the fitness of the cells, the leakiness of the vector that harbors the ParE1 molecule resulted to be enough to reach 10^4 CFU ml^{-1} **(Figure 1.8C).** At this point, when ParE1 was

expressed the cells tend to grow better **(Figure 1.8C),** and much better when the ParE1* L47A non-toxic variant was induced **(Figure 1.8D).** In summary, these data suggest that ParD1-ParE1 constitutes a dual toxin-antitoxin system where ParE1 prevents and reverses ParD1 toxicity, while ParD1 prevents but does not reverse ParE1 toxicity.

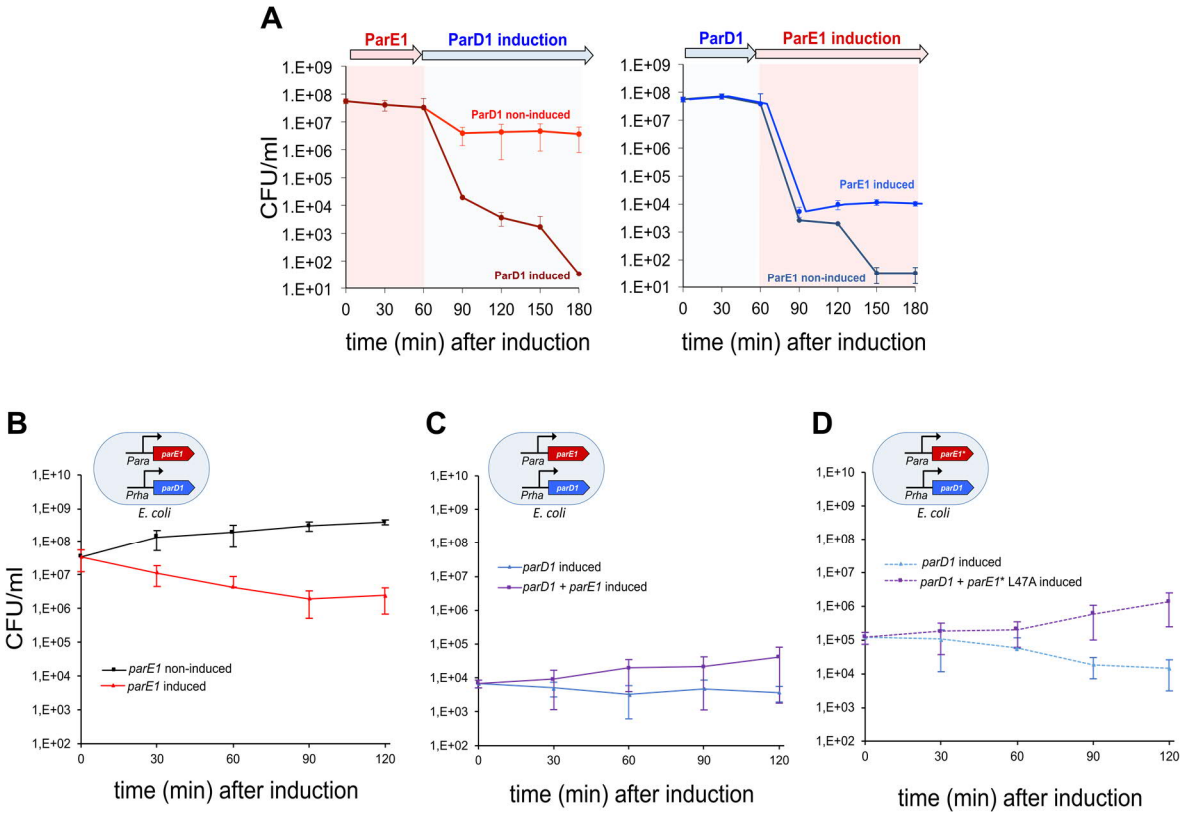

Figure 1.8: Expression of either ParD1 or ParE1 lead to effects in cell viability. ParE1 toxicity is not rescued by co-expression of ParD1 while the ParD1 effect in growth is rescued by co-expression of ParE1.

A. Exponentially growing *E. coli* cells harboring *parE1* (TTG-SD6) under the P_{ara} control and *parD1* under P_{rha} control were grown under repression conditions (0.2% glucose), divided in two cultures (time zero), washed twice and re-suspended in fresh LB media containing either 0.2% of arabinose to induce the ParE1 expression (right figure) or 0.2% rhamnose to induce ParD1 (left figure). After one hour, cells were washed again and re-suspended in fresh LB media containing the same (light red or dark blue) or the opposite (dark red or light blue) sugar to co-express the second molecule. ParD1 did not rescue the ParE1 effect on the cells (dark red line, right figure) and the CFU ml^{-1} decreased even more than when only ParE1 was expressed (light red line, right figure). Conversely, ParE1 rescue ParD1 toxicity (light blue, left figure) while the CFU ml^{-1} continued decreasing when only ParD1 was expressed (dark blue, left figure). **B.** Exponentially growing cells harboring the *parE1* (TTG-SD6) under the P_{ara} control and *parD1* under the P_{rha} control were divided in two (time zero): half of the culture served as a control (black line) while the second half was treated with 0.2% arabinose (red line). ParE1 expression caused a CFU ml^{-1} reduction. **C.** *E. coli* cells from B were grown under ParD1 expression conditions (0.2% rhamnose), until mid-exponential growth phase and then divided in two: half of the culture served as a control (blue line) while the second half was expressed with 0.2% arabinose (purple line). ParD1 had an effect in growth since cells only reached 10^4 CFU ml^{-1}, co-expression of ParE1 rescued this effect. **D.** Exponentially growing *E. coli* cells harboring the *parE1** L47A (TTG-SD6) less toxic variant under the P_{ara} control and *parD1* under the P_{rha} control, were grown and experiments were performed as C. ParD1 has an effect in growth while the ParE1* L47A variant seemed to better rescue ParD1 toxicity in comparison with the wild type ParE1 (C). M.Sc Frederik Kramer contributed to the death prevention experiments.

3.2 The *S. pyogenes parDE2* Operon Encodes a Bona-Fide Toxin-Antitoxin System

Bacteria often encode several TA copies within the chromosome, yet the role of redundant copies belonging to the same TA family is not well understood. *S. pyogenes* encodes two ParDE-like TA systems and this section describes the characterization of the bicistronic *parDE2* operon. The results indicated that *parDE2* is a bona-fide TA system that does not cross talk with the *parDEF1* module. Furthermore, ParE2 was less toxic than ParE1 in *E. coli* while it appeared to be more toxic in the absence of the antitoxin chromosomal copy in *S. pyogenes*. Interestingly, ParD2 also displayed toxicity when solely expressed in *S. pyogenes,* but this characteristic was not detected in *E. coli* where the potential native target might be absent. The ParD2 non-canonical activity correlates with the ParD1 toxicity described in the section 3.1. Overall, these findings provide more insights into the mechanism TA systems use to modulate bacterial behavior. The questions addressed in this section also highlight the importance of designing better molecular tools to understand the ParDE-like mechanisms and their roles in the natural host *S. pyogenes*.

The *parDE2* locus is an operon conserved among *S. pyogenes* serotypes

Two genes typically comprise the second ParDE-like TA system encoded in the chromosome of *S. pyogenes* **(Figure 2.1A)** and RT-PCR analysis have confirmed their operon architecture (**Figure 2.1B)**; *SPy_1926* is the first gene of the operon encoding the putative ParD2 antitoxin protein and *SPy_1927* the second gene encoding the putative toxin, named ParE2. Eleven nucleotides of the end of the antitoxin gene overlap with the start of *parE2* toxin gene-encoding region. Analysis of previously reported transcriptome data of our model organism (Le Rhun et al., 2017) showed low levels of *parDE2* expression at mid-exponential growth phase in rich media (Le Rhun et al., 2017), indicating that this TA system is active but might not play a pivotal role under normal growth conditions **(Figure 2.1A)**.

The *parDE2* locus as well as its surrounding genomic context had high sequence similarity among different *S. pyogenes* serotypes (> 82% of identity) **(Figure 2.2C).** Upstream of the *parDE2* operon are several genes involved in sugar metabolism, while downstream putative genes implicated in transcription and a putative DNA integrase are encoded **(Figure 2.2C)**. The presence of the hypothetical DNA integrase gene may imply the foreign origin of this TA locus as an integrative element that has remained over the evolution of *S. pyogenes* species.

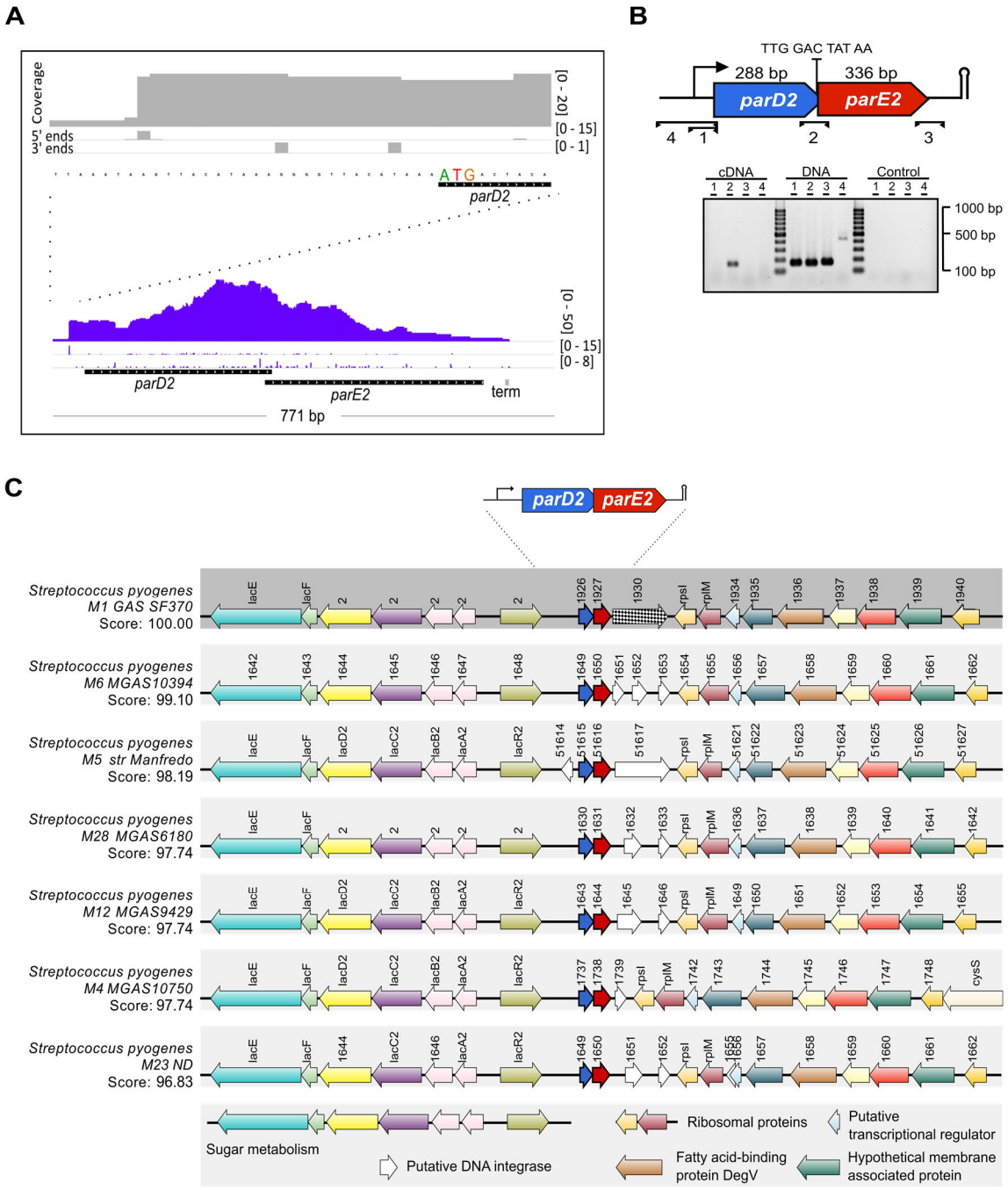

Figure 2.1: parDE2 is an operon conserved among S. pyogenes serotypes.
A. RNAseq analysis revealed that the *parDE2* locus is co-transcribed in the *S. pyogenes* M1 GAS (expression signal depicted in purple). The coverage of reads and the coverage of the 5' and 3' ends are given into brackets (image captured from Integrative Genomics Viewer) (Robinson et al., 2011; Thorvaldsdottir et al., 2013). The red box indicates the predicted Rho-independent terminator (TransTermHP v2.07 prediction downloaded from Le Rhun et al., 2017). Analysis performed in collaboration with Dr. Anaïs Le Rhun from the Max Planck Unit for the Science of Pathogens. **B.** The *parDE2* operon architecture was confirmed by RT-PCR analysis: *parD2* antitoxin in blue, *parE2* toxin in red. 11 nucleotides overlap the antitoxin and toxin sequences. Gene sizes are shown above the open reading frames (ORFs) and lines with arrows below the ORFs represent RT-PCRs performed. The genes *parD2* and *parE2* formed a bicistronic operon (positive PCR line 2 and negative PCR line 1, 3 and 4 from cDNA). Positive (DNA) and negative (water) controls are also showed. **C.** The *parDE2* operon is conserved among different *S. pyogenes* serotypes and the genomic context includes a

putative DNA integrase and genes involved in sugar metabolism among others depicted in colors. A BLAST-base analysis was performed using SyntTax web server (http://archaea.u-psud.fr/synttax).

ParDE2 is a bona fide TA system

In order to test whether the predicted TA system is functional, I made use of the same strategy applied to characterize the *parDEF1* TA operon (described in section 3.1). With the aim to compare the toxic phenotype of ParE2 with ParE1, I maintained the same features when cloning the *parE2* gene in the low copy plasmid pBAD33P_{ara}, including 6 nucleotides left between the ribosome binding side and the methionine-encoding triplet (SD6). However, due to the less toxic phenotype observed with the *parE2* TTG native start codon, the experiments were instead performed with the ParE2 (ATG-SD6) variant, which was shown to be toxic when induced in the heterologous host *E. coli* in comparison with the non-induced conditions **(Figure 2.2A).** Interestingly, unlike the results of ParE1 expression, ParE2 expression did not lead to a constant reduction in CFU ml^{-1}, which might suggest a different mechanism by which ParE2 acts in *E. coli* **(Figure 1.2A)**. Moreover, the randomly acquired L48A mutation permitted growth, suggesting the importance of the L48 residue for ParE2 toxicity or stability (**Figure 2.2A).** Next, I was interested on the characterization of the *E. coli* phenotype after two hours of ParE2 expression, which resulted in a less prominent cell elongation phenotype in comparison with ParE1 **(Figure 1.2C)**, while the DNA appeared to be present over the whole cell area (**Figure 2.3B)**.

Next, I determined the antitoxin activity by cloning *parD2* in the low copy vector pZE12P_{lac}. However, a complete depletion of ParE2 toxicity when co-expressed together with the pZE12P_{lac} empty vector was observed (data not shown), while the addition of only the inductor IPTG did not reduce ParE2 toxicity. I hypothesized that the pZE12P_{lac} effect on rescuing the ParE2 toxicity might be due to the effect the toxin has on the cells, essentially ParE2 toxin may interfere with plasmid replication/transcription. This might also explain why ParE2 is less toxic than ParE1, since it could be affecting its own expression. Experiments with the high copy pAH160P_{rha} empty vector also showed depletion of the ParE2 toxicity **(Figure 2.2C)** but to a lesser extent in comparison with pZE12P_{lac}, allowing further studies. Therefore, the putative antitoxin *parD2* was cloned into pAH160P_{rha} and co-transformed with the toxin in the pBAD33P_{ara} vector. Cells were grown under antitoxin expression conditions with rhamnose and at mid-exponential growth phase only half of the culture was induced with arabinose to produce the toxin, while the second half served as a control. As expected, co-expression of ParD2 efficiently counteracted the toxicity of its cognate toxin ParE2 **(Figure**

2.2D) confirming its antitoxin capacity. Furthermore, in order to study the antitoxin-toxin interaction I cloned and induced in *S. pyogenes*, the extra-chromosomally N-terminus FLAG-tagged ParD2 variant that efficiently retained the antitoxin function **(Figure 2.2E)**. ParD2 was pulled-down and MS analysis confirmed that ParD2 interacts with ParE2 *in vivo* (data not shown). Overall, the ParE2 toxicity, the ParD2 capacity to prevent ParE2 activity and the ParD2-ParE2 interaction *in vivo* confirmed that ParDE2 is a bona-fide TA system.

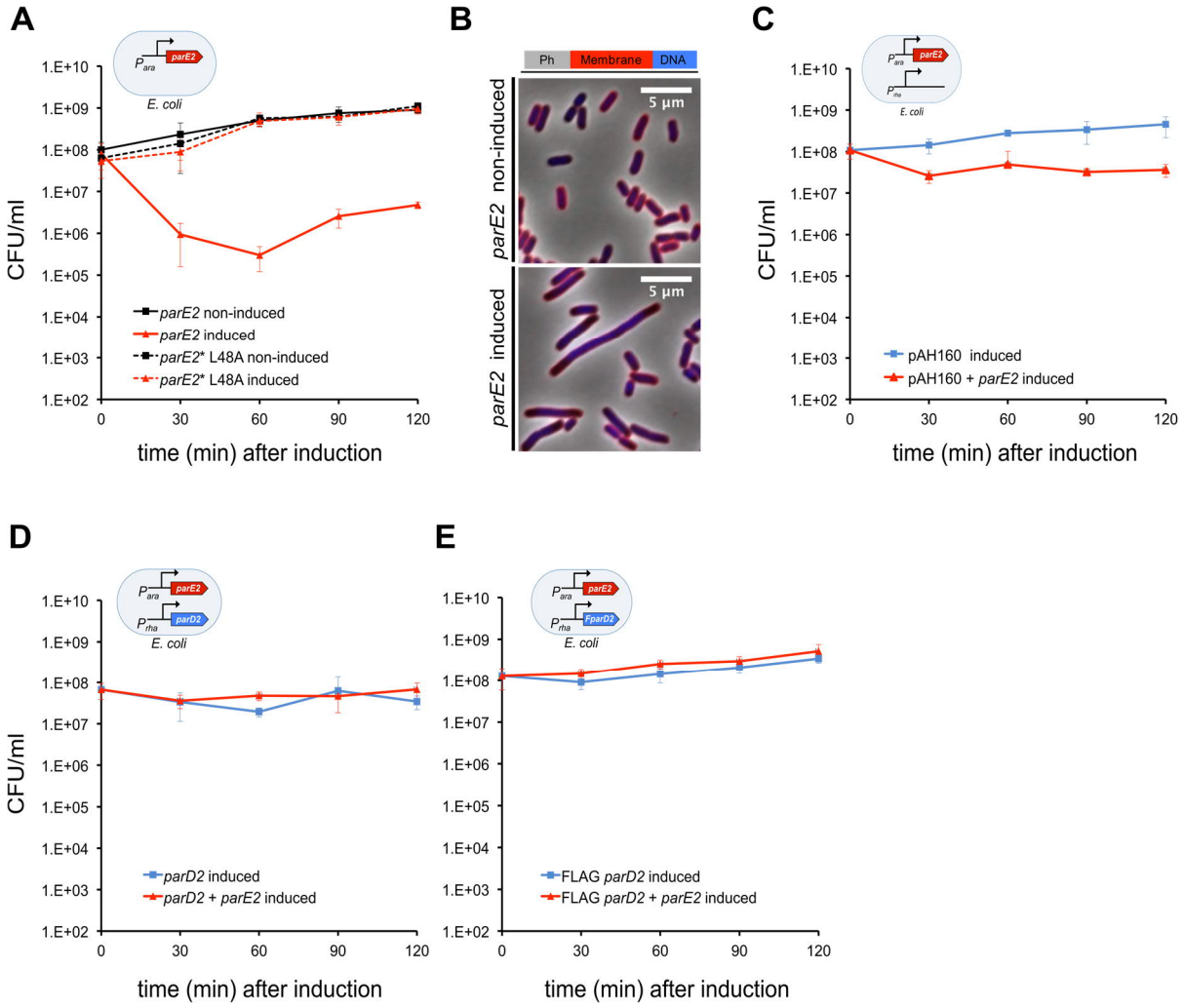

Figure 2.2: *parDE2* is a bona-fide TA system.

A. Exponentially growing *E. coli* cells harboring the toxin *parE2* (ATG-SD6) under the P_{ara} control were divided in two (time zero); half was treated with 0.2% D-glucose to repress P_{ara} (black) while 0.2% of arabinose was added to the second half (red) to induce toxin expression. The CFU ml^{-1} were counted every 30 min during 2 hours. Expression of the ParE2 toxin for one hour resulted *E. coli* abrogation of growth while after 2 hours of ParE1 expression the cells seemed to resume growth. The toxin ParE2* L48A variant did not have a detrimental effect in the cells (red and black dotted lines). Error bars represent the standard deviation of at least three biological replicates. **B.** Samples from A 120 minutes after ParE2 (ATG-SD6) expression were stained with FM4-64 (membranes; red) and Hoechst (DNA; blue) and observed by fluorescence and Ph microscopy. The toxin ParE2 led mild cell elongation and nucleoid condensation indicating that DNA-topology and cell division were

strongly affected. Representative images are shown. **C.** Exponentially growing *E. coli* cells in LB media supplemented with 0.2% rhamnose harboring *parE2* (ATG-SD6) under the P_{ara} control and the pAH160 empty vector under the P_{rha} control were divided in two (time zero): half of the culture served as a control and the second half was induced with 0.2% arabinose. Induction of the ParE2 expression led to a reduction of CFU ml^{-1}. **D.** The death prevention experiments in exponentially growing *E. coli* cells harboring *parE2* (ATG-SD6) under the P_{ara} control and *parD2* under the P_{rha}, control were performed as described in C, pre-expression the ParD2 protein. ParD2 expression efficiently prevents ParE2 toxicity. **E.** Death prevention experiment performed as described in C, pre-expression the N-terminal FLAG-tag ParD2 protein showed that it prevented ParE1 toxicity. M.Sc. Frederik Kramer contributed to the death prevention experiments.

ParDE2 does not cross talk with the ParDE1 TA system

TA cross talk has been reported for some TAs in different bacteria between modules that belong to different families (Walling and Butler, 2016; Wessner et al., 2015). Moreover, studies of TA paralogs in *E. coli* 0157:H7 have revealed cross talk between the chromosomal CcdB toxin that is neutralized by the plasmidic CcdA antitoxin, while the plasmidic toxin is not neutralized by the chromosomal antitoxin (Wilbaux et al., 2007). Conversely, evidence of cross talk was neither detected in between the two chromosomal *parDE* loci from *V. cholerae* (Yuan et al., 2011) nor among the three *parDE* loci encoded by distinct but paralogous TA loci in *Caulobacter crescentus* (Fiebig et al., 2010). I aimed to study the putative cross talk that might exist between the two ParDE-like TA systems from *S. pyogenes.* A certain level of antitoxin and toxin similarity is required for the cross interaction to occur between two TA modules. Protein sequence alignments have revealed that the TA molecules from both systems are not homologs since ParE toxins share 26% identity while ParD antitoxins share only 21% identity **(Figure 2.3A and 2.3B)**. This observation implied that each antitoxin would be able to only counteract the toxicity of its cognate toxin and not the ParE-like toxin belonging to the second locus. To confirm our *in silico* predictions, mismatched pairs of toxin from the second locus and antitoxin from the first locus and vice versa were introduced into *E. coli* and their effects on growth and viability were assayed as described above in the death prevention experiments. As shown before **(Figure 1.4B)** ParD1 is toxic in *E. coli*, therefore the starting point of this experiment is 10^4 CFU ml^{-1}, due to its deleterious effect. From this time point onwards, the ParE2 toxic phenotype was not rescued by the previous presence of ParD1 in the cells **(Figure 2.3C)**. Moreover, it was obvious that ParE2 did not rescue the ParD1 effect either **(Figure 2.3C)**, in comparison with the cognate ParE1-ParD1 pair **(Figure 1.9C)**. To further investigate this phenomenon, the same experiment with the opposite set up was performed and ParD2 was not able to fully prevent the ParE1 toxicity either **(Figure 2.3D)**. Finally, pull down experiments in *S. pyogenes* and MS analysis did not detect ParE2 when ParD1 was induced **(Figure 1.2G)**, indicating that ParDE1 and ParDE2 do not interact *in vivo*.

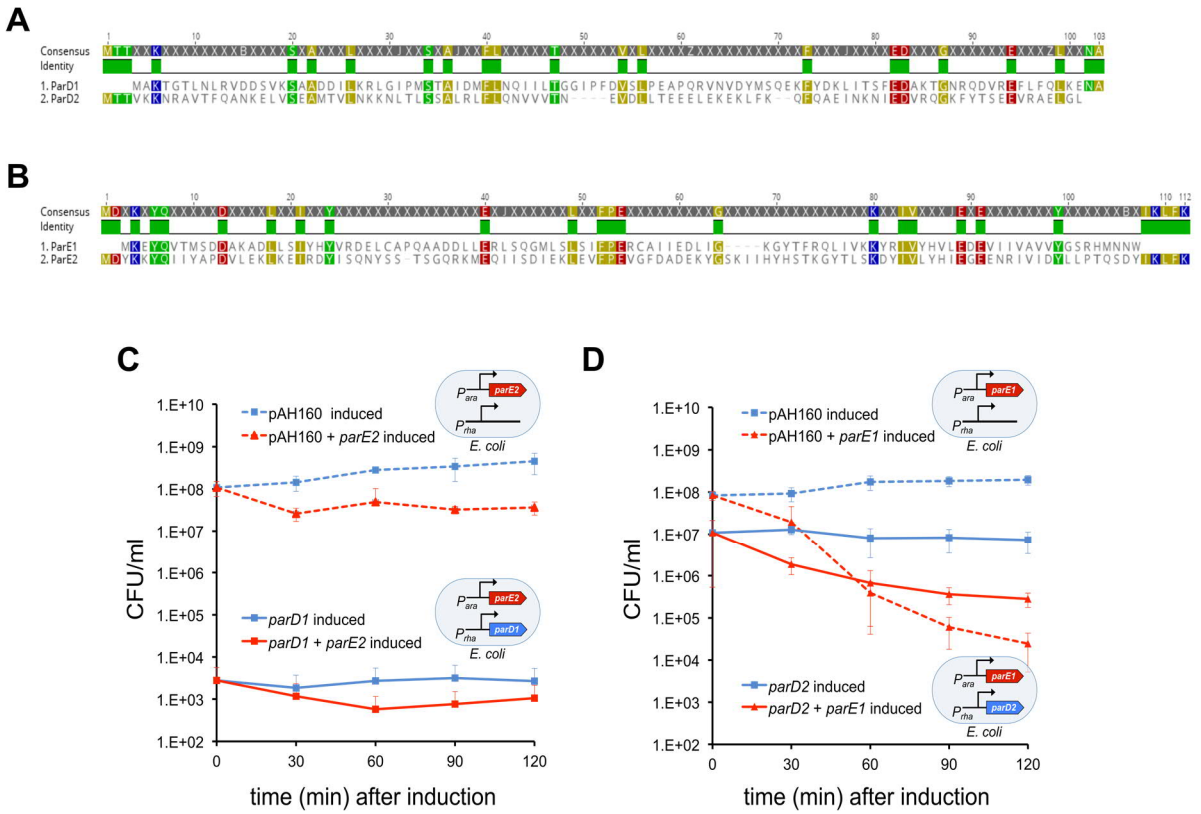

Figure 2.3: ParDE1 and ParDE2 do not cross talk in the heterologous host *E. coli*

A-B. Protein alignments highlighting the most conserved residues in colors. The proteins compared A. ParD1 and ParD2, or B. ParE1 and ParE2 were not highly conserved. **C.** ParE2 growth prevention experiments by the ParD1 non-cognate antitoxin. Two independent experiments are shown: i) Control experiment performed as described in **2.2C**, cell harboring *parE2** (ATG-SD6) under the P_{ara} control and the pAH160P_{rha} empty vector showed one fold change CFU ml^{-1} reduction upon ParE2 expression. ii) Cell harboring *parE2* (ATG-SD6) under the P_{ara} control and *parD1* under the P_{rha} control were grown and experiment was performed as described in **2.2D**. The growth effect of ParD1 pre-expression was again evident and there was CFU ml^{-1} reduction upon ParE2 expression, which suggested non-cross interaction of ParD1 and ParE2. **D.** ParE1 growth prevention experiments by the ParD2 non-cognate antitoxin. Two independent experiments are shown: i) Control experiment performed as described in **2.2C**, cell harboring *parE1* (TTG-SD6) under the P_{ara} control and the pAH160P_{rha} empty vector showed 4 fold change CFU ml^{-1} reduction upon ParE1 expression. ii) Cell harboring *parE1* (TTG-SD6) under the P_{ara} control and *parD2* under the P_{rha} control were grown and experiment was performed as described in **2.2D.** ParD2 did not prevent ParE1 toxicity.

Overexpression of the antitoxin ParD2 causes cell division halt in *S. pyogenes*

As it has been previously described in section 3.1, I also aimed to assess the ParDE2 TA function in the natural host *S. pyogenes*. For this purpose, I studied the growth of the wild type and *ΔparDE2* mutant strain upon extra-chromosomal expression of each TA component from the low copy vector pEC85P_{tet} under the control of the tetracycline promoter. As for ParE1, cloning the wild type ParE2 led to random mutations. The ParE2* L48A variant with the native start codon (TTG) did not show toxicity in wild type liquid cultures **(Figure 2.4A)**.

Conversely, ParE2* L48A (start codon ATG) variant leads to a non-toxic phenotype in *E. coli* **(Figure 2.2A),** but reduced growth in liquid *S. pyogenes* wild type strain cultures **(Figure 2.4B)**. This phenotype did not hold when the experiment was performed in solid media in the wild type strain **(Figure 2.4C)**; namely, expression of ParE2* L48A (start codon ATG) did not reduce CFU ml^{-1}. Conversely, expression of the same ParE2* L48A (ATG) variant led to non-viable cells when transformed in the *ΔparDE2* mutant strain **(Figure 2.4D)**. These findings could suggest that ParE2 needs the chromosomal antitoxin molecule to prevent its effect and that the toxicity can be rescued in the wild type background.

Moreover, I assessed the antitoxin phenotype in *S. pyogenes* by following the same methodology. Surprisingly, expression of N-terminal FLAG-tagged ParD2 that retained its antitoxin activity **(Figure 2.2E)** also led to a toxic phenotype in both the wild type strain and the *ΔparDE2* mutant strain **(Figure 2.4C and 2.4D)** that was not preliminary observed when performing the experiments in *E. coli* **(Figure 2.2)**. As for ParD1 **(Figure 1.3A and 1.3B)**, it is expected that the chromosomal copy of the toxin could rescue the detrimental effect of the antitoxin in the wild type strain. However, the putative capacity of ParD proteins to block the transcription from its own operon should be taken into consideration when expressing this molecule. High quantities of ParD2 could potentially reduce the transcription of *parD2* but also *parE2* toxin from the chromosome. This could explain why the ParD2 expression from the plasmid quickly kills the wild type strain.

Unexpectedly, plasmidic expression of the whole *parDE2* operon also led to a detrimental effect on growth in both the wild type and in the *ΔparDE2* mutant strain **(Figure 2.4C and 2.4D)**. Largely, these data do not conclude the canonical TA function ParDE2 should have; instead, these findings highlight an unknown missing piece that we have not considered in the natural host. In addition, these findings support the idea that equal plasmidic amounts of toxin- antitoxin molecules will not be sufficient to lead to growth rescue, highlighting the importance of validating the TA bona-fide function by varying the different levels of molecule expression in the natural host.

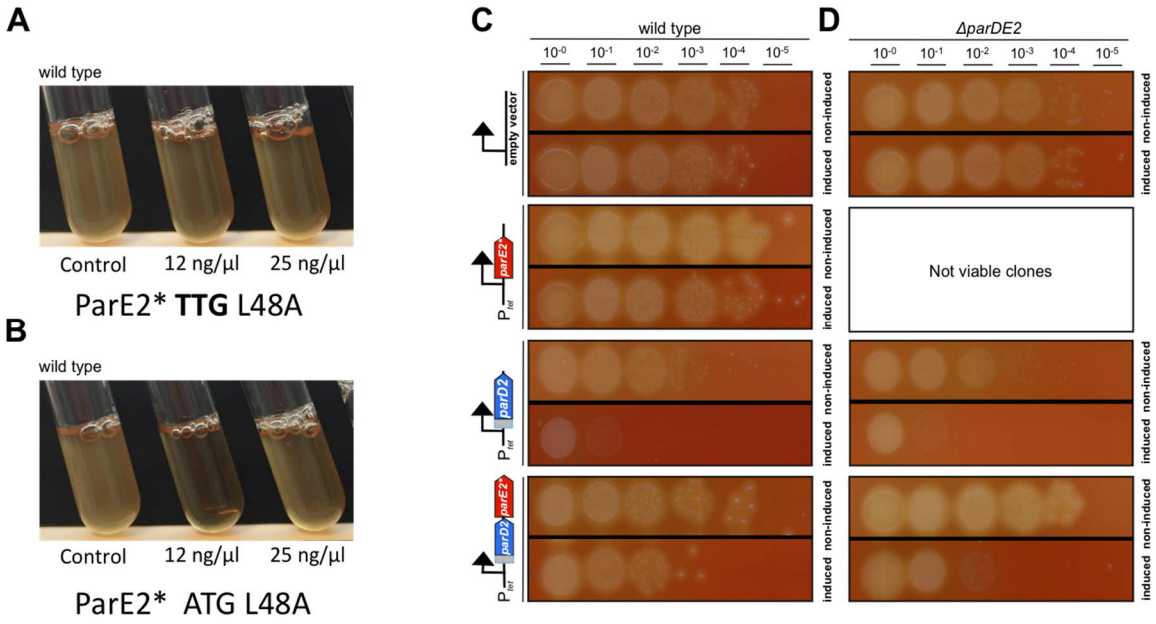

Figure 2.4: Both ParE2 and ParD2 have a deleterious effect in *S. pyogenes.*

A-B. *S. pyogenes* overnight cultures of cells harboring the pEC85P$_{tet}$ empty vector or harboring either *parE2** (TTG L48A) (A) or *parE2** (ATG L48A) (B) were normalized to the same optical density (OD$_{620nm}$ 0.2), and 1/100 dilution was inoculated in fresh THY media without or with the inducer AHT (12 or 25 ng ml^{-1}). The *parE2** (ATG L48A) expression showed to be more toxic than the *parE2** (TTG L48A) variant. **C-D**. *S. pyogenes* overnight cultures of either wild type cells (C) or *ΔparDE2* mutant background (D), harboring the pEC85P$_{tet}$ empty vector or either *parE2** (ATG L48A), N-terminal FLAG-tagged *parD2* or N-terminal FLAG-tagged *parD2-parE2* under the control of the tetracycline promoter, were normalized to the same optical density (OD$_{620nm}$ 0.2), and serial dilutions (10^{-1} to 10^{-5}) were spotted in TSA-blood with and without the inductor (AHT 50 ng ml^{-1}). Induction of the FLAG-tagged ParD1 expression and the whole ParDE2 operon led to reduce CFU ml^{-1} in both strains, while transformation of *parE2** (ATG L48A) led to not viable clones in the *parDE2* mutant background.

The non-canonical ParD2 toxicity does not affect *E. coli*

In order to further characterize ParD2, I investigated the ParD2 protein features and confirmed that ParD2 is similar to ParD1 in terms of the two main domains typical of ParD-like proteins **(Figure 2.5A)**. As ParD1, ParD2 harbors the RHH fold in the N-terminal, which is hypothesized to bind DNA (Oberer et al., 2002); it also contains the putative toxin-neutralization domain in the C-terminus with a rather structured conformation composed by two well-defined α-helical shapes **(Figure 2.5A)**. This feature shared with ParD1 could lead to a more stable protein as it has been previously described for other antitoxins (Dalton and Crosson, 2010). Similar to ParD1, ParD2 has no special features that could explain its toxic influence. Finally, phylogenetic studies grouped ParD2 in a cluster composed by hypothetical proteins belonging to other *S. pyogenes* strains, **(Figure 1.5B)**.

Next, the detrimental effect of the antitoxin was assessed in *E. coli* by growth arrest experiments. For this purpose, I used the high copy vector pAH160P$_{rha}$ previously used for the death prevention experiments. As depicted in **Figure 2.5B**, expression of ParD2 did not lead to a decrease in CFU ml^{-1} in comparison with the non-induced conditions. I have also tested the toxicity of the N-terminal FLAG-tagged ParD2 variant that displayed detrimental effects in *S. pyogenes*, and did not observe toxicity upon expression in *E. coli* (**Figure 2.5C).** Taken together this information implied that ParD2 only has a negative effect in its natural host when overexpressed ectopically. Further experiments are needed to confirm that the ParD1 and ParD2 phenotypes are not an artifact due to the artificial expression from a plasmid in the natural host. Expression of the TA molecules from the *S. pyogenes* chromosome should be considered, especially to study the native ParD target.

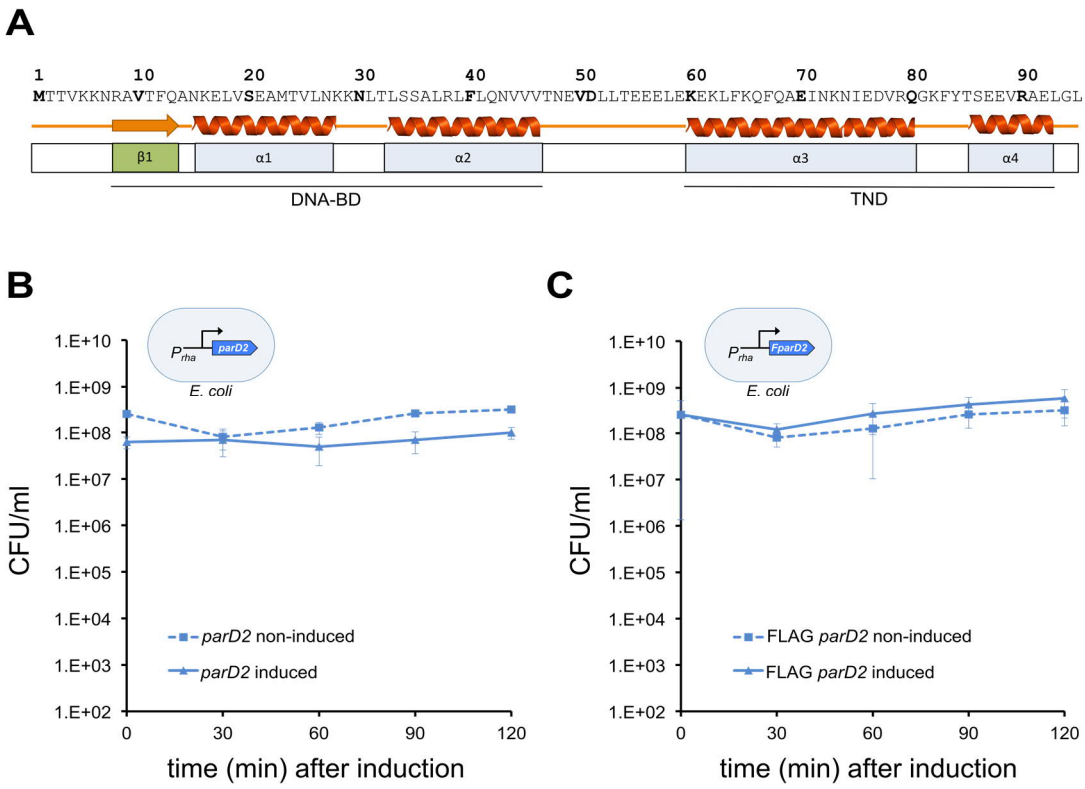

Figure 2.5: ParD2 is not toxic in *E. coli*

A. The ParD1 secondary structure prediction obtained from the SWISS-MODEL tool (Waterhouse et al., 2018), showed a β-sheet (β1: orange arrow) and two α-helix (α1, α2: orange spirals) on the hypothetical DNA-binding (DNA-BD) domain located at the N-terminus while two α-helix (α3, α4: orange spirals) on the putative toxin neutralization domain (TND) at the C-terminus of the protein. **B-C.** Killing assays performed as described in **1.4B**, *E. coli* exponentially growing cultures harboring either *parD2* (B) or N-terminal FLAG-tagged *parD2* (C) under the P$_{rha}$ control of promoter, indicated that ParD2 and FLAG-tagged ParD2 expression did not have any impact in *E. coli* growth.

3.3 ParE1 and ParE2 Arrest DNA Replication by Targeting Gyrase and Topoisomerase IV

Typical ParE toxins affect DNA topology by interacting with the DNA gyrase leading to double strand breaks that will induce cell elongation and eventually lead to cell death. The phenotypes observed upon ParE1 (section 3.1) and ParE2 (section 3.2) expression in *E. coli* - mainly cell elongation and nucleoid condensation - correlate with this hypothesis. In this section, I described the characterization of the ParE1 and ParE2 targets by *in vivo* studies in *E. coli* and *in vitro* assays. Assuming that multiple copies of the putative target will prevent killing by ParE1 or ParE2, we co-expressed each toxin together with either gyrase, its homolog topo IV or each of their subunits, to evaluate death prevention. We observed prevention of ParE1 and ParE2 toxic effect in the cells when co-expressed with topo IV E. These results implied that the ParE toxins could potentially interact and inhibit topo IV, a characteristic that has not been characterized yet for this toxin family. Moreover, I provided evidence that all ParE-like toxins tested indeed abrogate topoisomerase IV activity *in vitro*. On the other hand, co-expression of gyrase together with either ParE1 or ParE2 toxins caused stronger killing implying a gyrase poisoning effect by the toxin, which was a characteristic shared with the ParE3 toxin from *E. coli*. Interestingly, *in vitro* studies showed that ParE1, ParE2 and ParE3 from *E. coli,* indeed poison gyrase similar to a typical CcdB toxin. Furthermore, different phenotypes and killing ratios observed upon expression of *S. pyogenes* ParE proteins and ParE-like homologs from other organisms in *E. coli,* prompted us to hypothesize that their target affinities towards gyrase and/or topo IV might vary. Collectively, this chapter expand the view and diversity of mechanism employed by TA modules to control bacterial behavior.

The ParE1 and ParE2 toxicity is modulated upon co-expression of topoisomerases

The DNA condensation and cell elongation phenotype that we observed upon ParE1 and ParE2 expression in *E. coli* **(Figure 1.2C and 2.2C)** is in agreement with the phenotype observed in the coccoid *S. pyogenes* when ParE1 is expressed **(Figure 1.3D).** This phenotype generally observed is typical when cells experience DNA damage (Fiebig et al., 2010; Harms et al., 2015). A similar phenotype is common for other ParE-like proteins that influence DNA replication, stability and topology by targeting DNA gyrase (Gupta et al., 2016; Hallez et al., 2010; Jiang et al., 2002; Yuan et al., 2010). We speculated that multiple copies of the putative target in the cell could potentially rescue cell growth upon ParE expression by capturing and thereby inactivating the toxin and thereby allowing the free molecules of the target to fulfill their physiological function. We explored this hypothesis by growth rescue experiments, co-

expressing the *S. pyogenes* ParE toxins from the P_{ara} inducible promoter located on one vector and from a second vector under the P_{rha} control either the whole gyrase protein or its subunits: gyrase A or gyrase B (Harms et al., 2015). Co-expression of either ParE1 or ParE2 toxins with only one of the two-gyrase subunits had no effect on cell survival **(Figure 3.1A and 3.1B)**. Conversely, co-expression of the full complex of gyrase AB with either ParE1 (**Figure 3.1A)** or ParE2 (**Figure 3.1B)** exhibited an additive effect, which resulted in a stronger phenotype instead of rescuing the growth, namely cells died faster than cells in which only ParE1 or ParE2 was expressed. This result suggest that the gyrase function is poisoned by ParE1 and ParE2, which results in unrepaired double stand breaks and thus cell killing.

The topoisomerase IV (topo IV) shares sequence, folding and function similarity with gyrase (Sissi and Palumbo, 2010). In fact, other toxins such as FicT have been shown to target both enzymes: gyrase and topo IV (Harms et al., 2015). Only one report correlated the topo IV and gyrase inhibition activity with different *E. coli* ParE synthetic peptides *in vitro* (Barbosa et al., 2012). Thus, I decided to test whether co-expression of topo IV and its subunits topo IV E or topo IV C will modulate the ParE1 and ParE2 effect on cell growth **(Figure 3.1A and 3.1B)**. Expression of the whole topo IV enzyme and topo IV C did not have an effect on ParE1 **(Figure 3.1A)** neither on ParE2 **(Figure 3.1B)** toxicity. Nevertheless, expression of the topo IV subunit E rescued growth upon expression of both toxins in comparison with the control conditions where expression of either of the two ParE-like proteins resulted in cell death **(Figure 3.1A and 3.1B)**. This observation suggests that the ParE toxins from *S. pyogenes* also target topo IV and that an excess of the topo IV E subunit prevents ParE1 and ParE2 toxicity, implying a putative toxin-topo IV E protein interaction.

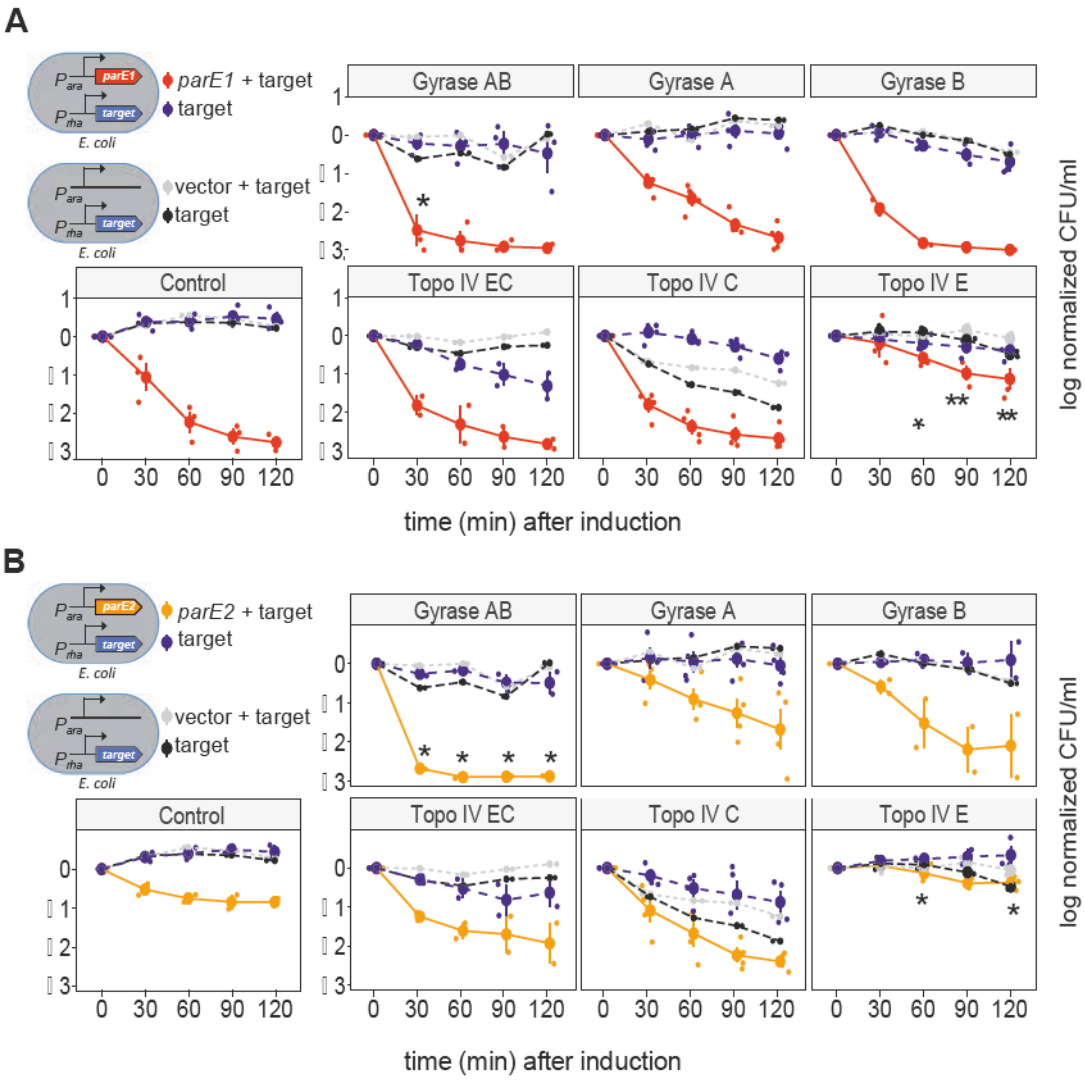

Figure 3.1: Co-expression of ParE-like toxins with either topo IV E or gyrase modulate ParE1 and ParE2 toxicity.

A-B. Two independent experiments are shown in each panel: i) To account for growth defects due to target expression, exponentially growing strains carrying pAH160P_{rha} with each target and the pBAD33P_{ara} empty vector were grown under target expression conditions until mid-exponential growth phase (time-zero): half of the culture served as a control (black line) while the second half was treated with arabinose 0.2% (grey line) and the CFU ml^{-1} were followed for 2 hours. The topo subunit C has an effect in growth in comparison with the control conditions where non-target was tested. ii) *E. coli* cells harboring the toxin *parE1* (TTG-SD6) (A) or *parE2* (ATG-SD6) (B) under the P_{ara} control and each of the potential toxin targets under the P_{rha} control in the pAH160 vector were grown under target expression conditions until mid-exponential growth phase (time zero). Half of the culture served as a control (blue line) and the second half was treated with arabinose 0.2% to induce the toxin (A. *parE1:* red line, B. *parE2:* yellow line) and the growth was followed as previously described. Pairwise comparison using t-test was performed to determine the significance between the toxin-expression conditions with and without the target (control). Co-expression of gyrase AB and either ParE1 (A) or ParE2 (B) resulted in faster killing ($p < 0.05$) while the topo IV subunit E prevented killing by ParE1 (A) and ParE2 (B) ($p < 0.05$) in comparison with the control conditions where only the toxin was expression. Error bars denote standard error of at least three biological replicates and CFU ml^{-1} normalized to time zero are plotted in log_{10} scale.

ParE-like toxins have similar effects in *E. coli*

The effect of ParE-like proteins have on the topo IV activity has not been characterized, yet. To test whether *S. pyogenes* ParE proteins are unique in their ability to target topo IV and gyrase or whether this is a general characteristic of ParE-like toxins, we compared the ParE1 (SPyParE1) and ParE2 (SPyParE2) with closely related homologs. To select ParE-like candidates we performed protein sequence-base comparisons, retrieving all the toxin sequences belonging to the RelE/ParE superfamily from the TABD database (Xie et al., 2018). Principal component analysis branded the toxins in two different clusters: ParE and RelE **(Figure 3.2A)**. The differences between the two clusters are independent of the taxonomical assignment. We confirmed that SPyParE1 and SPyParE2 belong to the ParE superfamily **(Figure 3.2A)**, wherein some of its most similar counterparts previously characterized are ParE3 from *E. coli* (EcParE3) (Hallez et al., 2010), ParE2 from *M. tuberculosis* H37Rv (MtbParE2) (Gupta et al., 2016) **)** and ParE1 and ParE2 from *Vibrio cholerae* (VcParE1 and VcParE2) (Yuan et al., 2010). Earlier reports suggest that MtbParE2 has a bacteriostatic effect since it damages the ATPase activity of the gyrase subunit B (Gupta et al., 2016), while EcParE3 and VcParE2 are bactericidal due to their putative interaction with the gyrase DNA binding side, subunit A (Hallez et al., 2010, Yuan et al., 2010), which leads to unrepaired double strand breaks.

To obtain a better insight on the toxicity of the ParE-like molecules in *E. coli*, I performed killing experiments and DNA damage assessment upon expression of each toxin protein. For this purpose, I also included the well characterized CcdB protein from *V. fisheri* (VfCcdB) that strongly effects gyrase as a control (Yuan et al., 2010). In general, SPyParE1 and VfCcdB presented similar killing rates upon expression, while EcParE3 reduces viable cells less prominently **(Figure 3.2B)**. Strikingly, MtbParE2 did not kill the standard strain *E. coli* MG1655; instead MtbParE2 only kills TOP10 cells at a similar ratio when compared with EcParE3. Moreover, SPyParE2 and VcParE2 had a weaker effect on growth, while VcParE1 had almost no effect. Next, I evaluated the DNA damage upon toxin expression. A typical ParE-like toxin will activate the SOS-response, a cascade of genes whose expression is triggered in order to respond to DNA breaks and allow correct DNA replication (Baharoglu and Mazel, 2014). SulA is one of the proteins strongly expressed upon DNA-damage who stops cell division by binding to FtsZ monomers, the initiating protein in this process (Justice et al., 2000; Mukherjee et al., 1998). The strain *E. coli* MG1655 AT15 (*λatt::*P_{sulA}*-gfp*) wherein the promoter of the gene *sulA* has been fused to the GFP-encoding gene was used to evaluate the SOS-response. In addition, Ciprofloxacin (CPX), which is an antibiotic that arrest DNA

replication and triggers SOS response, was used as a control for this experiment. As shown in **Figure 3.2C**, SPyParE1 strongly induced the SOS-response in comparison with the non-induced conditions, and this effect is similar but less prominent in the CPX treated conditions and upon expression of SPyParE2, EcParE3, VcParE2 and VfCcdB **(Figure 3.2C)**. Interestingly, even with weaker killing ratios, the toxins still prominently induced the SOS response. The weaker phenotype upon SPyParE2 and VcParE2 expression might be potentially rescued by the *E. coli* SOS response so it does not have a strong influence on growth. Conversely, the resilient effect that CPX, SPyParE1 or VfCcdB have in the cells might lead to unrepaired DNA strand breaks and therefore cells die faster.

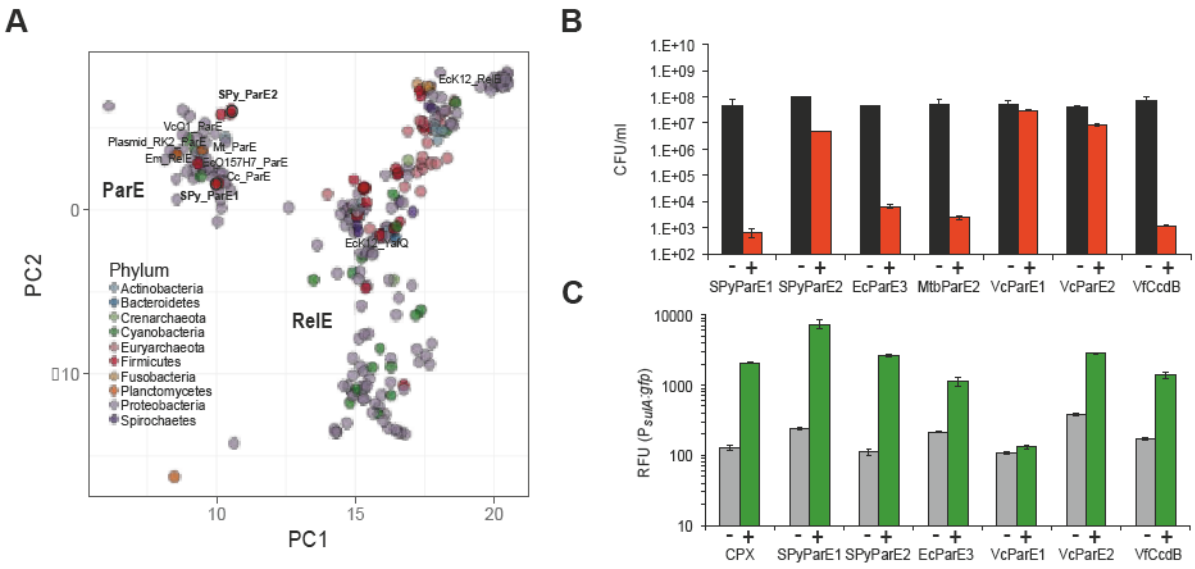

Figure 3.2: Expression of ParE1-like toxins lead to similar phenotypes in *E. coli*.

A. Principal component analysis of the ParE/RelE family members retrieved form the TADB database (Xie et al., 2018) showed that this toxin family is more abundant in proteobacteria and the members are not grouped by phylum. SPyParE1 and SPyParE2 clustered with typical ParE-like toxins such as EcParE3, MtbParE2, VcParE1 and VcParE2. Analysis performed in collaboration with Dr. Eric JC. Galvez from the Max Planck Unit for the Science of Pathogens **B.** Exponentially growing *E. coli* cells harboring SPyParE1 (TTG-SD6), EcParE3 (ATG-SD6), MtbParE2 (TTG-SD6) or VfCcdB (TTG-SD6) and in less extent SPyParE2 (ATG-SD6), VcParE1* (TTG-SD6), VcParE2* (TTG-SD6) under the P_{ara} promoter displayed reduction of CFU ml^{-1} 1 hour after toxin expression (red bars) in comparison with non-expressed conditions (black bars). Error bars represent standard deviation of at least three biological replicates **C.** Exponentially growing *E. coli* cells (*λatt::psulA-gfp*) harboring each toxin under the P_{ara} control were grown as described in Figure 1C and expression was induced (green bar) or repressed (grey bar) for 2 hours, to measure the GFP signal. The SOS response was induced by all proteins tested, except for VcParE1*. CPX treated samples were used as controls. The data was normalized to the OD_{600nm} measurements and relative fluoresce units (RFU) were plotted in a log_{10} scale. Error bars represent standard deviation of at least three biological replicates.

If the ParE toxins preferentially target one topoisomerase or another, the phenotypical outcome could potentially differ upon toxin expression. Namely, an effect on gyrase will lead

to high nucleoid condensation and an effect on topo IV mainly to cell elongation and unsegregated DNA (Harms et al., 2015; Kato et al., 1990). In order to explore the phenotype, I compared cells under the microscope after two hours of each toxin expression **(Figure 3.3)**. The control conditions have shown normal cell size of around 2 µm while the DNA molecule was spread over the cell area, similar to the VcParE1 expression conditions, which did not display toxicity, consistent with the SOS response and growth arrest results **(Figure 3.2B and 3.2C)**. SpyParE1 seemed to have the greatest effect as the cells showed stronger cell elongation and a highly compact nucleus while SPyParE2 and EcoParE3 led to milder cell elongation and a different DNA pattern **(Figure 3.3)**. The nucleoid condensation was a consistent phenotype also observed in cells treated with CPX and upon VfCcdB expression, wherein cell elongation was not as prominent as when SPyParE1 was expressed **(Figure 3.3)**. Moreover, expression of VcParE2 and MtbParE2 (TOP10 *E. coli* cells) led to less cell elongation while the DNA pattern looked normal **(Figure 3.3)**. These data indicate that ParE-like toxins could potentially harbor different affinities or dissimilar targets.

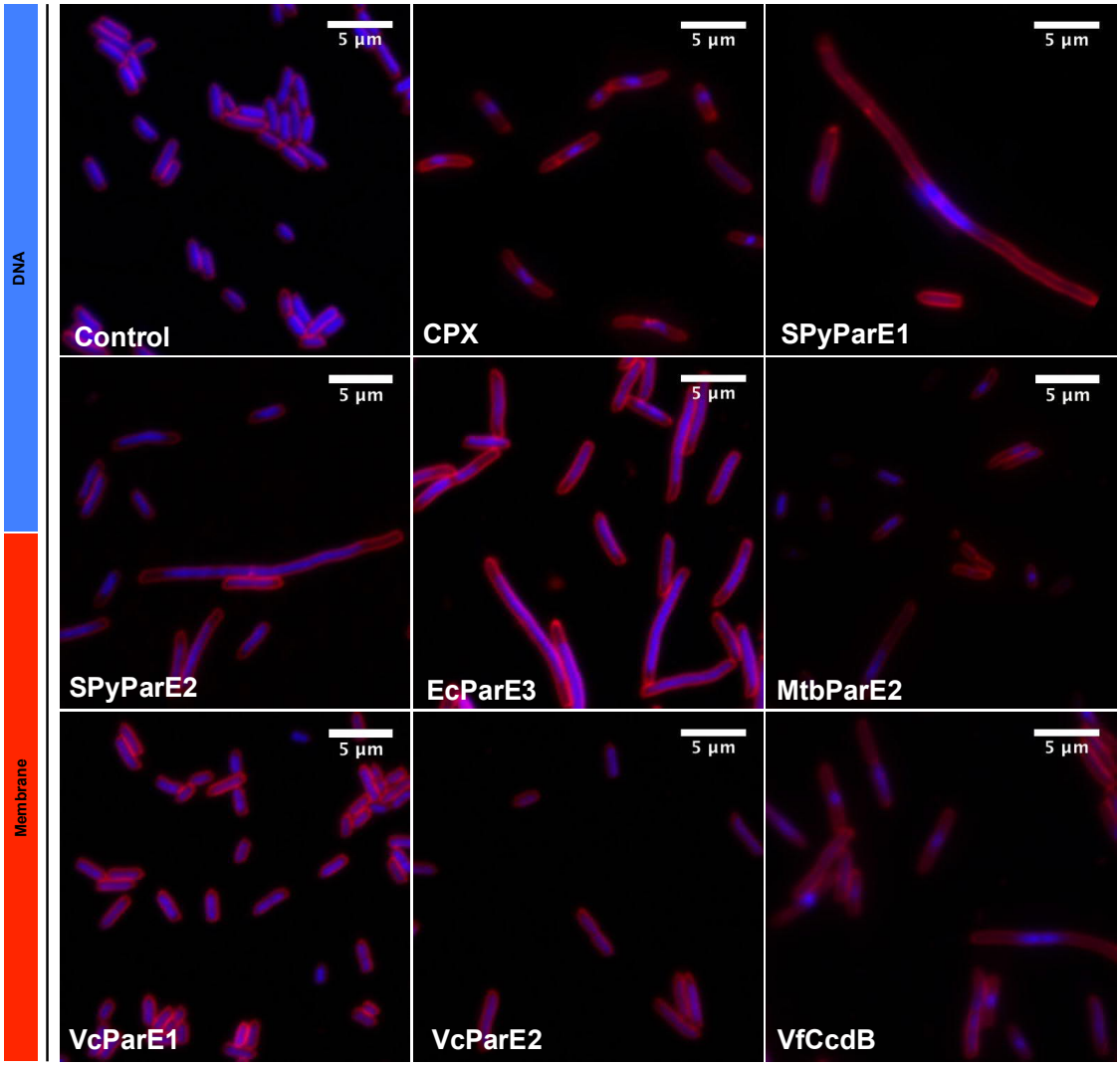

Figure 3.3: Expression of ParE1-likes proteins lead to strong phenotypes in *E. coli.*

Fluorescence microscopy of samples from **3.2B**, 120 minutes upon toxin induction showed cell elongation and nucleoid condensation upon induction of each toxin and in a less extent under CPX, MtbParE2, VcParE1 and VcParE2 treated conditions. Sample preparation was performed as described for **1.2C**. Representative pictures are shown.

Other ParE-like toxins are counteracted by Topo IV subunit E

In order to further investigate whether the toxicity of SPyParE1 and SPyParE2 is an exclusive characteristic modulated upon co- expression of gyrase and topo IV E, I performed growth rescue experiments under putative target expression in comparison with the homolog EcParE3 and the unrelated toxin VfCcdB. Co-expression of EcParE3 and either the full gyrase complex or each of the gyrase subunits led to similar killing as for SPyParE1 and SPyParE1 **(Figure 3.4)**. It is well known that VfCcdB poisons the gyrase and has a high affinity to gyrase

subunit A the DNA interacting domain involved in cleavage and sealing; as expected, co-expression of gyrase A rescued growth upon VfCcdB expression **(Figure 3.4).** The growth effect by EcParE3 expression was rescued by co-expression of the topo IV subunit E, suggesting that the ability to target topo IV is not exclusive for SPyParE1 and SPyParE1 **(Figure 3.4)**. Topo IV E harbors the ATPase activity; therefore, toxin interaction with this subunit will probably lead to inhibition of the topoisomerase activity. Finally, expression of both the whole topo IV enzyme and topo IV C led to unviable cells even with the leakage of EcParE3 in non-induced conditions, these findings might suggest a particular consequence of EcParE3 that bane the activity of multiples copies of topo IV of topo IV C (**Figure 3.4**). Assuming that all toxins were expressed at the same level under the conditions evaluated here, the results imply that ParE-like toxins might have the same target, but their mechanism of interaction might vary since all toxins shown distinct levels of killing, SOS response induction and phenotypes in *E. coli.*

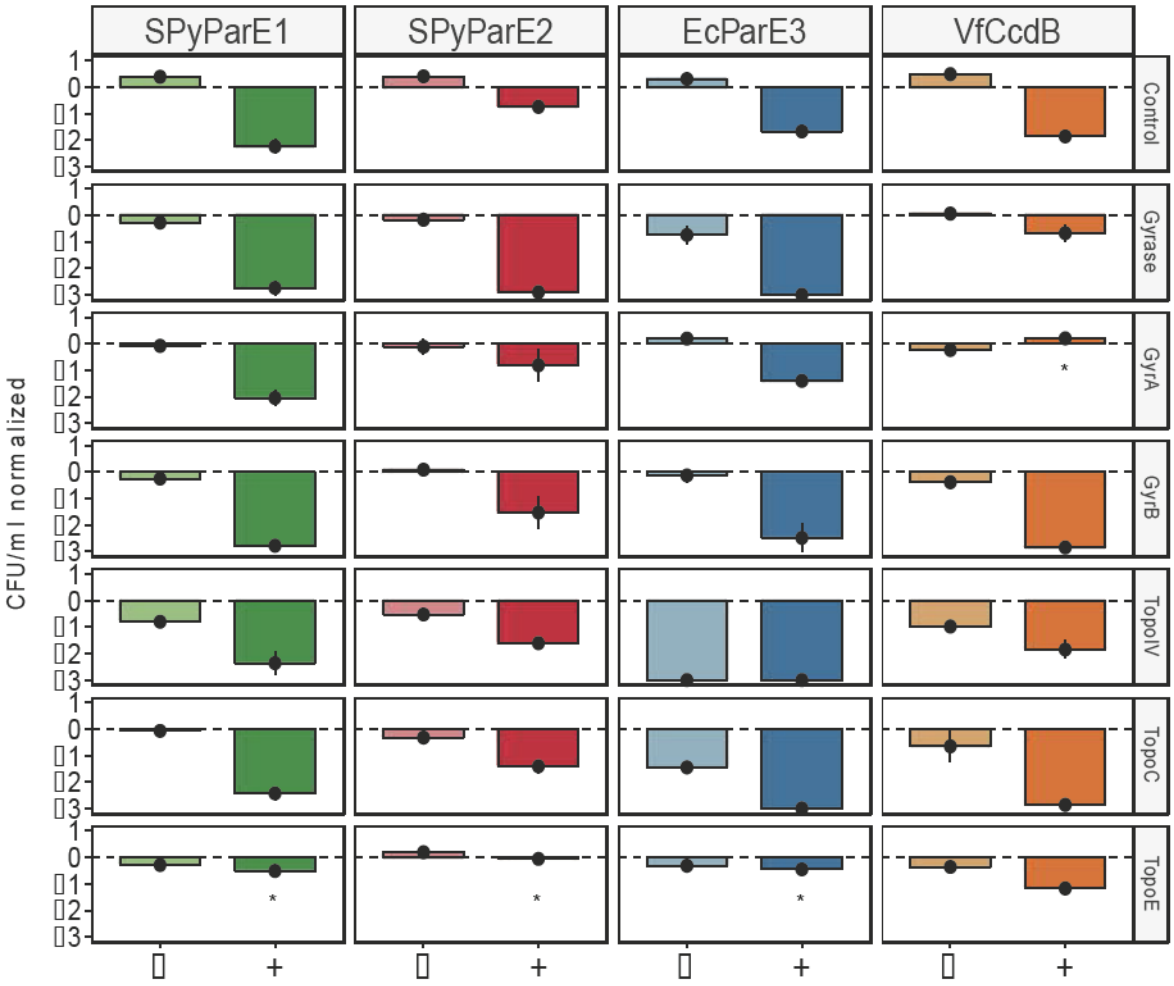

Figure 3.4: SPyParE1, SPyParE2 and EcParE3 toxicity are modulated by gyrase and topo IV E co-expression.

Growth prevention experiments of *E. coli* cells harboring each toxin under the P_{ara} control and each of the putative toxin targets under the P_{rha} control, (as described in 3.1). Data below "0" represented killing, and around "0" or above represented growth. Co-expression of gyrase and SPyParE1, SPyParE2 or EcParE3 led to stronger killing while co-expression of gyrase A and CcdB led to growth. Topo IV E expression prevents the growth effect by SPyParE1, SPyParE2 and EcParE3 expression. Experiments were performed as previously described in Figure 3.3, and the plot represented the CFU ml^{-1} count normalized to time zero (log_{10} scale) upon expression of each toxin for 1 hour. Error bars denote standard error of at least three biological replicates. Pairwise comparison using t-test was performed to determine the significance between the toxin-expression conditions with and without the target (control).

The SPyParE1, SPyParE2 and EcParE3 toxins poison Gyrase and inhibit Topoisomerase IV

SPyParE1, SPyParE2 and EcParE3 might target the gyrase with a putative different mechanism to what have been typically described for CcdB (Bahassi et al., 1999; Bernard and Couturier, 1992; De Jonge et al., 2010), since they appeared to act on the whole gyrase complex. I observed that SPyParE1, SPyParE2 and EcParE3 targeted and potentially can interact with the topo IV subunit E, resulting in inhibition of topo IV. To confirm these *in vivo* findings I performed biochemical assays to analyze the effect of the ParE toxins on the *E. coli* recombinant DNA gyrases and topo IV proteins. I aimed to express SPyParE1 in *E. coli* for protein purification and repetitively acquired random mutations, possible due to the detrimental effect on cell growth. Therefore, I decided to use an *in vitro* translation system to produce the toxin proteins of interest. First, the *E. coli* gyrase supercoiling activity was assessed incubating the recombinant enzyme with a relaxed plasmid substrate in the presence of each toxin. In addition, the topoisomerase interfacial poison CPX that stimulates the formation of DNA cleavage complexes and the catalytic inhibitor novobiocin (NOV), which inhibits the topoisomerase activity were also included. As expected, gyrase alone was able to supercoil a relaxed plasmid, whereas the presence of CPX blocked the gyrase resealing capacity resulting in accumulation of topoisomers of the plasmid while NOV abrogated the gyrase function leading to absence of supercoiled plasmid **(Figure 3.5A)**. Finally, the supercoiled fraction of the substrate was significantly reduced in the presence of SPyParE1, SPyParE2 and EcParE3 similar to what we observed with VfCcdB confirming that all these toxins inhibit the gyrase function.

As mentioned above, topo IV has not been reported as a potential ParE target thus, the effect of the different toxins on the topo IV relaxation activity was tested **(Figure 3.5B)**. In the absence of any drug the expected topoisomers were formed, which indicates normal topo IV activity while in the presence of CPX the linear form accumulates due to the inhibition of

DNA-breaks sealing by topo IV **(Figure 3.5B)**. In contrast, NOV abrogated topo IV activity and the supercoiled form of the plasmid accumulated. The presence of SPyParE1, SPyParE2 and EcParE3 also resulted in the accumulation of supercoiled plasmid, while VfCcdB did not have an effect on the relaxation activity **(Figure 3.5B)**, suggesting that the ParE toxins inhibit topo IV like NOV, which is in concordance with our *in vivo* results **(Figure 3.4)**.

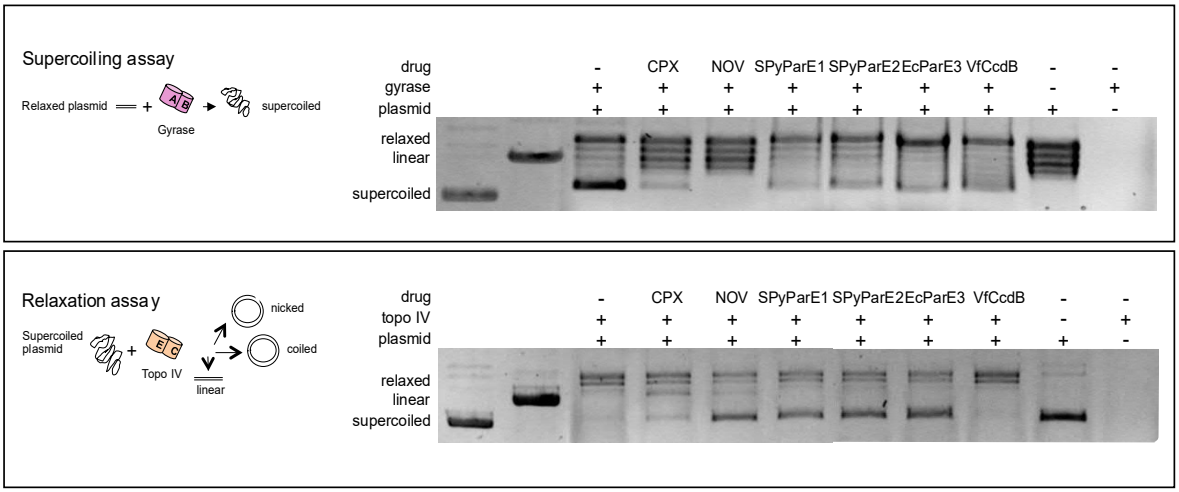

Figure 3.5: SPyParE1, SPyParE2 and EcParE3 target *E. coli* gyrase and topoisomerase IV recombinant proteins

A. The drugs CPX, NOV and the toxins SPyParE1, SPyParE2, EcParE3 or VfCcdB (*in vitro* translated proteins) affected the gyrase capacity to supercoil a relaxed plasmid. **B.** CPX poisoned topo IV when relaxing a supercoiled vector leading to a linear form while NOV, SPyParE1, SPyParE2 and EcParE3 abrogated the topo VI relaxation activity leading to the accumulation of the supercoiled form. VfCcdB did not impair topo IV activity. Representative pictures of at least three biological replicates are shown.

The effect of the more toxic SPyParE1 molecule versus the homolog EcParE3 was also tested with the recombinant gyrase and topo IV proteins from the closely related organism *Streptococcus pneumonia (*Spn). I have also included to these experiments the MtbParE2 molecule that was toxic only in top10 *E. coli* cells **(Figure 3.2 and 3.3**) and is known to be specific towards gyrase subunit B (Gupta et al., 2016). The results indicated that the Spn gyrase partially supercoiled the template in the presence of EcParE3 or MtbParE2, but only SPyParE1 led to the formation of a linear product, which is a typical attribute of a poison that impairs the re-resealing activity of the gyrase **(Figure 3.6A)**. This observation also indicates that SPyParE1 might have more affinity to the Spn gyrase than ParE3 from *E. coli*. Equally, the relaxation experiments revealed the same results obtained with the recombinant topo IV from *E. coli* **(Figure 3.6B).** Importantly, topo IV also has the ability to decatenate DNA molecules, a process that plays an important role in the separation of daughter DNA molecules during cell division (Vos et al., 2011). Therefore, we also studied the decatenation activity of

Spn topo IV on kinetoplast DNA (kDNA) as a substrate. In the absence of drugs, Spn topo IV decatenates kDNA into monomers while CPX, NOV and high concentrations of SPyParE1, EcParE3 or MtbParE2 completely abrogate the decatenation activity, which confirmed that these toxins can inhibit topo IV **(Figure 3.6C).** The results showed that the ParE-like toxins tested can target both gyrase and topo IV, however, their specificity might vary leading to the different phenotypes observed *in vivo*.

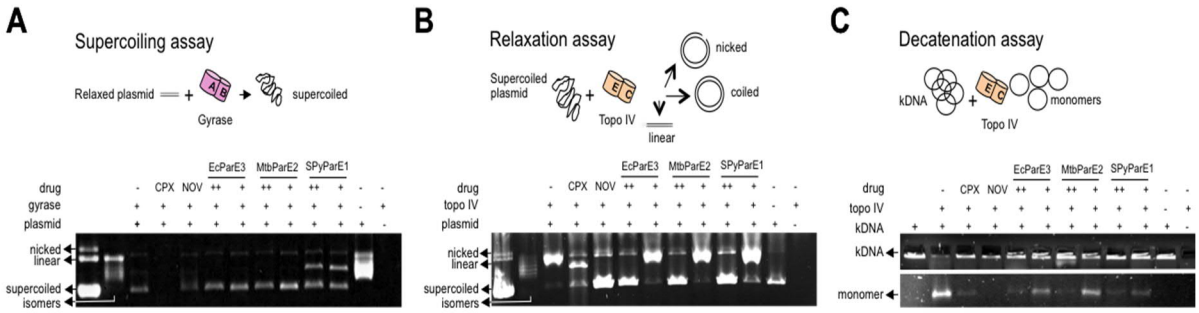

Figure 3.6: SPyParE1 strongly poisons *S. pneumonia* gyrase when compared with ParE counterparts while all ParE-like toxins tested inhibit topo IV activities *in vitro*.

A. The drugs CPX, NOV and two different quantities of EcParE3, MtbParE2 and SPyParE1 (*in vitro* translated toxins) affected the gyrase capacity to supercoil a relaxed plasmid. SPyParE1 strongly poison gyrase leading to the linear from of the vector **B.** CPX poisoned topo IV when relaxing a supercoiled vector leading to a linear form of the vector, while NOV or high concentrations of EcParE3, MtbParE2 or SPyParE1 abrogated the topo VI relaxation activity leading to the accumulation of the supercoiled form of the vector. **C.** In the absence of drugs topo IV decatenates kDNA into monomers while CPX, NOV or high concentrations of EcParE3, MtbParE2 or SPyParE1 abrogated the topo VI decatenation activity leading to the accumulation of the kDNA substrate on the gel wells. Representative pictures of at least three biological replicates are shown.

3.4 The TA Operons *parDEF1* and *parDE2* are Stress Response Elements in *S. pyogenes*

Toxin-Antitoxin systems can provide certain advantages to bacteria, for e.g. biofilm formation, post-segregational killing, abortive infection, and expression of persistence stage have been related to these modules. In this section, I present insights into the role of the two chromosomally encoded ParDE-like TA systems in *S. pyogenes*. First, I assessed the phenotypical characteristics of the *ΔparDE1* and *ΔparDE2* mutants in comparison with the wild type strain and did not find a difference neither in growth nor in biofilm formation, leading to the conclusion that the absence of single TA modules does not impair *S. pyogenes* fitness under these conditions. TA systems are also well defined as stress-response elements. Namely, upon stress, the antitoxin degradation will not only liberate the toxin to inhibit growth, but will also loosen the repression of the TA promoter. Thus, we assessed the TA transcript levels in wild type strain upon exposure to different stress conditions. The findings suggest that both *parDEF1* and *parDE2* are stress response elements up-regulated upon treatment with the multiple factorial inducer ethanol (EtOH) and serine hydroxamate (SHX) that mimics amino acid starvation. In both cases the *parDEF1* mRNA was more abundant than the *parDE2* mRNA. Surprisingly, additional mRNA transcripts below the expected size of the *parDE2* mRNA, were evident upon SHX treatment and absent in the control conditions. We hypothesize that a post-transcriptional regulation of the *parDE2* mRNA might occur upon stress in *S. pyogenes*.

The absence of *parDE1* and *parDE2* does not impair *S. pyogenes* fitness

Redundant TA copies can be found in the chromosome of some bacteria, yet their role is not well understood. Single or multiple deletions of TA modules might not lead to a reduction in fitness when compared with the wild type strain (Shan et al., 2017). However, I wanted to assess this possibility by phenotypical comparisons between the single TA mutants and the wild type strain. First, I studied the fitness of *S. pyogenes* by counting CFU ml^{-1} during the exponential phase of growth. As depicted in **Figure 4.1A** the TA mutants and the wild type strain presented the same growth trend indicating that the lack of each TA module does not affect growth. Moreover, no phenotypically differences were observed by microscopy analysis (data not shown).

The direct correlation of TAs with biofilm formation has been debated due to the multifactorial reasons that lead to the same phenotype in bacteria (Kim et al., 2009; Kolodkin-

Gal et al., 2009). Mutations in the *yafQ/dinJ* TA system, or interruption of the *hipA* toxin gene was reported to result in a prominent decrease in biofilm formation, as well as *mazEF* deletion. In order to assess whether *parDEF1* and *parDE2* affect biofilm formation I grew the cells in polystyrene coated plates at two different temperatures (25°C or 37°C) and quantified the bilayer formed after 24 hours of incubation by coomassie blue staining. No statistical differences were observed when comparing the TA mutants with the wild type strain **(Figure 4.1B and 4.1C)**. Nevertheless, at 25°C the biofilm formation of the *ΔparDE2* mutant tends to be higher implying that ParDE could act as a biofilm repressor (**Figure 4.1C).** Further experiments are required to confirm this phenotype and test whether the lack of *parDE2* favors biofilm formation of *S. pyogenes*.

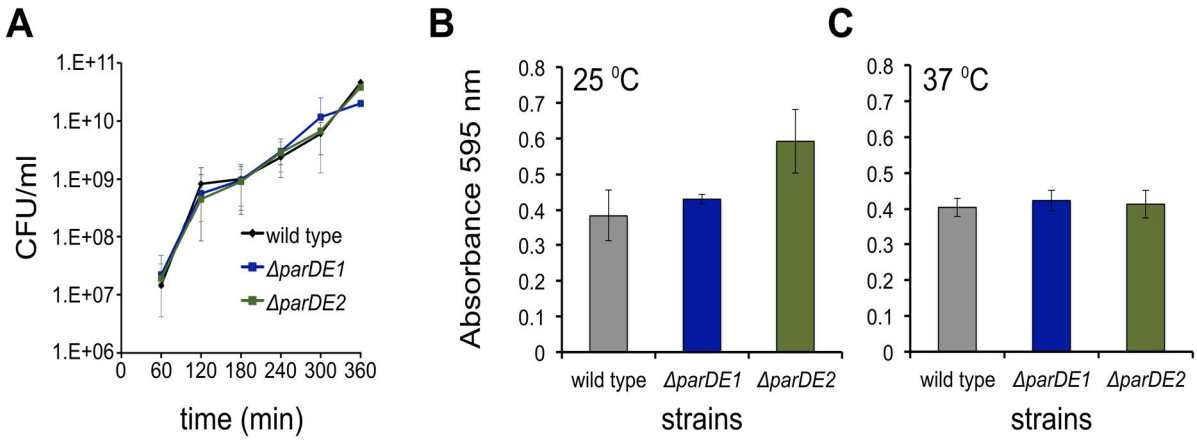

Figure 4.1: The absence of *parDE1* and *parDE2* do not affect *S. pyogenes* growth nor biofilm formation.

A. *S. pyogenes* wild type, *ΔparDE1* and *ΔparDE2* growth curves in THY media showed that the absence of each TA operon did not impair growth. **B-C.** *S. pyogenes* wild type, *ΔparDE1* and *ΔparDE2* biofilm formation experiments were done by growing the cells in polystyrene 96 well plates and quantifying the bio layer (crystal violet) on the bottom after 24 hours of incubation at either 25°C (B) or 37°C (C). The absence of the TA operons did not impair biofilm formation.

ParDEF1 and ParDE2 are stress response elements

As TA systems are also known to be involved in stress response, I aimed to study the *parDEF1* and *parDE2* regulation upon different stress conditions that mimic the conditions *S. pyogenes* might potentially face *in vivo*, e.g. oxidative, osmotic, heat-shock stress and antibiotic treatments. The different stress inducers of these conditions were tested at the selected compound concentrations that did not lead to death but growth arrest **(Figure 4.2A)**. We then added the chosen concentration of each inducer to *S. pyogenes* wild type cultures at early exponential phase of growth, and collected RNA samples at different time points to follow

the TA transcript abundance by performing qRT-PCR of the antitoxin mRNA molecule, assuming that both the antitoxin and the toxin are equally co-transcribed. Conditions such as oxidative and osmotic stress did not trigger *parD1* neither *parD2* mRNA antitoxin expression **(Figure 4.2B and 4.2C)**, unlike the general stress inducer ethanol that caused an increase in abundance of antitoxin mRNA transcripts **(Figure 4.2B and 4.2C)**.

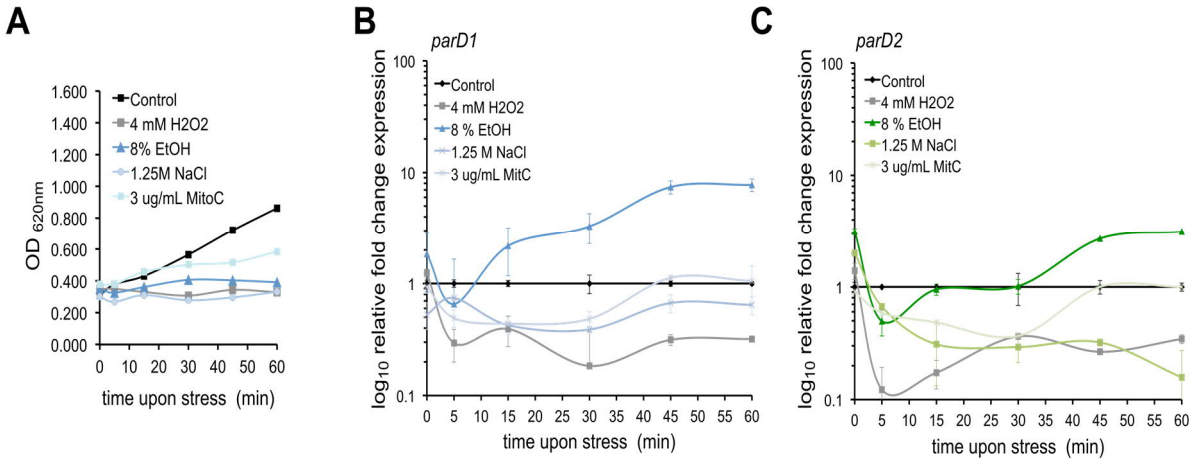

Figure 4.2: The general stress inductor ethanol triggers the *S. pyogenes* TAs transcription.

A. Early exponentially growing cells treated with different stress inducers for one hour, showed to arrest *S. pyogenes* growth (OD_{620nm} followed for one hour). Error bars represent the standard deviation of at least three biological replicates **B-C.** RNA samples were taken from *S. pyogenes* cultures grown until early exponential phase, treated with different stress inducers as described in A. qRT-PCR analysis (using cDNA as template) showed to trigger the *parD1* mRNA (B) and in less extent *parD2* mRNA (C) transcription upon 8% ethanol treatment. The relative fold change was calculated by using the *trfA* housekeeping gene and normalized to the control conditions. Error bars represent the standard deviation of at least three biological replicates**.** M.Sc. Cristian Aparicio contributed to the qRT-PCR analysis.

We wondered whether the concentration of ethanol used was indeed arresting the growth but not killing the cells. Therefore, we added 8% or 10% of ethanol to *S. pyogenes* wild type cultures at early exponential phase and followed growth by measuring the optical density **(Figure 4.3A)** and by counting the CFU ml^{-1} **(Figure 4.3B).** Results confirmed that 8% ethanol was indeed arresting the growth but not leading to cell death. We next quantified the TA mRNA levels, but this time we assessed the antitoxin and toxin mRNA transcripts and found that *parDE1* and to a lesser extent *parDE2* operons are indeed induced by ethanol treatment **(Figure 4.3C)**. In general, the transcriptional induction of TA loci is probably due to the antitoxin degradation by the proteases triggered by stress (reviewed by Harms et al., 2018). We also assessed the expression of the gene encoding the ClpP protease possibly involved in antitoxin degradation in *S. pyogenes* and observed an up regulation under ethanol treatment with the highest expression 5 minutes upon stress induction **(Figure 4.3C)**. Finally, we confirmed our previous observation by Northern blot assays targeting the *parE1* or *parE2*

toxin mRNA and observed that the *parE1* and *parE2* transcripts were evident 15 and 45 minutes upon ethanol addition, respectively **(Figure 4.3D)**. The effect that ethanol might have in the cells is rather general and although this stress is not a physiological condition that *S. pyogenes* is likely to encounter *in vivo*, the results imply that the TAs from *S. pyogenes* might be stress response elements.

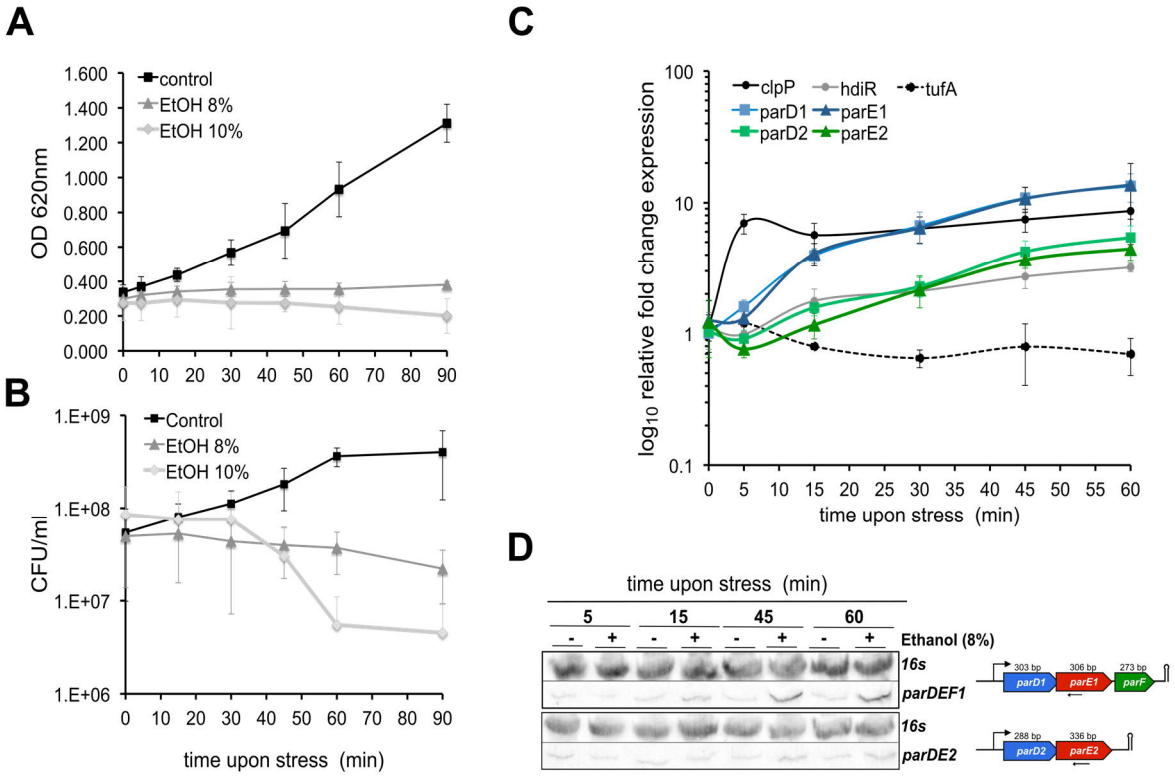

Figure 4.3: The general stress inductor ethanol triggers parDEF1 and parDE2 transcription.

A-B. Growth curve by measuring OD_{620nm} (A) and CFU ml^{-1} counting (B) upon stress induction as described in **4.2**, with ethanol at two different concentrations, revealed that the 8% did not impair growth while 10% killed the cells (B). **C.** RNA samples of cultures treated with 8% ethanol were taken from experiments performed as described in **4.2B-C**, and qRT-PCR analysis (using cDNA as template) showed to trigger *parD1*, *parE1* and in less extent *parD2*, *parE2,* as well as the controls *clpP* and in a less extent *htrA* transcription. Error bars represent the standard deviation of at least three biological replicates. M.Sc. Cristian Aparicio contributed to the qRT-PCR analysis. **D.** The *parDEF1* and in less extent *parDE2* operon are up regulated upon ethanol stress conditions. RNA samples were taken from *S. pyogenes* cultures grown until early exponential phase, treated with 8% ethanol for 1 hour. Northern blot analyses were performed using a probe targeting the 16S rRNA as a loading control and a probe targeting the *parE1* and *parE2* gene, respectably to detect the toxin-antitoxin (TA) mRNAs. A representative picture is shown.

The *parDEF1* and *parDE2* operons are triggered upon amino acid starvation

Next, I decided to separately test each of the cellular consequences potentially caused by high concentrations of ethanol, starting with amino acid starvation, which is the most common condition that triggers TA systems (reviewed by Harms et al., 2018). Serine hydroxamate (SHX) was shown to induce amino acid starvation and has been used to test TA

expression in other bacteria (Christensen et al., 2001b). SHX is an analogue of L-serine that inhibits charging of Seryl-tRNA synthetase and therefore induces the synthesis of ppGpp (guanosine tetraphosphate), which is the master regulator of the stringent response in *E. coli* (Traxler et al., 2008). Different concentrations of SHX were tested to select a quantity that might cause stress without killing the cells **(Figure 4.4A).** Interestingly, all tested concentrations below 15 mg ml^{-1} arrested growth but did not lead to death **(Figure 4.4A).** We selected 5 mg ml^{-1} to further evaluate the TA influence at the transcriptional level **(Figure 4.4B).** In agreement with our previous findings, our preliminary Northern blot analysis using a probe specific for the toxin mRNA demonstrated up-regulation of both *S. pyogenes* TA loci under amino acid starvation **(Figure 4.4B)**. Surprisingly, additional bands below the expected size of the *parDE2* operon were evident 10, 20 and 30 minutes upon SHX addition, but were absent in the control conditions. The mRNA encoding the toxin that is being detected by the probe increased over the time, which might suggest a putative processing of the mRNA.

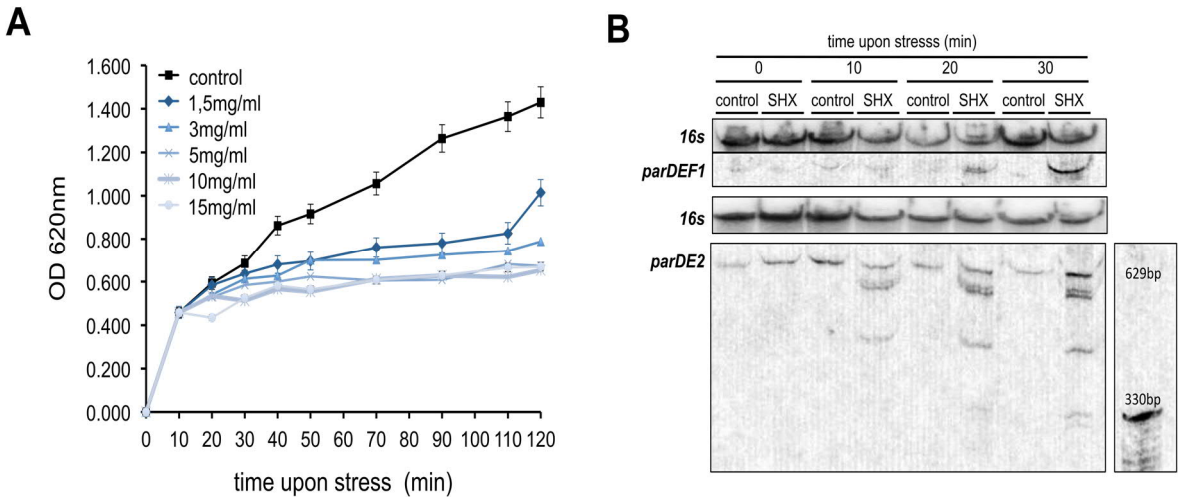

Figure 4.4: The parDEF1 and parDE2 operon expression is up regulated upon amino acid starvation.

A. *S. pyogenes* wild type growth curve by measuring OD_{620nm} upon stress induction with SHX at different concentrations revealed that none of the concentration tested impaired growth. **B.** The *parDEF1* and in less extent *parDE2* operon were up regulated upon SHX stress conditions. The *parDE2* mRNA transcript seemed to be processed since several bands below the mRNA TA transcript size were detected. RNA samples were taken from *S. pyogenes* cultures grown until early exponential phase, treated with SHX 5mg ml^{-1} for 30 minutes. Northern blot analysis were performed using a probe targeting the 16S rRNA for loading control and a probe targeting the *parE1* and *parE2* gene, respectably to detect the toxin-antitoxin (TA) mRNAs. A representative picture of three replicates is shown.

3.5 ClpXP is Responsible for the ParD1 and ParD2 Antitoxin Degradation

In a conventional TA type II system, the antitoxin is a less stable protein prone to degradation by the bacterial proteolytic machinery. This might be the main mechanism by which the toxin is freed to cause an influence bacterial physiology. In this section, I describe the characterization of the ParDEF1 and ParDE2 post-translational regulation through antitoxin degradation. ParD1 and ParD2 proteins were unstable in the wild type strain while stable in the *ΔclpP and ΔclpX* mutant backgrounds, suggesting that the ClpXP proteolytic machinery is implicated in the antitoxin degradation. Moreover, both antitoxins displayed different half-life in the wild type strain. Although the secondary structure prediction hypothesizes rather structured C-terminal domains, the conformation and ClpXP accessibility of certain residues may differ between the antitoxins. Additional factors for antitoxin degradation may be involved; ParF1 could decrease ParD1 stability, since the protein was not detectable when co-induced with ParF1. Finally, the long half-life of the wild type ParD2 was significantly reduced when 15 of the C-terminal residues were removed, indicating the importance of this domain for its stability. Further experiments in different stress conditions and in the presence of the cognate toxin will give us more insights into the activation of these ParDE-like modules.

ParD1 is an unstable protein degraded by ClpXP

To further characterize ParD1 I analyzed the *in silico* protein features that might give an idea of the domain/region which is less stable or prone to degradation by bacterial proteases. As already shown in **Figure 1.4A**, the C-terminal domain of ParD1 is predicted to be structured with a well-defined α-helical shape. This characteristic could lead to a more stable protein structure when comparing it with other antitoxins that typically have intrinsically disordered C-terminal domains (Madl et al., 2006; Oberer et al., 2007). To confirm our bioinformatic predictions, I expressed the N-terminal FLAG tagged ParD1 variant that was previously shown to be an active antitoxin **(Figure 1.2F)** and followed the protein levels in the wild type strain by Western blot analysis after protein synthesis was stopped. As shown in **Figure 5.1A** the antitoxin ParD1 was unstable with a half-life of approximately 20 minutes **(Figure 1.5B)**. In addition to ClpP protease, the Gram-positive bacterium *S. pyogenes* harbors the ClpX, ClpE and ClpC ATPases. In order to identify the protease complexes responsible for the degradation of ParD1, different *clp* mutant backgrounds were constructed. ParD1 showed stability in the in the *ΔclpP* and *ΔclpX* mutants in comparison with the wild type and

ΔclpC and *ΔclpE* mutant strains, suggesting that ClpXP is the protease complex responsible for ParD1 degradation **(Figure 5.1A)**.

Structural flexibility of an antitoxin may not completely explain its susceptibility to proteolysis; specific C-terminal residues may also be implicated in the recognition for degradation. Some reports have identified the presence of ClpX degradation tags in many ClpX substrates, such as: SsrA-tag in streptococci (Tao and Biswas, 2015), the LPF C-terminal domain in *Streptococcus mutants* (Jana et al., 2016) and other ClpXP consensus recognition-signals (reviewed by Baker and Sauer, 2012). The ParD1 antitoxin does not contain any of the known C-terminal ClpXP recognition residues. However, hydrophobic or solvent-exposed regions of the protein may be recognized for degradation too. In order to identify the residues that might be involved in the ParD1 recognition, I performed protein stability experiments by testing a ParD1 antitoxin variant lacking the last 5 residues at the C-terminus. Results revealed that the last 5 C-terminal residues of ParD1 were not implicated in antitoxin recognition, since this antitoxin variant had an equal rate of degradation as the wild type antitoxin **(Figure 5.1C)**.

Finally, I wanted to assess the ParD1 stability in the presence of ParF1 that did not display toxin or antitoxin function in the cell **(Figure 1.2E)**. For this purpose I ectopically co-expressed the two molecules from the same promoter and followed ParD1 stability over time. Since no signal was detected from ParD1-ParF1 expressed cultures in comparison with the solely ParD1 expression, I next aimed to detect ParD1 by Western blot after pull down of ParD1. Interestingly, less ParD1 protein was visible only when ParF1 was co-expressed suggesting that ParF1 might be implicated in the ParD1 stability **(Figure 5.1D)**. However, the ParD1 and ParF1 interaction might be transient or weak, since ParF1 was not detected from the ParD1 pull down experiments and MS analysis previously described in the section 3.1. Additional efforts are needed to further characterize the role ParF1 might play in *S. pyogenes*.

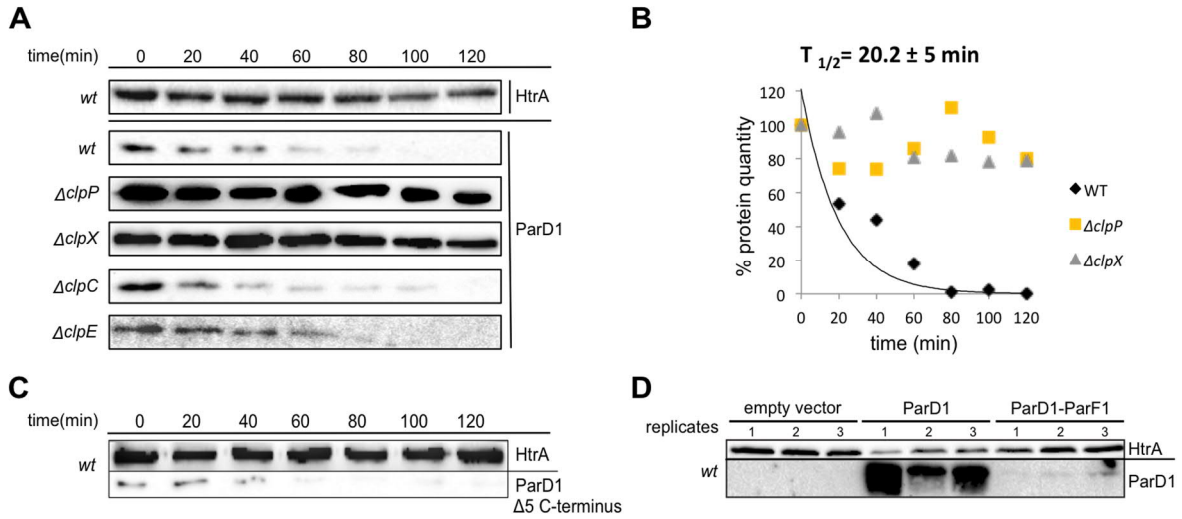

Figure 5.1: ParD1 degradation is ClpXP dependent and possibly mediated by ParF1.

A. The *in vivo* ParD1 stability was assessed in *S. pyogenes* wild type and *ΔclpP, ΔclpX ΔclpC* and *ΔclpE* deletion mutant strains harboring the plasmid pEC85P_{tet}ΩFLAGtag-SPy_*parD1*. Western blots were performed from samples taken at mid-exponential phase of growth upon translation arrest every 20 minutes for 2 hours and the protein HtrA was detected as loading control. The ParD1 antitoxin was unstable in the wild type strain while stable in the *ΔclpP* and *ΔclpX* mutants. **B.** A half-life of approximately 20 minutes was determined for the ParD1 protein by measuring the western blot signal by Image J **C.** The *in vivo* ParD1 Δ5 C-terminus variant stability assays in *S. pyogenes* wild type strain (as described in A), showed the same degradation ratio as the wild type ParD1 protein (A). **D.** *In vivo* N-terminus FLAG-tagged ParD1 pull downs as described in **1.2G** revealed a weaker signal upon co-expression with ParF1.

ParD2 is a more stable protein and also degraded by ClpXP

Next, I was interested in characterizing the degradation rate of ParD2. As it has been previously described **(Figure 2.5A)** the protein features determined *in silico* correlate with what was observed for ParD1. Namely, ParD2 also harbors a well-defined α-helical structure in the C-terminal implying that ParD2 might be a stable protein. I also followed the protein levels by Western blot analysis upon expression of the N-terminal FLAG-tagged ParD2 variant that was functional as an antitoxin **(Figure 2.2E)**. ParD2 appeared to be less prompt for degradation when compared with ParD1, with a half-life of roughly 47 minutes **(Figure 5.2A and 5.2B)**. In agreement with the ParD1 results, ParD2 was completely stable in the *ΔclpP* mutant, suggesting that ClpP is the protease responsible for ParD2 degradation. Moreover, ParD2 exhibited stability in the *ΔclpX* mutant when compared with the *ΔclpC and ΔclpE* mutant backgrounds, which suggest that ClpX might be the main chaperone involved in ParD2 degradation. Interestingly, the ParD2 protein tends to be also stable in the *ΔclpC* mutant strain but in a less extent in comparison with *ΔclpX*, therefore I cannot completely rule out whether only ClpX or both ClpX and ClpC chaperons are involved in ParD2 degradation. Additional

experiments will confirm this finding; ClpXP or ClpCP might be responsible for the ParD2 degradation under distinct conditions.

As for ParD1, ParD2 did not contain any SsrA-tag (Tao and Biswas, 2015), LPF C-terminal domain (Jana et al., 2016) or any other ClpXP consensus recognition-signal previously reported (reviewed by Baker and Sauer, 2012). However, the C-terminus might contain important features since the deletion of the last 15 C-terminal residues of ParD2 appeared to influence the stability of the protein. This variant had a half-life of less than 20 minutes compared to the half-life in the wild type strain **(Figure 5.2C)**. Association of the last C-terminus residues with a yet unknown stabilizing interaction partner might explain the greater stability of ParD2 in the wild type strain. Nevertheless, the deleted 15 C-terminal residues could also lead to changes in the protein structure that make the molecule more susceptible to proteolytic degradation.

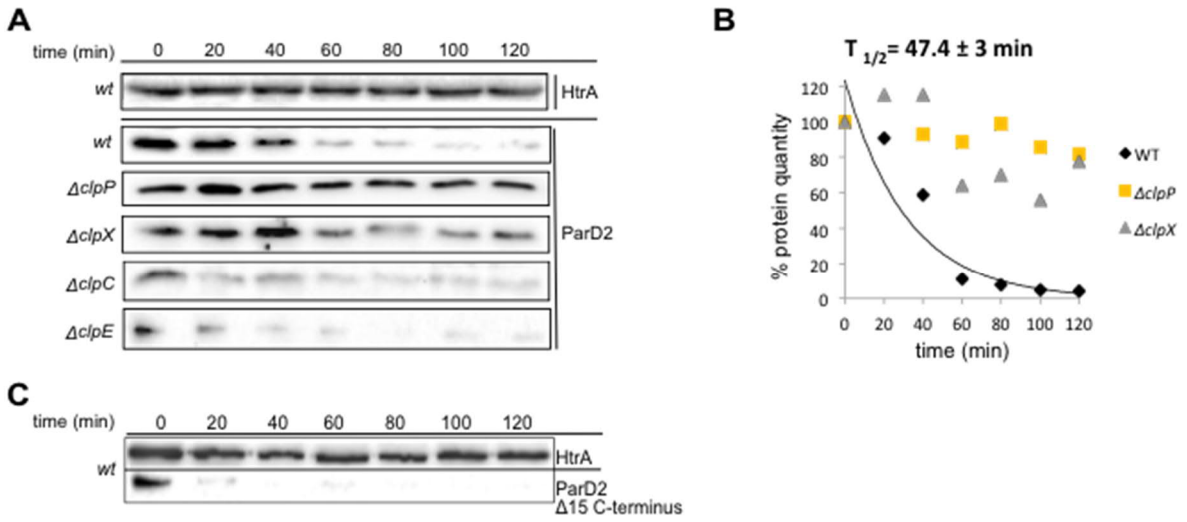

Figure 5.2: ParD2 degradation is ClpXP dependent.

A. The *in vivo* ParD2 stability assays were assessed in *S. pyogenes* wild type and *clpP, clpX, clpC* and *clpE* deletion mutant strains harboring the plasmid pEC85P$_{tet}$ΩFLAGtag-SPy_*parD2*. Western blots were performed from samples taken at mid-exponential phase of growth upon translation arrest every 20 minutes for 2 hours and the protein HtrA was detected as loading control. The ParD2 antitoxin was unstable in the wild type strain while more stable in the *ΔclpP* and *ΔclpX* mutants. **B.** A half-life of approximately 47 minutes was determined for the ParD2 protein. **C.** The *in vivo* ParD2 Δ15 C-terminal variant stability assays in *S. pyogenes* wild type strain (as described in A), showed a faster degradation ratio in comparison with the ParD2 native protein (A).

4 DISCUSSION

The role of many chromosomally encoded TA copies is not well understood and strikingly their diversity in Gram-positive bacteria cocci is not fully appreciated. This work describes the functional characterization of two chromosomal *parDE*-like TA homologs in the human pathogen *S. pyogenes*: the tri-party TA system *parDEF1* and the bicistronic *parDE2* operon. *S pyogenes* is characterized by its remarkable ability to endure diverse host conditions by mechanisms that are still unraveled. To date, this is the first report about chromosomally encoded TA systems in *S. pyogenes* and in this section, the features that provide the basis to understand their molecular mechanism for controlling bacterial growth will be discussed.

4.1 The TA genomic context might correlate with its role

The biological roles of chromosomally encoded TA systems have been a matter of discussion and controversy in the last years and two main roles have been related to them: DNA-stabilization or stress response. TAs related with DNA stabilization were first described in plasmids where typical ParDE-like TA systems are predicted to be addiction molecules that need to be maintained so that the vector remains in the offspring, a concept known as PSK (Roberts et al., 1994b). Presumably, ParDE systems encoded within bacterial chromosomes are important for stabilization of DNA-regions that need to be kept during infection. As a matter of fact, a previous report suggests that *parDE* modules encoded in the chromosome II of *Vibrio cholerae* could potentially stabilize DNA regions that might be needed for bacteria (Yuan et al., 2011). Moreover, the $CopA_{so}$-$ParE_{so}$ TA operon has been recently shown to stabilize a conjugative and integrative element within the chromosome of *Shewanella oneidensis* (Yao et al., 2018). Thus, the analysis of the TA genomic context could give us potential clues for their cellular function; in *S. pyogenes* the genomic contexts of the *parDEF1* operon shows putative prophage and antibiotic-resistant genes conserved among different serotypes **(Figure 1.1C)**, suggesting that this region could be under positive selection during the evolution of this species. I speculate that this genomic area somehow gives to *S. pyogenes* a selective advantage and that the *parDEF1* operon might be involved in its maintenance. The findings also suggest that this TA module might be originated from a phage since genomic composition revealed that *parDEF1* is present in a region with low GC content compare to the

chromosomal GC composition in *S. pyogenes.* Additional effort is needed to test whether the putative prophage region gets lost upon deletion of the *parDEF1* TA element.

On the other hand, the *parDE2* locus is also highly conserved among *S. pyogenes* serotypes and its genomic context contains hypothetical genes implicated in diverse functions **(Figure 2.1C)**. A putative integrase homolog of the bacteriophage MM1 from *S. pneumonia* is the only sign of a foreign DNA incorporation event, however, in our strain this gene seems to be non-functional since it is truncated **(Figure 2.1C)**. Furthermore, the GC content analysis showed in average the same value compare to the genomic content. Due to the lack of evidence we cannot hypothesize that the *parDE2* locus is involved in PSK, instead, it might be for instance a foreign selfish element or an altruistic programmed cell death system that gets triggered to sacrifices part of its host population in adverse conditions.

4.2 ParDEF1 and ParDE2 TA modules are stress response elements in *S. pyogenes*

Beside DNA-stabilization another important function of chromosomal TA systems is cellular stress response, providing to the bacterial population an advantage to survive when facing adverse conditions (reviewed by Gerdes et al., 2005). The basal expression of TA systems in *S. pyogenes* is low. Conversely, among many stress conditions tested, the *parDEF1* and in a less extent the *parDE2* operon responded to a non-lethal concentration of ethanol that has a rather general cellular effect **(Figure 4.2 and 4.3)**. Ethanol can decrease pH, induce protein damage and aggregation, disrupt the fatty acid composition and function of the membrane, and has profound effects on nutrient transport and metabolism, especially the catabolism of amino acids (Chatterjee et al., 2006). The ethanol stress induction might trigger TA-unrelated pathways that lead to a disruption of many functions, including destabilization of protein structures. It has been reported that the stimulation of TA transcriptions occurs due to the lack of TA promoter repression by the unstable antitoxin (Christensen et al., 2001b). Therefore, TA levels of expression under ethanol conditions indicated that the repression from the TA operon was released due to either a compromised antitoxin structure or acceleration of the antitoxin proteolysis. It will be interesting to determine whether the degradation of the antitoxin protein upon stress could result in a faster induction of the system and thus can prompt toxin release.

It has been reported that many chromosomal TAs are overexpressed during amino acid starvation in *E. coli* (reviewed by Gerdes et al., 2005). Since this is one of the cellular

effects of ethanol, we assessed TA expression under SHX treatment in *S. pyogenes,* which is a structural analog of L-serine that inhibits charging of seryl-tRNA and thereby induces amino acid starvation (Christensen et al., 2001b). We observed an increasing abundance of the TA mRNA upon SHX addition, suggesting that *parDEF1* and *parDE2* are stress response elements which are activated under amino acid starvation conditions and the thereby induced stringent response **(Figure 4.4B)**.

Interestingly, the mRNA encoding the *parE2* toxin that is being detected by the probe in the NB analysis has shown the appearance of multiple bands below the expected TA operon size which might suggest a putative transcript processing **(Figure 4.4B)**. Upregulation of the *relBE* TA systems has been observed upon SHX challenge in *E. coli* (Christensen et al., 2001b). The same study observed multiple bands corresponding to the TA mRNA detected that do not correspond to the expected TA operon size, but the authors did not comment on that. Recent reports have suggested an additional layer of TA regulation at the post-transcriptional level that involved mRNAses, where specific cleavages in the antitoxin mRNA were found but interestingly also in the toxin transcripts (Altuvia et al., 2018; Lybecker et al., 2014). I hypothesize that RNases may be involved in the regulation of TA transcripts upon stress; this may represent a potential novel mechanism of TA post-transcriptional regulation. However, induction of the second massager ppGpp upon amino acid starvation could also inhibit or disrupt transcription of stable RNA operons by direct interaction with the RNA polymerase during stringent response (reviewed by Chatterji and Kumar Ojha, 2001; Syal and Chatterji, 2015). This process might lead to a drop-off of the RNA polymerase that leads to different sizes of the same mRNA transcript. If the expression of the TAs is fast and tightly regulated, it would be plausible to have a system where the antitoxin mRNA is degraded to deplete production of the antitoxin protein - on top of its proteolytic regulation - under stress conditions. Additional experiments will be important to validate this hypothesis assessing the stability of the antitoxin mRNA or its disappearance over the time upon stress. This, together with the fact that the toxin mRNA and protein are predicted to be more stable than the antitoxin mRNA and protein molecules, would suggest a tight control of the TA systems at multiple levels.

Furthermore, some reports have suggested the involvement of TA modules in other cellular functions such as biofilm formation; however, their direct correlation has been debated. As an example, MqsR is a particular type II toxin from *E. coli* b3022 that cross talk with the quorum sensing molecule AI-2, while its MqsA antitoxin represses general stress response regulators leading to reduce amount of the second messenger c-di-GMP and overall

reduction of biofilm formation (Sun et al., 2017; Yamaguchi et al., 2009). Other reports showed that mutations of *yafQ/dinJ* or *mazEF* TA systems or interruption of the HipA toxin gene resulted in a prominent decrease in biofilm formation (Kolodkin-Gal et al., 2009). Our results showed that *parDE1* and *parDE2* are not implicated in this process in *S. pyogenes*, since the single TA mutant backgrounds did not show an impaired biofilm formation capacity **(Figure 4.1B and 4.1C)**. Nevertheless, cumulative TA mutants that I did not test might have clearer phenotypic outcomes (Kim et al., 2009).

Finally, It is important to note that a recent report claimed a new role of a ParDE module from *Pseudomonas aeruginosa* (Pa) (Muthuramalingam et al., 2018). Muthuramalingam and co-workers identified a protective function of the PaParE toxin against quinolones antibiotic treatment, since both the toxin and this type of antibiotics outcompete for binding the same target. This is an effect that relies on the amount of toxin that in high quantities might lead to cell death (Muthuramalingam et al., 2018). Will be interesting to test this hypothesis in *S. pyogenes*.

4.3 The ParD-like molecules from *S. pyogenes* are toxic

We have collected strong evidence to propose ParD1 as a new type of antitoxin that has a deleterious effect in the cell*:* 1) ParD1 reversibly decreased viability when overexpressed, 2) ParD1 induced nucleoid condensation, mild cell elongation and aberrant cell septum, 3) its toxicity is exclusive since ParD homologs did not show the same effect in *E. coli* and 4) its phylogenetic origin is not shared with proteins belonging to the ParD cluster. We stress that the ParD1 target must be highly conserved among Gram-negative and Gram-positive bacteria, since ParD1 is toxic in both the heterologous host *E. coli* and in *S. pyogenes*.

The remarkable nucleoid localization in the cells overexpressing ParD1 in comparison with the non-induced conditions prompted me to consider that ParD1 might be targeting a DNA-related function important during cell division or chromosomal segregation **(Figure 1.3E and 1.7)**. In addition, the ParD1 phenotype in *E. coli* looks similar to the CPX treated conditions suggesting a potential DNA topological effect thereby possibly inducing the SOS response **(Figure 3.3 and 1.7A)**. Nevertheless, the SOS response was not triggered upon ParD1 expression in *E. coli* **(Figure 1.7C)**, suggesting that DNA strand breaks are not a consequence of ParD1 toxicity. DNA replication and chromosomal segregation are processes that occur simultaneously with cell division (Reviewed by Surovtsev and Jacobs-Wagner, 2018); DNA replication or segregation arrest will lead to an ongoing cell division that will eventually halt,

which is evident by the cell elongation phenotype in *E. coli* **(Figure 1.7A and 1.7D)** and cell swelling in *S. pyogenes* **(Figure 1.3E)**. Furthermore, ParD1 might also affect RNA or protein synthesis, since those are main processes that influence the cells at different levels; however, transcription and translation arrest do not normally cause the observed nucleoid localization upon ParD1 expression.

Interestingly, the cell septum was not visible upon ParD1 expression in *E. coli* elongated cells **(Figure 1.7A and 1.7D)** while in *S. pyogenes* it appears to be abnormal **(Figure 1.3E)**. This phenotype is typical in Gram-positive bacteria lacking proteins important for septum formation (Fleurie et al., 2014; Stamsås et al., 2018). In *S. pneumoniae* the deletion of mid-cell anchored protein Z (MapZ) resulted in delocalization of the septum formation protein FtsZ, which subsequently leads to abnormal cell morphogenesis, asymmetric division and aberrant chromosomes (Fleurie et al., 2014). It has been shown that a deletion of *ftsZ* inhibits cell division in *Bacillus subtilis* and *Staphylococcus aureus* (Arjes et al., 2014). Indeed, inhibited cell division lead to an arrest in the initiation of new rounds of DNA replication, which might lead to cell growth halt but not to the strong killing observed upon ParD1 expression. Yet, FtsZ constitutes a good ParD1 target since it is well conserved among bacteria; however, toxins that impair the FtsZ ring formation will induce a lemon-like morphology that we did not observe in *E. coli* (Heller et al., 2017). Effects in other genes involved in septum formation might also lead to the phenotype observed in *S. pyogenes* upon ParD1 expression. In *S. pneumoniae* and *Staphylococcus aureus*, the coordinator of zonal elongation CozE mediates control of cell division by interacting with the division protein EzrA, and the mutation of the *cozE* gene leads to a similar outcome (Stamsås et al., 2018). For now, I cannot rule out whether ParD1 is directly or indirectly affecting septum formation in the cell. Further antitoxin pull down experiments could potentially elucidate whether ParD1 has a proteinaceous target in the cell.

ParD1 does not share a high level of similarity with ParD2 **(Figure 2.3A)** and in fact, phylogenetic analysis predicted that ParD2 belongs to the same family but clusters with a different group of hypothetical antitoxins predicted in other *S. pyogenes* strains **(Figure 1.5B)**. The N-terminal FLAG-tagged ParD2 variant was toxic in *S. pyogenes* **(Figure 2.4C and 2.4D),** having a detrimental effect similar to the one observed with the N-terminal tagged ParD1 protein. Interestingly neither of both, the FLAG-tagged ParD2 variant nor the wild-type ParD2 were toxic in *E. coli* **(Figure 2.5B and 2.5C)**. These findings imply that both *S. pyogenes* ParD-like molecules target an important function that leads to killing but does not necessarily mean that they both share the same target. In addition, the lack of toxicity by ParD2 in *E. coli* could

be due to either less specificity or the absence of the cellular target in this heterologous system.

Remarkably, studies in *E. coli* with functional ParD1 variants **(Figure 1.4C)**; have revealed that the N-terminal naturally acquired suppressor mutations (N8I and K3A) that led to non-toxic phenotypes, in addition, a mutation (G5A) intentionally planned resulted in a more toxic outcome **(Figure 1.4D)**. Moreover, ParD2 harbors the same predicted secondary structure and the RHH fold found in the ParD1 N-terminal side that potentially interacts with DNA and might be involved in the target recognition. Intriguingly, among some of the amino acids that both share the residue K and N at the N-terminus that showed to be important for ParD1 toxicity are conserved in ParD2. The N-terminus similarity between the two *S. pyogenes* ParD proteins could highlight important features that support the involvement of this region in the non-canonical antitoxin target recognition. Therefore, I do not exclude that the *S. pyogenes* ParD-like antitoxins have a DNA related target.

Even though they are not reports about deleterious effects upon antitoxin overexpression in bacteria, some reports shown that antitoxins can also act as transcriptional regulators (Brown et al., 2009; Hu et al., 2012; Wang et al., 2011). The MqsA (from the MqsAR TA system) and DinJ (from the DinJ-YafQ TA system) antitoxins, influence the general stress response by transcriptionally regulating the *rpoS* gene encoding the sigma-S factor, which is the master regulator of stress response (Brown et al., 2009; Hu et al., 2012; Wang et al., 2011). In addition, MqsA is a stable antitoxin that also binds the promoter DNA-regions of some genes important for *E. coli* cell physiology e.g. *mcbR* and *spy*, via its C-terminus domain (Brown et al., 2009; Wang et al., 2011). Thus, we speculate that *S. pyogenes* ParD-like antitoxins are potential transcriptional regulators and that their N-terminal side plays an important role in the bacterial DNA-promoter recognition. Antitoxins are more diverse than previously recognized and are perhaps vital in mediating bacteria stress responses, their implications as transcriptional regulators need to be explored in detail.

4.4 ParD1-ParE1 migth constitute a dual toxin-antitoxin system

The findings presented in this work suggest that *parDEF1* is a non-canonical TA system: 1) the antitoxin-toxin genes are typically co-transcribed in the natural host and up-regulated under stress conditions, 2) in *S. pyogenes* and in the heterologous host *E. coli,* ParD1 and ParE1 reduce viable cells when overexpressed ectopically, 3) ParD1 prevents but

not reverses the ParE1 toxicity while ParE1 rescues the ParD1 deleterious effect and 4) The ParD1 antitoxin is typically degraded by ClpXP, which might have an implication in the regulation of TA activity. I speculate that the *parDEF1* operon migth work as a dual-TA system where two of its molecules need to co-exist in the host to allow growth. Regarding the *parDE2* operon that is indeed a bona fide TA system, more evidence is needed to elucidate its putative TA dual function.

In typical ParDE-like TA systems, the prevention versus reversion of toxicity has been investigated. Prevention of toxicity by the antitoxin implies that both molecules interact before the toxin can reach its target. Reversion of toxicity denotes that the antitoxin is able to sequester the toxin even after it has reached the target. As an example, the well-characterized ParD antitoxin encoded in the RK2 plasmid has shown to be able to prevent and reverse ParE toxicity *in vitro* (Jiang et al., 2002). Conversely, *in vitro* studies showed that ParD2 from *V. cholerae* is able to prevent ParE2 toxicity, but is unable to rescue an already poisoned gyrase by the toxin (Yuan et al., 2010). CcdB is a gyrase poison from the *ccdAB* TA system and constitutes an example of a toxin that causes cell filamentation and nucleoid condensation when expressed in *E. coli.* It has been described that the CcdB effect on gyrase can be prevented and reversed by the antidote CcdA, (Bahassi et al., 1999; Kampranis et al., 1999). Our data showed that ParD1 did not reverse ParE1 toxicity in the heterologous system *E. coli*, instead, we observed a cumulative effect that led to stronger killing **(Figure 1.8A)**. Conversely, ParE1 efficiently reversed the ParD1 effect leading to cell growth **(Figure 1.8A)**. These findings could have important implications; if one molecule (ParE1) is able to compete with the target of the second molecule (ParD1) for binding, it will counteract the toxic effect leading to growth rescue. Conversely, if one molecule (ParD1) does not sequester the second molecule (ParE1) within the toxin-target complex, the toxicity will lead to irreversible decreace in cell-viability. We suggest that ParE1 is a toxin that irreversibly kills, while ParD1 is a toxin that reversibly kills its host when released from the TA complex.

4.5 The ParDE1 and ParDE2 TA paralogs do not cross talk

TA cross talk has been reported in some bacteria, as an example TA paralogous in *E. coli 0157:H7* showed a cross talk interaction in between the chromosomal CcdB toxin that is neutralized by the plasmidic CcdA antitoxin while the plasmidic toxin is not neutralized by the chromosomal antitoxin (Wilbaux et al., 2007). Since ParDEF1 and ParDE2 constitute paralogous TA systems it is tempting to expect cross-functionality, however, the low protein

similarity among them suggest the absence of an interaction **(Figure 2.3A)**. Mismatched pairs of toxin and antitoxins were introduced into *E. coli* and their effects on growth and viability were assayed. I observed that ParD1 did not protect cells from ParE2 toxicity and vice versa, taking into account that ParD1 also has a detrimental effect on cell growth **(Figure 2.3C)**. Conversely, ParD2 did not fully protect the cells from ParE1 toxicity. Nevertheless, a slide reduction of killing by ParE1 was observed in comparison with the control conditions where ParE1 (the only molecule induced) seemed to have a stronger effect **(Figure 2.3D)**. This phenomenon is attributed to the to the dilution effect of the *E. coli* machinery needed to translate and transcribe two molecules in parallel leading to fewer toxin copies. The absence of the non-cognate ParE toxin molecules in both of the *in vivo* N-terminus FLAG-tagged ParD pull-down assays **(Figure 1.2G)**, further confirmed that ParDEF1 and ParDE2 do not cross talk in *S. pyogenes*. Studies of chromosomal paralogous TA loci in other organisms including the two ParDE copies from *V. cholerae* and the three ParDE modules in *C. crescentus*, also failed to detect evidence of cross talk between antitoxin and toxins encoded by distinct TA loci (Fiebig et al., 2010; Yuan et al., 2011). Nevertheless, another recent report showed that a single mutation in the VapB1 antitoxin allows it to counteract the toxicity of both, its cognate toxin VapC1 and its non-cognate toxin VapC2 from *Haemophilus influenza* (Walling and Butler, 2016). Moreover, Wessner and coworkers have described the crosstalk between chromosomally encoded type I and type II TA systems (Wessner et al., 2015). For now, there is not enough evidence to exclude these possibilities in *S. pyogenes*.

4.6 ParE-like toxins are gyrase poisons and topo IV inhibitors

I provided evidence that ParE1 and ParE2 are toxic for the cell upon expression in *S. pyogenes* **(Figure 1.3 and 2.4)** and in the heterologous host *E. coli* **(Figure 1.2A and 2.2A)**. The observed phenotype in *E. coli* **(Figure 1.2C and 2.2B)** was associated with impaired DNA topology and DNA replication that eventually affect cell division, which is consistent with the existing literature (Harms et al., 2015; Kato et al., 1990). The importance of topoisomerases for the successful completion of DNA replication by preventing the buildup of torsional stress is well established (Postow et al., 2001). The gyrase is essential; mainly important during initiation, elongation, and termination of the DNA replication and has been reported to be the target of typical ParE-like toxins (Gupta et al., 2016; Hallez et al., 2010; Jiang et al., 2002; Yuan et al., 2010). This work confirmed that gyrase is one of the ParE1 and ParE2 cellular targets since co-expression of each of the toxins and gyrase modulated the toxicity leading to stronger killing **(Figure 3.1)**. These results suggest that both ParE toxins interact with the

gyrase and thereby transform it into a cellular poison that introduces DNA double-strand breaks that lead to SOS response. As a comparison, CcdB is a well know molecule with a particular way of harming the gyrase; it has a lethal effect when poisoning the gyrase-DNA complex, but could also prevent cell death through the formation of a CcdB-GyrA subunit complex that sequesters the toxin away from the gyrase complex (Bahassi et al., 1999; Kampranis et al., 1999) **(Figure 3.4)**. Conversely, ParE-like toxins might interact only with the whole gyrase complex when bound to the DNA molecule inducing double strand breaks; which would explain why co-expression of the ParE toxins with either the gyrase or its subunits did not rescue growth **(Figure 3.1)**. In addition, I demonstrated *in vitro* that SPyParE1, SPyParE2 and EcParE3 are indeed gyrase poisons, rather than inhibitors similar to VfCcdB, since they equally damage the supercoiling activity of the gyrase complex **(Figure 3.5A)**. Moreover, the most toxic SPyParE1 displayed stronger effects than EcParE3 and MtbParE2 on the gyrase recombinant protein from *S. pneumonia*, which is closer related to *S. pyogenes* validating the prominent specificity to its natural target **(Figure 3.6A)**.

Gyrase and topo IV are highly similar topoisomerases. However, unlike gyrase, topo IV mainly influences chromosomal stabilization during cell division, thus interfering with the separation of newly replicated DNA molecules (Reviewed by Sissi and Palumbo, 2010). It has been described that the nucleoid condensation is likely a consequence of DNA gyrase inhibition, while inactivation of topo IV is known to result in DNA catenation and knotting which induces the so call "*partition*" phenotype namely cell filamentation and sequestration of unsegregated DNA (Harms et al., 2015; Kato et al., 1990). The SPyParE1 and to a lesser extent the SPyParE2 and EcParE3 phenotypes seem to be a cumulative effect on both the gyrase and topo IV activity **(Figure 3.3)**. Toxins that target gyrase and their cross-interaction with Topo IV could be expected since these two enzymes are similar; in fact synthetic peptides based on the plasmidic ParE from *E. coli* have shown to inhibit both enzymes *in vitro* (Barbosa et al., 2012). This work provided the first *in vivo* and *in vitro* experimental evidence that the chromosomal SPyParE1, SPyParE2, EcParE3, and MtbParE2 toxins indeed target topo IV, highlighting the broader functional spectrum of ParE toxins.

The results displayed a remarkable growth rescue effect of the topo IV subunit E upon either SPyParE1, SPyParE2 or EcParE3 toxin co-expression, unlike the opposite phenomenon when the topo IV E homolog the gyrase subunit B is co-expressed with each ParE toxin **(Figure 3.1 and 3.4).** Furthermore, topo IV E harbors the ATPase activity; ParE interaction with this subunit would lead to complete inhibition of the topo IV relaxation and/or decatenation activity. Alike, *in vitro* results demonstrated that the ParE-like toxins tested

inhibiting topo IV like NOV, a catalytic inhibitor that abrogates the ATP activity of topoisomerases **(Figure 3.5B, 3.6B, and 3.6C)**. In addition, these data correlated with the SPyParE1, EcParE3 and MtbParE2 effect on the recombinant protein from *S. pneumonia*, validating the broad spectrum of these toxins on topoisomerases **(Figure 3.6B and 3.6C)**. These findings suggest that the ParE-like mechanism of targeting either gyrase or topo IV might vary due to putative different specificities toward these enzymes and their subunits; this would explain why SPyParE1 and EcParE3 poison gyrase but inhibit topo IV. Finally, our findings indicate that ParE activity on topo IV might be an exclusive feature of this kind of toxins as VfCcdB does not harm the topo IV enzyme as previously reported (Smith et al., 2012) **(Figure 3.4 and 3.5B)**.

Overall, our findings stress the functional diversity of ParE-like toxins ability to target two essential bacterial enzymes. Gyrase and to a lesser extent topo IV are found in nearly all bacteria but are absent in humans, this characteristic makes them interesting antibiotic targets (reviewed by Vos et al., 2011). Fluoroquinolones are antibiotics that target topoisomerases; their misusage has raised bacterial resistance, underlining the importance of finding new compounds with a novel mode of action. A major challenge in designing quinolone-like drugs that overcome target-mediated resistance relies on the ability to identify substituents that mediate strong interaction with bacterial topoisomerases, and do not interact with the human topo type II enzymes (Aldred et al., 2013; Mayer and Janin, 2014). In addition, topoisomerase poisons such as CcdB and ParE or FtsZ-MrB inhibitors such as CbtA act by direct stoichiometric interaction with their targets so that strong effects are achieved without enzymatic activity (Heller et al., 2017). This characteristic makes them attractive drugs due to the lack of cofactors or special conditions that enzymes need to function. Nevertheless, it will be interesting to elucidate the nature and real requirements of ParE-like toxins interaction with their targets.

4.7 The ParD antitoxins are subjected to degradation by the ClpXP protease

This work also showed that the antitoxins ParD1 and ParD2 are intrinsically unstable in the wild type strain **(Figure 5.1A and 5.2A)**. ParD1 presented a half-life of 20 minutes while ParD2 showed a relatively long half-life of 47 minutes under normal growth conditions **(Figure 5.1B and 5.2B)**. The half-lives of unstructured antitoxins such as RelB, HipB or ParD range from 15 to 18 minutes (Reviewed by Gerdes et al., 2005), whereas more structured antitoxins, such as YefM (Cherny and Gazit, 2004) or DinJ (Prysak et al., 2009) display a half-life of almost an hour. The antitoxin degradation rates might change upon stress; this will potentially

lead to a controlled toxin release. The MqsA antitoxin, for instance, has a structured C-terminus, however, presents a short half-life of around 1.25 min during oxidative stress, in comparison with the half-live of almost an hour under normal growth conditions (Brown et al., 2009). It will be interesting to test this hypothesis for ParD1 and ParD2 under amino acid starvation that appeared to trigger both TA systems *in vivo*.

ParD-like proteins are predicted to exist as dimers in solution and exhibit high thermal stability and excellent refolding properties after heat-induced denaturation (Oberer et al 1999, 2002). The *in vivo* pull-down revealed three putative conformations for the N-terminal FLAG-tagged ParD1: prominently a monomer and in a less extent a dimer and a hypothetical degradation product below the expected size of the native ParD1 protein **(Figure 1.2G)**. In the *in vivo* stability experiments the monomeric band is the only one detected and followed over the course of the experiment by WB, as it is the more prominent **(Figure 5.1A)**. These findings might suggest that there is another uncharacterized post-translational event occurring that leads to the short version of ParD1, which might have important regulatory roles.

It has been recently described that the ClpAP protease is a universal factor that degrades the ParD antitoxin from the RK2 plasmid and that ClpXP plays a minimal role in this process in the Gram-negative bacteria *E. coli*, *C. crecentus* and *Pseudominas putida* (Dubiel et al., 2018). In *S. pyogenes*, both ParD1 and ParD2 are degraded by the ClpXP protease *in vivo*. Similar to our findings, the only *S. pyogenes* antitoxin characterized up to date, ε (epsilon) from the native pSM19035 vector is also degraded by $ClpXP_{B.s.}$ protease *in vitro* and *in vivo* in the Gram-positive bacterium *Bacillus subtilis* (Brzozowska and Zielenkiewicz, 2014), suggesting a similar post-translational regulation path of chromosomally encoded antitoxins in our model organism. This information highlight that the machinery responsible for ParD-like antitoxin degradation varies depending on the organism. Interestingly, regulated protein degradation often depends on additional factors such as the toxin that protects the antitoxin from proteolysis (Dubiel et al., 2018). Moreover, previous reports have shown that the ClpAP protease is able to bind DNA regardless of the sequence or DNA form, which increases the ClpA ATPase activity and the ParD proteolysis efficiency (Dubiel et al., 2018; Kubik et al., 2012). It would be interesting to investigate whether the ParE1 and ParE2 are more stable than ParD1 and ParD2, and whether it stabilizes the antitoxin and/or protects it from degradation as well as whether a DNA molecule plays a role in the process in *S. pyogenes*.

Although ParD1 and ParD2 did not show high sequence identity with any typical antitoxin prone to degradation, some hydrophobic residues that could be protease recognition

sites in the C-terminus are similar to the ones present in the DinJ antitoxin, which is typically structured and degraded by ClpXP and Lon proteases in *E. coli* (Ruangprasert et al., 2017). It was recently reported that a C-terminal loop predicted next to the last α-helix of DinJ is solvent exposed and is a potent recognition site for proteolysis (Ruangprasert et al., 2017). I attempted to evaluate the implication of the last residues of *S. pyogenes* ParD-like antitoxins on its recognition for proteolysis and observed that 5 residues (after the last C-terminus α-helix) of ParD1 did not have an implication for its stability **(Figure 5.1C)**. Interestingly, deletion of the last 15 residues of ParD2 led to a faster degradation rate **(Figure 5.2C)**. This can be due to defects on protein folding that provoke precipitation or due to the removal of a feature that is needed for its stability or interaction with a potential protective partner.

Antitoxin degradation might also rely on adaptors (reviewed by Kirstein et al., 2009); the adaptor molecule TrfA for instance (homolog to MecA from *Bacillus subtilis*) is involved in antitoxin degradation by ClpCP in *Staphylococcus aureus* (Donegan et al., 2014). Additional molecules might be involved in the recognition of ParD1 in *S. pyogenes*. The *parF1* gene also part of the *parDEF1* operon in most of the *S. pyogenes* serotypes did not show toxic nor antitoxin activity. Moreover, ParD1 pull down experiments displayed lower amounts of ParD1 detected by WB when co-induced with ParF1 **(Figure 5.1D).** Therefore, it is tempting to speculate that ParF1 might somehow influence the stability of ParD1. Finally, the ParF1 function and potential interactions with the TA components and with other proteins could also be related to a specific condition, such as stress-related conditions that have not been tested yet.

5 CONCLUSION AND FUTURE PERSPECTIVES

TA characterization provides new insights to tackle bacterial infections: on the one hand, chromosomally encoded TA systems might constitute important antibiotic targets, on the other hand, toxins might serve as drugs to treat infections since they modulate bacterial growth. In this study, the characterization of two ParDE-like stress response TA systems encoded within the chromosome of *S. pyogenes* was described. We provided a general understandings regarding the mode of action of the ParE toxins, their broader target recognition and TA regulation. The two systems contain ParE-like toxins that have a lethal effect on DNA replication by poisoning the gyrase and inhibiting the topo IV, which is a feature shared with other chromosomal ParE-like toxins from different organisms **(Figure XIII and XV)**. Both ParD1 and ParD2 proteins are typically degraded by the ClpXP protease, important for the triggering of the system **(Figure XIII and XV)**.

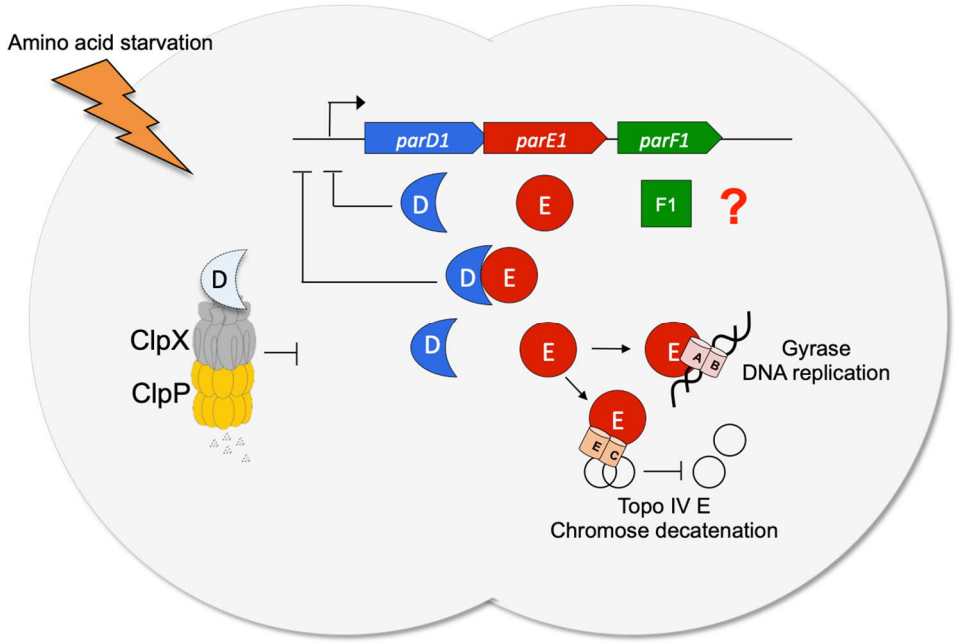

Figure XIII: The *parDEF1* TA system in *S. pyogenes*:

The ParDEF1 TA system is triggered by amino acid starvation conditions. Upon antitoxin degradation by ClpXP, the freed toxin accumulates and targets both gyrase and topo IV causing cell death. The function of ParF1 is not known yet.

The *parDEF1* TA system may function as an addiction module that stabilized a putative prophage region in the chromosome of *S. pyogenes*, It contains a third molecule ParF1, that may play a role in the stability of ParD1 and which function is currently under study **(Figure XIII)**. We presented evidence of a dual TA function that in particular ParD1-ParE1 displayed in both the heterologous host *E. coli* and in *S. pyogenes*. We hypothesize that the excess of ParE1 leads to irreversible lose in cell-viability since co-expression of ParD1 did not result in growth. Conversely, the excess of ParD1 reversible decrease cell-viability, which is aliviated by co-expression of ParE1. The coexistence of both ParD1 and ParE1 in a yet unknown ratio leads to cell growth **(Figure XIV)**. We speculate that ParD1 migth have a target well conserved among Gram-positive and Gram-negative bacterial species. Further experiments are needed to elucidate the nature of the ParD1 target that could be a protein or a DNA molecule. Moreover, we will attempt to test whether the ParD1 N-terminal region is involved in ParD1-DNA interaction which might be the key element implicated in target recognition as a putative transcriptional regulator.

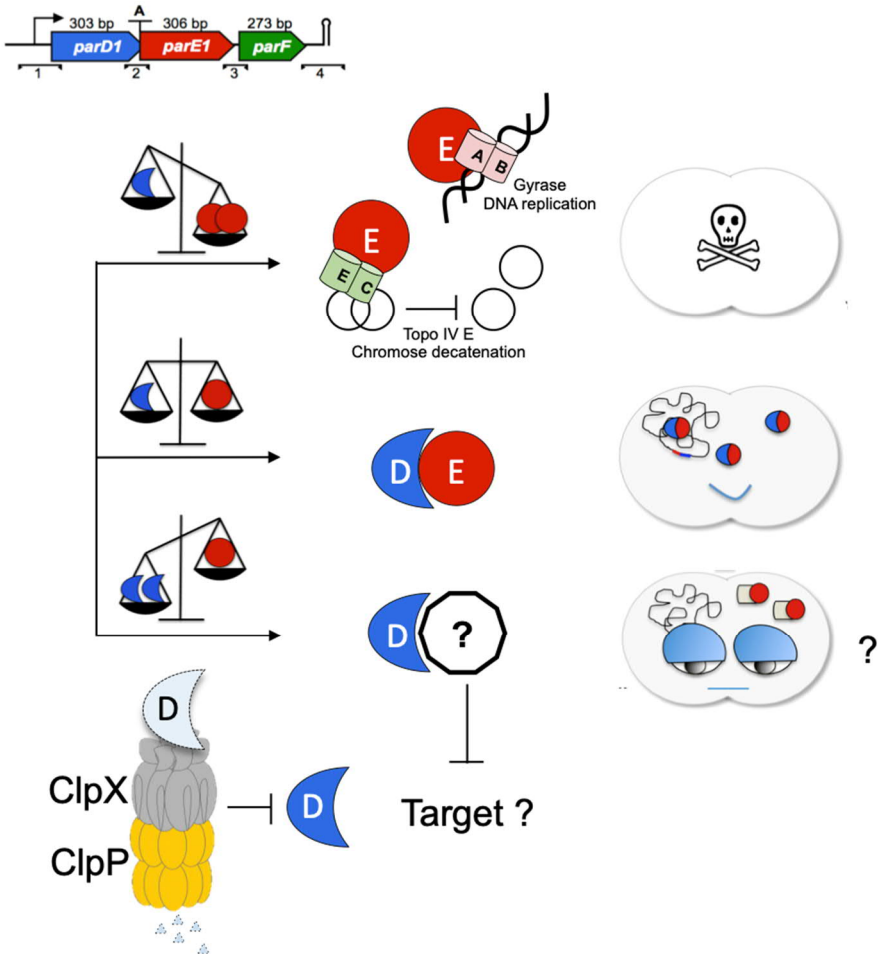

Figure XIV: The ParDE1 migth constitute a dual TA system:

ParE1 accumulation leads to cell killing, in this condition DNA replication and chromosomal decatenation are arrested due to toxin interaction with both gyrase and topo IV. The AT-T complex

allows cell growth while freed ParD1 accumulation leads to non-viable cells, a state from which the cells can be rescued by the presence of ParE1.

The ParDE2 TA module has commonly described bona fide TA characteristics **(Figure XV)**. Nevertheless, ParD2 showed to be toxic in *S. pyogenes* which may also suggest its TA-dual function which needs to be further evaluated. Interestingly, we observed a putative *parDE2* post-transcriptional regulation via TA mRNA processing under amino acid starvation. These data imply an additional layer of TA regulation upon stress exposure that has been proposed for TA systems but never experimentally proven. Further studies analysing the whole TA transcript will elucidate the nature of this putative mRNA cleavage and will provide evidence of the potential mRNase involved in TA mRNA regulation in *S. pyogenes*.

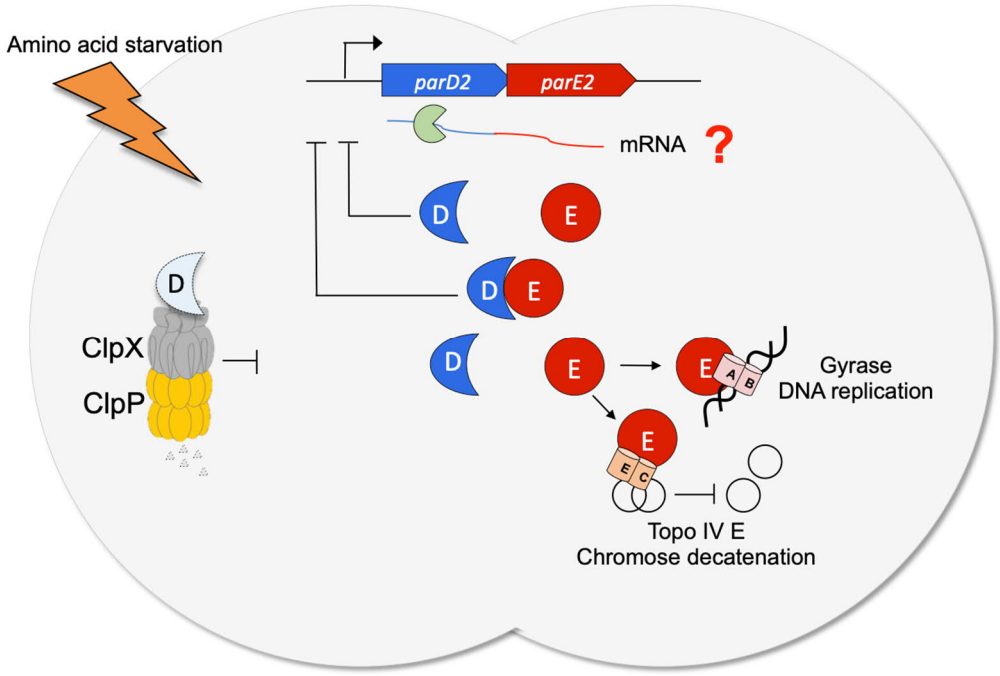

Figure XV: The *parDE2* TA system in *S. pyogenes*:

The *parDE2* TA system is triggered by amino acid starvation, a condition in which a potential TA mRNA post-transcriptional regulation occurs. Upon antitoxin degradation by ClpXP the freed toxin accumulates and targets both gyrase and topo IV causing cell death.

The bases to understand the molecular mechanism by which chromosomal ParDE-like TA systems function in the Gram-positive bacterium *S. pyogenes* were elucidated. Further analysis will help us to understand the role of these modules during bacterial infection and the generated knowledge should provide the foundation for the study of TA elements and their use as either new antibiotic targets or molecular tools to kill bacterial pathogens.

6 REFERENCES

Aakre, C.D., Phung, T.N., Huang, D., and Laub, M.T. (2013). A bacterial toxin inhibits DNA replication elongation through a direct interaction with the β Sliding Clamp. Mol. Cell *52*, 617–628.

Afif, H., Allali, N., Couturier, M., and Van Melderen, L. (2001a). The ratio between CcdA and CcdB modulates the transcriptional repression of the *ccd* poison-antidote system: Autoregulation of the *ccd* operon. Mol. Microbiol. *41*, 73–82.

Alawneh, A.M., Qi, D., Yonesaki, T., and Otsuka, Y. (2016). An ADP-ribosyltransferase Alt of bacteriophage T4 negatively regulates the *Escherichia coli* MazF toxin of a toxin-antitoxin module: ADP-ribosylation of *E. coli* MazF by T4 Alt. Mol. Microbiol. *99*, 188–198.

Aldred, K.J., Schwanz, H.A., Li, G., McPherson, S.A., Turnbough, C.L., Kerns, R.J., and Osheroff, N. (2013). Overcoming target-mediated quinolone resistance in topoisomerase IV by introducing metal-ion-independent drug–enzyme interactions. ACS Chem. Biol. *8*, 2660–2668.

Aldred, K.J., Kerns, R.J., and Osheroff, N. (2014). Mechanism of Quinolone Action and Resistance. Biochemistry *53*, 1565–1574.

Altuvia, Y., Bar, A., Reiss, N., Karavani, E., Argaman, L., and Margalit, H. (2018). In vivo cleavage rules and target repertoire of RNase III in *Escherichia coli.* Nucleic Acids Res. 46, 19, 10380-10394.

Arjes, H.A., Kriel, A., Sorto, N.A., Shaw, J.T., Wang, J.D., and Levin, P.A. (2014). Failsafe mechanisms couple division and DNA replication in bacteria. Curr. Biol. *24*, 2149–2155.

Baharoglu, Z., and Mazel, D. (2014). SOS, the formidable strategy of bacteria against aggressions. FEMS Microbiol. Rev. *38*, 1126–1145.

Bahassi, E.M., O'Dea, M.H., Allali, N., Messens, J., Gellert, M., and Couturier, M. (1999). Interactions of CcdB with DNA Gyrase: Inactivation of gyrA, poisoning of the gyrase-DNA complex, and the antidote action of ccdA. J. Biol. Chem: *274*, 10936–10944.

Baker, T.A., and Sauer, R.T. (2012). ClpXP, an ATP-powered unfolding and protein-degradation machine. Biochim Biophys Acta *1823*, 15–28.

Balaban, N.Q. (2004). Bacterial Persistence as a Phenotypic Switch. Science *305*, 1622–1625.

Barbosa, L.C.B., Garrido, S.S., Garcia, A., Delfino, D.B., Santos, L. do N., and Marchetto, R. (2012). Design and synthesis of peptides from bacterial ParE toxin as inhibitors of topoisomerases. Eu. J. Med. Chem. *54*, 591–596.

Berghoff, B.A., and Wagner, E.G.H. (2017). RNA-based regulation in type I toxin–antitoxin systems and its implication for bacterial persistence. Curr: Genet. *63*, 1011–1016.

Berghoff, B.A., Hoekzema, M., Aulbach, L., and Wagner, E.G.H. (2017). Two regulatory RNA elements affect TisB-dependent depolarization and persister formation: RNA-based regulation of depolarization and persistence. Mol. Microbiol. *103*, 1020–1033.

Bernard, P., and Couturier, M. (1992). Cell killing by the F plasmid CcdB protein involves poisoning of DNA-topoisomerase II complexes. J. Mol. Biol. *226*, 735–745.

Bessen, D.E., and Kalia, A. (2002). Genomic localization of a T serotype locus to a recombinatorial zone encoding extracellular matrix-binding proteins in *Streptococcus pyogenes*. Infect. Immun. *70*, 1159–1167.

Blower, T.R., Short, F.L., Rao, F., Mizuguchi, K., Pei, X.Y., Fineran, P.C., Luisi, B.F., and Salmond, G.P.C. (2012). Identification and classification of bacterial Type III toxin–antitoxin systems encoded in chromosomal and plasmid genomes. Nucleic Acids Res. *40*, 6158–6173.

Bordes, P., Sala, A.J., Ayala, S., Texier, P., Slama, N., Cirinesi, A.-M., Guillet, V., Mourey, L., and Genevaux, P. (2016). Chaperone addiction of toxin–antitoxin systems. Nat. Commun. *7*, 13339.

Brantl, S. (2012). Bacterial type I toxin-antitoxin systems. RNA Biol. *9*, 1488–1490.

Brantl, S., and Jahn, N. (2015). sRNAs in bacterial type I and type III toxin-antitoxin systems. FEMS Microbiol. Rev. *39*, 413–427.

Brown, J.M., and Shaw, K.J. (2003). A novel family of *Escherichia coli* toxin-antitoxin gene pairs. J. Bacteriol. *185*, 6600–6608.

Brown, B.L., Grigoriu, S., Kim, Y., Arruda, J.M., Davenport, A., Wood, T.K., Peti, W., and Page, R. (2009). Three dimensional structure of the MqsR:MqsA Complex: a novel TA pair comprised of a toxin homologous to RelE and an antitoxin with unique properties. PLoS Pathog. *5*, e1000706.

Brown, B.L., Lord, D.M., Grigoriu, S., Peti, W., and Page, R. (2013). The *Escherichia coli* toxin MqsR destabilizes the transcriptional repression complex formed between the Antitoxin MqsA and the *mqsRA* operon promoter. J. Biol. Chem. *288*, 1286–1294.

Brzozowska, I., and Zielenkiewicz, U. (2014). The ClpXP protease is responsible for the degradation of the epsilon antidote to the zeta toxin of the *Streptococcal* pSM19035 Plasmid. J. Biol. Chem. *289*, 7514–7523.

Bugrysheva, J.V., and Scott, J.R. (2010). The ribonucleases J1 and J2 are essential for growth and have independent roles in mRNA decay in *Streptococcus pyogenes*: RNases J1/J2 in *S. pyogenes*. Mol. Microbiol. *75*, 731–743.

Camacho, A.G., Misselwitz, R., Behlke, J., Ayora, S., Welfle, K., Meinhart, A., Lara, B., Saenger, W., Welfle, H., and Alons, J.C. (2002). In vitro and in vivo stability of the 2ζ2 protein complex of the broad host-range *Streptococcus pyogene*s pSM19035 addiction System. Biol. Chem. *383*.

Caparon, M.G., and Scott, J.R. (1991). Genetic manipulation of pathogenic streptococci. Meth. Enzymol. *204*, 556–586.

Castro-Roa, D., Garcia-Pino, A., De Gieter, S., van Nuland, N.A.J., Loris, R., and Zenkin, N. (2013). The Fic protein Doc uses an inverted substrate to phosphorylate and inactivate EF-Tu. Nat. Chem. Biol. *9*, 811–817.

Chatterjee, I., Somerville, G.A., Heilmann, C., Sahl, H.-G., Maurer, H.H., and Herrmann, M. (2006). Very low ethanol concentrations affect the viability and growth recovery in post-stationary-phase *Staphylococcus aureus* populations. Appl. Environ. Microbiol. *72*, 2627–2636.

Chatterji, D., and Kumar Ojha, A. (2001). Revisiting the stringent response, ppGpp and starvation signaling. Curr. Opin. Microbiol. *4*, 160–165.

Cherny, I., and Gazit, E. (2004). The YefM antitoxin defines a family of natively unfolded proteins implications as a novel antibacterial target. J. Biol. Chem. *279*, 8252–8261.

Cheverton, A.M., Gollan, B., Przydacz, M., Wong, C.T., Mylona, A., Hare, S.A., and Helaine, S. (2016). A Salmonella toxin promotes persister formation through acetylation of tRNA. Mol. Cell *63*, 86–96.

Chibani-Chennoufi, S., Bruttin, A., Dillmann, M.-L., and Brussow, H. (2004). Phage-host interaction: an ecological perspective. J. Bacteriol. *186*, 3677–3686.

Chopin, M.-C., Chopin, A., and Bidnenko, E. (2005). Phage abortive infection in lactococci: variations on a theme. Curr. Opin. Microbiol. *8*, 473–479.

Chowdhury, N., Kwan, B.W., and Wood, T.K. (2016). Persistence increases in the absence of the alarmone guanosine tetraphosphate by reducing cell growth. Sci. Rep. *6*.

Christensen, S.K., and Gerdes, K. (2003a). RelE toxins from bacteria and Archaea cleave mRNAs on translating ribosomes, which are rescued by tmRNA. Mol. Microbiol. *48*, 1389–1400.

Christensen, S.K., and Gerdes, K. (2003b). RelE toxins from Bacteria and Archaea cleave mRNAs on translating ribosomes, which are rescued by tmRNA: tmRNA counteracts RelE. Mol. Microbiol. *48*, 1389–1400.

Christensen, S.K., Mikkelsen, M., Pedersen, K., and Gerdes, K. (2001a). RelE, a global inhibitor of translation, is activated during nutritional stress. Proc. Natl. Acad. Sci. U.S.A. *98*, 14328–14333.

Christensen, S.K., Mikkelsen, M., Pedersen, K., and Gerdes, K. (2001b). RelE, a global inhibitor of translation, is activated during nutritional stress. Proc. Natl. Acad. Sci. U S A *98*, 14328–14333.

Christensen, S.K., Pedersen, K., Hansen, F.G., and Gerdes, K. (2003). Toxin-antitoxin loci as stress-response-elements: ChpAK/MazF and ChpBK cleave translated RNAs and are counteracted by tmRNA. J. Mol. Biol. *332*, 809–819.

Christensen-Dalsgaard, M., Jørgensen, M.G., and Gerdes, K. (2010). Three new RelE-homologous mRNA interferases of *Escherichia coli* differentially induced by environmental stresses. Mol. Microbiol. *75*, 333–348.

Conlon, B.P., Rowe, S.E., Gandt, A.B., Nuxoll, A.S., Donegan, N.P., Zalis, E.A., Clair, G., Adkins, J.N., Cheung, A.L., and Lewis, K. (2016). Persister formation in *Staphylococcus aureus* is associated with ATP depletion. Nat. Microbiol. *1*.

Culviner, P.H., and Laub, M.T. (2018). Global analysis of the *E. coli* toxin MazF reveals widespread cleavage of mRNA and the inhibition of rRNA maturation and ribosome Biogenesis. Mol. Cell. *70*, 868-880.e10.

Cunningham, M.W. (2000). Pathogenesis of group A *streptococcal* infections. Clin. Microbiol. Rev. *13*, 470–511.

Dalton, K.M., and Crosson, S. (2010). A conserved mode of protein recognition and binding in a ParD−ParE toxin−antitoxin complex. Biochem. *49*, 2205–2215.

De Jonge, N., Hohlweg, W., Garcia-Pino, A., Respondek, M., Buts, L., Haesaerts, S., Lah, J., Zangger, K., and Loris, R. (2010). Structural and thermodynamic characterization of *Vibrio fischeri* CcdB. J. Biol.l Chem. *285*, 5606–5613.

Deutscher, J., Francke, C., and Postma, P.W. (2006). how phosphotransferase system-related protein phosphorylation regulates carbohydrate metabolism in bacteria. Microb. Mol. Biol. Rev. *70*, 939–1031.

Dienemann, C., Bøggild, A., Winther, K.S., Gerdes, K., and Brodersen, D.E. (2011). crystal structure of the VapBC toxin–antitoxin complex from shigella flexneri reveals a hetero-octameric DNA-binding assembly. J. Mol. Biol. *414*, 713–722.

Donegan, N.P., Marvin, J.S., and Cheung, A.L. (2014). Role of adaptor TrfA and ClpPC in Controlling Levels of SsrA-tagged proteins and antitoxins in *Staphylococcus aureus.* J. Bacteriol. *196*, 4140–4151.

Dörr, T., Vulić, M., and Lewis, K. (2010). Ciprofloxacin causes persister formation by inducing the TisB toxin in *Escherichia coli*. PLoS Biol. *8*, e1000317.

Dubiel, A., Wegrzyn, K., Kupinski, A.P., and Konieczny, I. (2018). ClpAP protease is a universal factor that activates the *parDE* toxin-antitoxin system from a broad host range RK2 plasmid. Sci. Rep. *8*.

Durand, S., Gilet, L., and Condon, C. (2012a). The essential function of *B. subtilis* RNase III is to silence foreign toxin genes. PLoS Genet. *8*, e1003181.

Durand, S., Jahn, N., Condon, C., and Brantl, S. (2012b). Type I toxin-antitoxin systems in *Bacillus subtilis*. RNA Biol. *9*, 1491–1497.

Edgar, R.C. (2004). MUSCLE: multiple sequence alignment with high accuracy and high throughput. Nucleic Acids Res. *32*, 1792–1797.

Erental, A., Sharon, I., and Engelberg-Kulka, H. (2012). Two programmed cell death systems in *Escherichia coli*: an apoptotic-like death is inhibited by the *mazEF*-mediated death pathway. PLoS Biol. *10*, e1001281.

Fernández de Henestrosa, A.R., Ogi, T., Aoyagi, S., Chafin, D., Hayes, J.J., Ohmori, H., and Woodgate, R. (2002). Identification of additional genes belonging to the LexA regulon in *Escherichia coli*: Novel LexA-regulated genes in *E. coli.* Mol. Microbiol. *35*, 1560–1572.

Ferretti, J.J., McShan, W.M., Ajdic, D., Savic, D.J., Savic, G., Lyon, K., Primeaux, C., Sezate, S., Suvorov, A.N., Kenton, S., et al. (2001). Complete genome sequence of an M1 strain of *Streptococcus pyogenes*. Proc Natl Acad Sci U S A *98*, 4658–4663.

Fiebig, A., Castro Rojas, C.M., Siegal-Gaskins, D., and Crosson, S. (2010). Interaction specificity, toxicity and regulation of a paralogous set of ParE/RelE-family toxin-antitoxin systems. Mol. Microbiol. *77*, 236–251.

Fineran, P.C., Blower, T.R., Foulds, I.J., Humphreys, D.P., Lilley, K.S., and Salmond, G.P.C. (2009). The phage abortive infection system, ToxIN, functions as a protein–RNA toxin–antitoxin pair. PNAS *106*, 894–899.

Finn, R.D., Coggill, P., Eberhardt, R.Y., Eddy, S.R., Mistry, J., Mitchell, A.L., Potter, S.C., Punta, M., Qureshi, M., Sangrador-Vegas, A., et al. (2016). The Pfam protein families database: towards a more sustainable future. Nucleic Acids Res. *44*, D279–D285.

Fleurie, A., Lesterlin, C., Manuse, S., Zhao, C., Cluzel, C., Lavergne, J.-P., Franz-Wachtel, M., Macek, B., Combet, C., Kuru, E., et al. (2014). MapZ marks the division sites and positions FtsZ rings in *Streptococcus pneumoniae*. Nature *516*, 259–262.

Flynn, J.M. (2004). Modulating substrate choice: the SspB adaptor delivers a regulator of the extracytoplasmic-stress response to the AAA+ protease ClpXP for degradation. Genes. Dev. *18*, 2292–2301.

Fonfara, I., Le Rhun, A., Chylinski, K., Makarova, K.S., Lécrivain, A.-L., Bzdrenga, J., Koonin, E.V., and Charpentier, E. (2014). Phylogeny of Cas9 determines functional exchangeability of dual-RNA and Cas9 among orthologous type II CRISPR-Cas systems. Nucleic Acids Res. *42*, 2577–2590.

Forde, A., and Fitzgerald, G.F. (1999). Bacteriophage defence systems in lactic acid bacteria. Antonie Van Leeuwenhoek *76*, 89–113.

Forterre, P., Gribaldo, S., Gadelle, D., and Serre, M.-C. (2007). Origin and evolution of DNA topoisomerases. Biochimie *89*, 427–446.

Fozo, E.M. (2012). New type I toxin-antitoxin families from “wild” and laboratory strains of *E. coli*: Ibs-Sib, ShoB-OhsC and Zor-Orz. RNA Biol. *9*, 1504–1512.

Fozo, E.M., Hemm, M.R., and Storz, G. (2008a). Small toxic proteins and the antisense RNAs that repress them. Microbiol. Mol. Biol. Rev. *72*, 579–589.

Fozo, E.M., Kawano, M., Fontaine, F., Kaya, Y., Mendieta, K.S., Jones, K.L., Ocampo, A., Rudd, K.E., and Storz, G. (2008b). Repression of small toxic protein synthesis by the Sib and OhsC small RNAs. Mol. Microbiol. *70*, 1076–1093.

Franch, T., Gultyaev, A.P., and Gerdes, K. (1997). Programmed cell death by hok/sok of plasmid R1: Processing at the hok mRNA 3′-end triggers structural rearrangements that allow translation and antisense RNA binding. J. Mol. Biol.*273*, 38–51.

Galluzzi, L., Vitale, I., Aaronson, S.A., Abrams, J.M., Adam, D., Agostinis, P., Alnemri, E.S., Altucci, L., Amelio, I., Andrews, D.W., et al. (2018). Molecular mechanisms of cell death: recommendations of the Nomenclature Committee on Cell Death 2018. Cell Death & Differentiation *25*, 486–541.

Garcia-Pino, A., Balasubramanian, S., Wyns, L., Gazit, E., De Greve, H., Magnuson, R.D., Charlier, D., van Nuland, N.A.J., and Loris, R. (2010). Allostery and intrinsic disorder mediate transcription regulation by conditional cooperativity. Cell *142*, 101–111.

Garcia-Pino, A., De Gieter, S., Talavera, A., De Greve, H., Efremov, R.G., and Loris, R. (2016a). An intrinsically disordered entropic switch determines allostery in Phd–Doc regulation. Nat. Chem. Biol. *12*, 490–496.

Garcia-Pino, A., De Gieter, S., Talavera, A., De Greve, H., Efremov, R.G., and Loris, R. (2016b). An intrinsically disordered entropic switch determines allostery in Phd–Doc regulation. Nat. Chem. Biol. *12*, 490–496.

Gerdes, K., and Wagner, E.G.H. (2007). RNA antitoxins. Curr. Opin. Microbiol. *10*, 117–124.

Gerdes, K., Rasmussen, P.B., and Molin, S. (1986). Unique type of plasmid maintenance function: postsegregational killing of plasmid-free cells. PNAS. *83*, 3116–3120.

Gerdes, K., Nielsen, A., Thorsted, P., and Wagner, E.G.H. (1992). Mechanism of killer gene activation. Antisense RNA-dependent RNase III cleavage ensures rapid turn-over of the stable Hok, SrnB and PndA effector messenger RNAs. J. .Mol. Biol. *226*, 637–649.

Gerdes, K., Christensen, S.K., and Løbner-Olesen, A. (2005). Prokaryotic toxin–antitoxin stress response loci. Nat. Rev. Micro. *3*, 371–382.

Germain, E., Castro-Roa, D., Zenkin, N., and Gerdes, K. (2013). Molecular mechanism of bacterial persistence by HipA. Mol. Cell. *52*, 248–254.

Goeders, N., Chai, R., Chen, B., Day, A., and Salmond, G. (2016). Structure, evolution, and functions of bacterial type III Toxin-Antitoxin Systems. Toxins *8*, 282.

Goormaghtigh, F., Fraikin, N., Putrinš, M., Hallaert, T., Hauryliuk, V., Garcia-Pino, A., Sjödin, A., Kasvandik, S., Udekwu, K., Tenson, T., et al. (2018a). Reassessing the role of Type II toxin-antitoxin systems in formation of *Escherichia coli* type II persister cells. MBio *9*.

Goormaghtigh, F., Fraikin, N., Putrinš, M., Hauryliuk, V., Garcia-Pino, A., Udekwu, K., Tenson, T., Kaldalu, N., and Van Melderen, L. (2018b). Reply to Holden and Errington, “type ii toxin-antitoxin systems and persister cells.” MBio *9*.

Granok, A.B., Parsonage, D., Ross, R.P., and Caparon, M.G. (2000). The RofA binding site in *Streptococcus pyogenes* is utilized in multiple transcriptional pathways. J. Bacteriol. *182*, 1529–1540.

Gryllos, I., Levin, J.C., and Wessels, M.R. (2003). The CsrR/CsrS two-component system of group A *Streptococcus* responds to environmental Mg2+. PNAS. *100*, 4227–4232.

Gupta, M., Nayyar, N., Chawla, M., Sitaraman, R., Bhatnagar, R., and Banerjee, N. (2016). The chromosomal parDE2 toxin-antitoxin system of *Mycobacterium tuberculosis* H37Rv: genetic and functional characterization. Front. Microbiol. *7*, 886.

Gurnev, P.A., Ortenberg, R., Dörr, T., Lewis, K., and Bezrukov, S.M. (2012). Persister-promoting bacterial toxin TisB produces anion-selective pores in planar lipid bilayers. FEBS Letters *586*, 2529–2534.

Guzman, L.M., Belin, D., Carson, M.J., and Beckwith, J. (1995). Tight regulation, modulation, and high-level expression by vectors containing the arabinose PBAD promoter. J. Bacteriol. *177*, 4121–4130.

Hallez, R., Geeraerts, D., Sterckx, Y., Mine, N., Loris, R., and Van Melderen, L. (2010). New toxins homologous to ParE belonging to three-component toxin-antitoxin systems in *Escherichia coli* O157:H7. Mol. Microbiol. *76*, 719–732.

Hansen, S., Vulić, M., Min, J., Yen, T.-J., Schumacher, M.A., Brennan, R.G., and Lewis, K. (2012). Regulation of the *Escherichia coli* HipBA toxin-antitoxin system by proteolysis. PLoS ONE *7*, e39185.

Harms, A., Stanger, F.V., Scheu, P.D., de Jong, I.G., Goepfert, A., Glatter, T., Gerdes, K., Schirmer, T., and Dehio, C. (2015). Adenylylation of gyrase and topo IV by FicT toxins disrupts bacterial dna topology. Cell Rep. *12*, 1497–1507.

Harms, A., Fino, C., Sørensen, M.A., Semsey, S., and Gerdes, K. (2017). Prophages and growth dynamics confound experimental results with antibiotic-tolerant persister cells. MBio *8*, e01964-17.

Harms, A., Brodersen, D.E., Mitarai, N., and Gerdes, K. (2018). Toxins, targets, and triggers: an overview of toxin-antitoxin biology. Mol. Cell *70*, 768–784.

Harrison, J.J., Wade, W.D., Akierman, S., Vacchi-Suzzi, C., Stremick, C.A., Turner, R.J., and Ceri, H. (2009). The chromosomal toxin gene *yafQ* Is a determinant of multidrug tolerance for *Escherichia coli* growing in a biofilm. Antimicrob. Agents. Chemothe. *53*, 2253–2258.

Helaine, S., Cheverton, A.M., Watson, K.G., Faure, L.M., Matthews, S.A., and Holden, D.W. (2014). Internalization of *Salmonella* by macrophages induces formation of nonreplicating persisters. Science *343*, 204–208.

Heller, D.M., Tavag, M., and Hochschild, A. (2017). CbtA toxin of *Escherichia coli* inhibits cell division and cell elongation via direct and independent interactions with FtsZ and MreB. PLoS Genet. *13*, e1007007.

Holden, D.W., and Errington, J. (2018). Type II Toxin-Antitoxin Systems and Persister Cells. MBio *9*.

Hu, Y., Benedik, M.J., and Wood, T.K. (2012). Antitoxin DinJ influences the general stress response through transcript stabilizer CspE: DinJ regulates the general stress response. Environ.l Microbiol. *14*, 669–679.

Hynes, W., and Sloan, M. (2016). Secreted Extracellular Virulence Factors. In *Streptococcus pyogenes* : Basic biology to clinical manifestations, J.J. Ferretti, D.L. Stevens, and V.A. Fischetti, eds. (Oklahoma City (OK): University of Oklahoma Health Sciences Center), p.

Jana, B., Tao, L., and Biswas, I. (2016). Strain-Dependent Recognition of a Unique Degradation Motif by ClpXP in *Streptococcus mutan*s. MSphere *1*.

Jankevicius, G., Ariza, A., Ahel, M., and Ahel, I. (2016). The toxin-antitoxin system DarTG catalyzes reversible ADP-ribosylation of DNA. Mol. Cell *64*, 1109–1116.

Jensen, R.B., and Gerdes, K. (1995). Programmed cell death in bacteria: proteic plasmid stabilization systems. Mol. Microbiol. *17*, 205–210.

Jiang, Y., Pogliano, J., Helinski, D.R., and Konieczny, I. (2002). ParE toxin encoded by the broad□host□range plasmid RK2 is an inhibitor of *Escherichia coli* gyrase. Mol. Microbiol. *44*, 971–979.

Johnson, E.P., Strom, A.R., and Helinski, D.R. (1996). Plasmid RK2 toxin protein ParE: purification and interaction with the ParD antitoxin protein. J. Bacteriol. *178*, 1420–1429.

Justice, S.S., García-Lara, J., and Rothfield, L.I. (2000). Cell division inhibitors SulA and MinC/MinD block septum formation at different steps in the assembly of the *Escherichia coli* division machinery. Mol. Microbiol. *37*, 410–423.

Kampranis, S.C., Howells, A.J., and Maxwell, A. (1999). The interaction of DNA gyrase with the bacterial toxin CcdB: evidence for the existence of two gyrase-CcdB complexes 1 1Edited by I. B. Holland. J. Mol. Biol. *293*, 733–744.

Kato, J., Nishimura, Y., Imamura, R., Niki, H., Hiraga, S., and Suzuki, H. (1990). New topoisomerase essential for chromosome segregation in *E. coli*. Cell *63*, 393–404.

Katoh, K., Misawa, K., Kuma, K., and Miyata, T. (2002). MAFFT: a novel method for rapid multiple sequence alignment based on fast Fourier transform. Nucleic Acids Res. *30*, 3059–3066.

Kawano, M. (2005). Detection of 5'- and 3'-UTR-derived small RNAs and cis-encoded antisense RNAs in *Escherichia coli.* Nucleic Acids Res. *33*, 1040–1050.

Kawano, M. (2012). Divergently overlapping *cis* -encoded antisense RNA regulating toxin-antitoxin systems from *E. coli*: *hok* / *sok* , *ldr* / *rdl* , *symE* / *symR*. RNA Biology *9*, 1520–1527.

Kawano, M., Aravind, L., and Storz, G. (2007). An antisense RNA controls synthesis of an SOS-induced toxin evolved from an antitoxin. Mol. Microbiol. *64*, 738–754.

Kelley, L.A., Mezulis, S., Yates, C.M., Wass, M.N., and Sternberg, M.J.E. (2015). The Phyre2 web portal for protein modeling, prediction and analysis. Nat. Protoc. *10*, 845.

Keren, I., Shah, D., Spoering, A., Kaldalu, N., and Lewis, K. (2004). Specialized persister cells and the mechanism of multidrug tolerance in *Escherichia coli.* J. Bacteriol. *186*, 8172–8180.

Kim, Y., Wang, X., Ma, Q., Zhang, X.-S., and Wood, T.K. (2009). Toxin-antitoxin systems in *Escherichia coli* influence biofilm formation through YjgK (TabA) and fimbriae. J. Bacteriol. *191*, 1258–1267.

Kirstein, J., Molière, N., Dougan, D.A., and Turgay, K. (2009). Adapting the machine: adaptor proteins for Hsp100/Clp and AAA+ proteases. Nat. Rev. Micro. *7*, 589–599.

Koga, M., Otsuka, Y., Lemire, S., and Yonesaki, T. (2011). *Escherichia coli rnlA* and *rnlB* compose a novel toxin-antitoxin system. Genetics. *187*, 123–130.

Kolodkin-Gal, I., Verdiger, R., Shlosberg-Fedida, A., and Engelberg-Kulka, H. (2009). A differential effect of *E. coli* toxin-antitoxin systems on cell death in liquid media and biofilm formation. PLoS ONE *4*, e6785.

Korch, S.B., and Hill, T.M. (2006). Ectopic Overexpression of wild-type and mutant hipA genes in *Escherichia coli*: effects on macromolecular synthesis and persister formation. J. Bacteriol. *188*, 3826–3836.

Kubik, S., Wegrzyn, K., Pierechod, M., and Konieczny, I. (2012). Opposing effects of DNA on proteolysis of a replication initiator. Nucleic Acids Res. *40*, 1148–1159.

Kumar, P., Issac, B., Dodson, E.J., Turkenburg, J.P., and Mande, S.C. (2008). Crystal structure of *Mycobacterium tuberculosis* YefM Antitoxin reveals that it is not an intrinsically unstructured protein. J. Mol. Biol. *383*, 482–493.

Lambert, J.M., Bongers, R.S., and Kleerebezem, M. (2007). Cre-lox-based system for multiple gene deletions and selectable-marker removal in *Lactobacillus plantarum*. Appl Environ. Microbiol. *73*, 1126–1135.

Lancefield, R.C. (1962). Current knowledge of type-specific M antigens of group A *streptococci*. J. Immunol. *89*, 307–313.

Le Breton, Y., Belew, A.T., Valdes, K.M., Islam, E., Curry, P., Tettelin, H., Shirtliff, M.E., El-Sayed, N.M., and McIver, K.S. (2015). Essential genes in the core genome of the human pathogen *Streptococcus pyogenes*. Scientific Reports *5*.

Le Rhun, A., Beer, Y.Y., Reimegård, J., Chylinski, K., and Charpentier, E. (2016). RNA sequencing uncovers antisense RNAs and novel small RNAs in *Streptococcus pyogenes*. RNA Biol. *13*, 177–195.

Lehnherr, H., and Yarmolinsky, M.B. (1995). Addiction protein Phd of plasmid prophage P1 is a substrate of the ClpXP serine protease of *Escherichia coli*. PNAS. *92*, 3274–3277.

Leplae, R., Geeraerts, D., Hallez, R., Guglielmini, J., Drèze, P., and Van Melderen, L. (2011). Diversity of bacterial type II toxin–antitoxin systems: a comprehensive search and functional analysis of novel families. Nucleic Acids Res. *39*, 5513–5525.

Le Rhun, A., Lécrivain, A.-L., Reimegård, J., Proux-Wéra, E., Broglia, L., Della Beffa, C., and Charpentier, E. (2017). Identification of endoribonuclease specific cleavage positions reveals novel targets of RNase III in *Streptococcus pyogenes*. Nucleic Acids Res. gkw1316.

Levchenko, I., Seidel, M., Sauer, R.T., and Baker, T.A. (2000). A specificity-enhancing factor for the ClpXP degradation machine. Science *289*, 2354–2356.

Lewis, K. (2010). Persister cells. Ann. Rev. Microbiol. *64*, 357–372.

Lima-Mendez, G., Toussaint, A., and Leplae, R. (2007). Analysis of the phage sequence space: The benefit of structured information. Virology *365*, 241–249.

Lobato-Márquez, D., Moreno-Córdoba, I., Figueroa, V., Díaz-Orejas, R., and García-del Portillo, F. (2015). Distinct type I and type II toxin-antitoxin modules control *Salmonella* lifestyle inside eukaryotic cells. Sci. Rep. *5*.

Lutz, R., and Bujard, H. (1997). Independent and tight regulation of transcriptional units in *Escherichia coli* via the LacR/O, the TetR/O and AraC/I1-I2 regulatory elements. Nucleic Acids Res. *25*, 1203–1210.

Lybecker, M., Zimmermann, B., Bilusic, I., Tukhtubaeva, N., and Schroeder, R. (2014). The double-stranded transcriptome of *Escherichia coli*. PNAS. *111*, 3134–3139.

Madl, T., Van Melderen, L., Mine, N., Respondek, M., Oberer, M., Keller, W., Khatai, L., and Zangger, K. (2006). Structural basis for nucleic acid and toxin recognition of the bacterial antitoxin CcdA. J. Mol. Biol. *364*, 170–185.

Magnuson, R.D. (2007). Hypothetical functions of Toxin-Antitoxin systems. J. Bacteriol. *189*, 6089–6092.

Magnuson, R., and Yarmolinsky, M.B. (1998). Corepression of the P1 addiction operon by Phd and Doc. J. Bacteriol. *180*, 6342–6351.

Maisonneuve, E., Castro-Camargo, M., and Gerdes, K. (2013). RETRACTED: (p)ppGpp controls bacterial persistence by stochastic induction of toxin-antitoxin activity. Cell *154*, 1140–1150.

Masuda, H., Tan, Q., Awano, N., Wu, K.-P., and Inouye, M. (2012). YeeU enhances the bundling of cytoskeletal polymers of MreB and FtsZ, antagonizing the CbtA (YeeV) toxicity in *Escherichia coli*: YeeU enhances bundling of MreB and FtsZ filaments. Mol. Microbiol. *84*, 979–989.

Mayer, C., and Janin, Y.L. (2014). Non-quinolone Inhibitors of Bacterial Type IIA Topoisomerases: A Feat of Bioisosterism. Chem. Rev. *114*, 2313–2342.

McCool, J.D., Long, E., Petrosino, J.F., Sandler, H.A., Rosenberg, S.M., and Sandler, S.J. (2004). Measurement of SOS expression in individual *Escherichia coli* K-12 cells using fluorescence microscopy: SOS expression using fluorescence microscopy. Mol. Microbiol.*53*, 1343–1357.

Meier-Kolthoff, J.P., Auch, A.F., Klenk, H.-P., and Göker, M. (2013). Genome sequence-based species delimitation with confidence intervals and improved distance functions. BMC Bioinform. *14*, 60.

Meinhart, A., Alonso, J.C., Strater, N., and Saenger, W. (2003). Crystal structure of the plasmid maintenance system / : Functional mechanism of toxin and inactivation by 2 2 complex formation. PNAS. *100*, 1661–1666.

Melderen, L., Bernard, P., and Couturier, M. (1994). Lon-dependent proteolysis of CcdA is the key control for activation of CcdB in plasmid-free segregant bacteria. Mol. Microbiol. *11*, 1151–1157.

Monti, M.C., Hernández-Arriaga, A.M., Kamphuis, M.B., López-Villarejo, J., Heck, A.J.R., Boelens, R., Díaz-Orejas, R., and van den Heuvel, R.H.H. (2007). Interactions of Kid–Kis toxin–antitoxin complexes with the *parD* operator-promoter region of plasmid R1 are piloted by the Kis antitoxin and tuned by the stoichiometry of Kid–Kis oligomers. Nucleic Acids Res. *35*, 1737–1749.

Mora, M., Bensi, G., Capo, S., Falugi, F., Zingaretti, C., Manetti, A.G.O., Maggi, T., Taddei, A.R., Grandi, G., and Telford, J.L. (2005). Group A Streptococcus produce pilus-like structures containing protective antigens and Lancefield T antigens. PNAS. *102*, 15641–15646.

Moyed, H.S., and Bertrand, K.P. (1983). hipA, a newly recognized gene of *Escherichia coli* K-12 that affects frequency of persistence after inhibition of murein synthesis. J. Bacteriol. *155*, 768–775.

Mukherjee, A., Cao, C., and Lutkenhaus, J. (1998). Inhibition of FtsZ polymerization by SulA, an inhibitor of septation in *Escherichia coli.* PNAS. *95*, 2885–2890.

Muthuramalingam, M., White, J.C., and Bourne, C.R. (2016). Toxin-antitoxin modules are pliable switches activated by multiple protease pathways. Toxins (Basel) *8*.

Muthuramalingam, M., White, J.C., Murphy, T., Ames, J.R., and Bourne, C.R. (2018). The toxin from a ParDE toxin-antitoxin system found in *Pseudomonas aeruginosa* offers protection to cells challenged with anti-gyrase antibiotics. Mol. Microbiol.

Mutschler, H., Gebhardt, M., Shoeman, R.L., and Meinhart, A. (2011). A novel mechanism of programmed cell death in bacteria by toxin–antitoxin systems corrupts peptidoglycan synthesis. PLoS Biol. *9*, e1001033.

Neher, S.B. (2003). Latent ClpX-recognition signals ensure LexA destruction after DNA damage. Genes Develop.*17*, 1084–1089.

Norton, J.P., and Mulvey, M.A. (2012). Toxin-Antitoxin systems are important for niche-specific colonization and stress resistance of uropathogenic *Escherichia coli*. PLoS Patho. *8*, e1002954.

Oberer, M., Zangger, K., Prytulla, S., and Keller, W. (2002). The antitoxin ParD of plasmid RK2 consists of two structurally distinct moieties and belongs to the ribbon-helix-helix family of DNA-binding proteins. Biochem. J. *361*, 41–47.

Oberer, M., Zangger, K., Gruber, K., and Keller, W. (2007). The solution structure of ParD, the antidote of the ParDE toxin antitoxin module, provides the structural basis for DNA and toxin binding. Protein Sci. *16*, 1676–1688.

Oberto, J. (2013). SyntTax: a web server linking synteny to prokaryotic taxonomy. BMC Bioinform. *14*, 4.

Ogura, T., and Hiraga, S. (1983). Mini-F plasmid genes that couple host cell division to plasmid proliferation. PNAS *80*, 4784–4788.

Osterlund, A., and Engstrand, L. (1997). An intracellular sanctuary for *Streptococcus pyogenes* in human tonsillar epithelium--studies of asymptomatic carriers and in vitro cultured biopsies. Acta Otolaryngol. *117*, 883–888.

Otsuka, Y., and Yonesaki, T. (2012). Dmd of bacteriophage T4 functions as an antitoxin against *Escherichia coli* LsoA and RnlA toxins: T4 phage Dmd as an antitoxin. Mol. Microbiol. *83*, 669–681.

Overgaard, M., Borch, J., Jørgensen, M.G., and Gerdes, K. (2008). Messenger RNA interferase RelE controls *relBE* transcription by conditional cooperativity. Mol. Microbiol. *69*, 841–857.

Page, R., and Peti, W. (2016). Toxin-antitoxin systems in bacterial growth arrest and persistence. Nat. Chem. Biol. *12*, 208–214.

Pall, G.S., and Hamilton, A.J. (2008). Improved northern blot method for enhanced detection of small RNA. Nat. Protoc. *3*, 1077–1084.

Pecota, D.C., and Wood, T.K. (1996). Exclusion of T4 phage by the hok/sok killer locus from plasmid R1. J. Bacteriol. *178*, 2044–2050.

Pedersen, K., and Gerdes, K. (1999). Multiple hok genes on the chromosome of *Escherichia coli*. Mol. Microbiol. *32*, 1090–1102.

Petty, N.K., Evans, T.J., Fineran, P.C., and Salmond, G.P.C. (2007). Biotechnological exploitation of bacteriophage research. Trends Biotech. *25*, 7–15.

Pfaffl, M.W. (2001). A new mathematical model for relative quantification in real-time RT-PCR. Nucleic Acids Res. *29*, e45.

Pilla, G., and Tang, C.M. (2018). Going around in circles: virulence plasmids in enteric pathogens. Nat. Rev. Microbiol. *16*, 484–495.

Postow, L., Crisona, N.J., Peter, B.J., Hardy, C.D., and Cozzarelli, N.R. (2001). Topological challenges to DNA replication: conformations at the fork. PNAS *98*, 8219–8226.

Prysak, M.H., Mozdzierz, C.J., Cook, A.M., Zhu, L., Zhang, Y., Inouye, M., and Woychik, N.A. (2009). Bacterial toxin YafQ is an endoribonuclease that associates with the ribosome and blocks translation elongation through sequence-specific and frame-dependent mRNA cleavage. Mol. Microbiol. *71*, 1071–1087.

Ramage, H.R., Connolly, L.E., and Cox, J.S. (2009). Comprehensive functional analysis of *Mycobacterium tuberculosis* toxin-antitoxin systems: implications for pathogenesis, stress responses, and evolution. PLoS Genet. *5*, e1000767.

Ringquist, S., Shinedling, S., Barrick, D., Green, L., Binkley, J., Stormo, G.D., and Gold, L. (1992a). Translation initiation in *Escherichia coli:* sequences within the ribosome-binding site. Mol. Microbiol. *6*, 1219–1229.

Ringquist, S., Shinedling, S., Barrick, D., Green, L., Binkley, J., Stormo, G.D., and Gold, L. (1992b). Translation initiation in *Escherichia coli*: sequences within the ribosome-binding site. Mol. Microbiol. *6*, 1219–1229.

Roberts, R.C., and Helinski, D.R. (1992). Definition of a minimal plasmid stabilization system from the broad-host-range plasmid RK2. J. Bacteriol. *174*, 8119–8132.

Roberts, R.C., Ström, A.R., and Helinski, D.R. (1994a). The parDE Operon of the Broad-host-range Plasmid RK2 Specifies Growth Inhibition Associated with Plasmid Loss. J. Mol. Biol. *237*, 35–51.

Roberts, R.C., Ström, A.R., and Helinski, D.R. (1994b). The parDE operon of the broad-host-range plasmid RK2 Specifies growth inhibition associated with plasmid loss. J. Mol, Biol, *237*, 35–51.

Robinson, J.T., Thorvaldsdóttir, H., Winckler, W., Guttman, M., Lander, E.S., Getz, G., and Mesirov, J.P. (2011). Integrative genomics viewer. Nat, Biotech, *29*, 24–26.

Rocker, A., Peschke, M., Kittilä, T., Sakson, R., Brieke, C., and Meinhart, A. (2018). The ng_ζ1 toxin of the gonococcal epsilon/zeta toxin/antitoxin system drains precursors for cell wall synthesis. Nat. Comm. *9*.

Ruangprasert, A., Maehigashi, T., Miles, S.J., and Dunham, C.M. (2017). Importance of the *E. coli* DinJ antitoxin carboxy terminus for toxin suppression and regulated proteolysis: Functional characterization of the *E. coli* DinJ-YafQ complex. Mol. Microbiol. *104*, 65–77.

Rycroft, J.A., Gollan, B., Grabe, G.J., Hall, A., Cheverton, A.M., Larrouy-Maumus, G., Hare, S.A., and Helaine, S. (2018). Activity of acetyltransferase toxins involved in Salmonella persister formation during macrophage infection. Nat. Comm. *9*.

Sala, A., Bordes, P., and Genevaux, P. (2014). Multiple Toxin-Antitoxin Systems in *Mycobacterium tuberculosis*. Toxins *6*, 1002–1020.

Sambrook, J., and Russell, D.W. (2001). Molecular Cloning: A Laboratory Manual (CSHL Press).

Samson, J.E., Spinelli, S., Cambillau, C., and Moineau, S. (2013). Structure and activity of AbiQ, a lactococcal endoribonuclease belonging to the type III toxin-antitoxin system: AbiQ, a type III toxin-antitoxin system. Mol. Microbiol. *87*, 756–768.

Sberro, H., Leavitt, A., Kiro, R., Koh, E., Peleg, Y., Qimron, U., and Sorek, R. (2013). Discovery of Functional Toxin/Antitoxin Systems in Bacteria by Shotgun Cloning. Mol. Cell *50*, 136–148.

Schneider, C.A., Rasband, W.S., and Eliceiri, K.W. (2012). NIH Image to ImageJ: 25 years of image analysis. Nat. Meth. *9*, 671–675.

Sevin, E.W., and Barloy-Hubler, F. (2007). RASTA-Bacteria: a web-based tool for identifying toxin-antitoxin loci in prokaryotes. Gen. Biol. *8*, R155.

Shan, Y., Brown Gandt, A., Rowe, S.E., Deisinger, J.P., Conlon, B.P., and Lewis, K. (2017). ATP-Dependent Persister Formation in *Escherichia coli*. MBio *8*, e02267-16.

Shih, Y.-L., and Rothfield, L. (2006). The Bacterial Cytoskeleton. Microbiol. Mol. Biol. Rev. *70*, 729–754.

Short, F.L., Monson, R.E., and Salmond, G.P. (2015). A Type III protein-RNA toxin-antitoxin system from *Bacillus thuringiensis* promotes plasmid retention during spore development. RNA Biol. *12*, 933–937.

Sissi, C., and Palumbo, M. (2010). In front of and behind the replication fork: bacterial type IIA topoisomerases. Cell. Mol, Life Sci, *67*, 2001–2024.

Smith, A.S.G., and Rawlings, D.E. (1997). The poison-antidote stability system of the broad-host-range *Thiobacillus ferrooxidans* plasmid pTF-FC2. Mol, Microbiol, *26*, 961–970.

Smith, A.B., López-Villarejo, J., Diago-Navarro, E., Mitchenall, L.A., Barendregt, A., Heck, A.J., Lemonnier, M., Maxwell, A., and Díaz-Orejas, R. (2012). A common origin for the bacterial toxin-antitoxin systems *parD* and *ccd*, Suggested by analyses of toxin/target and toxin/antitoxin interactions. PLoS ONE *7*, e46499.

Sorek, R., Kunin, V., and Hugenholtz, P. (2008). CRISPR — a widespread system that provides acquired resistance against phages in bacteria and archaea. Nat. Rev. Microbiol. *6*, 181–186.

Stamatakis, A. (2014). RAxML version 8: a tool for phylogenetic analysis and post-analysis of large phylogenies. Bioinformatics *30*, 1312–1313.

Stamsås, G.A., Myrbråten, I.S., Straume, D., Salehian, Z., Veening, J.-W., Håvarstein, L.S., and Kjos, M. (2018). CozEa and CozEb play overlapping and essential roles in controlling cell division in *Staphylococcus aureus*: CozE proteins control staphylococcal cell division. Mol. Microbiol.

Steiner, K., and Malke, H. (2001). relA-Independent Amino Acid Starvation Response Network of *Streptococcus pyogenes*. J. Bacteriol. *183*, 7354–7364.

Stevens, D.L., Bisno, A.L., Chambers, H.F., Dellinger, E.P., Goldstein, E.J.C., Gorbach, S.L., Hirschmann, J.V., Kaplan, S.L., Montoya, J.G., and Wade, J.C. (2014). Executive summary: practice guidelines for the diagnosis and management of skin and soft tissue infections: 2014 update by the infectious diseases society of america. Clinical Infectious Diseases *59*, 147–159.

Sun, C., Guo, Y., Tang, K., Wen, Z., Li, B., Zeng, Z., and Wang, X. (2017). MqsR/MqsA toxin/antitoxin system regulates persistence and biofilm formation in *Pseudomonas putida* KT2440. Front. Microbiol. *8*.

Surovtsev, I.V., and Jacobs-Wagner, C. (2018). Subcellular organization: a critical feature of bacterial cell replication. Cell *172*, 1271–1293.

Syal, K., and Chatterji, D. (2015). Differential binding of ppGpp and pppGpp to *E. coli* RNA polymerase: photo-labeling and mass spectral studies. Genes Cells *20*, 1006–1016.

Szekeres, S., Dauti, M., Wilde, C., Mazel, D., and Rowe-Magnus, D.A. (2007). Chromosomal toxin-antitoxin loci can diminish large-scale genome reductions in the absence of selection: Chromosomal addiction loci minimize gene loss. Mol. Microbiol. *63*, 1588–1605.

Tan, Q., Awano, N., and Inouye, M. (2011). YeeV is an *Escherichia coli* toxin that inhibits cell division by targeting the cytoskeleton proteins, FtsZ and MreB: YeeV targets the cytoskeleton proteins. Mol. Microbiol. *79*, 109–118.

Tanouchi, Y., Lee, A.J., Meredith, H., and You, L. (2013). Programmed cell death in bacteria and implications for antibiotic therapy. Trends. Microbiol. *21*, 265–270.

Tao, L., and Biswas, I. (2015). Degradation of SsrA-tagged proteins in streptococci. Microbiology (Reading, Engl.) *161*, 884–894.

Thisted, T., and Gerdes, K. (1992). Mechanism of post-segregational killing by the hok/sok system of plasmid R1. J. Mol. Biol. *223*, 41–54.

Thorvaldsdottir, H., Robinson, J.T., and Mesirov, J.P. (2013). Integrative Genomics Viewer (IGV): high-performance genomics data visualization and exploration. Brief. Bioinform. *14*, 178–192.

Tian, Q.B., Ohnishi, M., Murata, T., Nakayama, K., Terawaki, Y., and Hayashi, T. (2001). Specific protein–DNA and protein–protein interaction in the hig gene system, a plasmid-borne proteic killer gene system of plasmid Rts1. Plasmid *45*, 63–74.

Traxler, M.F., Summers, S.M., Nguyen, H.-T., Zacharia, V.M., Smith, J.T., and Conway, T. (2008). The global, ppGpp-mediated stringent response to amino acid starvation in *Escherichia coli.* Mol. Microbiol. *68*, 1128–1148.

Tripathi, A., Dewan, P.C., Siddique, S.A., and Varadarajan, R. (2014). MazF-induced growth inhibition and persister generation in *Escherichia coli*. J. Biol. Chem. *289*, 4191–4205.

Tsatsaronis, J.A., Walker, M.J., and Sanderson-Smith, M.L. (2014). Host responses to group A Streptococcus: Cell Death and Inflammation. PLoS Pathogens *10*, e1004266.

Tsuchimoto, S., and Ohtsubo, E. (1993). Autoregulation by cooperative binding of the PemI and PemK proteins to the promoter region of the pem operon. Mol. Gen. Genet. *237*, 81–88.

Tsuchimoto, S., Nishimura, Y., and Ohtsubo, E. (1992). The stable maintenance system pem of plasmid R100: degradation of PemI protein may allow PemK protein to inhibit cell growth. J. Bacteriol. *174*, 4205–4211.

Unterholzner, S.J., Poppenberger, B., and Rozhon, W. (2013). Toxin–antitoxin systems: Biology, identification, and application. Mobile Genetic Elements *3*, e26219.

Van Acker, H., Sass, A., Dhondt, I., Nelis, H.J., and Coenye, T. (2014). Involvement of toxin-antitoxin modules in *Burkholderia cenocepacia* biofilm persistence. Patho. .Dis. *71*, 326–335.

Van Melderen, L. (2010). Toxin–antitoxin systems: why so many, what for? Curr. Opi. Microbiol. *13*, 781–785.

Vos, S.M., Tretter, E.M., Schmidt, B.H., and Berger, J.M. (2011). All tangled up: how cells direct, manage and exploit topoisomerase function. Nat. Rev. Mol. Cell Biol. *12*, 827–841.

Wagner, E.G.H., and Unoson, C. (2012). The toxin-antitoxin system tisB-istR1: Expression, regulation, and biological role in persister phenotypes. RNA Biol. *9*, 1513–1519.

Walker, M.J., Barnett, T.C., McArthur, J.D., Cole, J.N., Gillen, C.M., Henningham, A., Sriprakash, K.S., Sanderson-Smith, M.L., and Nizet, V. (2014). Disease manifestations and pathogenic mechanisms of Group A Streptococcus. Clin. Microbiol. Rev. *27*, 264–301.

Walling, L.R., and Butler, J.S. (2016). Structural determinants for antitoxin identity and insulation of cross talk between homologous toxin-antitoxin systems. J. Bacteriol. *198*, 3287–3295.

Wang, X., Kim, Y., Hong, S.H., Ma, Q., Brown, B.L., Pu, M., Tarone, A.M., Benedik, M.J., Peti, W., Page, R., et al. (2011). Antitoxin MqsA helps mediate the bacterial general stress response. Nat. Chem. Biol. *7*, 359–366.

Wang, X., Lord, D.M., Cheng, H.-Y., Osbourne, D.O., Hong, S.H., Sanchez-Torres, V., Quiroga, C., Zheng, K., Herrmann, T., Peti, W., et al. (2012). A new type V toxin-antitoxin system where mRNA for toxin GhoT is cleaved by antitoxin GhoS. Nat. Chem. Biol. *8*, 855–861.

Wang, X., Lord, D.M., Hong, S.H., Peti, W., Benedik, M.J., Page, R., and Wood, T.K. (2013). Type II toxin/antitoxin MqsR/MqsA controls type V toxin/antitoxin GhoT/GhoS: Type V TA pair GhoT/GhoS is regulated by MqsR. Environ. Microbiol.*15*, 1734–1744.

Waterhouse, A., Bertoni, M., Bienert, S., Studer, G., Tauriello, G., Gumienny, R., Heer, F.T., de Beer, T.A.P., Rempfer, C., Bordoli, L., et al. (2018). SWISS-MODEL: homology modelling of protein structures and complexes. Nucleic Acids Res. *46*, W296–W303.

Waterhouse, A.M., Procter, J.B., Martin, D.M.A., Clamp, M., and Barton, G.J. (2009). Jalview Version 2--a multiple sequence alignment editor and analysis workbench. Bioinformatics *25*, 1189–1191.

Weel-Sneve, R., Kristiansen, K.I., Odsbu, I., Dalhus, B., Booth, J., Rognes, T., Skarstad, K., and Bjørås, M. (2013). Single transmembrane peptide DinQ Modulates membrane-dependent activities. PLoS Gen. *9*, e1003260.

Wen, J., Won, D., and Fozo, E.M. (2014). The ZorO-OrzO type I toxin–antitoxin locus: repression by the OrzO antitoxin. Nucleic Acids Res. *42*, 1930–1946.

Wen, J., Harp, J.R., and Fozo, E.M. (2017). The 5′ UTR of the type I toxin ZorO can both inhibit and enhance translation. Nucleic Acids Res. *45*, 4006–4020.

Wessner, F., Lacoux, C., Goeders, N., Fouquier d'Hérouel, A., Matos, R., Serror, P., Van Melderen, L., and Repoila, F. (2015). Regulatory crosstalk between type I and type II toxin-antitoxin systems in the human pathogen *Enterococcus faecalis*. RNA Biol. *12*, 1099–1108.

Wilbaux, M., Mine, N., Guerout, A.-M., Mazel, D., and Van Melderen, L. (2007). Functional Interactions between Coexisting Toxin-Antitoxin Systems of the *ccd* Family in *Escherichia coli* O157:H7. J. Bacteriol. *189*, 2712–2719.

Wilson, A.T. (1959). The relative importance of the capsule and the M-antigen in determining colony form of group A streptococci. J. Exp. Med. *109*, 257–270.

Winther, K.S., and Gerdes, K. (2011). Enteric virulence associated protein VapC inhibits translation by cleavage of initiator tRNA. PNAS *108*, 7403–7407.

Wood, D.N., Chaussee, M.A., Chaussee, M.S., and Buttaro, B.A. (2005). Persistence of *Streptococcus pyogenes* in Stationary-Phase Cultures. J. Bacteriol. *187*, 3319–3328.

Wozniak, R.A.F., and Waldor, M.K. (2009). A toxin-antitoxin system promotes the maintenance of an integrative conjugative element. PLoS Genet. *5*, e1000439.

Xie, Y., Wei, Y., Shen, Y., Li, X., Zhou, H., Tai, C., Deng, Z., and Ou, H.-Y. (2018). TADB 2.0: an updated database of bacterial type II toxin-antitoxin loci. Nucleic Acids Res. *46*, D749–D753.

Yamaguchi, Y., Park, J.-H., and Inouye, M. (2009). MqsR, a Crucial Regulator for Quorum Sensing and Biofilm Formation, Is a GCU-specific mRNA Interferase in *Escherichia coli*. J. Biol. Chem. *284*, 28746–28753.

Yao, J., Guo, Y., Wang, P., Zeng, Z., Li, B., Tang, K., Liu, X., and Wang, X. (2018). Type II toxin/antitoxin system ParE $_{SO}$ /CopA $_{SO}$ stabilizes prophage CP4So in *Shewanella oneidensis*: ParE $_{SO}$ /CopA $_{SO}$ stabilizes prophage CP4So. Environ. Microbiol. *20*, 1224–1239.

Yuan, J., Sterckx, Y., Mitchenall, L.A., Maxwell, A., Loris, R., and Waldor, M.K. (2010). *Vibrio cholerae* ParE2 poisons DNA gyrase via a mechanism distinct from other gyrase inhibitors. J. Biol. Chem. *285*, 40397–40408.

Yuan, J., Yamaichi, Y., and Waldor, M.K. (2011). The three *Vibrio cholerae* chromosome II-encoded ParE toxins degrade chromosome I following loss of chromosome II. J. Bacteriol. *193*, 611–619.

Zielenkiewicz, U., Kowalewska, M., Kaczor, C., and Ceglowski, P. (2009). In Vivo Interactions between Toxin-Antitoxin Proteins Epsilon and Zeta of Streptococcal Plasmid pSM19035 in *Saccharomyces cerevisiae*. J. Bacteriol. *191*, 3677–3684.

(2016). *Streptococcus pyogenes* : Basic Biology to Clinical Manifestations (Oklahoma City (OK): University of Oklahoma Health Sciences Center).

7 APPENDIX

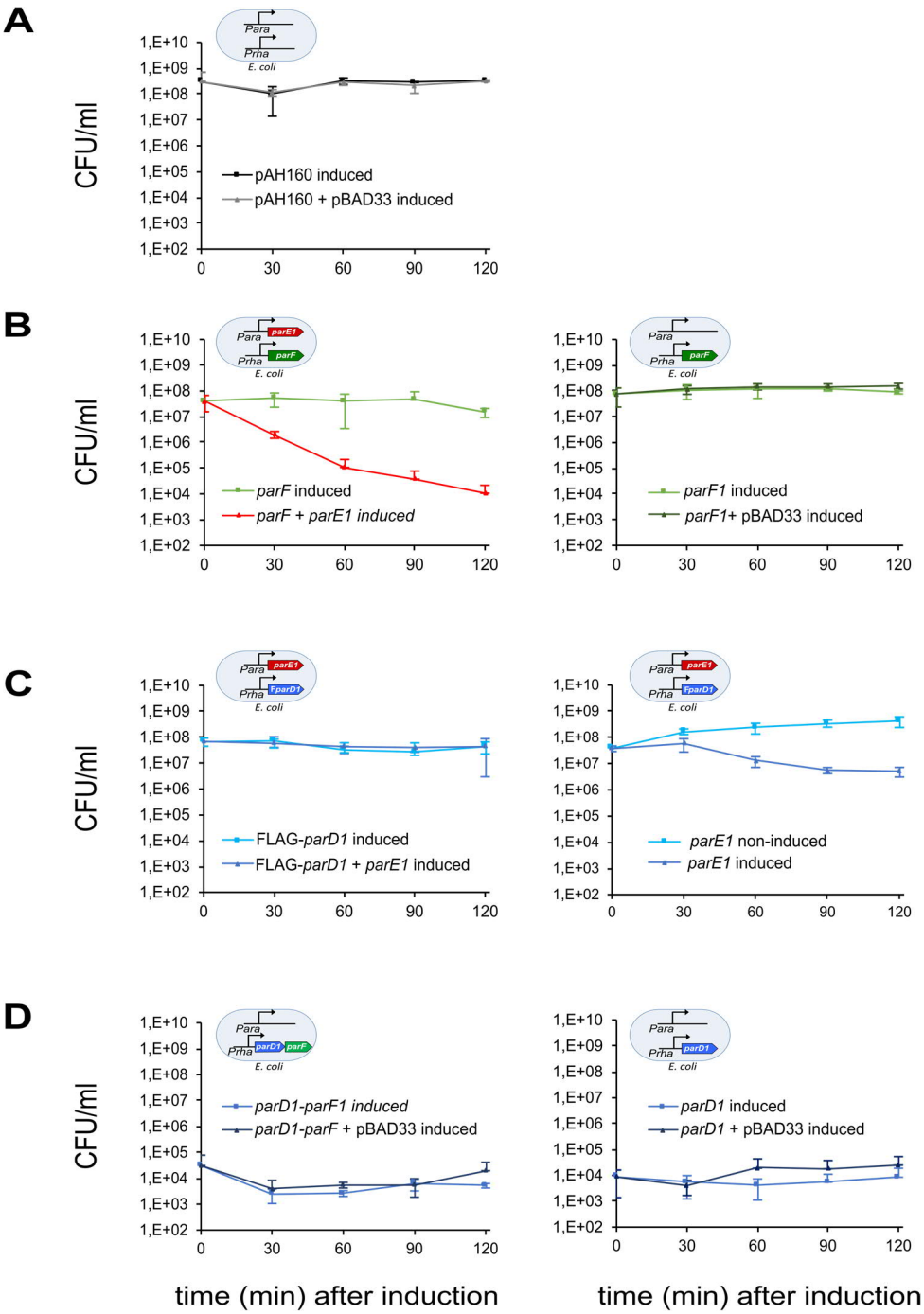

Figure S1: Controls death prevention experiments

Death prevention experiments of exponentially growing *E. coli* cells harboring two vectors the pBAD33P$_{ara}$ empty or harboring the toxin parE1 (TTG-SD6) and the pAH160P$_{rha}$ empty or harboring parF1, FLAG-tagged ParD1 or *parD1-parF1.* In all cases the cultures started in pAH160P$_{rha}$ expression conditions (0.2% rhamnose), except for **C** (right panel). **A.** Induction of the empty plasmids did not have an effect in growth. **B.** ParF1 did not prevented ParE1 toxicity (right panel) and ParF1 is not toxic (left panel). **C.** The FLAG-*parD1* variant prevented ParE1 toxicity (right panel) and absence of FLAG-*parD1* pre-expression led to killing by ParE1 (left panel). **D.** FLAG-*parD1* pre-expression led to less growth and this outcome is not modulated by co-expression of *parF1* (right panel) neither by the empty vector (left panel).

Table 2: Strains and plasmids used in this study

Strain	Relevant Characteristics	Source
Escherichia coli		
EC2618	*E. coli K-12,* MG1655*, F-, λ; ilvG, rfb-50, rph-1*	Kim Lewis lab
EC2620	*E. coli* MG1655 AT15, *λatt::PsulA*-gfp	Kim Lewis lab
RDN204	Top10 (*mcrA*, Δ(*mrr-hsd*RMS-*mcrBC*), Phi80*lacZ(del)M15*, Δ*lacX74*, *deoR*, *recA1*, *araD139*, Δ(*ara-leu*)7697, *galU*, *galK*, *rpsL(SmR)*, *endA1*, *nupG)*	Invitrogen (Host for cloning)
Streptococcus pyogenes		
EC2514	*Streptococcus pyogenes M1 GAS SF370*	ATCC 700294
EC2559	EC2514 Δ*SPy_parDE1::lox72*	This study
EC2568	EC2514 Δ*SPy_parDE2::lox72*	This study
EC2761	EC2514 Δ*SPy_clpE::lox72*	This study
EC2763	EC2514 Δ*SPy_clpC::lox72*	This study
EC1521	EC2514 Δ*SPy_clpP::lox72*	Laboratory collection
EC1376	EC2514 Δ*SPy_clpX::lox72*	Laboratory collection
Plasmid	**Relevant Characteristics**	**Source**
Killing assays		
pEC1055	pBAD33P_{ara}	(Guzman et al., 1995)
pEC1484	pBAD33P_{ara}ΩSPy_*parE1*(TTG-SD6)	This study
pEC1601	pBAD33P_{ara}ΩSPy_*parE1*(TTG-SD6) L47A	This study
pEC1315	pBAD33P_{ara}ΩSPy_*parE2*(ATG-SD6)	This study
pEC1603	pBAD33P_{ara}ΩSPy_*parE2*(ATG-SD6) L48A	This study
pEC2378	pBAD33P_{ara}Ω*EcoO157:H7_parE3*(ATG-SD6)	This study
pEC2379	pBAD33ΩMtbH37Rv_*parE2*(ATG-SD6)	This study
pEC2513	pBAD33ΩVc_*parE1** L48P (ATG-SD6)	This study
pEC2514	pBAD33ΩVc_*parE2** I86T (ATG-SD6)	This study
pEC2493	pBAD33P_{ara}Ω*Vfi_ccdB*(TTG-SD6)	This study
Growth rescue assays		
pEC1057	pZE12P_{lac}	(Lutz and Bujard, 1997)
pEC2138	pZE12P_{lac}ΩSPy_*parD1*	This study
pEC1369	pZE12P_{lac}ΩSPy_*parD1 F49L*	This study
pEC2141	pZE12P_{lac}ΩFLAGtag-SPy_*parD1*	This study
pEC2139	pZE12P_{lac}ΩSPy_*parF1*	This study
pEC1091	pZE12ΩSPy_1926	This study
Death prevention experiments		
pEC2119	pAH160P_{rha}	(Harms et al., 2015a)
pEC2198	pAH160P_{rha}ΩSPy_*parD1*	This study
pEC2199	pAH160P_{rha}ΩFLAG-tag-SPy_*parD1*	This study
pEC2310	pAH160P_{rha}ΩSPy_*parD1*- FLAG-tag	This study
pEC2383	pAH160P_{rha}ΩSPy_*parD1 K3A*	This study
pEC2343	pAH160P_{rha}ΩSPy_*parD1 N8I*	This study
pEC2385	pAH160P_{rha}ΩSPy_*parD1 G6A*	This study
pEC2202	pAH160P_{rha}ΩSPy_*parF1*	This study
pEC2205	pAH160P_{rha}ΩSPy_*parD1- parF1*	This study
pEC2200	pAH160ΩSPy_*parD2*	This study
pEC2201	pAH160ΩFLAG-tag-SPy_ *parD2*	This study
pEC2120	pAH160P_{rha}Ω*gyrB*	(Harms et al., 2015)
pEC2121	pAH160P_{rha}Ω*parE*	(Harms et al., 2015)
pEC2122	pAH160P_{rha}Ω*gyrB-gyrA*	Christoph Dehio lab
pEC2123	pAH160P_{rha}Ω*parE-parC*	Christoph Dehio lab
pEC2160	pAH160P_{rha}Ω*parC*	This study
pEC2161	pAH160P_{rha}Ω*gyrA*	This study
***S. pyogenes* experiments**		
pEC85	*repDEG*-pAM β1, aphIII-Pjh1, ColE1	Laboratory collection
pEC1487	pEC85ΩP_{tet}FLAGtag-SPy_*parD1*	This study
pEC2203	pEC85ΩP_{tet}FLAGtag-SPy_*parD1-parF1*	This study
pEC1824	pEC85ΩP_{tet}SPy_*parE1* (ATG-L47A)	This study
pEC1488	pEC85ΩP_{tet}FLAGtag-SPy_*parD2*	This study

pEC1820	pEC85ΩP$_{tet}$FLAGtag-SPy_*parE2* (TTG L48A)	This study
pEC1821	pEC85ΩP$_{tet}$FLAGtag-SPy_*parE2* (ATG L48A)	This study
pEC2162	pEC85ΩP$_{tet}$ FLAGtag-SPy_*parD2-parE2*	This study
pEC1072	pUC19Ωup*SPy_0550-lox66-erm-lox71-dwSPy_0552*	This study
pEC1071	pUC19Ωup*SPy_1926*-lox66-erm-lox71-dw*SPy_1927*	This study
pEC536	pEU8517ΩP$_{tet}$ (pCR-XL-TOPO (Invitrogen) back-bone)	(Bugrysheva and Scott, 2010)
pEC454	pUC19Ωlox66-erm-lox71	Laboratory collection
pEC455	pEC85ΩßgalP$_{gyrA}$*cre*	Laboratory collection

Table 3: Oligonucleotides used in this study

OLIGO	Sequence 5´-3´ [a]	F/R[b]	Target/ Purpose[c]
RT-PCR and NB analysis			
OLEC5128	AAACGTGATACAATGTCGTTA	F	RT-PCR 1: *SPy_0549*end - *SPy_0550*start
OLEC5129	CATTAACTCGTTGAGGCGC	R	
OLEC4693	TGAGTCAGGAGAAGTTTTATGATAAGC	F	RT-PCR 2: *SPy_0550*end - *SPy_552*start, qRT-PCR and NB
OLEC4694	GCTCAGCAAATCTGCTTTAGCATCATC	R	
OLEC4695	TCGCATTGTATATCATGTTCTGGAAG	F	RT-PCR3: *SPy_0552*end- *SPy_0553*start and qRT-PCR
OLEC4696	TGCCAAATAGGTCAGGTATCGGAG	R	
OLEC5130	CAACTGATGGAACTTTGGTG	F	RT-PCR 4: *SPy_0553*end- *SPy_0555*start
OLEC5131	GCCCTCCTTATTTTGGGGTAC	R	
OLEC4699	TGAAAATCTGTCTCAATTACCGAGTC	F	RT-PCR 1: UPSpy_1926- Spy_1926start
OLEC4700	ACTGTCATTGCTTCGCTTACCA	R	
OLEC4701	TGAGGATGTTCGTCAAGGGAAGT	F	RT-PCR2: *SPy_1926*end- *SPy_1927*start, qRT-PCR and NB
OLEC4702	ACGCTGACCTGATGTTGAGG	R	
OLEC4703	ACTTGCTTCCTACTCAAAGCGACT	F	RT-PCR3: Spy_1927end- DWSpy_1927
OLEC4704	GCCTAGCTTCGTAGTCTTTGGCT	R	
OLEC4719	TACCATGTCTACTTAAGAGG	F	RT-PCR4: UPSpy_1926- Spy_1926start
OLEC4700	ACTGTCATTGCTTCGCTTACCA	R	
OLEC5923	*CTACCTATATGTCAACACACCAG*	F	qRT-PCR *clpP*
OLEC5924	*CATTGGCTGGTGGATCATATAC*	R	
OLEC5362	GATGGCAACTCCGCTTACGTTG	F	qRT-PCR *htrA*
OLEC5363	GTTCCTAGTGGGCTGCCGATAG	R	
OLEC6677	AAGCTCTTGAAGGCGACACT	F	qRT-PCR *tufA*
OLEC6678	TGACACGAACAGTACCACGG	R	
OliRN243	CGTTGTACCAACCATTGTAGC	R	16S rRNA, NB
Sequencing			
OLEC8101	GCTAGTTATTGCTCAGCGG	F	MCS pAH160
OLEC8102	GGAAATGCGGTGAGCATCAC	R	
OLEC4208	CTGTTTCTCCATACCCGTT	F	MCS pBAD33
OLEC4210	CACTTCTGAGTTCGGCAT	R	
OLEC4112	TGTCTCATGAGCGGATACATA	F	MCS pZE12
OLEC4114	GATCCTCATCCTGTCTCTTGA	R	
OliRN228	GGAACGAAAACTCACGTTAA	F	MCS pEC85
OLEC787	TGTGGTTACGTGGTTTTTAAC	R	
***In-vitro* translation**			
OLEC8194	aagctttaatacgactcactataggaacataaggagaaacaataATGAAA GAATATCAGGTCACCATGT	F	*SPy_parE1*
OLEC8195	caaaaaacccctcaagacccgtttagaggccccaaggggttatgctatttttttTT ACCAATTATTCATATGACG	R	
OLEC8196	aagctttaatacgactcactataggaacataaggagaaacaataATGGAC TATAAGAAATATCAGATTATCTAT	F	*SPy_parE2*
OLEC8197	caaaaaacccctcaagacccgtttagaggccccaaggggttatgctatttttttTT ATTTGAATAACTTTATATAGTCGCT	R	
OLEC8912	aagctttaatacgactcactataggaacataaggagaaacaataATGACG CGCAGGCTGCGCGTCCATAAC	F	*Mtb_parE2* from genomic DNA MtbH37Rv (Kaufmann lab)
OLEC8913	caaaaaacccctcaagacccgtttagaggccccaaggggttatgctatttttttT CACTCGAAGGTGCGGCCAGAGATCTC	R	
OLEC9665	aagctttaatacgactcactataggaacataaggagaaacaataATGTAT AAGCTTAGCGGAAAAGCTGT	F	*Ec_parE3* from *E. coli O157:H7* DNA (DSM 17076)

OLEC8911	caaaaaaccccctcaagacccgtttagaggccccaaggggttatgctatttttttTTACCAGTGACGGCGAGGTTCCATC	R	
OLEC9670	aagctttaatacgactcactataggaacataaggagaaacaataATGTCTCAATTTACGCTATATAAAAAC	F	*Vf_ccdB* from pBAD33*ccdBv.f.* (Yuan et al., 2010)
OLEC9671	caaaaaaccccctcaagacccgtttagaggccccaaggggttatgctatttttttTTAAATGCCAGTGATTAAAAAATCAAT	R	
Toxin cloning (restriction ligation mediated cloning)			
OLEC4421	CCCCCTCTAGAGTCGACTA**AAGGA**AAAAAATTGAAGGGAAATTGCTTATTGAAAGAA (XbaI)	F	*SPy_parE1*
OLEC4077	TTCGCATGCTTACCAATTATTCATATGACGTGA (SphIR)	R	
OLEC8811	CCCCCTCTAGAGTCGACTA**AAGGA**AAAAAAATGACGCGCAGGCTGCGCGTCCATAAC (XbaI)	F	*Mtb_parE2* from genomic DNA MtbH37Rv (Kaufmann lab)
OLEC8813	TTCGCATGCTCACTCGAAGGTGCGGCCAGAGATCTC (SphIR)	R	
OLEC9661	CCCCCTCTAGAGTCGACTA**AAGGA**AAAAAATTGAGCGTTTACCTCAATATGCAAAAT (XbaI)	F	*Vc_parE1* from pBAD33*parE1* *(Yuan et al., 2011)*
OLEC9662	TTCGCATGCTTAAGAAACAAAGCGTGACTGTTTGAG (SphIR)	R	
OLEC9659	CCCCCTCTAGAGTCGACTA**AAGGA**AAAAAATTGAAACCATTTAATCTTACCGTCGCC (XbaI)	F	*Vc_parE2* from pBAD33*parE2* *(Yuan et al., 2010)*
OLEC9660	TTCGCATGCTTATGCGCCGAATATTGGGTTCACATC (SphIR)	R	
OLEC8846	CCCCCTCTAGAGTCGACTA**AAGGA**AAAAAAATGTATAAGCTTAGCGGAAAAGCTGT (XbaI)	F	*Ec_parE3* from *E. coli O157:H7* DNA (DSM 17076)
OLEC8847	TTCGCATGCTTACCAGTGACGGCGAGGTTCCATC (SphIR)	R	
OLEC9663	CCCCCTCTAGAGTCGACTA**AAGGA**AAAAAATTGTCTCAATTTACGCTATATAAAAAC (XbaI)	F	*Vf_ccdB* from pBAD33*ccdBv.f.* (Yuan et al., 2010)
OLEC9664	TTCGCATGCTTAAATGCCAGTGATTAAAAAATCAAT(SphIR)	R	
Antitoxin cloning (restriction ligation mediated cloning for pZE12P$_{lac}$ and Gibson mediated cloning for pAH160P$_{rha}$)			
OLEC8231	AATGAAATTCCTGCAGATAGGAGGAACAATTTTATGGCTAAAACGGGAACTTTGAAT	F	*SPy_parD1* to clone into pAH160
OLEC8232	GCCGGCCGATATCCAATTGAGATCTGCCATATGTTAAGCATTTTCCTTCAATTGAAA	R	
OLEC8237	AATGAAATTCCTGCAGATAGGAGGAACAATTTTATGGATTACAAGGATGACGATGACAAGGCTAAAACGGGAACTTTGAAT	F	FLAG-tagged *SPy_parD1* to clone into pAH160
OLEC8232	GCCGGCCGATATCCAATTGAGATCTGCCATATGTTAAGCATTTTCCTTCAATTGAAA	R	
OLEC8231	AATGAAATTCCTGCAGATAGGAGGAACAATTTTATGGCTAAAACGGGAACTTTGAAT	F	*SPy_parD1* to construct pAH160 Ω*SPy_parD1–parF1*
OLEC7978	CATACATCACTCTCCCTTACTTTAAGCATTTTCCTTCAATTGAAA	R	
OLEC7979	AGTAAGGGAGAGTGATGTATGGAACTCGTAAAGACGATACAAATT	F	*SPy_parF1* to construct pAH160 Ω*SPy_parD1–parF1*
OLEC8236	GCCGGCCGATATCCAATTGAGATCTGCCATATGTCATTCTGTCAATTCCTTAAATG	R	
OLEC8233	AATGAAATTCCTGCAGATAGGAGGAACAATTTTATGACTACAGTAAAAAAAAACAGAGCG	F	*SPy_parD2* to clone into pAH160
OLEC8234	GCCGGCCGATATCCAATTGAGATCTGCCATATGTTATAGTCCAAGTTCAGCCCTCAC	R	
OLEC8238	AATGAAATTCCTGCAGATAGGAGGAACAATTTTATGGATTACAAGGATGACGATGACAAGACTACAGTAAAAAAAAACAGAGCG	F	FLAG-tagged *SPy_parD2* to clone into pAH160
OLEC8234	GCCGGCCGATATCCAATTGAGATCTGCCATATGTTATAGTCCAAGTTCAGCCCTCAC	R	
OLEC7974	GCGGGTACCATGGCTAAAACGGGAACTTTGAAT (KpnI)	F	*SPy_parD1* to clone into pZE12
OLEC7975	GCGGGATCCTTAAGCATTTTCCTTCAATTGAAA (BamHI)	R	
OLEC8017	GCGGGTACCATGGATTACAAGGATGACGATGACAAGGCTAAAACGGGAACTTTGAAT (KpnI)	F	FLAGtag-*SPy_parD1* to clone into pZE12

OLEC7975	GCGGGATCCTTAAGCATTTTCCTTCAATTGAAA (BamHI)	R	
OLEC7976	GCGGGTACCATGGAACTCGTAAAGACGATACAAATT (KpnI)	F	*SPy_parF1* to clone into pZE12
OLEC7977	GCGGGATCCTCATTCTGTCAATTCCTTAAATGC (BamHI)	R	
OLEC4415	GCGGGTACCATGACTACAGTAAAAAAAAACAGAGCG (KpnI)	F	*SPy_parD2* to clone into pZE12
OLEC4100	GCGGGATCCTTATAGTCCAAGTTCAGCCCTCAC (BamHI)	R	
OLEC8018	GCGGGTACCATGGATTACAAGGATGACGATGACAAGACTACAGTAAAAAAAAAACAGAGCG	F	FLAGtag-*SPy_parD2* to clone into pZE12
OLEC8019	GCGGGATCCTTATAGTCCAAGTTCAGCCCTC (BamHI)	R	
pEC85 cloning (Gibson mediated cloning)			
OLEC4839	GAATTCAGGCCGGCCAAAAAAGG	F	pEC85
OLEC4840	GGATCCTCTAGAGTCGACCTGCAG	R	
OLEC5258	CCGCTGCATGCCTGCAGGTCGACTCTAGAGGATCCTATGAGATAATGCCGACTGTAC	F	P_{tet} from the pEC536
OLEC6249	CTTGTCATCGTCATCCTTGTAATCCATTCTAGATCACCTCCTTAACTAG	R	
OLEC6250	ATGGATTACAAGGATGACGATGACAAGGCTAAAACGGGAACTTTGAAT	F	FLAGtag-*SPy_parD1*
OLEC5261	CACTTTTGTGGGCCTTTTTTGGCCGGCCTGAATTCCATTAAGCATTTTCCTTCAAT	R	
OLEC6250	ATGGATTACAAGGATGACGATGACAAGGCTAAAACGGGAACTTTGAAT	F	FLAGtag-*SPy_parD1*, to construct FLAGtag-*SPy_parD1-parF1*
OLEC7978	CATACATCACTCTCCCTTACTTTAAGCATTTTCCTTCAATTGAAA	R	
OLEC7979	AGTAAGGGAGAGTGATGTATGGAACTCGTAAAGACGATACAAATT	F	*SPy_parF1*, to construct FLAGtag-*SPy_parD1-parF1*
OLEC7980	CACTTTTGTGGGCCTTTTTTGGCCGGCCTGAATTCTCATTCTGTCAATTCCTTAAATGC	R	
OLEC6251	ATGGATTACAAGGATGACGATGACAAGACTACAGTAAAAAAAAACAGAGCG	F	FLAGtag-*SPy_parD2*
OLEC5263	CACTTTTGTGGGCCTTTTTTGGCCGGCCTGAATTCTTATAGTCCAAGTTCAGCCCTC	R	
OLEC8515	TTTCAATTGAAGGAAAATGCTTATTGAAAGAATATCAGGTCACCATGT	F	*SPy_parE1*
OLEC7981	CACTTTTGTGGGCCTTTTTTGGCCGGCCTGAATTCTTACCAATTATTCATATGACG	R	
OLEC5218	CTCGAATAGATCTTCGAGTCTAGTTAGAGGAAA**TTG**GACTATAAGAAATATCAGATTATC	F	*SPy_parE2*
OLEC5219	CTCGAATAGATCTTCGAGTCTAGTTAGAGGAAA**ATG**GACTATAAGAAATATCAGATTATC	F	
OLEC5220	CACTTTTGTGGGCCTTTTTTGGCCGGCCTGAATTCTTATTTGAATAACTTTATATAGTCGCT	R	
OLEC6251	ATGGATTACAAGGATGACGATGACAAGACTACAGTAAAAAAAAACAGAGCG	F	FLAG-tag-*SPy_parD2-parE2*
OLEC7982	CACTTTTGTGGGCCTTTTTTGGCCGGCCTGAATTCTTATTTGAATAACTTTATATAGTCGCT	R	
Toxin targets (Gibson mediated cloning)			
OLEC8009	CATATGGCAGATCTCAATTGGATATCGGCCGGC	F	pAH160
OLEC8010	CATAAAATTGTTCCTCCTATCTGCAGGAATTTCATT	R	
OLEC8203	AATGAAATTCCTGCAGATAGGAGGAACAATTTTATGAGCGACCTTGCGAGAGAAA	F	*Ec_gyrA* from pEC2122
OLEC8204	GCCGGCCGATATCCAATTGAGATCTGCCATATGTTATTCTTCTTCTGGCTCGTCG	R	
OLEC8205	AATGAAATTCCTGCAGATAGGAGGAACAATTTTATGAGCGATATGGCAGAGC	F	*Ec_parC* from pEC2123
OLEC8206	GCCGGCCGATATCCAATTGAGATCTGCCATATGTTACTCTTCGCTATCACCGC	R	
Mutants construction (TOPO XL cloning or restriction ligation mediated cloning for pUC19)			

OLEC1943	TACCGTTCGTATAGCATACATTATACGAAGTTATCCGT AGCGGTTTTCAAAATTTGCAACC	F	lox66-*ermAM/B*-lox71 cassette from the pEC454 vector
OLEC1932	TACCGTTCGTATAATGTATGCTATACGAAGTTATTTATT TCCTCCCGTTAAATAATAGATAACTATTAAA	R	
OLEC4225	CGCGAATTCAAGTAAGAGACAATCATCTGA (EcoRI)	F	Upstream *SPy_parD1*
OLEC4228	TATAATGTATGCTATACGAACGGTATGTATCACGTTTT TAGATTGAC	R	
OLEC4232	ATAGCATACATTATACGAACGGTAAGTAAGGGAGAGT GATGTATG	F	Downstream *SPy_parE1*
OLEC4235	GCGGGATCCTCCTGGAATAACGACCTTATC (BamHI)	R	
OLEC4237	AGAAAATCTGTAGGATCATCC		Up- Upstream *SPy_parD1,* SEQ mutant
OLEC4241	GGAGTTAAAGAGATGGTTGTA		Down- Downstream *SPy_parE1,* SEQ mutant
OLEC4147	CGCGAATTCGTGGTGAATGTCGTGAAATTA (EcoRI)	F	Upstream *SPy_parD2*
OLEC4148	TATAATGTATGCTATACGAACGGTATTTATGTAACCCC TTTATGTAACT	R	
OLEC4185	ATAGCATACATTATACGAACGGTACACGTTAAAAGCCT TAGCAGTCT	F	Downstream *SPy_parE2*
OLEC4186	GCGGGATCCAGTCATTTGACTACTAGCATGTCC (BamHI)	R	
OLEC4155	AATTCTATTGCGACGTACAGT	F	Up- Upstream *SPy_parD2,* SEQ mutant
OLRC4158	TTACAAGCATTTTGCAAGTCT		Down- Downstream *SPy_parE2,* SEQ mutant
OLEC5005	GGAAGTAGTCTTGAAAAGTCCAAG	F	Upstream *SPy_clpE*
OLEC5006	TATAATGTATGCTATACGAACGGTAAATATACCTCCGA GGGTTTATCTA	R	
OLEC5007	ATAGCATACATTATACGAACGGTACGTTAGCTAAGAGA GTTTCTATAAG	F	Downstream *SPy_clpE*
OLEC5008	TCTTTTAAGAAAATTGCTGGCTTC	R	
OLEC5005	CGCGAATTCGGTCAACGGCTTCACATGACTAC (EcoRI)	F	Nested PCR to mutate *SPy_clpE*
OLEC5206	GCGGGATCCGTCTGAATAGCTGGCTGCTG (BamHI)	R	
OLEC4997	GATGTGAGAGCGAGTAGAGTTGA	F	Upstream *SPy_clpC*
OLEC4998	TATAATGTATGCTATACGAACGGTATTTAATTGCTTCC CTTTCTGTCAATTC	R	
OLEC4999	ATAGCATACATTATACGAACGGTATTTCCATATAAAAG GTGGATCATCC	F	Downstream *SPy_clpC*
OLEC5000	CATCGTTGCCCACACGCTC	R	
OLEC5209	CGCGAATTCATGTGTTACTCTTAGTGAGT (EcoRI)	F	Nested PCR to mutate *SPy_clpC*
OLEC5210	GCGGGATCCTGGCTTTCAAGGCTTCAAC (BamHI)	R	

[a] *italic*: sequence annealing to the template; underlined: restriction site; lowercase: t7 promoter/terminator; highlighted grey: FLAG-tag, sequence in bold; ribosome binding side or start codon.

[b] F: forward primer; R: reverse primer.

[c] RT-PCR: retro-transcription PCR; qRT-PCR: quantitative retro-transcription; NB: used for Northern blot analysis; MCS: multiple cloning side; SEQ: sequencing; SPy: *S. pyogenes*; Ec: *E. coli*; Mtb: *Mycobacterium tuberculosis* H37Rv; Vc: *Vibrio Cholerae*; Vf (*v.f.*): *Vibrio Fischeri*; *SPy_0550: parD1; SPy_0552: parE1; SPy_0553: parF1; SPy_1926: parD2; SPy_1927: parE2.*

ACKNOWLEDGMENTS

I express my gratitude to Prof. Dr. Emmanuelle Charpentier for her support, trust, and help in my research. Special acknowledge to Dr. Alexander Elsholz for his guidance and support as well as to my thesis committee members, Prof. Dr. Kenn Gerdes, Prof. Dr. Marc Erhardt and Prof. Dr. Kürsad Turgay for their advice in my Ph.D. project. I am also very thankful to the HZI Graduate School, the Helmholtz Institute for Infection Research, the Max Planck Institute for Infection Biology, the ZIBI Graduate School and the Max Planck Unit for the Science of Pathogens for the financial support and for the several career development opportunities provided.

I would like to express my deep gratitude to my friends, Dr. James Tsatsaronis, Dr. Thibaud Renault, Dr. Majda Bratovic and Dr. Anais Le Rhun, for their endless support during the past years. Thank you for your mentorship, patient guidance, enthusiastic encouragement and all the great advice without which this thesis would have not been possible. Exceptional acknowledgments to all members of the REGI/RIIB group. Thank you for all the help, technical support and friendship. I am especially grateful to Frank Hille, Vanessa Muñoz, Laura Broglia, Andres Mauer, Shi Pey Wong, Ines Fanfara, Anna Laure Lecrivain. It has been a pleasure to work with you guys and have the privilege to have you as friends. Thanks to Frederik Kramer, Daniel Troitzsch, Leticia Rodriguez, Sandra Augustin, Christian Aparicio and Maik Damm for their extraordinary help, commitment and for trusting me, you have all made my labor worth it. I am also very grateful to Tim Sullivan and Jackson Emanuel for the English proofreading of this document.

My gratitude also goes to all the amazing friends I had the pleasure to meet in Braunschweig and Berlin. You made this journey an astonishing experience that will remain in my mind and will remind me of the family I have in Europe. Most importantly, I want to thank my best friend, favorite colleague, Dr. Eric J.C. Galvez B, who has been next to me during my scientific career and has made this Ph.D. a family project. Finally, I wish to thank all my family, who has provided me through moral and emotional support in my life. Gracias papi y mami por ayudarme a sobrellevar la distancia, y por hacerme el ser humano que soy.

DECLARATION

Erklärung:

Hiermit erkläre ich, die Dissertation selbstständig und nur unter Verwendung der angegebenen Hilfen und Hilfsmittel angefertigt zu haben. Ich habe mich anderwärts nicht um einen Doktorgrad beworben und besitze keinen entsprechenden Doktorgrad. Ich erkläre, dass ich die Dissertation oder Teile davon nicht bereits bei einer anderen wissenschaftlichen Einrichtung eingereicht habe und dass sie dort weder angenommen noch abgelehnt wurde. Ich erkläre die Kenntnisnahme der dem Verfahren zugrunde liegenden Promotionsordnung der Lebenswissenschaftlichen Fakultät der Humboldt-Universität zu Berlin vom 5. März 2015.

Weiterhin erkläre ich, dass keine Zusammenarbeit mit gewerblichen Promotionsbearbeiterinnen/Promotionsberatern stattgefunden hat und dass die Grundsätze der Humboldt-Universität zu Berlin zur Sicherung guter wissenschaftlicher Praxis eingehalten wurden.

Declaration:

I hereby declare that I completed the doctoral thesis independently based on the stated resources and aids. I have not applied for a doctoral degree elsewhere and do not have a corresponding doctoral degree. I have not submitted the doctoral thesis, or parts of it, to another academic institution and the thesis has not been accepted or rejected. I declare that I have acknowledged the Doctoral Degree Regulations which underlie the procedure of the Faculty of Life Sciences of Humboldt-Universität zu Berlin, as amended on 5th March 2015.

Furthermore, I declare that no collaboration with commercial doctoral degree supervisors took place, and that the principles of Humboldt-Universität zu Berlin for ensuring good academic practice were abided by.

.....
Datum / Unterschrift
Date / signature